NEUTRONS
FOR SOCIETY

ANNUAL REPORT
2017

INSTITUT LAUE-LANGEVIN

50 years of service to science and society

THE FIVE DECADES OF THE ILL

1967–1977

The ILL was founded on 19 January 1967 with the signing of an agreement between France and Germany. The reactor went critical on 31 August, ramping up to full power between 16–21 December. The UK becomes an Associate on 1 January 1973.

1978–1989

The 'deuxième souffle' modernisation programme is launched. Spain and Switzerland join the ILL. The Grenoble outstation of the EMBL moves to the ILL site.

1990–1999

Replacement of the reactor vessel during a five-year long shutdown. Austria, Russia, Italy and the Czech Republic become members. The ESRF is built close to the ILL, thus sowing the seeds for the development of a unique site for scientific research.

2000–2007

The Millennium Programme is launched with the aim of radically modernising the ILL's infrastructure and instrument suite. At the end of its first phase, it has already boosted the efficiency of the ILL's instrument suite by a factor of 14. Sweden, Belgium, Poland and Hungary join the ILL.

2008–2017

The second phase of the Millennium Programme is completed, with a total budget of about 80 k€ and a global instrument efficiency gain factor of about 25. Major reinforcements and security measures are undertaken on the ILL reactor (post-Fukushima event). The Endurance phase I modernisation plan is launched. Slovakia and India join the ILL.

This year the Institute celebrated its 50th anniversary and yet remains in the prime of youth! The ILL was founded on 19 January 1967, and since then it has firmly established itself as a pioneer in neutron science and technology and has taken on a truly international dimension.

The unique research conducted at the ILL is essential to solving some of the major challenges facing modern society. To maintain its status as leader in neutron science, the Institute has constantly upgraded its instruments, infrastructure and scientific equipment during the last 50 years. Even today, the ILL is still looking resolutely to the future with its latest modernisation programme: Endurance.

1967
2017

PUBLISHING INFORMATION

Editors:
Giovanna Cicognani and Mark Johnson
Scientific advisors:
Gabriel Cuello, Emmanuel Farhi, Philipp Gutfreund,
Ingo Hoffmann, Tobias Jenke, Anne Martel,
Estelle Mossou, Jacques Ollivier, Andrea Piovano,
Navid Qureshi, Thomas Saerbeck and
Bruno Tomasello
Production team:
Giovanna Cicognani, Virginie Guerard,
Robert Corner and Susan Tinniswood
Design:
Morton Ward Limited
Photography:
Serge Claisse – ILL (unless otherwise specified)

Further copies can be obtained from:
Institut Laue-Langevin
Communication Unit
CS 20156, F-38042 Grenoble Cedex 9
communication@ill.eu
www.ill.eu

Contents

WHAT IS THE ILL

EXPERIMENTAL AND USER PROGRAMME

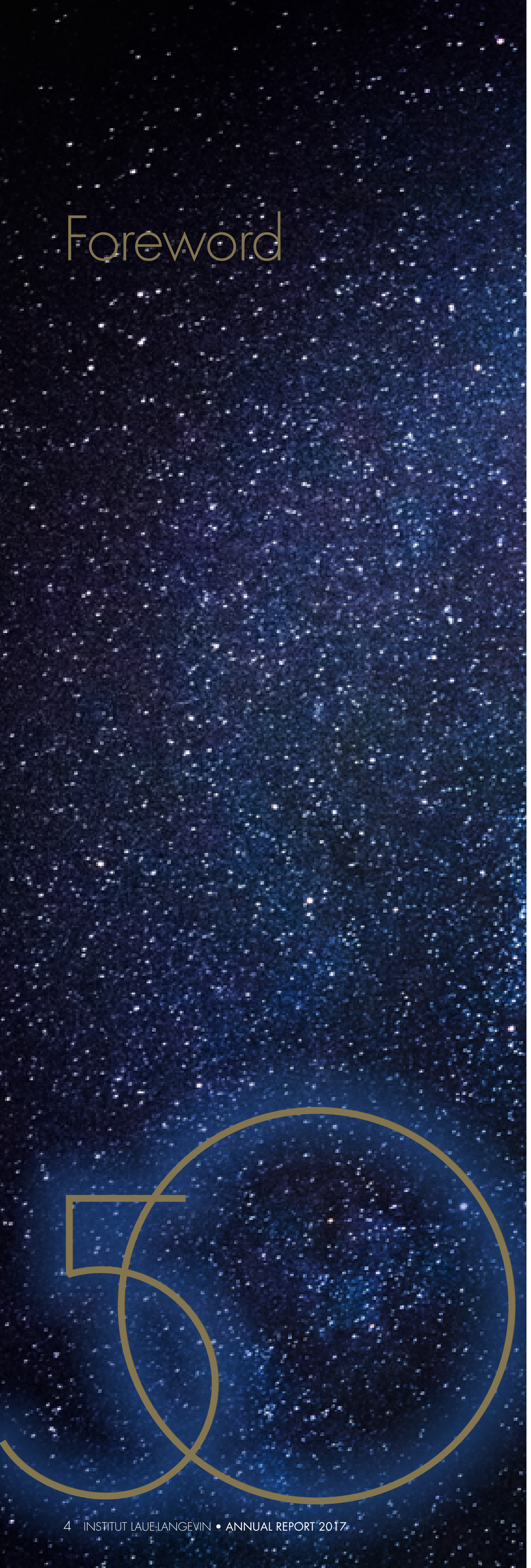

Foreword

This past year saw the turn of the UK to chair the ILL Steering Committee, and I had the honour and pleasure to serve in that capacity for a second time.

The year started with the celebration of a remarkable 50 years of the ILL, on 19 January. The UK ambassador to France, the Rt. Hon. Lord Llewellyn, along with dignitaries from the other Associate and Scientific Member countries, enjoyed meeting staff and touring the ILL prior to the afternoon event. The 'legendary' Professor Bill Stirling returned as Master of Ceremonies for that event, which saw many staff and users, past and present, come together. I would like to take this opportunity to congratulate Bill on receipt of his C.M.G. (Companion of the Order of St Michael and St George) for services to British science and international science collaboration, in the UK New Year Honours for 2018.

We also said a fond farewell to Dr. Charles Simon, who completed his five-year appointment as French Associate Director and head of Projects and Techniques at the end of September. Charles has had a long association with the ILL, serving as part of the French delegation to the Steering Committee prior to his appointment, and will continue to work with the ILL in his new role as science advisor for the French neutron roadmap in CNRS. In October we welcomed the appointment of his successor, Jérôme Estrade; Jérôme brings a wealth of experience in the operation of nuclear facilities to the management team.

In June, the UK hosted the Steering Committee meeting in Abingdon. Prior to that there was a meeting between delegates from the ESS and the ILL, during which the two facilities signed a Memorandum of Understanding for closer ties and joint working in some areas, including attendance at our respective Council meetings. This new way of working will see the first joint ESS/ILL user meeting being held in 2018.

During the summer months the ILL had to make the difficult announcement that, for a number of reasons, it would not be able to operate more than one user cycle in 2017. The loss of scientific output from the facility was not taken lightly by the Associates, who have been closely monitoring the situation. The Director and management team have the full support of the Associates as they make the changes necessary to resolve the issues; the Associates welcome the positive changes in the way of working across the ILL, whilst emphasising that this approach must continue. We look forward to a return to the usual excellent level of scientific output in 2018, over the course of which the operation of three cycles is planned.

In November we all headed to Rome for the autumn Steering Committee meeting to celebrate 20 years of Italian Scientific Membership of the ILL. I thank the Italian CNR for hosting the event and we all hope that successful collaboration between Italy and the ILL will continue in future years.

Looking to the future, 2018 is an important year for the ILL as we aim to renew the contracts of the Scientific Members. The Associates have worked with the Scientific Member countries to draft a revised contract, and I hope that this time next year we will be able to announce that all the contracts have been renewed.

Grahame Blair
Chair of the ILL Steering Committee

Director's foreword

The year 2017 was marked most specially by the celebration of the ILL's 50th anniversary. The past fifty years have seen the most pronounced increase in scientific knowledge ever witnessed in human history. The concomitant technological revolution has changed our world profoundly, and, despite undeniably problematic side-effects, has dramatically improved living conditions for people all over the globe. The unique and outstanding analytical capabilities of the ILL have pulsed at the very heart of this process. The ILL's history has been marked by steady gains in performance and continuous adaptation of its services to the changing needs of its users, qualities that have allowed it to maintain its position as the world's leading provider of neutrons for scientific applications. The scientific highlights you will find in this report bear testimony to this fact.

The success of the past poses obligations for the future. With the help of the Endurance Programme, the ILL is currently accelerating the modernisation of its scientific infrastructure. You will find plenty of information on Endurance in this report. The timely launch of its second phase in 2019 is fundamental to maintaining the ILL's excellence in instrumentation. The ILL places particular emphasis on fine-tuning its services and instrumentation to the rapidly evolving needs of its user communities. We are making particular efforts to monitor the different fields of research in order to be able to respond in the future with the most appropriate technical support. The advice of our Scientific Council and its Subcommittees is of invaluable help in this context.

The reliability of the Institute's neutron source has been an integral part of its success. Reliable operations are guaranteed by the continuous renewal of key reactor components. The ILL is known for its high nuclear safety standards, and we will sustain our efforts in this area with continuous improvement as our goal. In 2017 our responsibilities in the fields of reactor maintenance and ever higher standards of nuclear safety, together with the need to adapt to changes in regulations, prevented the ILL from running a full user programme. These efforts have, however, left us fitter for the future. We now fulfil all technical conditions for sustained and successful operations beyond the next decade.

I hope that you enjoy reading this annual report, and that I may have the opportunity of meeting you, as an ILL user or otherwise, this year at the ILL.

Helmut Schober
ILL Director

About the ILL

The Institut Laue-Langevin (the ILL) is an international research centre providing world-leading facilities in neutron science and technology. Neutrons are used at the ILL to probe the microscopic structure and dynamics of a broad range of materials at molecular, atomic and nuclear level.

The ILL is owned by the three founding countries—France, Germany and the United Kingdom. These three Associate countries contributed some 65 M€ to the Institute in 2017, a sum enhanced by significant contributions from the ILL's Scientific Member countries—Austria, Belgium, the Czech Republic, Denmark, Italy, Poland, Slovakia, Spain, Sweden and Switzerland. The ILL's overall budget in 2017 amounted to approximately 101 M€.

The Institute operates the most intense neutron source in the world, based on a single-element, 58.3 MW nuclear reactor designed for high brightness. The reactor normally functions round-the-clock for four 50-day cycles per year, supplying neutrons to a suite of 40 high-performance instruments constantly maintained at the highest state of the art.

As a service institute, the ILL makes its facilities and expertise available to visiting scientists. It has a global user community, with approximately 2 000 researchers coming to work at the ILL every year from almost 40 countries. The 800 experiments they perform annually are pre-selected by a scientific review committee. Over 600 scientific papers are published annually, following the treatment and interpretation of data obtained by using our facilities. Around 140 of these articles are published in high-impact journals. This is a factor of two higher than the next most productive neutron source in the world.

The ILL's Director and two Associate Directors are appointed for a period of five years. They each represent one of the three Associate countries. The ILL Scientific Council, comprising external scientists from the Scientific Members countries, advises the directors on the scientific priorities of the Institute and the development of the instrument suite and technical infrastructure. It also assesses the scientific output of the Institute. The ILL's main governing body is the Steering Committee, composed of representatives of the Associates; it meets twice yearly. Scientific Member observers participate in the Steering Committee meetings, as do ILL senior management, the Chair of the Scientific Council and staff representatives. The Steering Committee lays down the general directives for management, and the Associates have ultimate responsibility for determining the operational and investment strategies employed by the Institute.

NEUTRONS AND SOCIETY

The scope of the research carried out at the ILL is very broad, embracing condensed matter physics, chemistry, biology, materials and earth sciences, engineering, and nuclear and particle physics. Much of it impacts on many of the challenges facing society today, from sustainable sources of energy, better healthcare and a cleaner environment, to new materials for information and computer technology. Neutron scattering experiments have, for example, given us new insights into the structure and behaviour of biological and soft condensed matter; this is important in designing better drug delivery systems and in improving the processing of polymers. They also provide a unique probe into phenomena such as high-temperature superconductivity and the molecular magnetism liable to provide the technology for computers of the future.

PREPARING FOR THE FUTURE

If the Institute has maintained its leading status in neutron science, it is because it has been constantly upgrading its instruments, infrastructure and scientific equipment over the last 50 years. The latest upgrade (the Millennium Programme) was completed in 2016 at an overall budget of about 80 k€ and has resulted in a global instrument efficiency gain factor of around 25. The Millennium Programme achieved its goals, but the need for ever more sensitive and powerful instrumentation is constant. The ILL is therefore perpetuating progress with its new Endurance Programme, which will continue to develop instrumentation and support services with a view to maintaining the Institute's world-leading position for another decade at least. Endurance phase I is currently running (2016–2019), with a second phase anticipated to run between 2019 and 2023.

© R. Cubitt

Why neutron scattering is useful

When used to probe small samples of materials, neutron beams have the power to reveal what is invisible using other forms of radiation. Neutrons can appear to behave as particles, waves or microscopic magnetic dipoles; with these very specific properties they can provide information that is often impossible to obtain using other techniques. Below are a few of the special characteristics of neutrons.

WAVELENGTHS OF TENTHS OF NANOMETERS

Neutrons have wavelengths varying from 0.01 to 100 nanometers. This makes them an ideal probe of atomic and molecular structures, whether composed of single atomic species or complex biopolymers.

ENERGIES OF MILLI-ELECTRONVOLTS

The milli-electronvolt energies associated with neutrons are of the same magnitude as the diffusive motions of atoms and molecules in solids and liquids, the coherent waves in single crystals (phonons and magnons) and the vibrational modes in molecules. Any energy exchange, therefore, of between 1 µeV (or even 1 neV with neutron spin-echo techniques) and 1 eV between the incoming neutron and the sample is easy to detect.

MICROSCOPICALLY MAGNETIC

Neutrons possess a magnetic dipole moment which makes them sensitive to the magnetic fields generated by unpaired electrons in materials. They therefore play an important role in the investigation of the magnetic behaviour of materials at the atomic level. In addition, as the neutron scattering effect of the atomic nuclei in a sample depends on the orientation of the spin of both the neutron and the atomic nuclei, neutron scattering techniques are ideal for detecting nuclear spin order.

ELECTRICALLY NEUTRAL

As neutrons are electrically neutral they can penetrate far into matter without doing damage. They are therefore precious allies for research into biological samples or engineering components under extreme conditions of pressure, temperature or magnetic field, or within chemical-reaction vessels.

HIGH SENSITIVITY AND SELECTIVITY

The scattering from nucleus to nucleus in a sample varies in a quasi-random manner, even for different isotopes of the same atom. This means that light atoms remain visible in the presence of heavy atoms, and atoms close to each other in the periodic table can be clearly distinguished. This makes it possible to use isotopic substitution (substituting deuterium for hydrogen, for example, or one nickel isotope for another), in order to vary the contrast in certain samples and thus highlight specific structural features.

Neutrons are also particularly sensitive to hydrogen atoms and are therefore essential for research into hydrogen storage materials, organic molecular materials and biomolecular samples or polymers.

SCIENTIFIC HIGHLIGHTS

The scientific highlights presented in this year's annual report demonstrate how research with neutrons continues to push back the frontiers of science.

2017 was a year of celebration for the ILL, starting with the 50th birthday of the Institute in January. We celebrated 20 years of Italian membership with a dedicated session on neutrons at the FISMAT conference in Trieste in October, sponsored by the FILL2030 European project, followed by a meeting of the ILL Steering Committee at the impressive CNR headquarters in Rome. Spain joined the ILL in 1987 and therefore reached 30 years of membership. Since there is a limit to how many celebrations can be held in a year, we will celebrate 31 years of membership with the Steering Committee meeting in Madrid this November. In view of these milestones, the Italian and Spanish contributions in the following highlights are flagged.

While we were disappointed not to be able to deliver the usual number of beam days in such a notable year, the opportunity was taken to advance Endurance projects (see page 74), reduce the backlog of untreated data and pursue scientific collaborations. More than 560 ILL publications have been recorded to date in 2017, which is a 5 % increase on 2016. Strikingly, more than 20 % of publications in 2017 use data from more than one ILL instrument, which is a marked increase on previous years and confirms the trend for combining data from several techniques in scientific publications.

This trend has several implications for the way we operate. Access to beamtime should be more flexible, so that data can be collected in the timeliest manner and to minimise the time to publication. In this context, and in view of the disruption to thesis work for example, because of the limited beamtime available in 2017, we have been promoting Director's Discretionary Time (DDT) for experiments that need to be performed quickly. Despite the name, the views of the proposal subcommittees are solicited in the evaluation of these requests. In addition, upon request short measurements will be made more widely available from the second cycle this year. This is called Easy Access, and has been available on D2B for room temperature, powder diffraction for a number of years. Easy Access will be available on all instruments under a wide range of experimental conditions for short measurements, to prepare or complete experiments and to collect individual data sets that may complement publications.

The quality and quantity of scientific output at the ILL depends on the number of neutrons delivered and the way we use them, but also the intrinsic quality of our instruments and the associated services. In addition to the reviews conducted within the framework of the Endurance upgrade programme, we review three instruments or services each year with help from the Scientific Council. In 2017, these were D16, D7 and the theory group. The need for upgrades for these instruments in Endurance Phase 2 was clearly endorsed, as was the need to expand and diversify the user communities. In the case of D7, an effort to bring in the solid-state chemistry community alongside the physics community studying magnetic diffuse scattering was encouraged. Software for data reduction and analysis is a key issue in attracting a new user community, and is being addressed specifically in the case of D7 and more generally by the Bastille project in the Endurance programme.

Another user group at the ILL we would like to know more about is industry, especially in the context of our motto 'neutrons for society'. The Industry Liaison Unit is now in the Science Division at the ILL, and we would like to measure and promote the impact of their use of neutrons. While direct 'customer' use of our instruments is easy to identify, indirect, collaborative use is more extensive (10–25 % of proposals) but more difficult to measure. Indirect use would typically involve industry sponsoring an academic research project using neutrons. On the proposal submission forms, we now request more precise information about industrial partners (which will of course be treated confidentially) and ask the subcommittees to evaluate the industrial relevance of proposals. Finally, in 2017, we and our neighbours the ESRF, were delighted to sign a Master Collaboration Agreement for direct and collaborative use of our facilities.

We hope that you enjoy the scientific highlights that follow, which illustrate the uniqueness and strengths of neutron techniques, qualities also found in the scientific infrastructure of the ILL. We look forward to a full year of scientific activity in 2018 in which our User Meeting will be a major event. The meeting is being organised by the ILL and ESS in Grenoble to take place on 10–12 October. With the neutron landscape in Europe in a state of transition, we feel that it is the perfect time to bring together a large part of the neutron community to share and collect information on developments at the two European facilities. This is a unique opportunity to shape the future and we strongly encourage you to participate. Further information and registration are available on the website: **http://neutrons4europe.com**.

Mark R. Johnson
Associate Director,
Head of Science Division

COLLEGE INTRODUCTIONS

COLLEGE 1 – APPLIED METALLURGY, INSTRUMENTATION AND TECHNIQUES

E. Farhi (College 1 Secretary)

College 1 deals with subjects ranging from metallurgy to applied sciences, archaeology, geology and instrumentation. Hence, it encompasses eclectic fields and their associated neutron scattering instruments at the ILL. If you are ever in doubt about which college your experiment proposal fits, consider College 1.

Currently, metallurgy represents about 40 per cent of our studies. This includes the characterisation of various steels and alloys (titanium-, nickel-, silicon- and aluminium-based) obtained by, for example, additive manufacturing or oxide dispersion-strengthening processing. Typical results include residual stress, fatigue and crack analysis.

Applied sciences studies represent another 40 per cent of subjects in College 1. Topics such as hydrogen storage, fuel cells, lithium and sodium batteries fall into this category, as typically do fibre reinforcement and soft matter industrial materials.

Geology, art and archaeology, as well as innovative instrumentation, complete the diverse landscape of proposals.

Most of our proposals are 'industry relevant' and many of the research groups have industry backing.

COLLEGE 2 – THEORY

B. Tommasello (College 2 Secretary)

College 2 embodies the theoretical expertise of the ILL. The Theory Group pursues research in synergy with the core mission of the Institute. Its diversity, spanning disciplines from solid-state physics to soft matter and beyond, expresses its functionality and synergy with the experimental challenges of other colleges. The year 2017 brought two new ILL theory postdocs: Elisa Rebolini, working on *ab initio* calculations and parallel coding for condensed matter systems; and Nicolàs Garcia, investigating entanglement in heterogeneous polymers. Hender Lopez-Silva also joined us in 2017, and will spend two years of his postdoctoral project (ANR-DFG ILL, Université Grenoble Alpes and the University of Tübingen) working on static and dynamic properties of antibody proteins in solutions. Last year also saw the NOTmeeting programme—a platform for junior scientists to discuss theory regularly in an informal set-up—take shape. The Theory Group looks forward to 2018 and to starting new projects and consolidating promising ones, one example being the collaboration between Jordan Hervy (PhD at LPMMC-UGA, Grenoble) and Dominique Bicout investigating stochastic processes for microtubule instabilities.

COLLEGE 3 – NUCLEAR AND PARTICLE PHYSICS

T. Jenke (College 3 Secretary)

The year 2017 was one of notable successes and several new challenges for College 3. In March, 90 experts in nuclear physics attended our workshop on 'Fission and Spectroscopy of Neutron-rich Nuclei' and congratulated the FIPPS team on a very successful first cycle of the instrument.

PN3 also celebrated its first cycle of the newly developed GAMS-6 spectrometer, which has already led to its first publications. Unfortunately, the instrument will not be available again until early 2021; the through-going beam tube H6/H7 had to be removed and considerable difficulties have been encountered in fabricating a replacement. At PF1B, the first campaign for Boron Neutron Capture Therapy (BNCT) was successfully completed. The ILL and TU München have agreed to set up the spectrometer PanEDM to search for an electric dipole moment of the neutron using the future UCN source SuperSUN. The spectrometer itself was delivered to the ILL at the end of 2017.

Consequently, the ILL now hosts flagship experiments in all fields of ultracold neutron physics: as well as PanEDM, GraviTRAP measures neutron lifetime and qBounce and GRANIT handle data for testing gravity at short distances.

COLLEGE 4 – MAGNETIC EXCITATIONS

J. Ollivier (College 4 Secretary)

College 4 deals with magnetic excitations. Subject areas encompass fields such as superconductors and frustrated magnetism, and extend to molecular magnets. In particular, results on low-dimensional frustrated systems leading to exotic excitations, as demonstrated uniquely by neutron scattering, continue to highlight the 2016 Nobel Prize for Physics as illustrated by this year's selected articles. Strong demand for superconductor research continues, with a clear shift to iron-based superconductors and a slight drop in beamtime requests for classical, high-temperature, copper-based superconductors. We have also seen a reduction in work on molecular magnets despite many successful experiments at the ILL in this field, as illustrated in this report. The coming and going of scientific fields is a fact of science, particularly at large-scale facilities offering specific techniques. In this case, the reorganisation of the community contributes to the fluctuation. Recent advances in the domain of quantum computing, in which molecular magnets may have an important role to play, may give new impetus to fundamental research in this area or move the field to a higher level of technological achievement.

COLLEGE 5A – CRYSTALLOGRAPHY

E. Mossou (College 5A Secretary)

The science related to College 5A allows detailed, atomic-level structural information to be obtained from well-ordered solid-state materials such as single crystals and polycrystalline powder materials. These studies make use of the large suite of ILL and CRG instruments, which cover a wide range of length-scale and resolution as well as diffuse scattering. Proposals in 2017 followed a similar trend to that of previous years, with functional materials and large structures such as solid electrolytes, hydrides, etc. being among the most prevalent. The rise observed over the last few years in *in situ*, *in operando* studies, particularly on lithium-ion batteries, is still very clearly present. These proposals represent more than 15 per cent of the total number. Interest in the study of organometallic and metal organic framework (MOF) systems also constitutes a significant proportion of experiments proposed. Most College 5A proposals have a very clear industrial relevance that is mostly exploited through academia.

COLLEGE 5B – MAGNETIC STRUCTURES

N. Qureshi (College 5B Secretary) and **T. Saerbeck** (vice-Secretary)

In 2017, only the Spring proposal review round took place. We received 130 proposals, which were discussed in the main group (diffraction) and focus group (small-angle scattering and reflectivity) to ensure that each was given appropriate scientific discussion during the subcommittee meeting.

There was strong interest, and many high-quality proposals, in the field of frustrated compounds with exotic ground states, especially in pyrochlore structures. Multiferroic and functional materials are as popular as ever, as demonstrated by the high number of proposals focusing on these systems. A rising trend in molecule-based systems, such as metal organic frameworks, molecular magnets and magnetic ionic liquids, was also observed.

Topics for SANS are spread across skyrmion lattice, vortex lattice and nanoparticle or grain studies. For skyrmions, new materials and phase diagrams with extended environmental conditions are being explored in addition to new bi-skyrmionic phases. Studies on vortex lattices have decreased in number, but it remains an active topic for studying different materials, for example heavy fermion superconductors. Studies on nanoparticles and grain structures are directed more towards time-resolved studies and applications. For reflectometry, strong interest lies in the investigation of structural and magnetic properties of emergent, thin-film materials, for example half-metals, topological insulators and nanoparticle arrangements, and the consequent proximity effects at interfaces between the different components.

COLLEGE 6 – STRUCTURE AND DYNAMICS OF LIQUIDS AND GLASSES

G. Cuello (College 6 Secretary)

Water (bulk and confined) attracts as much attention as ever from the College 6 community and materials science researchers. In particular, one of our highlight experiments deals with water organisation in nanochannels of imogolite nanotubes. This system provides tuneable diameters and surface chemistry, allowing the characterisation of water mobility in hydrophobic and hydrophilic tubes as a function of the diameter.

Ionic liquids are also a topic of great interest because of the use of aqueous solutions as alternatives to lithium-ion batteries, which raise safety, environmental and cost concerns. Another particular highlight project of College 6 aims to study the structure of Li ions around water hydrogen. This will give important insight into how water arranges in water-in-salt and water-in-bisalt electrolytes. This work benefits from the use of polarised neutrons to separate coherent and incoherent contributions to the structure factor.

We look forward to a full and stimulating programme of challenging experiments on liquid and amorphous systems in 2018.

COLLEGE 7 – SPECTROSCOPY IN SOLID-STATE PHYSICS & CHEMISTRY

A. Piovano (College 7 Secretary)

A broad variety of topics in solid-state physics and chemistry constitute the activities of College 7. They include fundamental studies of the physics governing intriguing phenomena, but also studies with an impact on society concerning the environment, energy and life sciences.

The suite of instruments available to the college includes the TOF machines IN4, IN5 and IN6-Sharp, the INS spectrometer LAGRANGE, the triple-axis instrument IN8 as well as the high-resolution instruments IN11 and IN16B. This suite of state-of-art instruments covers the complete Q and energy ranges.

More and more realistic calculations at the atomic scale, using either DFT approaches or model Hamiltonians, are necessary nowadays to rationalise and understand experimental data. There are, however, new open questions concerning, for example, the proper treatment of disordered systems, phonon lifetime calculations and others, for which analysis tools need to be developed by ILL staff and the user community.

COLLEGE 8 – STRUCTURE AND DYNAMICS OF BIOLOGICAL SYSTEMS

A. Martel (College 8 Secretary)

College 8 deals with biological samples, using different techniques to study macromolecular structure in solutions (SANS) and in crystals (LADI, D19), bio-mimicking surfaces (reflectometers, D16) and macromolecular dynamics (IN15, IN13, IN11). The systems studied are generally of health relevance, although fundamental science and materials science are also represented.

The information provided by these techniques is unique, thanks to the ability to distinguish macromolecules by their type (DNA versus protein), often taking advantage of deuteration to highlight a particular component of the system or focus on hydrogen bonds which are so often critical in enzymatic processes. The D-Lab is available to support users who wish to deuterate biological molecules, while the PSB platforms and the PSCM offer many techniques for complementary characterisation. The biology laboratories of the EMBL are also available to users for specific sample preparation.

COLLEGE 9 – SOFT CONDENSED MATTER

I. Hoffmann (College 9 Secretary) and **Ph. Gutfreund** (vice-Secretary)

The more than 140 proposals submitted to College 9 in the last proposal round underlines both the high level of overall activity in the field of soft condensed matter and the great demand for neutrons in the field.

Increasingly complex experiments need increasingly complex sample environments in which to study the influence of external stimuli and fields on complex systems. This demand is met by the ILL by, for example, providing new pressure cells for SANS and NSE or a new shear cell for IN15. As experiments often explore time-dependent processes, fast acquisition times are needed which are possible with the ILL's high-flux neutron beams. One way to achieve acquisition times of 100 ms or lower is the 'coherent summing' mode recently made available on the reflectometers D17 and FIGARO, and ongoing work to implement RAINBOWS' wavelength-dependent detection.

Another consequence of using more complex systems is the need for additional sample characterisation—the PSCM labs provide a large range of instruments for this purpose. In 2017 the laboratories hosted 650 experiments by internal and external users. As there is a particularly high demand for Dynamic Light Scattering (DLS), an additional new instrument was acquired.

More information on the support facilities mentioned above can be found on p.106.

Multi-domain proteins: combining neutrons and NMR makes the difference

Small-angle diffractometer D22
KWS1 and KWS2 beamlines at the Heinz Maier-Leibnitz Zentrum

Most eukaryotic proteins feature multiple domains connected by flexible linkers. These multi-domain proteins are at the core of many essential processes of life. Standard structural biology methods often fail to capture a detailed picture of their molecular mechanism due to inherent dynamics and transient binding. By integrating nuclear magnetic resonance (NMR) spectroscopy, segmental deuteration and small-angle neutron scattering (SANS), the structures and dynamics of multi-domain proteins can be efficiently determined to unravel their molecular functions.

AUTHORS
M. Sonntag and **M. Sattler** (Helmholtz-Zentrum Munich and Technical University of Munich, Germany)
F. Gabel (ILL and CEA-CNRS-UGA, Grenoble)
J. Hennig (EMBL Heidelberg, Germany)

ARTICLE FROM
Angew. Chem. Int. (2017) – doi:10.1002/anie.201702904

REFERENCES
[1] J. Hennig, C. Militti, G.M. Popowicz, I. Wang and M. Sonntag, Nature 515 (2014) 287
[2] A. Lapinaite, B. Simon, L. Skjaerven, M. Rakwalska-Bange, F. Gabel and T. Carlomagno, Nature 502 (2013) 519
[3] M. Sonntag, P.K.A. Jagtap, B. Simon, M.S. Appavou, A. Geerlof, Angew. Chem. Int. Ed. Engl. 56 (2017) 9322

To understand the functional mechanisms of multi-domain protein-ligand interactions, it is important to determine the structures in the bound state and observe how the domains rearrange upon binding to a ligand (**figure 1**). However, long, intrinsically disordered linker regions often prevent crystallisation or image reconstruction in cryo-electron microscopy. A combination of nuclear magnetic resonance (NMR) and small-angle scattering can overcome these problems. For larger systems, *e.g.* multi-protein-nucleic acid complexes, the use of small-angle neutron scattering (SANS) especially has been demonstrated to be a powerful alternative [1, 2]. Here, deuterium oxide (D_2O) concentrations in the solute's buffer can be varied to match the scattering density between the buffer and parts of the complex, depending on the subunit-selective deuteration scheme. SANS experiments can then provide centre-of-mass distance restraints between components of the complex. Until now, this approach has been limited to macromolecular complexes, reconstituted (*i.e.* reassembled) from deuterated and hydrogenated individual proteins in solution. But how can specific domains or regions within a single peptide chain be deuterated?

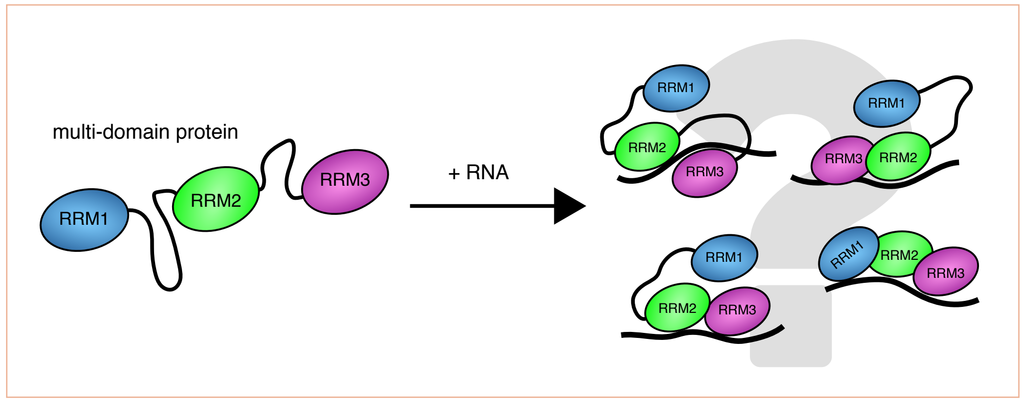

Figure 1

Cartoon representation of a multi-domain RNA-binding protein.
Left) the unbound protein comprises three canonical RNA recognition motif (RRM) domains connected by flexible linkers.
Right) upon RNA binding, domain rearrangements occur. An important task is determining the arrangements of individual domains upon binding to the ligand.

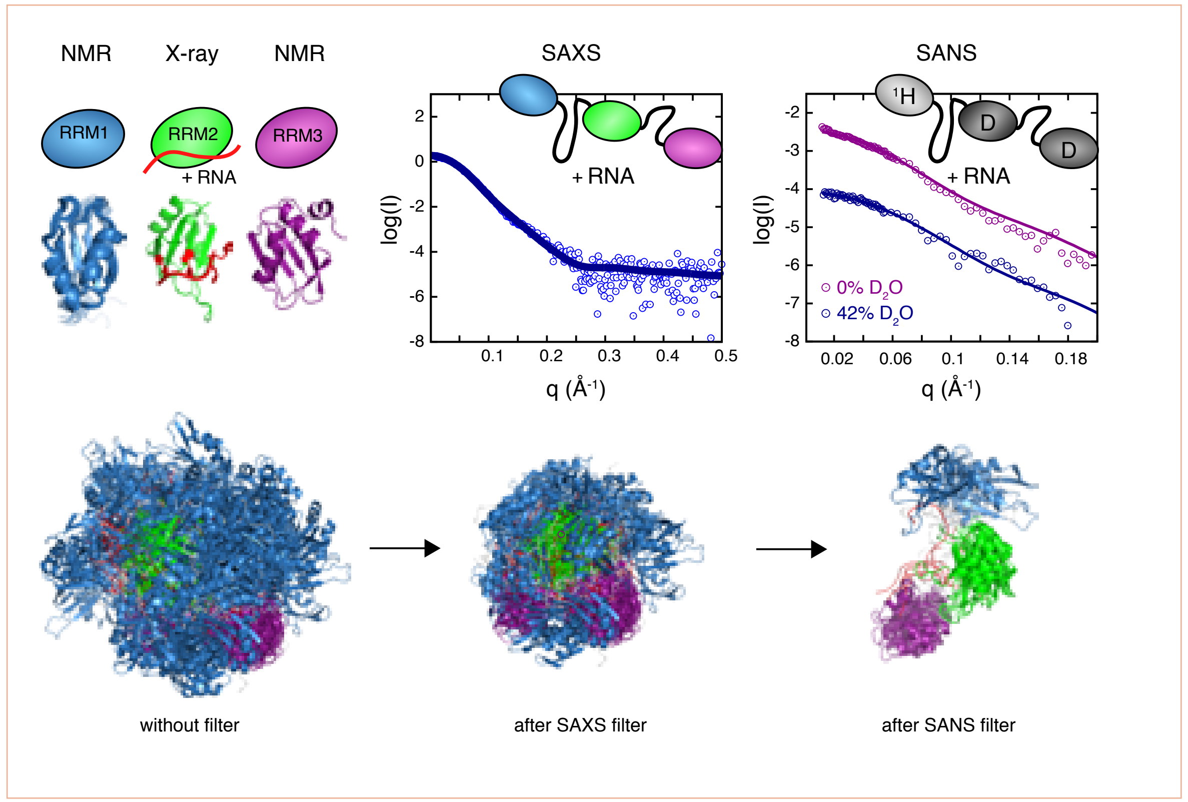

Figure 2

Schematic representation of the structural analysis. NMR and X-ray structures of individual domains are used for rigid body modelling of TIA-1 RRM123. The initial pool of 5 000 structures is first scored against the SAXS data on RRM123 bound to U15 (SAXS filter). The remaining 67 structures are then evaluated against the experimental SANS data at various H_2O:D_2O ratios (SANS filter). The SANS data provide unique information for defining the domain arrangements as represented by a final ensemble of structures.

In a recent publication, we employed sortase A-mediated protein ligation to fuse separately expressed domains with distinct isotope composition into a single peptide chain. In this way, it is possible to fuse a deuterated domain to a protonated domain of a multi-domain protein, enabling contrast-matching in SANS of sub-domain selectively deuterated samples [3]. As an example, we employed this approach for our structural analysis of the T-cell-restricted intracellular antigen-1 (TIA-1) protein, a key player at the level of post-transcriptional pre-mRNA processing. TIA-1 modulates alternative splicing of cancer-related pre-mRNAs by binding to uridine-rich (U-rich) pre-mRNA sequences downstream of weak 5′ splice sites (ss). The protein contains three canonical RNA recognition motif (RRM) domains, all connected by flexible linkers (**figure 1**). Even though structural studies are available on the individual domains and a tandem RRM2-RRM3 (RRM23) fragment, all in the free state, the domain arrangement in the RNA-bound state and the specific role of RRM1 for RNA binding remain unclear.

SANS data on domain-selective, segmentally deuterated TIA-1 constructs were recorded under several conditions (H_2O:D_2O ratio in the solvent) on D22 at the ILL, and on the KWS1 and KWS2 beamlines at the Heinz Maier-Leibnitz Zentrum (MLZ). Using sortase A-mediated protein ligation, the single-chain multi-domain protein was reconstituted from hydrogenated and deuterated RRM1 and RRM23 domains. The contrast-matching neutron data were used as a filtering step in rigid body modelling of the full-length protein.

Assembling all available structural information from NMR and X-ray crystallography (**figure 1**), a random pool of 5 000 structures was generated by randomising the linker connecting the three RNA binding domains. This initial pool was first scored against the experimental small-angle X-ray scattering (SAXS) data and the remaining structures against the SANS data (**figure 2**). Notably, the SANS data were of high discriminative power because the conformational space was drastically reduced. The final ensemble of five structures provides unique insights into the domain orientation and organisation of TIA-1 in the RNA-bound state. Although the full-length protein compacts upon RNA interaction, the neutron scattering data reveal that RRM1 is spatially more separated from the closely packed RRM2 and RRM3 domains. Moreover, RRM1 is detached from the RNA, which supports a minor role in protein-RNA interaction.

The protocol developed here for combining data, using X-rays, neutrons and nuclear spins, will be applicable to other challenging and dynamic multi-domain proteins carrying out crucial functions in eukaryotes.

Glycolipids *vs* phospholipids: dipoles make the difference

High-resolution diffractometer with variable vertical focusing D16

Membrane systems that naturally occur as densely packed membrane stacks (thylakoids in plants or myelin in the brain) contain high amounts of glycolipids, whose sugar headgroups display multiple small electric dipoles in the form of hydroxyl groups. The hydration repulsion between glycolipid membranes is of much shorter range than that between zwitterionic phospholipids, whose headgroups are dominated by a single large dipole. With molecular dynamics (MD) simulations, we were able to reproduce the repulsion forces between phospholipid membranes and between glycolipid membranes, as measured by neutron diffraction (ND) under controlled humidity. The simulations reveal that the repulsion between glycolipid membranes is solely governed by the hydrogen-bond balance between water and the sugars featuring water-like dipoles. Additional repulsion mechanisms, which require correlated large dipoles and are responsible for the stronger swelling of phospholipid membranes, are inoperative for the glycolipids. These results explain the tight cohesion between glycolipid bilayers from thylakoid membranes, which is essential for the biogenesis of photosynthetic membranes.

AUTHORS

E. Schneck (Max Planck Institute of Colloids and Interfaces, Potsdam, Germany)
M. Kanduč (Helmholtz-Zentrum Berlin, Germany)
A. Schlaich and **R.R. Netz** (Freie Universität Berlin, Germany)
A.H. de Vries (Groningen Biomolecular Sciences and Biotechnology Institute & University of Groningen, the Netherlands)
J. Jouhet and **E. Maréchal** (CNRS, Université Grenoble Alpes, CEA Grenoble, France)
B. Demé (ILL)

ARTICLE FROM

Nat. Commun. 8 (2017) – doi:10.1038/ncomms14899

REFERENCES

[1] B. Demé, C. Cataye, M.A. Block, E. Maréchal and J. Jouhet, FASEB J. 28 (2014) 3373
[2] L.J. Lis, M. McAlister, N. Fuller, R.P. Rand and V.A. Parsegian, Biophys. J. 37 (1982) 657
[3] V.A. Parsegian, N. Fuller and R.P. Rand, Proc. Natl Acad. Sci. USA 76 (1979) 2750
[4] E. Schneck, F. Sedlmeier and R.R. Netz, Proc. Natl Acad. Sci. USA 109 (2012) 14405
[5] M. Kanduč, A. Schlaich, A.H. De Vries, J. Jouhet, E. Maréchal, B.Demé, R.R. Netz and E. Schneck, Nat. Commun. 8 (2017) 14899

Naturally occurring neutral membrane lipids in various biological organisms can be divided into two main classes: phospholipids, among which phosphatidylcholines (PCs), whose headgroup is dominated by a single large electric dipole (**figure 1a**), are the main lipid type in most membranes; and glycolipids, such as di-galactosyldiacylglycerol (DGDG), whose saccharide headgroups display multiple small electric dipoles in the form of hydroxyl groups (**figure 1b**). Such glycolipids are found in high concentrations in densely packed membrane stacks like thylakoids (photosynthetic organelles in plants) or myelin sheaths in vertebrates. Both phospholipid and glycolipid membranes repel each other in water at short distance due to the hydrophilic lipid headgroups, a phenomenon commonly termed hydration repulsion.

Experiments have shown that the repulsion between glycolipid membranes is of much shorter range than that between phospholipid membranes [1–3], see **figure 2b**. In fact, as measured by neutron diffraction on D16 (**figure 2a**), the water layer between glycolipid membranes in excess water remains as thin as 1.2 nm, whereas it is typically around 3 nm for phospholipid membranes.

In order to gain insight into the underlying mechanisms, we used atomistic molecular dynamics (MD) simulations (**figure 1c**), which allow the description of biomolecular systems at full chemical detail. By using a recently developed simulation technique [4], our simulations quantitatively reproduce, with remarkable agreement, the experimental pressure-*versus*-distance curves between glycolipid and phospholipid membranes (**figure 2**) [5].

Figure 1

Chemical structures of a PC lipid **(a)** and of the glycolipid DGDG **(b)** as representatives of two fundamentally different lipid classes found in nature: lipids with a headgroup chemistry dominated by one large electric dipole, and lipids whose headgroups comprise multiple small electric dipoles in the form of OH groups. Both classes are schematically illustrated below the chemical structures, with dipoles indicated by arrows.
c) Simulation snapshot of interacting DGDG membranes.
With periodic boundary conditions in all three directions, the simulations represent a periodic stack of membranes. The simulation box is indicated by a bright rectangle. For illustration purposes, water molecules are only shown in the lower half of the box.

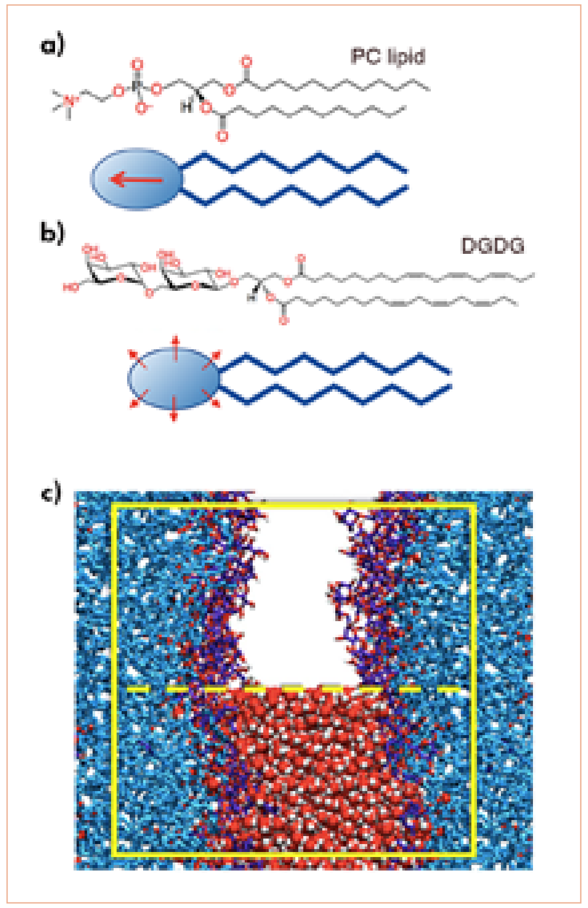

Figure 2

a) Neutron diffraction of DGDG membrane stacks in excess water, measured on D16. The inset is a plot of the Bragg reflection positions.
b) Pressure–distance curves of DGDG and PC lipid membranes as obtained in experiments (open symbols) and in the simulations (filled symbols). Straight dashed lines in the semi-logarithmic plots indicate that the best-matching exponential fits to the experimental data points for DGDG and to the combined experimental data sets for egg PC and DLPC.

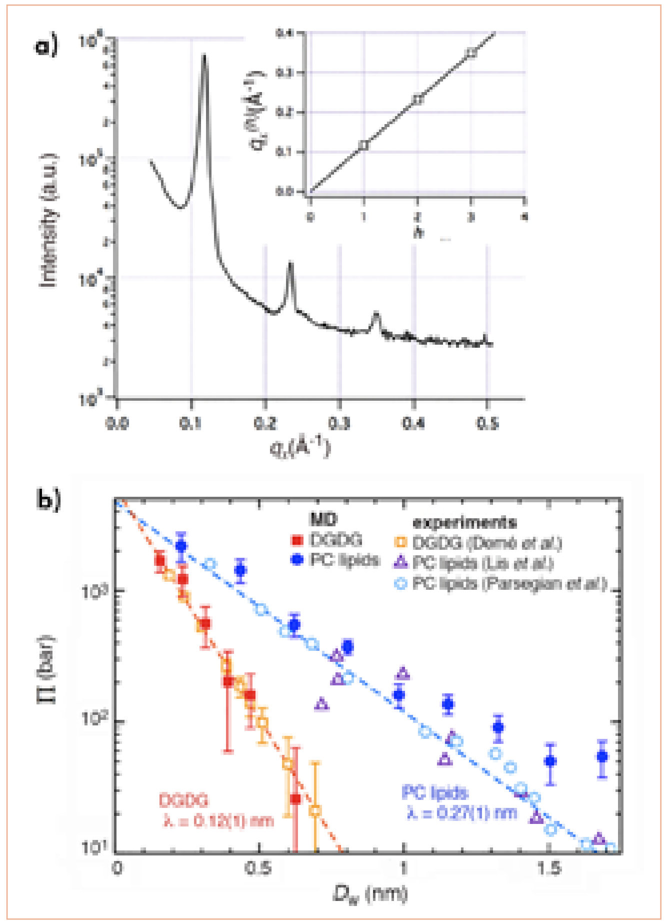

The simulations allow us to systematically decompose and analyse different contributions to the repulsive force. We show that repulsion in glycolipids is driven by the hydrogen-bond balance between water molecules and the sugar headgroups, which have water-like dipoles. For PC lipid membranes featuring large correlated dipoles, two additional repulsion mechanisms are relevant: repulsion due to water structuring effects and repulsion due to the entropy loss associated with a reduction of the lipid conformational freedom upon surface approach. Both mechanisms were found to be inoperative for the glycolipid membranes, so that the corresponding pressure–distance curve decays more rapidly than that of the phospholipid membranes (**figure 2b**) [5].

More generally, the results demonstrate that the characteristics of the repulsion between lipid membranes (or hydrophilic surfaces in general) in terms of strength, range and mechanisms are not governed by a universal, water-inherent mechanism but are highly sensitive to the headgroup chemistry [5]. Differences in the interactions are also exploited by nature in building membrane architectures: tightly packed membrane structures like thylakoids are built predominantly of glycolipids, whereas most other membrane types, where such adhesion is undesired, are rich in phospholipids.

A common critical dynamic regime for proteins upon melting

Backscattering spectrometer IN13

Proteins are molecular nano-machines that carry out essential metabolic processes in living organisms. Full knowledge of their structure and dynamics in their native, transition, intermediate and denatured states is a key goal of life and physical sciences. Here, we show that the amplitude of local fluctuations of a model protein in the presence of different environments rescales to the same value when approaching unfolding temperature, meaning that these machines can sustain up to a certain level of internal flexibility before abandoning their native structure and functionality.

AUTHORS
M. Katava, **G. Stirnemann** and **F. Sterpone**
(LBT/IBPC, CNRS UPR9080, Paris, France)
M. Zanatta (University of Verona, Italy)
S. Capaccioli, **M. Pachetti** and **K.L. Ngai**
(University of Pisa and CNR Pisa, Italy)
F. Natali (CNR-IOM, OGG @ ILL)
A. Paciaroni (University of Perugia, Italy)

ARTICLE FROM
PNAS (2017) – doi:10.1073/pnas.1707357114

REFERENCES
[1] G. Zaccai, Science 288 (2000) 1604
[2] A.L. Lee and J. Wand, Nature 424 (2003) 501
[3] M. Katava, G. Stirnemann, M. Zanatta, S. Capaccioli, M. Pachetti, K.L. Ngai, F. Sterpone and A. Paciaroni, Proc. Natl. Acad. Sci. USA 114 (2017) 9361
[4] K.A. Dill, K. Ghosh and J.D. Schmit, Proc. Natl. Acad. Sci. USA 108 (2011) 17876

The atomic traits of the dynamic mechanisms by which, upon increasing temperature, a protein structure is progressively destabilised and eventually transforms into a melted inoperative state, are still elusive. It has previously been proposed that besides playing a crucial role in the onset of protein biological activity [1], fast internal dynamics are also important in modulating the stability of proteins because they are a major component of conformational entropy [2].

Within this context, the amplitude of sub-nanosecond time scale structural fluctuations of proteins can be greatly reduced by sugar-glass matrices surrounding their surface, thus making their melting temperature T_m much higher than the one they have when dissolved in aqueous media. Since these internal sub-nanosecond protein motions are strongly driven by temperature, it is relevant to track changes in their amplitude along the pathway toward thermal unfolding.

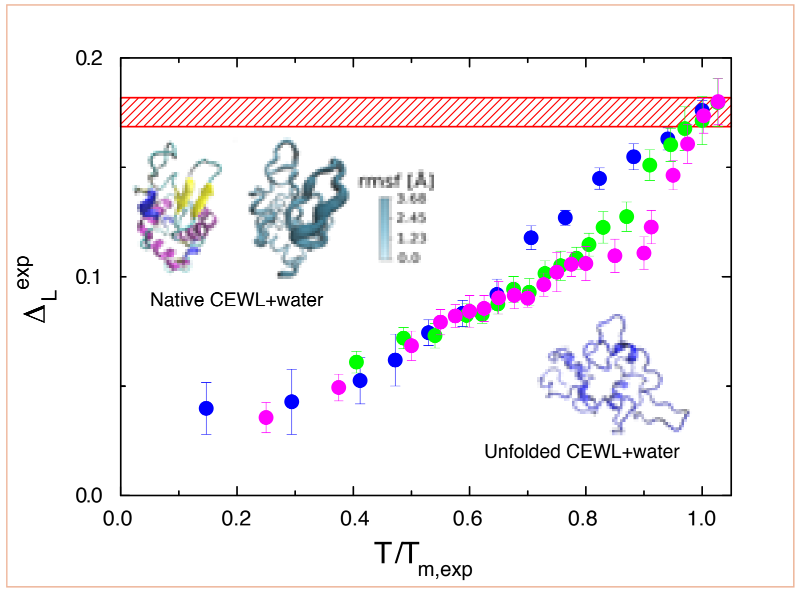

Figure 1

Scaling law of protein fast fluctuations by EINS. The experimental Lindemann parameter for CEWL is shown in the presence of different environments as a function of reduced temperature $T/T_{m,exp}$, for CEWL+water (blue), CEWL+glycerol (green) and CEWL+glucose (pink). All the solvents are perdeuterated. The red hatched area highlights the region of critical MSD corresponding to the protein melting in the different environments. Also shown are the structures of CEWL obtained by X-ray data **(upper inset, left)** and with the information on root mean squared fluctuations from MD simulations **(upper inset, right)**. The **lower inset** shows CEWL in an unfolded conformation.

Hence, we used the elastic incoherent neutron scattering (EINS) technique on the IN13 spectrometer to measure the mean squared displacement (MSD) of the model protein chicken egg white lysozyme (CEWL) in the presence of different solvent matrices, from water to glassy networks. In fact the unfolding temperature of CEWL is largely modulated by the environment, being 340 K, 370 K and 400 K when the shell around the protein surface consists of water, glycerol and glucose respectively, so we could sample increasingly stable systems in a wide temperature range up to melting point [3]. To support and interpret the protein measured by MSD, we also assessed the protein thermal response and melting *in silico* by performing atomistic molecular dynamics simulations based on the replica exchange with solute tempering (REST2) method [3].

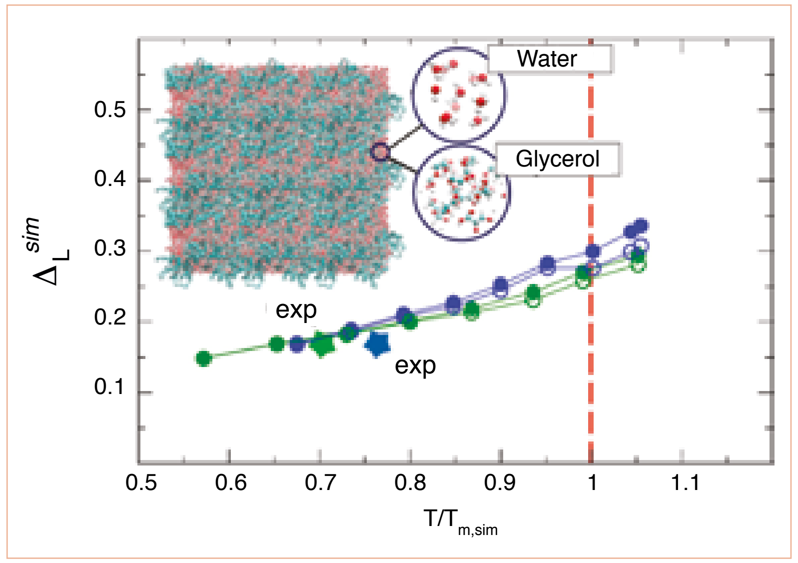

Figure 2

The Lindemann parameter obtained by combining the folded and unfolded states MSD from MD simulations, $MSD = f \cdot MSD_{folded} + (1-f)MSD_{unfolded}$, with f the fraction of folded states, for CEWL+H_2O (blue closed circles) and CEWL+glycerol (green closed circles). In the same graph we also show the folded-state contributions (same colours but open circles). The coloured stars indicate the experimental points of the two systems. The **inset** shows the alternative schemes employed to simulate CEWL+water and CEWL+glycerol.

Inspired by the Lindemann criterion, which states that crystals liquefy when the amplitude of atomic thermal vibrations exceeds a fraction of the interatomic spacing, we compared the MSD of CEWL normalised by the most-probable, non-bonded, near-neighbour distance *a*, in the presence of three different molecular environments, *i.e.* water, glycerol and glucose. We then defined the Lindemann parameter for proteins as $\Delta_L = 1/a(MSD/2)^{1/2}$. Quite strikingly, in **figure 1** we see that, even if its trend is largely tuned by the molecular environment, the Lindemann parameter of CEWL converges to a common value in proximity to its specific T_m. In other words, the fast internal dynamics of the biomolecule enter a common dynamical regime corresponding to the melting transition.

It is worth noting that the MSD measured by neutron scattering, and consequently the parameter Δ_L^{exp}, result from the combined amplitudes of fluctuations from folded and unfolded states, with a predominant contribution from the latter as the melting temperature is crossed. To dissect the separate contributions in native and unfolded states, we exploited molecular dynamics simulations of CEWL in water and glycerol environments [3]. Exploiting the two-state model, we combined the contributions to the MSD from folded and unfolded states to assess the *in silico* Lindemann parameter. As shown in **figure 2**, Δ_L^{sim} converges upon melting for CEWL in the presence of both water and glycerol, although to a larger value than Δ_L^{exp} owing to the shift of the *in silico* melting point with respect to the experimental one. **Figure 2** also shows that the difference between the MSD in folded and unfolded conformations is small.

One might question whether the threshold we found for thermal fluctuations upon melting can be generalised to proteins other than CEWL. Actually, we have found that the same value of the Lindemann parameter holds for different proteins; thus it seems that Δ_L^{exp} does not depend significantly on protein size, and that it is independent of the presence of a quaternary structure [3]. This common dynamic regime could correspond to conditions where a certain critical value of conformational entropy is reached, at high enough temperature, and unfolding events become predominant. We propose that this universal trend can also be used to predict the thermal stability of cells, under the hypothesis that the cell's death temperature corresponds to the denaturation catastrophe of its proteome [4].

The relationship we have found adds an important piece of information to our in-depth understanding of the folding and unfolding of proteins which are, in turn, crucial processes in the metabolism of cells, regulating biological activity and targeting proteins at different cellular locations. Such information could be also key to the biotechnology and pharmaceutical fields, where therapeutic principles based on proteins are worth many tens of billions in currency on the world market.

BIOLOGY AND HEALTH

High hydrostatic pressure specifically affects molecular dynamics and the shape of low-density lipoprotein particles

Time-of-flight spectrometers IN5 and IN6
Backscattering spectrometer IN13
SANS-II beamline at PSI

Low-density lipoproteins are natural nanoparticles circulating in the blood that play an important role in the proper functioning of human lipid metabolism. Here, by combining different neutron scattering methods we explored the effects of high hydrostatic pressure on the structural and dynamical features of two distinct low (space) density lipoprotein species—representing either normolipidemic or triglyceride-rich entities—that simulate some pathologies. Our results revealed that low-density lipoprotein particles are much more resistant to high pressure applications than are biological membranes.

AUTHORS
M. Golub, **N. Martinez** and **J. Peters** (Université Grenoble Alpes, LiPhy, IBS and ILL, Grenoble, France)
B. Lehofer and **R. Prassl** (Institute of Biophysics, Medical University of Graz, Austria)
J. Ollivier (ILL)
J. Kohlbrecher (PSI, Villigen, Switzerland)

ARTICLE FROM
Sci. Rep. 7 (2017) 46034 – doi:10.1038/srep46034

REFERENCES
[1] A.J. Lusis, Nature 407 (2000) 233
[2] C. Mikl, J. Peters, M. Trapp, K. Kornmueller, W.J. Schneider and R. Prassl, J. Am. Chem. Soc. 133 (2011) 13213

A key determinant of lipoprotein functionality in both health and disease is the molecular lipid composition of the individual lipoprotein particles, which also determines their molecular structure and dynamics. Low-density lipoproteins (LDL) are the principal carriers of cholesterol in the bloodstream, their primary function being to provide cholesterol for peripheral tissues. However, modified LDL particles are also associated with an increased risk of cardiovascular diseases such as atherosclerosis and coronary artery disease, which are among the most prevalent causes of death in Western civilisation [1]. LDLs are natural nanoparticles with a diameter of about 20 nm. They are composed of a hydrophobic lipid core primarily comprising cholesteryl ester and triglyceride molecules, surrounded by an amphiphilic monolayer of phospholipids. In the outer phospholipid shell a single copy of the apolipoprotein B100 is embedded.

Research has shown that minor changes in lipid composition or LDL particle size could affect their physiological function through modulation of protein flexibility or membrane fluidity. As LDL particles have shown distinct dynamical behaviour as a function of molecular composition and temperature that is comparable to cell membranes [2], we assumed that LDL particles, like lipid membranes, would be highly sensitive to pressure as well. Notably, the dynamic landscape for lipoprotein species under high hydrostatic pressure (HHP) has never been investigated before. Indeed, so far specific information on molecular motions, intrinsic flexibility and conformational stability is lacking, especially with respect to the structural integrity of LDL particles exposed to extreme external stress conditions. The high pressure cells available at the ILL are shown in **Figure 1**.

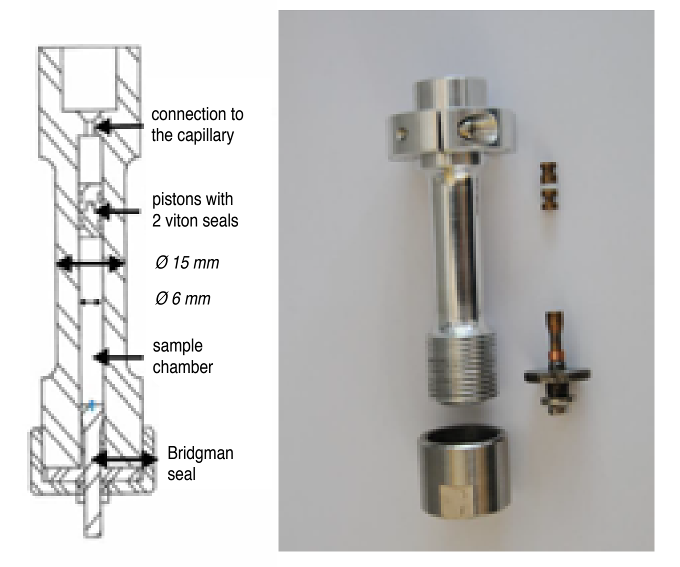

Figure 1
Cross-section (**left**) and photograph (**right**) of the aluminium pressure cell.

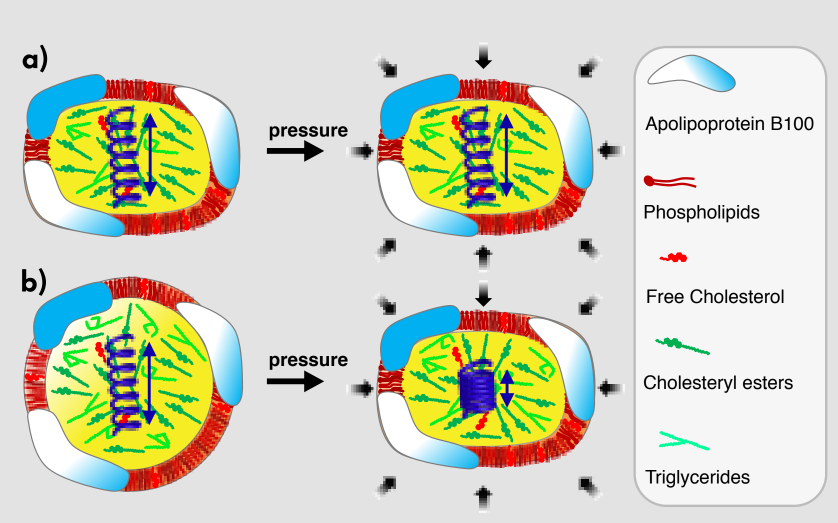

Figure 2
Sketch of the effects of high hydrostatic pressure (HHP) on LDL particles. The overall shape and dynamics of LDL particles with a normolipidemic lipid composition (N-LDL) were highly resistant to pressure applications **(a)**. The dynamics and structure of triglyceride-rich LDL particles (TG-LDL) was much more sensitive to HHP. At low pressure TG-LDL particles were rather spherical but approached the ellipsoidal morphology of N-LDL at high hydrostatic pressure **(b)**. The blue coil symbolises the altered dynamics within the particle.

To probe the structure and molecular dynamics of LDL under HHP (range from 20 to 3 000 bar), we combined data from different neutron scattering techniques: small-angle neutron scattering (SANS), elastic incoherent neutron scattering (EINS) and quasi-elastic neutron scattering (QENS). We compared two compositionally different LDL species, namely an LDL particle with a normolipidemic composition (N-LDL) and a triglyceride-rich form of LDL (TG-LDL).

The SANS experiments were performed on the SANS-II beamline of the Paul Scherrer Institute (PSI, Villigen, Switzerland). For the QENS experiments we used the time-of-flight spectrometers IN5 and IN6 at the ILL, while the EINS experiments were conducted on the thermal neutron backscattering spectrometer IN13. With these instruments we could combine elastic and quasi-elastic scattering data at two different time windows to identify various types of motions at the atomic scale. We found that HHP did not change the types of motion in LDL, but it did influence the portion of populations participating in the individual motions. Analysis of the QENS data recorded at HHP (3 000 bar) revealed no changes in the dynamics of N-LDL, whereas a significant difference for TG-LDL was found: the elastic part became much more pronounced, while the shape of the quasi-elastic broadening was not affected. This indicates that HHP influences the elastic intensity extracted from QENS data as well as the mean square displacement (MSD), which can be extracted from EINS measurements. In particular, TG-LDL showed a lower MSD value indicative of the reduced flexibility of motions and increased stiffness at HHP. The SANS data, which were analysed using a triaxial ellipsoid model, revealed that the shapes of the LDL particles were transformed from quasi-spherical to more elongated ellipsoids under high pressure. At low pressure, TG-LDL particles were rather spherical but approached the ellipsoidal morphology of N-LDL at HHP.

We determined that LDL copes surprisingly well with high-pressure conditions, although the lipid composition, especially the triglyceride content of the particles, affects the molecular dynamics and shape arrangement of LDL under pressure. We conclude that triglyceride-rich LDL particles, which are thought to mimic pathological conditions, are more pressure-sensitive than are their healthy counterparts. Our data suggest that a subtle interplay between the structural flexibility and intrinsic molecular dynamics of lipids and proteins partially compensates for variations in the chemical composition of the particles, particularly under extreme external stress conditions. A deeper understanding of the molecular parameters that determine the complexity of LDL particles could help to develop new concepts for the early diagnosis and target-specific therapy of atherosclerosis. A summary of our findings is given schematically in **Figure 2**.

Escaping the squeeze – soft particles at high densities

Small-angle scattering diffractometer D11

Soft particles such as polymeric microgels can form ultra-dense phases with intriguing properties, where the average centre-to-centre distance can be significantly smaller than the initial unperturbed particle diameter. However, despite efforts devoted to microgels at ultra-high densities, we know surprisingly little about their response to their environment at effective volume fractions above close packing. Small-angle neutron scattering (SANS) is an ideal method for obtaining this information. We therefore performed measurements on the small-angle instrument D11, using a so-called zero average contrast method in order to characterise the size and shape of microgels over a very large range of particle concentrations.

Figure 1

Schematic description of the temperature-induced swelling/de-swelling of thermo-responsive microgels.

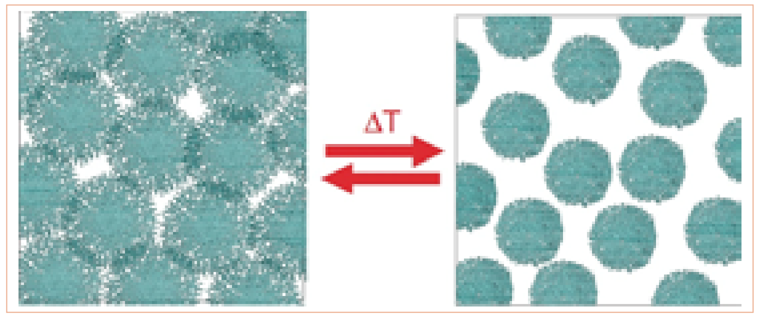

AUTHORS
P.S. Mohanty (University of Lund, Sweden and KIIT University, Bhubaneswar, India)
S. Nöjd, **J.J. Crassous**, **M. Obiols-Rabasa**, **A. Stradner** and **P. Schurtenberger** (University of Lund, Sweden)
R. Schweins (ILL)

ARTICLE FROM
Sci. Rep. 7 (2017) – doi:10.1126/sciadv.1700969

REFERENCES
[1] R. Bonnecaze and M. Cloitre, Adv. Polym. Sci. 236 (2010) 117
[2] D. Paloli, P.S. Mohanty, J.J. Crassous, E. Zaccarelli and P. Schurtenberger, Soft Matter 9 (2013) 3000
[3] P.S. Mohanty, S. Nöjd, K. van Gruijthuijsen, J.J. Crassous, M. Obiols-Rabasa, R. Schweins, A. Stradner and P. Schurtenberger, Sci. Rep. 7 (2017) 1487
[4] G.M. Conley, P. Aebischer, S. Nöjd, P. Schurtenberger and F. Scheffold, Sci. Adv. 3 (2017) e1700969

Thermo- and pH-responsive neutral or ionic polymer microgel particles present a particularly interesting class of colloids. They are formed by a cross-linked polymeric structure based on stimuli-responsive polymers such as poly(N-isopropylacrylamide) (PNIPAm) [1]. These particles can undergo reversible continuous or discontinuous volume transitions upon variations in external stimuli such as temperature, pH or ionic strength. Microgels possess a variable degree of softness and a tuneable interaction potential that can vary between hard-sphere and very soft repulsive. Moreover, the fact that soft microgels can interpenetrate to a certain degree allows the creation of states with densities far above close packing, so-called squeezed states, with interesting structural and dynamic properties. The thermo-responsive properties of microgels have, for example, been used to induce crystallisation or the onset of a glass transition through a variation in the temperature, and thus the particle size and the resulting volume fraction ϕ_{eff} (**figure 1**) [2].

However, do particles at very high packing fractions still have the same size and shape, or are they compressed and/or faceted? Despite the considerable amount of work that has been performed on microgels, our knowledge about particle size, shape and local structure as a function of particle volume fraction at high packing fractions is limited. And yet this information is crucial to any attempt to understand the behaviour of dense microgel suspensions. In particular, the extent to which the microgel particles interpenetrate or become compressed and faceted at effective volume fractions close to or beyond random close packing is very important. It is for this reason that we conducted a systematic investigation of the microgel structure at high effective volume fractions, using small-angle neutron scattering (SANS) experiments on the instrument D11 with mixtures of deuterated and hydrogenated microgels under so-called zero average contrast (ZAC) conditions to extract the particle form factor at all densities [3].

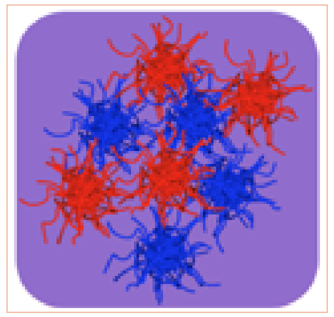

Figure 2

Schematic view of a zero average contrast experiment, where the colour represents the scattering length density of the hydrogenated and deuterated particles and the solvent, respectively.

Figure 3

Examples of the concentration-normalised scattered intensity $I(q)/\phi_{\text{eff}}$ as a function of the scattering vector q for a 50-50 mixture of hydrogenated and deuterated particles at a temperature T = 16.4 °C in a zero average contrast solvent mixture, for different values of the effective volume fraction $0.33 \leq \phi_{\text{eff}} \leq 1.68$. **Inset)** the corresponding intensities I(q) from SAXS, where the position q* of the maximum of the resulting structure factor peak is also indicated. The data are offset along the ordinate for clarity, with increasing ϕ_{eff} from bottom to top.

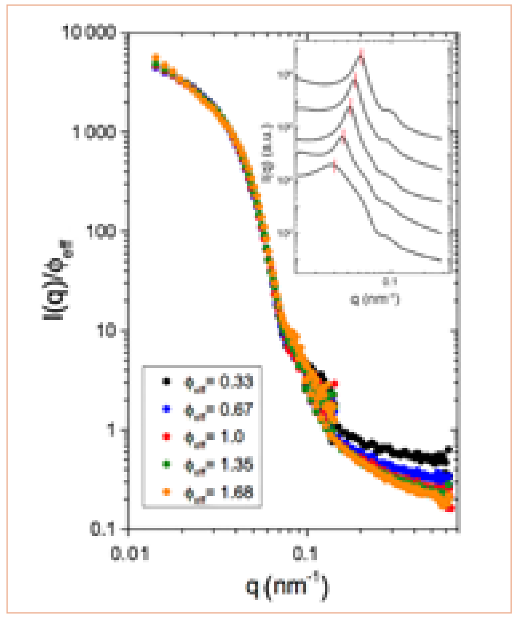

Figure 4

Normalised overall dimensions R_{SANS}/R_0 as a function of ϕ_{eff} obtained from SANS at T = 15 °C (solid black circles) and T = 27 °C (solid black triangles). The average normalised centre-to-centre distances a_s/a_0 from SAXS are shown as solid red circles for T = 15 °C and triangles for T = 27 °C, and data from confocal laser scanning microscopy are shown as solid red squares for T = 15 °C.

The solid red line represents the dependence of the normalised centre-to-centre distance on the number density of particles interacting *via* a soft repulsive potential given by $a_s/a_0 \sim 1/\phi_{\text{eff}}^{1/3}$. The location of the glass transition is indicated by the solid black arrow (T = 15 °C) and the black dashed arrow (T = 27 °C) at the bottom, and an estimate of the volume fraction ϕ where the outer shell touches the dense core of the nearest neighbour particles is given as the short solid black (T = 15 °C) and dashed (T = 27 °C) lines at the top.

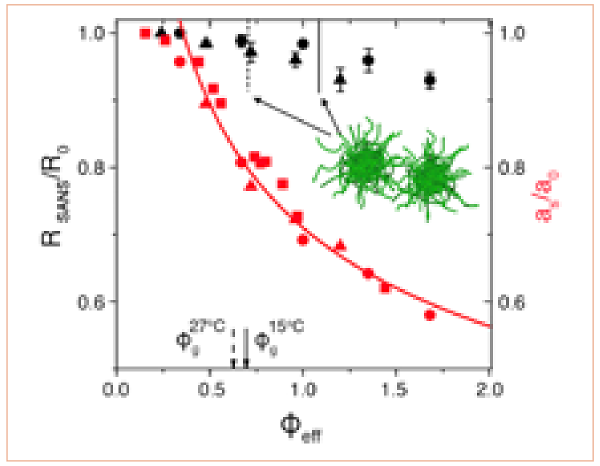

While the resulting scattering intensity in a traditional SANS or X-ray (SAXS) scattering experiment contains contributions from the particle size and structure (the particle form factor P(q)) and the positional correlations (structure factor S(q)), this is not the case for an equal number density mixture of hydrogenated and deuterated but otherwise identical particles under so-called zero average contrast conditions. Here, the scattering length density of the solvent (a mixture of H_2O and D_2O) is chosen to correspond to the average value of the two particles (**figure 2**), which results in a cancellation of all contributions to the measured structure factor and a resulting scattering intensity that reflects the average particle form factor only [3].

This is demonstrated in **figure 3**, where we see the concentration-normalised scattering intensities from suspensions of microgels at different concentrations from below to far above close packing. The datasets almost overlap at all concentrations and show no signs of an interaction peak normally present for colloidal particles with soft repulsive interactions at these concentrations. This is in quite clear contrast to the data from SAXS experiments using the same samples, as shown in the inset of **figure 3**, where the q-dependence of the scattering intensity is dominated by a well-pronounced peak in S(q), with a peak position at q* that moves to larger q-values with increasing concentration, reflecting the decreasing average centre-to-centre distance a_s.

Quantitative analysis of the scattering data using a so-called fuzzy sphere model for the structure of the microgels demonstrates that the effective particle radius R_{SANS} decreases only weakly for very high-volume fractions when compared with the unperturbed size at high dilutions, R_0 [3]. This is shown in **figure 4**, where the ratio R_{SANS}/R_0 is given together with the average centre-to-centre distance a_s normalised by the particle diameter a_0, as obtained from SAXS and confocal microscopy for two different temperatures. At high concentrations, where the sample undergoes a glass transition, particle size can be significantly larger than the average centre-to-centre distance between particles, indicating strong interpenetration without detectable shape deformation. It is interesting to note that a measurable decrease in particle size only occurs for concentrations where the soft outer corona of the particles touches the inner, more strongly cross-linked core. The conclusions from this study have recently been confirmed using super-resolution optical microscopy for similar microgels [4].

Our results clearly indicate that care must be taken when trying to use microgels as simple model systems to investigate phase transitions or look at various macroscopic viscoelastic properties. Their ability to interpenetrate and de-swell appears to depend strongly on particle softness, internal cross-link density distribution and temperature, which will certainly require a second look at some previously postulated microscopic structural models used to describe flow properties of dense suspensions of microgels.

Taming complex fluids for smarter lubricants and adhesives

Reflectometer FIGARO

Everyone is familiar with complex fluids: from daily items like ketchup or shampoo, through hi-tech motor oil in cars, to our own biological tissues. They all have a rich mechanical response: shear-thinning or -thickening, rod-climbing, memory effects and many more. They also present challenges, like shear-banding and surface slippage. Neutrons reveal the details of this complex interface under shear flow. In this paper we contribute to the design of better lubricants and adhesives, and maybe even of treatments for arthritis.

AUTHORS
A. Korolkovas and **P. Gutfreund** (ILL)
C. Rodriguez-Emmenegger and **A. de los Santos Pereira** (IMC Prague, Czech Republic)
A. Chennevière (LLB Paris, France)
F. Restagno (CNRS Paris, France)
M. Wolff and **F.A. Adlmann** (Uppsala University, Sweden)
A.J.C. Dennison (Sheffield University, UK)

ARTICLE FROM
Macromolecules 50.3 (2017) – doi:10.1021/acs.macromol.6b02525

REFERENCES

[1] A. Korolkovas, C. Rodriguez-Emmenegger, A.S. Pereira, A. Chennevière, F. Restagno, M. Wolff, F.A. Adlmann, A.J.C. Dennison and P. Gutfreund, Macromolecules 50.3 (2017) 1215
[2] A. Korolkovas, J.L. Barrat and P. Gutfreund, J. Chem. Phys. 145.12 (2016) 124113

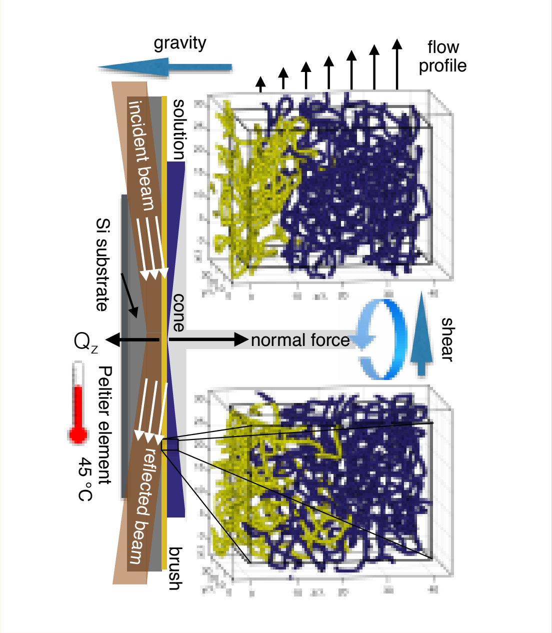

Figure 1

Experimental set-up and simulated polymer conformation. The experiments are conducted with the silicon-polymer interface horizontally oriented. The wave-vector transfer Q_z is perpendicular to the interface. Shear is applied by the rheometer *via* a titanium cone or plate.
Lower right panel) shows a conformation snapshot plotted from the simulation data. The interpenetration of the polymer brush (yellow) and free chains (blue) is clearly visible.
Upper right panel) with applied shear the free chains are pulled out of the brush, the mean thickness of the brush decreases and the interface becomes sharper.

A polymer brush is a unique type of surface functionalisation, consisting of long polymer chains densely tethered by one end to a surface. The conformation of a solvated brush is markedly different to that of chains in bulk solution, as the brush must stretch away from the surface to minimise contact with densely grafted neighbouring chains. Polymer brushes are of broad interest across a variety of sectors, since tuning interfacial properties (*e.g.* chemical composition, molecular weight, grafting density) can yield surface coatings with a high degree of control and in some cases completely new functionality.

The static properties of polymer brushes are well understood, thanks to extensive theoretical and experimental studies. Our knowledge of brush dynamics, however, is still incomplete, even though it is crucial for controlling flow. To help fill this gap, our study focused on the response of brushes to an applied shear stress while swollen and deeply interpenetrated with a bulk polymer solution, as illustrated in **figure 1**. The chains are strongly entangled and their relaxation time is about 1s, similar to the scale encountered in real world applications. However, the brush–bulk interface remains very challenging to investigate due to its complex, heterogeneous, strongly interacting, non-equilibrium and confined nature. We have therefore supplemented neutron reflectometry [1] with our recently developed computer simulations [2]. This combination enables greater insight into what is occurring at the interface, compared with applying the two approaches separately.

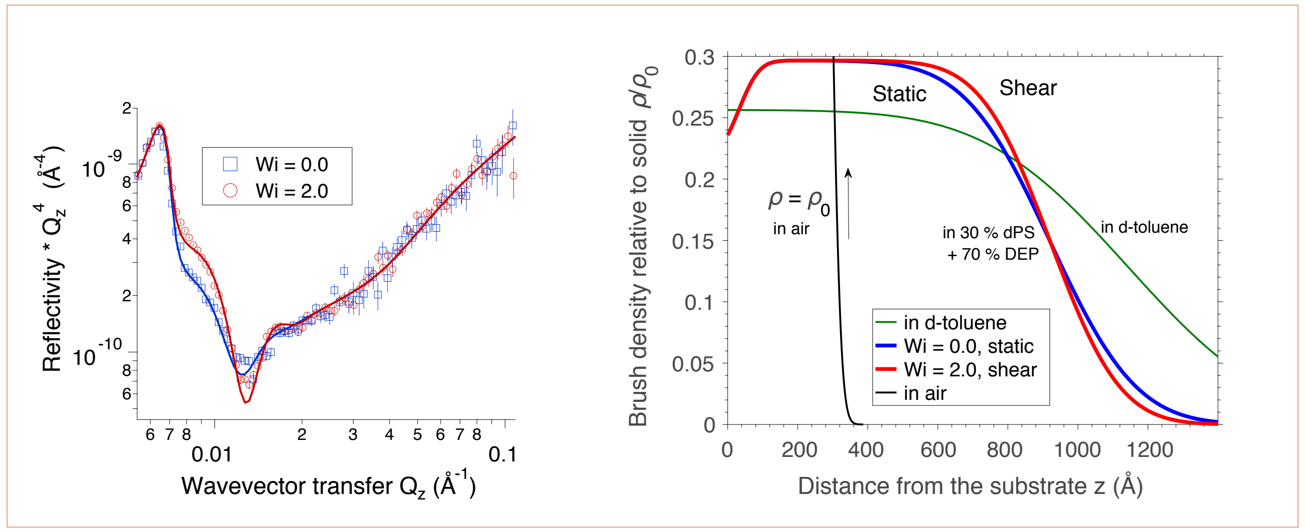

Figure 2

Left) neutron reflectivity of the entangled polymer brush system at equilibrium (blue squares), and under a strong shear flow (red circles).
Right) the fitted brush density profile reveals that the change in reflectivity is caused by the sharpening of the brush-bulk interface.

Due to deuterium labelling, neutrons can reveal a stark contrast between the polymer brush and the free chains in solution, which are otherwise chemically identical to polystyrene. Therefore, any change in the brush structure that may happen under shear flow will influence the neutron signal. As shown in **figure 2**, we observe up to a 50 % decrease in reflectivity when shearing. This result is consistent across a range of grafting densities and chain lengths, and confirms earlier *ex situ* studies of a similar system. Our coarse-grained computer simulations support this finding and provide additional information, such as the lateral brush structure, which is unobservable in the experiment.

We have shown both experimentally and computationally that the entangled polymer brush thickness decreases with shear. More precisely, we observed a shrinking of brushes proportional to the square of the applied shear rate, see **figure 3**. This non-linear effect is attributed to the normal stress difference, which is an excess pressure build-up perpendicular to the applied shear flow and is well known to occur in bulk entangled polymer fluids, where it leads to the so-called Weissenberg effect. The time scale of the brush collapse is determined by the reptation time of the free chains in solution rather than the internal dynamics of the brush. The brush thickness returns to equilibrium upon cessation of shear, and the effect can by cycled many times over. These observations are corroborated by a simple phenomenological theory, which states that the polymers tend to adopt a conformation as close as possible to the one in equilibrium. The overall deformation is smallest if the grafted chains shrink perpendicular to the flow, thereby hiding from some of the shear stress.

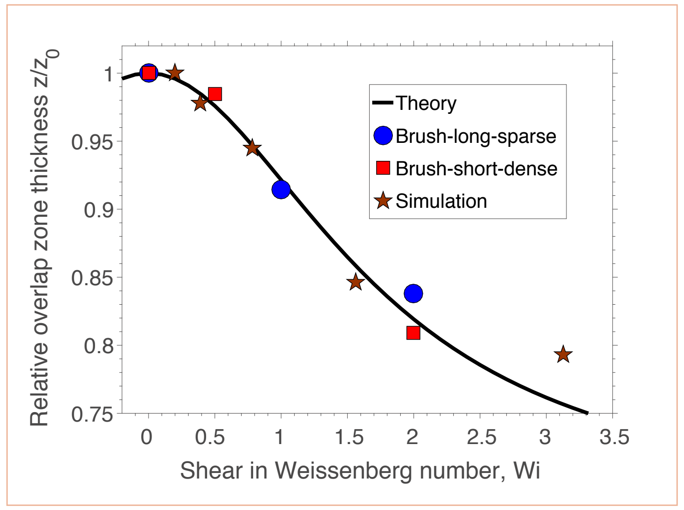

Figure 3

Brush thickness under shear, normalised to the equilibrium thickness. Only the brush–bulk overlap region is considered in this comparison.

Strain engineering of multiferroic properties in $TbMnO_3$ epitaxial thin films

Single-crystal four-circle diffractometer D10
Three-axis spectrometer RITA-II at PSI

Multiferroic materials are capable of hosting electric and magnetic order parameters simultaneously. The coupling of the order parameters and the possibility of cross-control by magnetic and electric fields [1] makes them attractive candidates for potential applications in device technology. Orthorhombic rare-earth manganites (o-$RMnO_3$: R = Gd - Lu) demonstrate multiferroicity induced by the ordering of Mn^{3+} spins and represent the family of spin-driven multiferroics [2]. $TbMnO_3$ is a prime example of materials demonstrating a ferroelectric (FE) order induced by the magnetic ordering of the ground state [3]. Neutron diffraction reveals that the system undergoes a transition at $T_N \sim 41$ K, from a paramagnetic to an amplitude-modulated antiferromagnetic phase, which is paraelectric. This is followed by the onset of an incommensurate spiral magnetic phase at $T_C \sim 28$ K, which induces a spontaneous FE ordering with polarisation pointing along the *c*-axis (P_c) [4, 5]. The multiferroic ground state in bulk $TbMnO_3$ was found to be uniquely modified by the application of external pressure and magnetic fields [6]. An alternative way to induce a significant modification of the ground state is the growth of strained thin films. The strain state depends on the substrate used and the growth orientation. Unlike the case of externally applied pressure, the strain in thin films is anisotropic and can play a prominent role in tuning physical properties [7]. For our studies of multiferroic properties in strain-engineered $TbMnO_3$ films, an 80 nm-thick (100)-oriented and 44 nm-thick (010)-oriented $TbMnO_3$ film was grown on (100) and (010)-oriented $YAlO_3$ substrates by pulsed laser deposition [8].

AUTHORS

S. Mukherjee, **C. Schneider** and **C. Niedermayer**
(PSI, Villigen, Switzerland)

ARTICLE FROM

Sci. Rep. *7* (2017) – doi:10.1038/srep44753

REFERENCES

[1] N.A. Spaldin and M. Fiebig, Science 309 (2005) 391
[2] S. Ishiwata *et al.*, Phys. Rev. B 81 (2010) 10041
[3] T. Kimura *et al.*, Nature 426 (2003) 55
[4] M. Kenzelmann *et al.*, Phys. Rev. Lett. 95 (2005) 087206
[5] T. Kimura *et al.*, Phys. Rev. B 71 (2005) 224425
[6] N. Terada *et al.*, Phys. Rev. B 93 (2016) 081104
[7] K. Shimamoto *et al.*, Phys. Rev. B 95 (2017) 184105
[8] K. Shimamoto *et al.*, Sci. Rep. *7* (2017) 44753
[9] M. Mochizuki *et al.*, Phys. Rev. B 84 (2011) 144409

The structural properties of $TbMnO_3$ films and corresponding growth-induced strain states were studied by X-ray diffraction. The magnetic order was determined by neutron diffraction with the single-crystal, four-circle diffractometer with three-axis energy analysis D10 at the ILL, and the cold-neutron, three-axis spectrometer RITA-II at the Paul Scherrer Institute (PSI), Switzerland. The largest challenge was to identify and optimise the experimental conditions in order to be able to perform neutron diffraction measurements on the very small scattering volume (mass ~ 70 μg) of a thin film within a reasonable time frame in the order of hours. The analyser option of the D10 instrument at the high-flux neutron source at the ILL helped to improve the signal-to-noise ratio significantly. In addition, the four-circle Euler cradle set-up provided access to a larger fraction of the Ewald sphere and enabled us to measure an adequate set of magnetic reflections with sufficiently large intensity. The nine-blade analyser option and the high *q*-resolution of the RITA-II spectrometer enabled us to unambiguously identify the magnetic order. There are very few experimental facilities available that can accommodate such demanding measurements, and these two instruments can definitely be considered the best adapted for this purpose. The electric properties of the thin films were determined by dielectric measurements and the second-harmonic generation technique.

The films demonstrated a highly crystalline orthorhombic phase and epitaxial growth. The lattice parameters of (100)-oriented films remained almost unchanged compared with bulk $TbMnO_3$. This implies that the mismatch of the in-plane lattice parameters between the film and the (100)-oriented substrate is minimal, allowing the film to relax towards the bulk-like phase. A more significant change of the lattice parameters was found for (010) films deposited on (010)-oriented substrates. The in-plane *a*- and *c*-axis lattice parameters experienced a compressive strain of 2.1 % and 0.4 %, respectively. The out-of-plane *b*-axis parameter became elongated due to a resulting tensile strain of 1.7 %. On the basis of these results we denote the investigated (010) film as strained and the (100) film as relaxed.

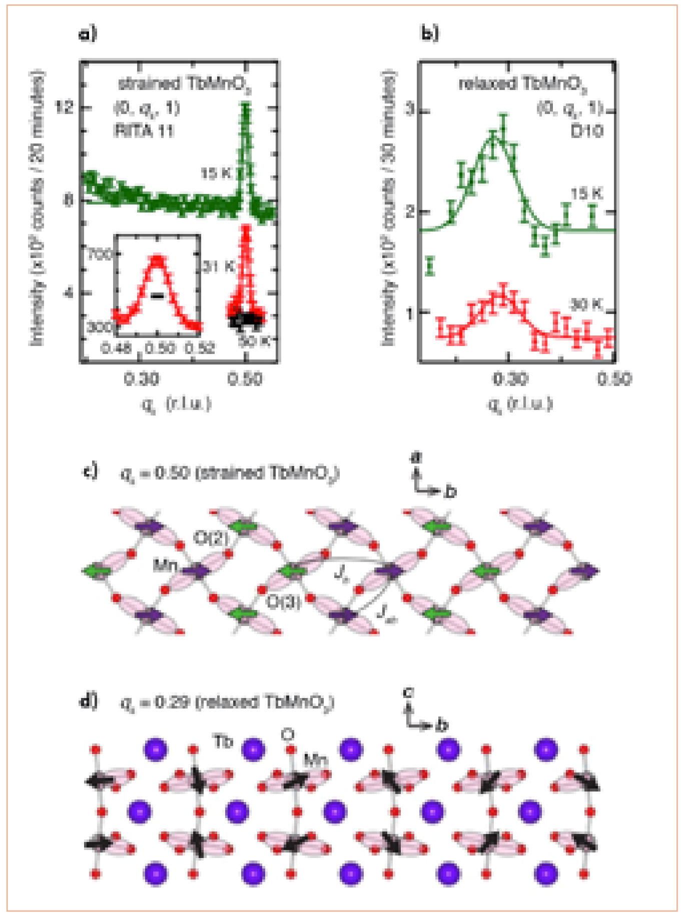

Figure 1

Magnetic reflections (0 *q* 1) measured at different temperatures for
a) the relaxed film and
b) the strained film.
Schematic images of the antiferromagnetic
c) spiral order in bulk and
d) *E*-type order in the strained film.

Magnetic reflections (0 *q* 1) revealed that the relaxed film reproduced a bulk-like spiral incommensurate antiferromagnetic order of the ground state with a magnetic modulation wave vector $q \sim 0.285\mathbf{b}^*$ (r. l. u), as shown in **figure 1** [3]. In contrast, the strained film showed a drastic modification of the magnetic ground state towards a commensurate *E*-type order with $q \sim 0.5\mathbf{b}^*$[8]. This strongly suggests a strain-induced tuning of the antiferromagnetic spin ordering at the Mn ion site. In addition to these studies we attempted to identify the orientation of the electric polarisation axis in the multiferroic phase. In accordance with the structural and magnetic studies, the polar ordering showed a switching from $P \parallel c$ induced by the spiral order for the relaxed film to $P \parallel a$ induced by the *E*-type order for the strained film. The other interesting feature found was a significant increase in the onset temperature of the FE ordering $T_{FE} \sim 41$ K for the strained film compared with bulk $TbMnO_3$ at $T_{FE} \sim 28$ K [4]. In addition, FE loop measurements of the strained film showed an enhancement of the spontaneous polarisation up to $P_a \sim 2$ μC/cm² compared with $P_c \sim 0.08$ μC/cm² observed in bulk $TbMnO_3$ [4].

We propose a simplistic description based on tuning of a specific spin-exchange interaction between Mn spins to explain the observed modification of the multiferroic properties under strain. In the theoretical explanation of multiferroicity in o-$RMnO_3$ by Mochizuki *et al.* [9], the ratio between the antiferromagnetic next-nearest neighbour exchange interaction along the *b*-axis (J_b) and the ferromagnetic nearest neighbour exchange interaction along the *ab* direction (J_{ab}) is found to play the most dominant role in defining the ground state. The interaction J_b between Mn spins is mediated by two staggered oxygen 2*p* orbitals. For a given J_{ab} value, it is proposed that the magnetic ground state shows a transition from a spiral phase at 0.5 meV < J_b < 1.2 meV to an *E*-type order at J_b > 2 meV. In the strained film, the increase of the *b*-axis results in an increased overlap of the oxygen orbitals, giving rise to an effective increase of the J_b-exchange interaction. This hypothetical scenario of a strain-induced modification of the microscopic mechanism explains the stabilisation of the *E*-type ground state in our $TbMnO_3$ thin films. Our studies also identify 'strain' as an effective tool for engineering the magnetic and ferroelectric properties of multiferroic materials. Our results identify neutron scattering as a suitable experimental technique for the study of magnetism in thin films despite their very limited scattering volume.

Ground state selection under pressure in the quantum pyrochlore magnet $Yb_2Ti_2O_7$

High-intensity two-axis diffractometer with variable resolution D20

New quantum states of matter often escape experimental observation. The magnetic properties of the rare-earth pyrochlore quantum magnet $Yb_2Ti_2O_7$ have eluded global understanding, while even the presence or absence of static magnetic order at low temperatures is controversial. Our recent study combined neutron diffraction and muon spin relaxation measurements in order to show why: isolated atomic defects (excess of Yb) create a local strain and induce a phase transition to a much more conventional magnetic state.

AUTHORS
E. Kermarrec (Paris Sud University, Orsay, France)
J. Gaudet and **B.D. Gaulin** (McMaster University, Hamilton ON, Canada)
R. Khasanov (PSI, Villigen, Switzerland)
C. Ritter (ILL)

ARTICLE FROM
Nat. Commun. (2017) – doi:10.1038/ncomms14810

REFERENCES
[1] S.T. Bramwell and M.J.P. Gingras, Science 294 (2001) 1495
[2] M.J.P. Gingras and P.A. McClarty, Rep. Prog. Phys. 77 (2014) 056501
[3] E. Kermarrec, J. Gaudet, K. Fritsch, R. Khasanov, Z. Guguchia, C. Ritter, K.A. Ross, H.A. Dabkowska and B.D. Gaulin, Nat. Commun. 8 (2017) 14810

A new quantum state of matter, dubbed ‘quantum spin ice’, may well exist at temperatures below 2 K in the rare-earth mineral $Yb_2Ti_2O_7$. In this state, the orientation of the magnetic moments of the electrons is analogous to the configuration of hydrogen-oxygen chemical bonds in the solid form of water, hence the reference to ice [1]. By using specific atoms with anisotropic magnetic properties, like the chemical element ytterbium (Yb), this state can acquire fascinating quantum properties such as the coherent superposition of states depicted by the famous Schrödinger’s cat, or new exotic quasi-particles of electronic character [2].

The experimental observation of such a quantum state in a large size material could revolutionise our ways of thinking of the collective behaviour of electrons in matter and further help to consider the future physical properties of quantum materials. Although $Yb_2Ti_2O_7$ has been the subject of intense research since 2000, physicists have not reached consensus on the nature of its magnetic state at very low temperatures: is it the so-called quantum spin ice, or a more ordinary ferromagnetic phase similar to the one that exists in fridge magnets?

Figure 1

a) Neutron diffraction measurements performed under hydrostatic pressure (P = 11 kbar) on $Yb_2Ti_2O_7$ on D20. The evolution of diffraction patterns with temperature (after subtraction of the nuclear scattering determined at 800 mK) shows the appearance of magnetic Bragg peaks for T ≤ 400 mK, a characteristic feature of a particular ferromagnetic phase with a magnetic moment of 0.33(5) μB at 100 mK.
b) Pressure–temperature (P–T) phase diagram established by μSR measurements on $Yb_2Ti_2O_7$. Empty black circles define the phase transition line between a collective paramagnetic state (PM, orange) and a ferromagnetic-like state (SFM, blue). The green region at low temperatures highlights the existence of an exotic non-magnetic phase (QSL), evidenced for P = 0.

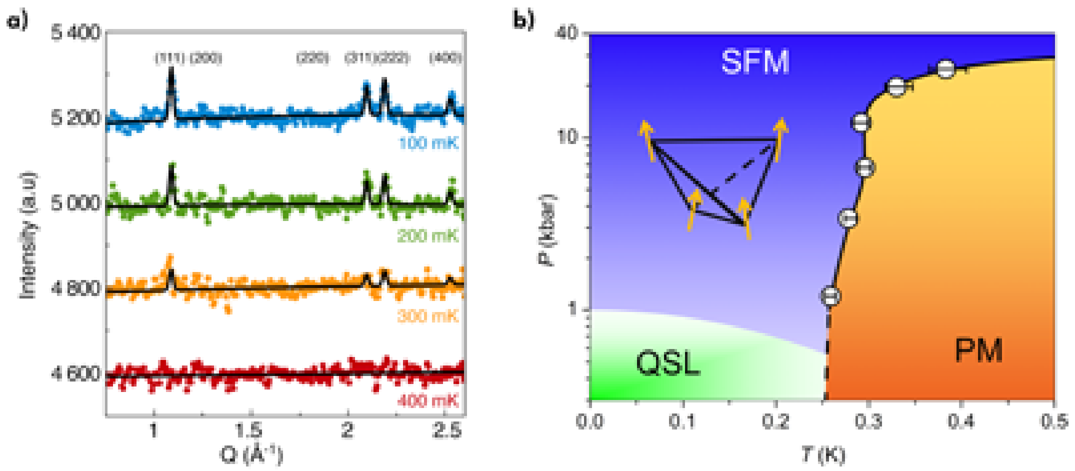

Figure 2

Representation of the two, interpenetrating, corner-sharing tetrahedra lattices of Yb^{3+} (blue, magnetic) and Ti^{4+} (yellow, non-magnetic) forming the pyrochlore structure. A few isolated atomic defects (Yb replacing Ti) could be responsible for a local strain and could strongly modify the electronic properties of the material. ©Edwin Kermarrec

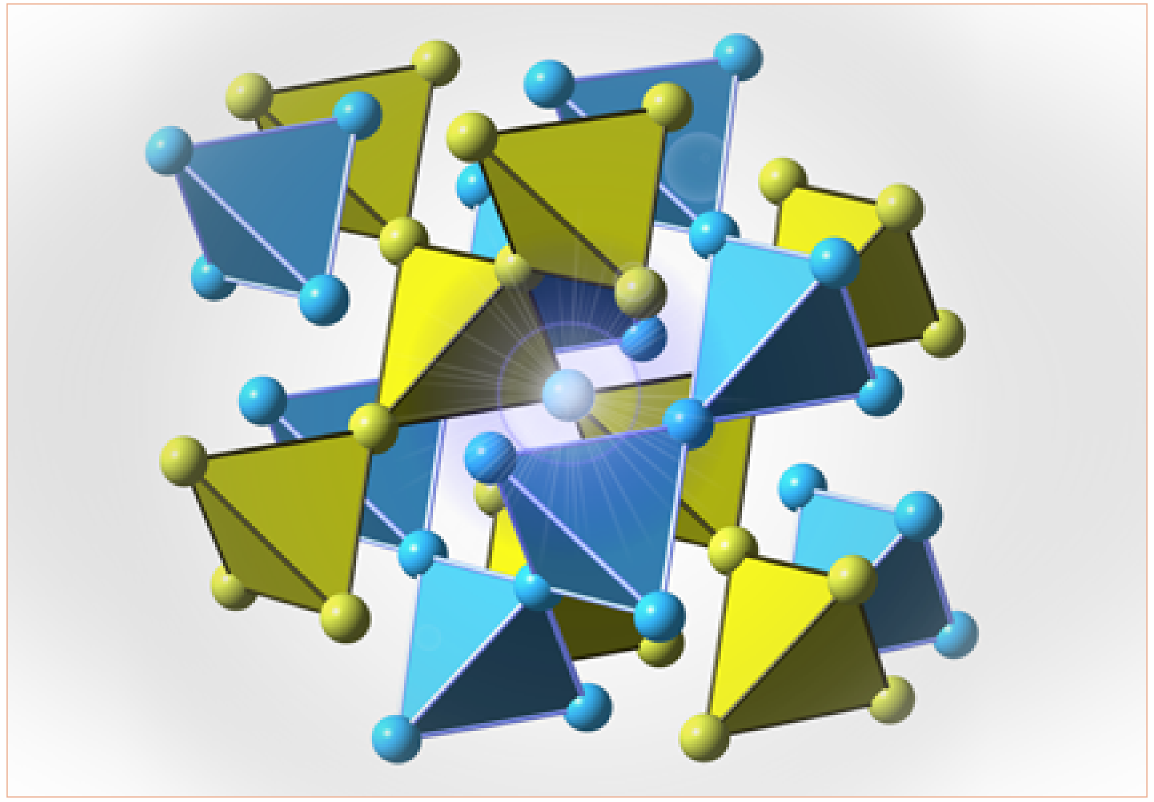

In our recent study, we show that a mysterious non-magnetic state exists at very low temperatures and that it is very sensitive to external perturbations such as the application of high pressure [3]. We used two spectroscopic techniques: muon spin relaxation (μSR) and neutron diffraction. The neutron experiment was conducted on the ILL’s D20 instrument, while the μSR measurements were carried out at the Paul Scherrer Institute. D20 is a versatile, two-axis powder diffractometer with a variety of applications, including thermodiffractometry, magnetism, kinetics, multi-stroboscopy and physisorption. The instrument is characterised by its extremely high neutron flux, which allowed us to detect a very small signal inside a heavy, high-pressure (11 kbar), low-temperature (100 mK) sample environment.

The results obtained from neutron scattering indicate that the magnetic state obtained under pressure is long-range ordered, with a static magnetic moment of 0.33(5) μ_B, as evidenced by the appearance of resolution-limited magnetic Bragg peaks (**figure 1a**). Previous neutron diffraction measurements have demonstrated, in real materials with the chemical formula $Yb_2(Yb_xTi_{1-x})_2O_7$, the presence of Yb atoms in excess localised on the titanium crystallographic site. The significant difference between the ionic radius of Yb^{3+} and Ti^{4+} creates a strong local strain, in a similar way to externally applied pressure (**figure 2**). Further μSR measurements allowed us to construct a pressure–temperature phase diagram under applied pressure (**figure 1b**). A non-magnetic phase is found to lie close by an ordered, splayed ferromagnetic phase.

These new measurements will help scientists reach a consensus on the nature of the magnetic state of $Yb_2Ti_2O_7$ at very low temperatures. Defects at the atomic scale could have a significant impact on the magnetic properties of $Yb_2Ti_2O_7$ at the macroscopic level, explaining previous findings that seemed controversial. The findings of the neutron diffraction experiment, together with the μSR measurements, provide the first step to better understanding how quantum states can arise in real materials. These findings also justify the need for close collaboration between solid-states physicists and chemists in order to conceive and understand the next generation of strongly correlated electron materials.

MAGNETISM

Field-induced magnetic instability within a superconducting condensate

Three-axis spectrometer IN12
Single-crystal diffractometer D23
Single-crystal four-circle diffractometer D10
Three-axis spectrometer Rita-II at PSI

Quantum phase transitions arise from inherent quantum effects in the zero-temperature limit. They separate phases with different organisation principles and may be tuned by external parameters such as pressure, chemical substitution or magnetic field. Here we provide evidence of a novel quantum phase transition that separates two antiferromagnetic phases with identical symmetry within a superconducting condensate. This suggests that the magnetic instability is driven not by magnetic degrees of freedom but by fluctuations related to the superconducting condensate.

AUTHORS
D.G. Mazzone, **J.L. Gavilano**, **C. Niedermayer, J. Okkels Birk** and **M. Kenzelmann** (PSI, Villigen, Switzerland)
S. Raymond, **E. Ressouche**, **G. Bastien**, **G. Knebel**, **D. Aoki** and **G. Lapertot** (Université Grenoble Alpes and CEA-Grenoble, France)
B. Ouladdiaf (ILL)

ARTICLE FROM
Sci. Adv. 3, e1602055 (2017) – doi: 10.1126/sciadv.1602055

REFERENCES
[1] M. Kenzelmann *et al.*, Science 321 (2008) 1652
[2] S. Gerber *et al.*, Nat. Phys. 10 (2014) 126
[3] S. Raymond *et al.*, J. Phys. Soc. Jpn. 83 (2014) 013707
[4] D.G. Mazzone *et al.*, Sci. Adv. 3 (2017) e1602055

Strong electronic fluctuations in the vicinity of quantum phase transitions (QPTs) are thought to trigger unconventional superconductivity. A prime candidate for magnetically driven superconductivity is the heavy-fermion compound $CeCoIn_5$ which is naturally located close to a spin-density wave (SDW) quantum critical point. The material condenses in an unconventional superconducting ground state with a well-established d_{x2-y2} symmetry at low temperatures. The system also features a magnetic field-induced QPT with emergent magnetic order inside the superconducting condensate [1, 2]. The SDW propagates along $\boldsymbol{Q} = (q, \pm q, 0.5)$ with $q \approx 0.45$ and collapses in a first-order transition at the superconducting upper critical field, providing evidence of a coupling between superconductivity and magnetism in this high-field Q-phase.

The origin and microscopic interpretation of the Q-phase is still under debate, and might be further clarified by the application of an auxiliary tuning parameter. The magneto-superconducting ground state is, however, both highly sensitive upon doping and found to be suppressed at very small impurity concentrations. Recent studies on $Nd_{0.05}Ce_{0.95}CoIn_5$ reveal magnetic order below $T_N = 0.8$ K and zero-field inside its superconducting phase ($T_c = 1.8$ K) which shares the magnetic wave vector of the high-field Q-phase in the undoped compound [3]. In the present study, we investigated the nature of the magnetic order in 5 % Nd-doped $CeCoIn_5$ as a function of magnetic field and its relation to the Q-phase [4].

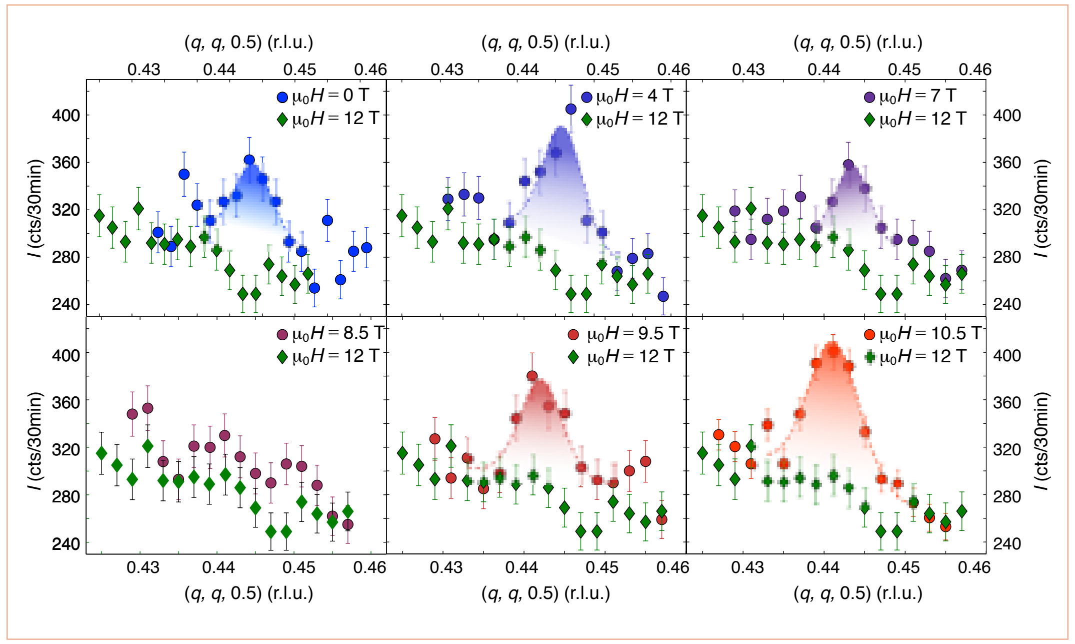

Figure 1

Diffracted neutron intensity measured at $T = 40$ mK and $H||[1\ \text{-}1\ 0]$. We observe a magnetic Bragg peak that first increases with increasing magnetic field and then vanishes around $\mu_0H^* \approx 8$ T. Magnetic order reappears at higher fields and collapses at the superconducting upper critical field.

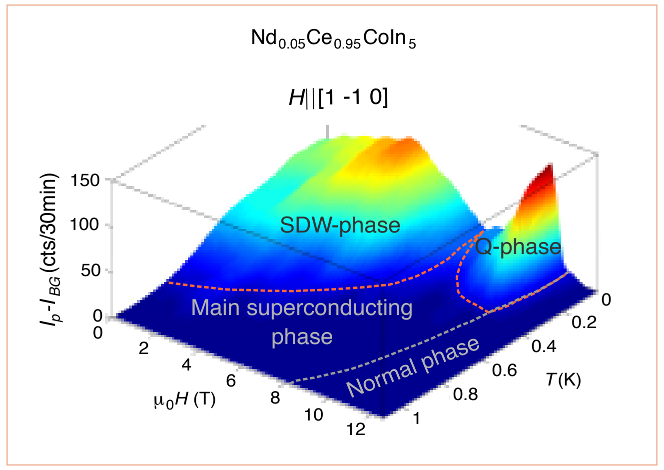

Figure 2

HT-phase diagram of $Nd_{0.05}Ce_{0.95}CoIn_5$ for $H||[1\ \text{-}1\ 0]$ with the main *d*-wave superconducting condensate, the SDW-phase and the Q-phase. The *z*-axis denotes the magnetic intensity, the white dashed line represents the superconducting upper critical field and the red dashed lines are the magnetic phase boundaries.

Neutron diffraction is a unique technique for studying magnetic order under extreme conditions, such as very low temperatures and high magnetic fields. Our results were obtained from the lifting-counter two-axis diffractometer D23, the single-crystal four-circle diffractometer D10 and the cold-neutron three-axis spectrometer IN12 at the ILL, Grenoble, France, and the cold-neutron triple-axis spectrometer Rita-II at the Swiss Spallation Neutron Source SINQ, Paul Scherrer Institut, Villigen Switzerland. **Figure 1** shows the field-dependence of the magnetic order along $Q = (q, q, 0.5)$ for $H||[1\ \text{-}1\ 0]$ and at $T = 40$ mK. We observe a magnetic Bragg peak that first increases with increasing magnetic field strengths and then vanishes around $\mu_0H^* \approx 8$ T. Above this magnetic instability, magnetic order surprisingly reappears at a similar wave vector and collapses around $\mu_0H \approx 11$ T. This provides direct evidence of two distinct magnetic phases in the material: a low-field SDW-phase that is stable for $H < H^*$, and a high-field phase that is denoted as Q-phase because it is closely related to the Q-phase of $CeCoIn_5$.

The HT-phase diagram of $Nd_{0.05}Ce_{0.95}CoIn_5$ is displayed in **figure 2**. Both magnetic phases are embedded inside the main superconducting *d*-wave condensate and separated by a field-induced QPT. The Q-phase collapses in a first-order transition at the superconducting upper critical field, providing evidence of a cooperative magneto-superconducting ground state at high magnetic fields and low temperatures. Thus, we demonstrate that the Q-phase is stable under 5 % of Nd substitution for Ce in $CeCoIn_5$.

Our neutron diffraction results, however, show that the magnetic symmetry (propagation vector, direction of the magnetic moment) is not affected at H^*. This demonstrates that the putative field-induced QPT cannot be driven purely by magnetic fluctuations but is attributed to another type of fluctuation. Since magnetic order is directly coupled to the superconductivity in the high-field Q-phase, we suggest that the superconducting condensate is modified at H^*.

In summary, we find a magnetic instability in superconducting $Nd_{0.05}Ce_{0.95}CoIn_5$ that separates two antiferromagnetic phases with the same symmetry. While the low-field SDW-phase is suppressed at $\mu_0H^* \approx 8$ T, the emergent high-field Q-phase features a direct coupling between superconductivity and magnetism. We provide evidence for a novel QPT that may be attributed to fluctuations related to the superconducting properties and which yields a cooperative magneto-superconducting ground state in the Q-phase.

Long-range order avoided in a low-dimensional magnet due to trapped domain walls

Diffuse scattering spectrometer D7
Three-axis spectrometer RITA-II at PSI

Local defects of the spin configuration in magnetic materials can be described as magnetic defects or emergent quasi-particles. Examples of such quasi-particles are the magnetic monopoles in spin-ice compounds [1]. Our study reveals that magnetic defects in the frustrated magnet $SrDy_2O_4$ play a key role in preventing long-range magnetic order. These results illustrate the general importance of local magnetic defects in frustrated magnets.

AUTHORS
N. Gauthier, **A. Fennell**, **A.-C. Uldry**, **B. Delley**, **R. Sibille**, **J.S. White**, **C. Niedermayer**, **V. Pomjakushin** and **M. Kenzelmann** (PSI, Switzerland)
B. Prévost, **A. Désilets-Benoit** and **A.D. Bianchi** (University of Montréal, Canada)
H.A. Dabkowska (Brockhouse Institute for Materials Research, Hamilton, Canada)
J. Nilsen and **L.-P. Regnault** (ILL)

ARTICLE FROM
PRB (2017) – doi:10.1103/PhysRevB.95.134430

REFERENCES
[1] C. Castelnovo, R. Moessner and S.L. Sondhi, Nature 451 (2008) 42
[2] W. Selke, Phys. Rep. 170 (1988) 213
[3] S. Redner and P.L. Krapivsky, J. Phys. A: Math. Gen. 31 (1998) 9229
[4] N. Gauthier *et al.*, Phys. Rev. B 95 (2017) 134430

Frustrated magnets present an interesting playground for investigating novel emergent properties. One prototypical example is the emergence of magnetic monopoles in spin-ice compounds [1]. These quasi-particles break the so-called ice rules and can be understood as local defects of the spin configuration. Magnetic monopoles play a crucial role in the low-temperature description of spin ices. By analogy, we have found that local defects in the low-dimensional frustrated magnet $SrDy_2O_4$ are responsible for the absence of long-range order down to milliKelvin temperatures. In this case, the defects correspond to domain walls in frustrated zigzag chains.

The compound $SrDy_2O_4$ is part of a large family of rare-earth-based frustrated magnets that exhibit a variety of properties, such as spin-liquid ground states and magnetic phases with coexisting order parameters. In $SrDy_2O_4$, magnetic correlations remain one-dimensional down to $T = 60$ mK. Experimentally, these correlations along the zigzag chains form planes in reciprocal space that can be probed by diffuse neutron scattering. In our experimental set-up, these planes appear as lines near half-integers of the reciprocal lattice component Q_l, as illustrated in **figure 1**. The neutron polarisation analysis of the D7 diffractometer at the ILL allows us to both determine unambiguously the magnetic origin of this scattering, and indicate the direction of the magnetic moments.

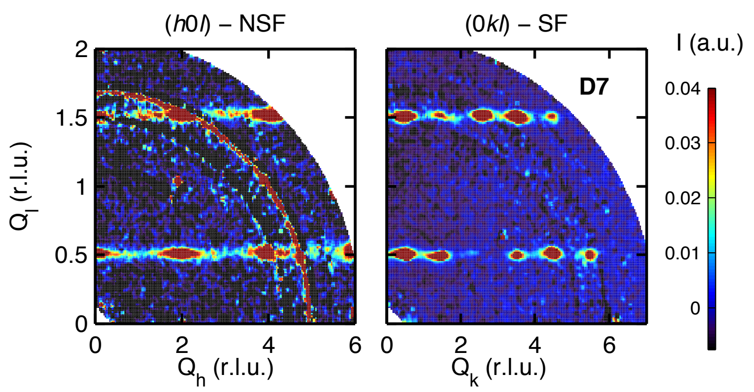

Figure 1

Magnetic diffuse scattering in the (*h*0*l*) and (0*kl*) reciprocal planes at T = 60 mK. The neutrons were polarised perpendicular to the scattering plane and measurements performed for non-spin-flip (NSF) and spin-flip (SF) scattering. These measurements were performed with the D7 diffractometer at the Institut Laue-Langevin.

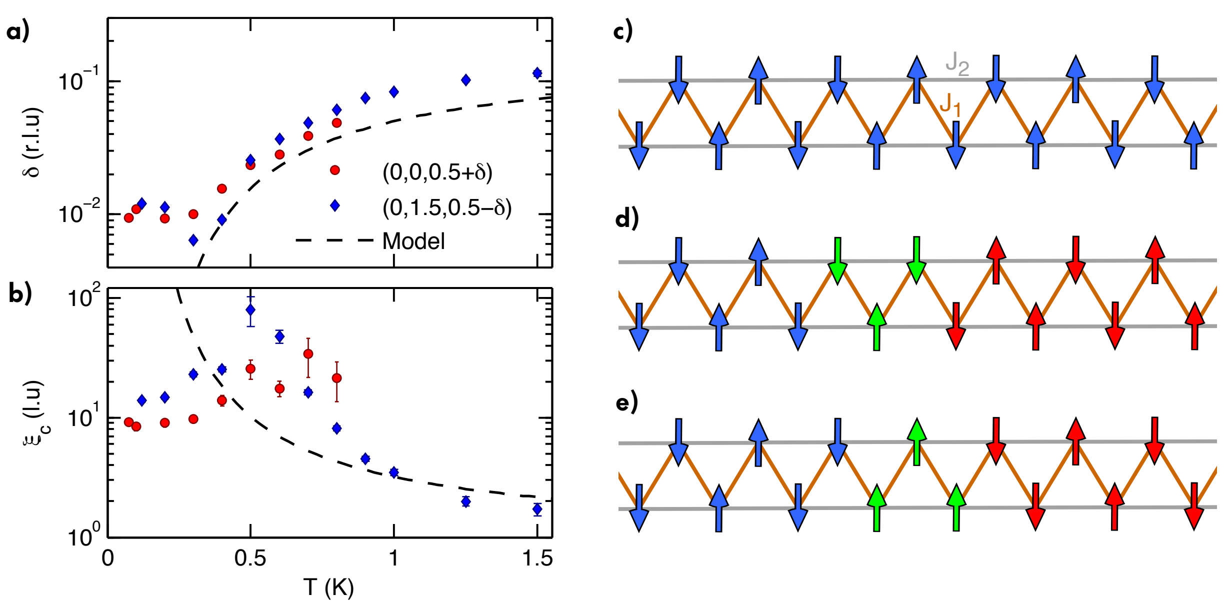

Figure 2

Temperature dependence of:
a) the incommensurate wave vector of the correlations, and
b) the correlation length along the chain. The dashed line corresponds to the model described in the text. These measurements were performed with the TASP and RITA-II three-axis spectrometers at PSI.
c) Ground state of the zigzag chains expected at T = 0 K.
d, **e)** Representation of two types of domain wall, shown as green arrows, separating the two different domains illustrated with blue and red arrows.

The results reveal the nature of short-range magnetic correlations. Specifically, the system converges at low temperatures towards an antiferromagnetic order on the zigzag chains illustrated in **figure 2c**. The correlations are well described above $T = 0.5$ K by a one-dimensional Ising model with nearest and next-nearest neighbour interactions [2], as shown in **figures 2a**, **b**. The model also predicts that the domain walls in the chains can propagate freely but that they decay very slowly [3]. There are two types of domain wall, which are illustrated by the green arrows in **figures 2d**, **e**. These domain walls appear as antiferromagnetic and ferromagnetic defects in **figures 2d** and **2e**, respectively. The slow dynamics of the defects are confirmed by AC susceptibility measurements that indicate an average relaxation time of almost one second at $T = 0.6$ K. The presence of a large density of domain walls is therefore expected within experimental time scales.

Like magnetic monopoles in spin ice, the domain walls in $SrDy_2O_4$ play a fundamental role at very low temperatures. In $SrDy_2O_4$, the magnetic defects become confined below $T = 0.5$ K due to a dimensionality crossover. The interchain interactions are responsible for this confinement, which prevents propagation of the defects and inhibits their decay mechanisms. Consequently, the formation of three-dimensional long-range order in this frustrated magnet is avoided [4]. The system instead reaches a metastable state with trapped domain walls. The local defects of the spin configuration emerge as an essential ingredient of the low temperature physics in the compound $SrDy_2O_4$, highlighting the fact that macroscopic properties can be dominated by localised effects in a variety of frustrated systems.

Higgs mode and its decay in a two-dimensional antiferromagnet

Three-axis spectrometer IN20

Neutron scattering experiments have revealed an excitation branch in a two-dimensional antiferromagnet that is analogous to the Higgs mode in particle physics. Theoretical predictions for the dispersion and decay of the mode in two dimensions can thus be systematically tested.

AUTHORS

A. Jain, **M. Krautloher**, **J. Porras**, **G.H. Ryu**, **D.P. Chen**, **J. Chaloupka**, **G. Khaliullin**, **B.J. Kim** and **B. Keimer** (Max Planck Institute for Solid State Research, Stuttgart, Germany)
A. Ivanov (ILL)
D.L. Abernathy (Oak Ridge National Laboratory, US)
J.T. Park (Technical University of Munich, Germany)

ARTICLE FROM

Nat. Phys. 13 (2017) – doi:10.1038/nphys4077

REFERENCES

[1] R. Matsunaga *et al.*, Phys. Rev. Lett. 111 (2013) 057002
[2] A. Jain, M. Krautloher, J. Porras, G.H. Ryu, D.P. Chen, D.L. Abernathy, J.T. Park, A. Ivanov, J. Chaloupka, G. Khaliullin, B. Keimer and B.J. Kim, Nat. Phys. 13 (2017) 633
[3] G. Khaliullin, Phys. Rev. Lett. 111 (2013) 197201
[4] S.-M. Souliou, J. Chaloupka, G. Khaliullin, G. Ryu, A. Jain, B.J. Kim, M. Le Tacon and B. Keimer, Phys. Rev. Lett. 119 (2017) 067201

The 'Mexican hat' potential with a circle of degenerate minima (red line in **figure 1**) epitomises the concept of spontaneous symmetry breaking in many areas of physics. When a system settles into a specific state along the circle, its ground becomes less symmetric than the Hamiltonian that describes it. The system then supports two types of oscillation: zero-energy oscillations along the brim of the 'hat', and oscillations perpendicular to it whose excitation requires energy (blue arrows in **figure 1**). In particle physics, the Mexican hat has achieved fame as a two-dimensional cartoon of the Higgs potential, where the oscillation modes correspond to massless and massive elementary particles, respectively. Theorists would love to see how our world would look if they changed this potential, but this is impossible—the Higgs potential is a basic and immutable property of nature. It turns out, however, that Mexican hat potentials also appear in solid-state and cold-atom physics, where their parameters can be adjusted so that theoretical predictions can be tested systematically. One such example—the electromagnetic potential in a superconductor, which supports phase and amplitude oscillations of the Cooper-pair condensate—actually predates the Higgs model in particle physics. However, the 'Higgs' amplitude mode of the superconducting condensate is difficult to observe and has been detected only recently in optical pump-probe experiments [1].

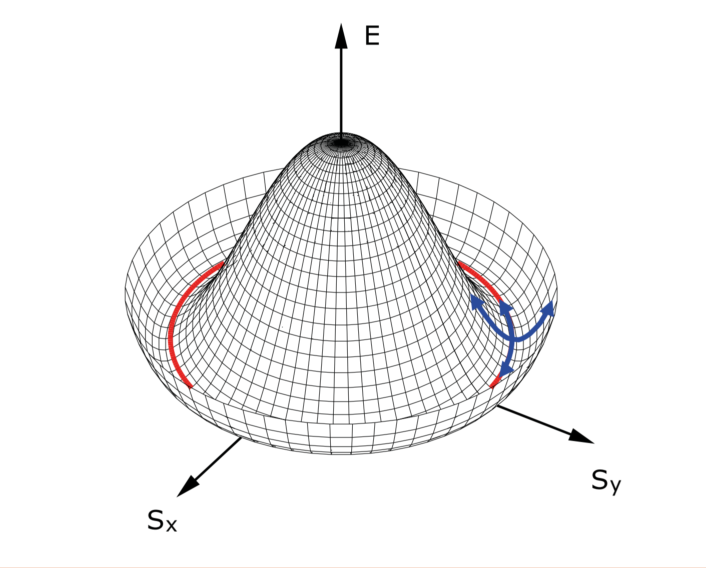

Figure 1

Mexican hat potential for a two-dimensional magnet. S is the spin, E is energy.

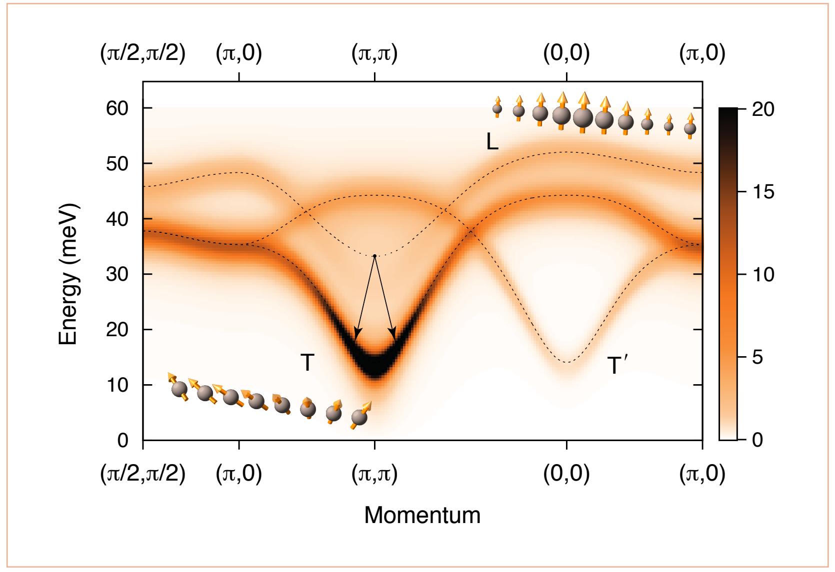

Figure 2

Dispersion of transverse magnons (marked T, T′) and the longitudinal Higgs mode (marked L) in Ca$_2$RuO$_4$ (from [2]).

Inelastic neutron scattering experiments [2] have now led to the discovery of a stable Higgs amplitude mode in an antiferromagnet, where it can be systematically tested over a wide range of energy and momentum. In an antiferromagnet, the Mexican hat potential is created by the effective magnetic field acting on a given electron spin by the surrounding spins. In the long-wavelength limit, it takes little energy to create a transverse spin wave (or magnon) that changes the direction of the spins (lower inset in **figure 2**). Magnons thus correspond to 'massless' phase oscillations, where the tip of the spin moves along the brim of the Mexican hat (**figure 1**). 'Higgs' modes, on the other hand, involve modulations of the length of the spins (upper inset in **figure 2**), perpendicular to the brim.

In ordinary antiferromagnets, such excitations are 'massive'; that is, they are found at high energies where they decay rapidly into transverse magnons. The recent experiments were motivated by theoretical work that predicted stable amplitude modes for magnets close to a quantum phase transition between an antiferromagnetically ordered state and a singlet state with no magnetic moment [3]. Such a singlet state can emerge in magnets where the orbital magnetic moment of the unpaired electrons cancels the magnetic moment arising from their spins. In the layered antiferromagnet Ca$_2$RuO$_4$, the magnetic moments reside on Ru^{4+} ions with valence electrons in the 4d shell. The strong spin-orbit coupling of these ions stabilises a substantial orbital moment antiparallel to the spin moment. The ordered moment in the antiferromagnetic state is therefore substantially lower than the spin-only moment. This situation is quite favourable for observing a 'soft' mode modulating the moment amplitude.

The growth of single crystals of a volume sufficient for inelastic magnetic neutron scattering experiments was challenging because Ca$_2$RuO$_4$ undergoes a metal-insulator transition associated with a large volume change just above room temperature. After developing a cooling protocol to avoid cracking of the crystals at this transition, about 100 sizeable specimens could be grown and co-aligned for the experiments. **Figure 2** shows a representation of the resulting spectrum. Three magnetic excitation branches can be seen. The two branches marked T and T′ are transverse magnon branches that involve oscillations of the moment direction; two such branches are present because the magnetic unit cell contains two Ru ions. The main branch, T, emanates from the antiferromagnetic ordering vector (marked (π,π) in **figure 2**) but its dispersion is quite different from that of a magnon in an ordinary Heisenberg antiferromagnet, which would turn around in the middle of the Brillouin zone and exhibit a minimum at (0,0). Instead, it exhibits a maximum at (0,0) which (along with the large magnon gap) is a signature of the large spin-orbit coupling that brings Ca$_2$RuO$_4$ close to a quantum phase transition into a singlet state.

The upper branch marked L is the Higgs amplitude mode, which turned out to be stable and well defined over much of the Brillouin zone. Only at the magnetic ordering vector does it decay into transverse magnons at a rate that can be calculated based on the magnetic Hamiltonian that also describes the magnon dispersions. The neutron data are in excellent agreement with the predictions. Based on the same calculations, evidence of the Higgs mode was also found later on in Raman scattering experiments [4]. These experiments thus establish a new platform for systematic research on the Higgs mode in two dimensions. Future experiments will address the dispersion and decay of amplitude modes in other magnets in which 4d valence electrons are arranged in different lattice geometries.

Evidence for a spinon Fermi surface in a triangular-lattice quantum-spin-liquid candidate

Three-axis low-energy spectrometer ThALES

A quantum spin liquid (QSL) shows no static order in the zero-temperature limit but presents highly entangled spins. In spite of decades of efforts, its experimental realisation remains a key challenge. In measurements of the triangular lattice YbMgGaO$_4$ we observed broad spin excitations covering a wide region of the Brillouin zone, with a clear upper excitation edge. Our results point to the existence of a QSL state with a two-dimensional spinon Fermi surface in the triangular antiferromagnet YbMgGaO$_4$.

AUTHORS
Y. Shen, **Y.-D. Li**, **H. Wo**, **S. Shen**, **B. Pan**, **Q. Wang**, **Y. Hao**, **G. Chen** and **J. Zhao** (Fudan University, Shanghai, China)
Y. Li and **Q. Zhang** (Renmin University, Beijing, China)
H.C. Walker (ISIS, UK)
P. Steffens and **M. Boehm** (ILL)
D.L. Quintero-Castro (HZB, Berlin, Germany)
L.W. Harriger (NIST, Gaithersburg, US)
M.D. Frontzek (ORNL, Tennessee, US)
L. Hao and **S. Meng** (CIAE, Beijing, China)

ARTICLE FROM
Nature (2016) – doi:10.1038/nature20614

REFERENCES
[1] L. Balents, Nature 464 (2010) 199
[2] Y. Li *et al.*, Sci. Rep. 5 (2015) 16419

In a QSL, magnetic ordering is prevented by strong frustration, leading to a highly degenerated ground state. It goes beyond the traditional Landau paradigm for conventional symmetry breaking phases and is often characterised by an emergent gauge structure and excitations with fractionalised quantum numbers. The latter can be measured by inelastic neutron scattering, which shows continuous spectra and contains information on topological symmetry. However, the identification of fractional excitations is usually constrained by various practical issues, including the lack of promising candidate materials. In the newly found QSL candidate, YbMgGaO$_4$, no static order is observed to the lowest measuring temperature, 0.03 K, far below its Curie-Weiss temperature, ~ -4 K [2]. Furthermore, the successful synthesis of sizeable single crystals makes it possible for use in inelastic neutron scattering experiments.

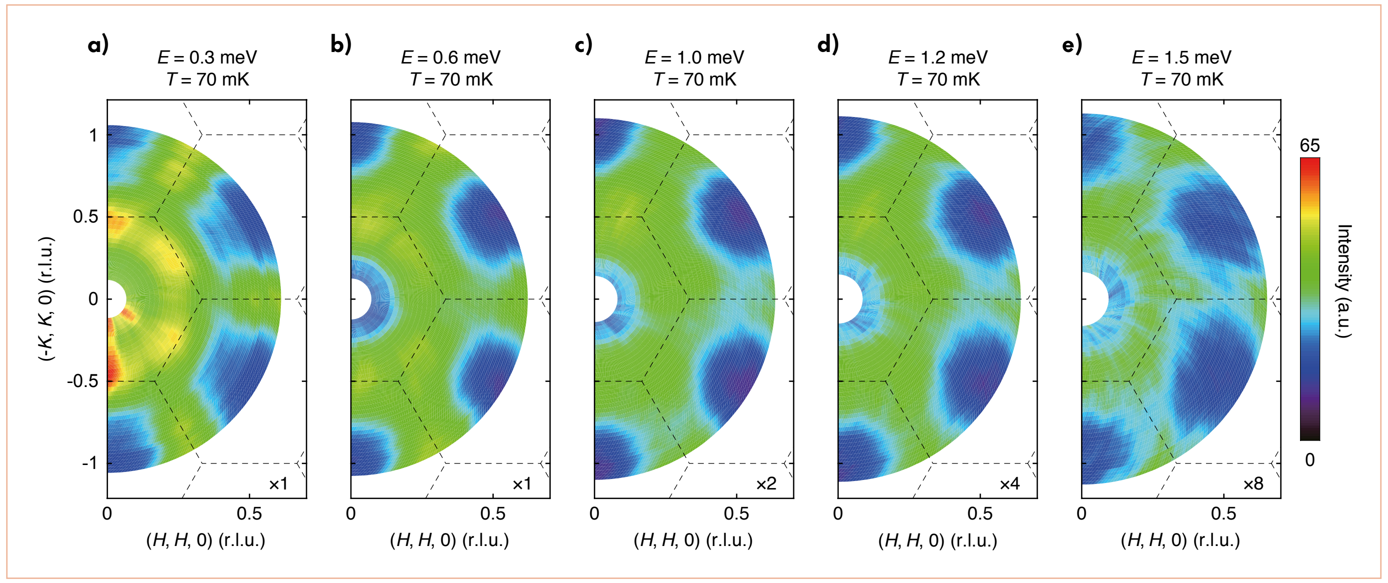

Figure 1

Constant-energy images at the indicated energies and T = 70 mK. The scattering intensity in **(c)**, **(d)** and **(e)** has been multiplied by 2, 4 and 8, respectively, for clarity. The dashed lines indicate the Brillouin zone boundaries.

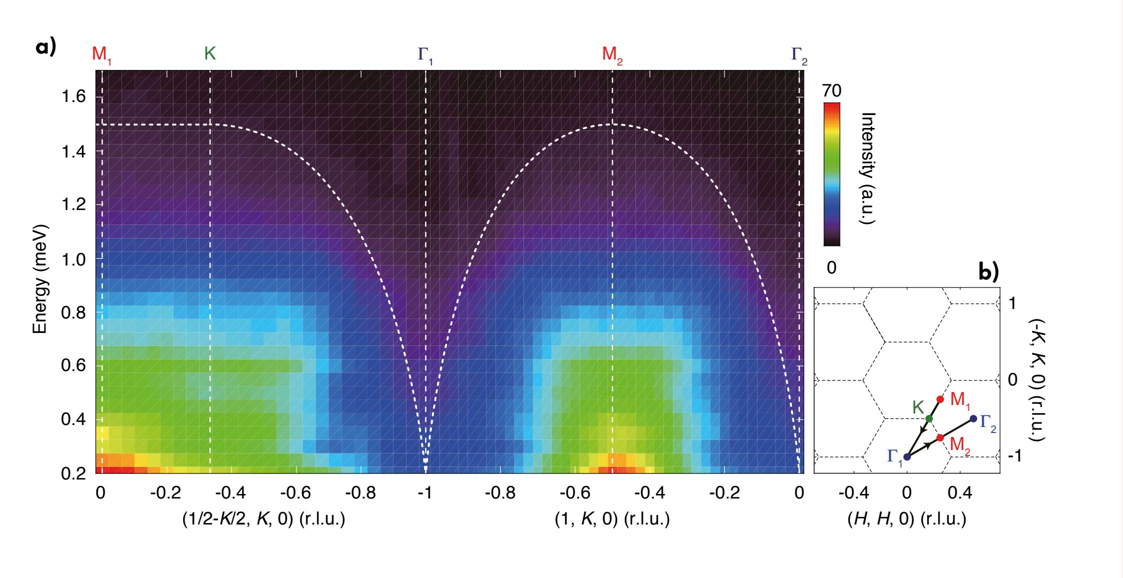

Figure 2

a) Energy dependence of the magnetic excitations along the high symmetry momentum directions illustrated by the black lines in **(b)**. Vertical dashed lines represent the high-symmetry points and dotted lines indicate the upper bounds.
b) Sketch of reciprocal space.

In the present experiment we used the three-axis low-energy spectrometer ThALES at the ILL to study the spin excitations in single-crystalline YbMgGaO$_4$ samples. **Figure 1** shows the constant-energy images measured with the FlatCone detector. Broad signals are revealed covering a large region of the Brillouin zone for all measured energies. The scattering spectra are mainly spread along the zone boundaries, leaving signals near the zone centre (Γ points) strongly suppressed. The intensity near M points is slightly enhanced at low energy (< 0.3 meV), while at higher energy the scattering is markedly isotropic around the boundaries.

The complete spectral distribution in energy-momentum (E-Q) space is presented in **figure 2**. The spectral intensity is rather broad in both the momentum and energy dimensions. As energy is increased, the spectral intensity is weakened gradually and vanishes above approximately 1.5 meV. No indication of spin gap can be probed within the instrument resolution (0.05 meV). Moreover, a V-shaped upper bound is revealed near the Γ points (dotted lines in **figure 2**), resulting in dispersive continuous excitations.

Unambiguously, such broad spectra are different from what we expect for magnon excitations, in which signals strongly peak at specific moments in reciprocal space leading to sharp spin-wave dispersion. Instead, the broad feature results from the spin fractionalisation in quantum materials. In the neutron scattering measurements, a spin-1 process neutron-spin-flip event creates a pair of deconfined spinons, each carrying half-integer spins and propagating separately. As a consequence, an excitation continuum structured in momentum space, very similar to the diffusive signals observed experimentally in **figures 1 and 2**, can be predicted. More specifically, the dispersive continuum with V-shaped upper bounds observed here can be explained by the particle–hole excitation created out of a spinon Fermi surface. These results indicate that YbMgGaO$_4$ is a QSL with a two-dimensional spinon Fermi surface.

Spiral spin-liquid and the emergence of a vortex-like state in $MnSc_2S_4$

Three-axis spectrometer IN22

The spiral spin-liquid, a disordered and fluctuating liquid of local spin spirals, was predicted to exist in spinels with a magnetic A-site but has never been observed. Using various single-crystal neutron diffraction techniques, we showed that $MnSc_2S_4$ supports a spiral spin-liquid that gives way to an unexpected series of ordered phases, which in turn can be driven into a vortex-like state by a magnetic field. $MnSc_2S_4$ is revealed as an excellent model material for the study of spiral spin-liquid and related questions.

AUTHORS

S. Gao (PSI, Villigen and University of Geneva, Switzerland)
O. Zaharko, **T. Fennell** and **Ch. Rüegg** (PSI, Villigen, Switzerland)
F. Bourdarot (CEA and Université Grenoble Alpes, Grenoble, France)

ARTICLE FROM

Nat. Phys. (2017) – doi:10.1038/nphys3914

REFERENCES

[1] D. Bergman, J. Alicea, E. Gull, S. Trebst and L. Balents, Nat. Phys. 3 (2007) 487
[2] S. Gao, O. Zaharko, V. Tsurkan, Y. Su, J.S. White, G.S. Tucker, B. Roessli, F. Bourdarot, R. Sibille, D. Chernyshov, T. Fennell, A. Loidl and Ch. Rüegg, Nat. Phys. 13 (2016) 157

Frustration is the inability of a system to satisfy all its interactions, which leads to degeneracies. In the absence of any perturbation, simple frustrated models present complications in the context of the third law of thermodynamics and are of interest for studying new emergent phenomena in many-body physics; since strong frustration tends to suppress conventional behaviour (such as long-range ordering), it is also useful as a design principle for new materials with novel properties. In spin systems, frustration can be imposed by geometry (*e.g.* antiferromagnetic interactions on triangular units), or by competition, as in the case of the J_1-J_2 model on the diamond lattice.

A spiral spin-liquid was predicted to occur in the J_1-J_2 model on the diamond lattice when $|J_1/J_2| > 0.125$ [1]. This model is relevant to spinels of general type AB_2O_4 where only the A-site is magnetic, as in $MnSc_2S_4$. Although there are plenty of these materials, no previous candidate has shown the signature of the spiral spin-liquid—a squared-ring of diffuse scattering, indicative of magnetic fluctuations at many possible incommensurate wave vectors. Using the first high-quality single crystals, we found an exact example of this spiral surface in $MnSc_2S_4$ at 2.9 K [2]. In theory, thermal fluctuations select certain wave vectors from the surface and the spiral spin-liquid undergoes an order-by-disorder transition.

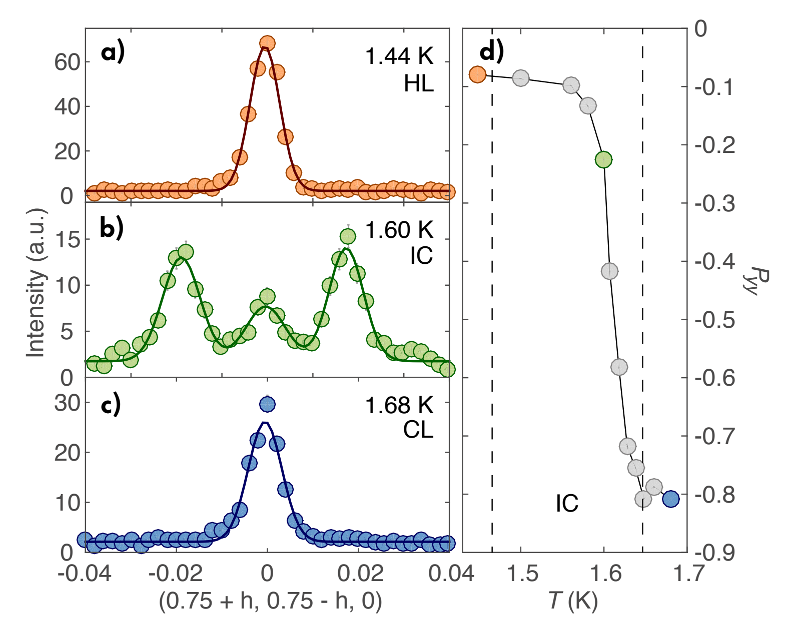

Figure 1

Magnetic Bragg scattering in the helical (HL, **a**), incommensurate (IC, **b**) and sinusoidally modulated collinear (CL, **c**) phases of $MnSc_2S_4$. Although the HL and CL phases have very similar Bragg scattering, a clear sign that they have different structures is the evolution of the P_{yy} element of the polarisation matrix, measured by spherical neutron polarimetry, on heating/cooling through the incommensurate phase (**d**).

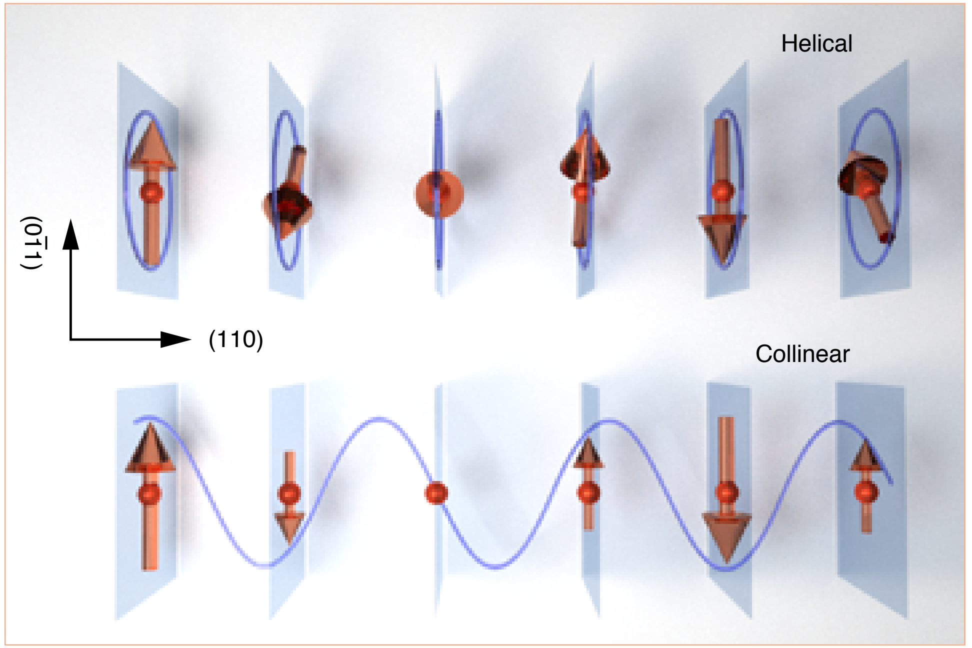

Figure 2

Schematic illustration of the different structures of helical and amplitude-modulated collinear phases.

On cooling, $MnSc_2S_4$ undergoes an ordering transition at T ~ 2.3 K with ***q*** = (0.75, 0.75, 0), which is a wave vector on the spiral surface, but an incommensurate phase (q' = (0.75+/-0.02, 0.75-/+0.02, 0) appears for 1.64 > T > 1.46 K followed by another transition to a structure that also has ***q*** = (0.75, 0.75, 0) (**figures 1 a–c**). The two commensurate phases are different, as is unambiguously shown by our spherical neutron polarimetry experiments, partly performed at IN22 with CRYOPAD. The temperature dependence of the P_{yy} element of the polarisation matrix measured at (0.75, 0.75,0) shows a continuous evolution from -0.8 to -0.1 as the sample is cooled through the incommensurate phase (IC) (**figure 1d**). Magnetic structure refinements show that the higher temperature collinear phase is a sinusoidally modulated collinear structure (CL), while the low temperature phase has a helical structure (HL) (**figure 2**).

The primary parameters of the J_1-J_2 model are set by observations of the spiral surface (its size and temperature dependence), but this sequence of ordered phases suggests that the order-by-disorder transition of the ideal model is replaced by a conventional ordering transition controlled by perturbations, and the observed structures suggest what these perturbations may be. The third neighbour interaction J_3 will select a ***q*** position for spiral order but does not determine whether the structure is cycloidal or helical. Dipolar interactions are predicted to favour a helical structure, and their anisotropy can also help to stabilise the collinear phase. Although these perturbations determine the ordering behaviour, they are small, meaning that the spiral spin-liquid of $MnSc_2S_4$ is rather ideal.

Both zero-field phases are single-q structures, but on cooling in an applied field a triple-q state is formed, also based on the vector (0.75,0.75,0). The three ***q***-vectors of a single triple-q domain are coplanar and sum to zero, and so four domains are possible; but when the field is applied along [111], their degeneracy is broken and a single domain structure is formed. The condition that the ***q***-vectors sum to zero has an analogue in the construction of a skyrmion lattice, but here the basis vectors are real and a vortex lattice is obtained instead.

$MnSc_2S_4$ has the most frustrated ratio of $|J_1/J_2|$ of any known spinel, which means that it realises an ideal spiral spin-liquid. However, a wealth of complex ordering phenomena in the zero and applied fields also appear below the spiral spin-liquid. Although it appears that the order-by-disorder transition is suppressed, $MnSc_2S_4$ represents an excellent model system for studying perturbations of this effect, as well as the spiral spin-liquid itself.

Portraying entanglement between molecular qubits with four-dimensional inelastic neutron scattering

Time-of-flight spectrometer IN5

Molecular nanomagnets are organometallic compounds that consist of a metallic core surrounded by organic ligands, which act to create magnetically isolated units [1]. While these compounds are interesting for testing fundamental concepts in quantum mechanics, they are also promising candidates for various technological applications, one of the most exciting of which is quantum information processing [2]. The detection and quantification of entanglement are crucial steps in quantum information science, and weakly-coupled molecular nanomagnets provide ideal test-beds for investigating entanglement between complex spin systems [3].

AUTHORS

E. Garlatti, **P. Santini**, **G. Amoretti** and **S. Carretta** (University of Parma, Italy)
T. Guidi (ISIS, UK)
S. Ansbro (ILL and University of Manchester, UK)
J. Ollivier and **H. Mutka** (ILL)
G. Timco, **I.J. Vitórica-Yrezábal**, **G.F.S. Whitehead** and **R.E.P. Winpenny** (University of Manchester, UK)

ARTICLE FROM

Nat. Commun. 8 (2017) – doi:10.1038/ncomms14543

REFERENCES

[1] D. Gatteschi, R. Sessoli and J. Villain, Molecular Nanomagnets, Oxford University Press (2006) 1086
[2] M.N. Leuenberger and D. Loss, Nature 410 (2001) 789
[3] I. Siloi and F. Troiani, Phys. Rev. B 86 (2012) 224404
[4] E. Garlatti, T. Guidi, S. Ansbro, P. Santini, G. Amoretti, J. Ollivier, H. Mutka, G. Timco, I.J. Vitórica-Yrezábal, G.F.S. Whitehead, R.E.P. Winpenny and S. Carretta, Nat. Commun. 8 (2017) 14543

To date, entanglement in molecular nanomagnets has only been experimentally demonstrated rather indirectly by macroscopic techniques or by fitting trial model Hamiltonians to experimental data. In this study we show that by exploiting the position-sensitive detectors of the IN5 spectrometer, four-dimensional inelastic neutron scattering enables us to portray entanglement in weakly-coupled molecular qubits and to quantify it [4]. We have used a prototype (Cr$_7$Ni)$_2$ supramolecular dimer as a benchmark to demonstrate the potential of this approach. Indeed, the neutron cross-section directly reflects dynamical correlations between individual atomic spins in the molecule, and distinguishes between intra-ring correlations associated with the composite nature of the molecular qubits and inter-ring spin-spin correlations which are a signature of entanglement between qubits.

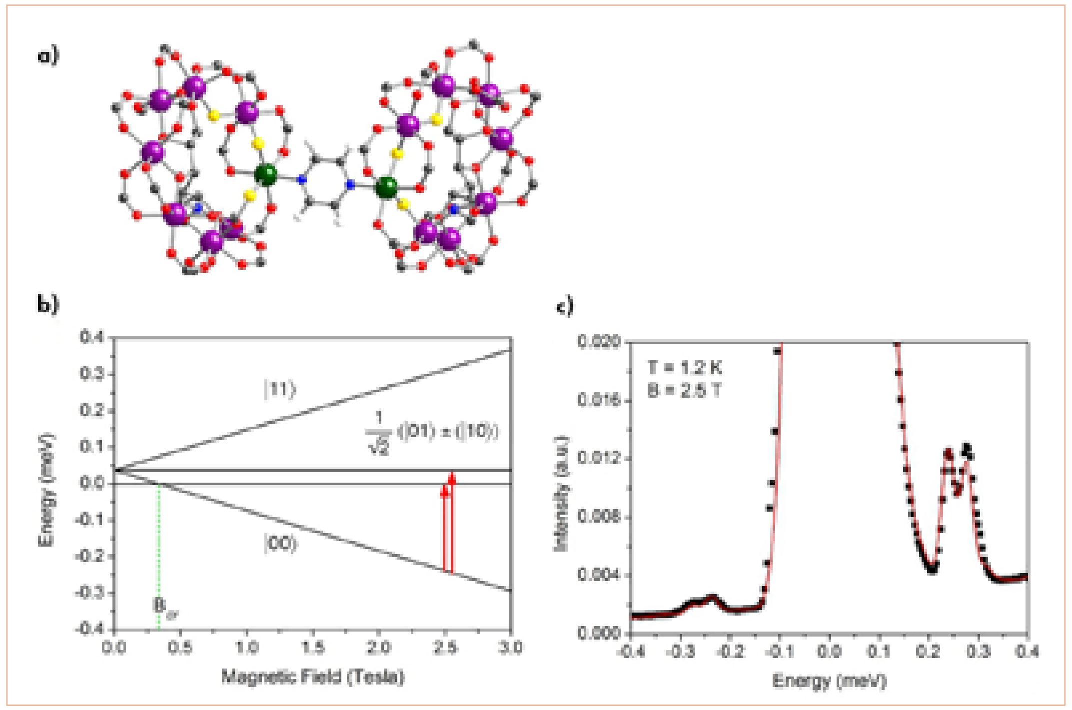

Figure 1

a) Molecular structure of the (Cr$_7$Ni)$_2$ supramolecular dimer (magenta, Cr; green, Ni; yellow, F; red, O; light blue, N; grey, C; C(CH$_3$)$_3$ groups and all H atoms omitted). The coupling between the rings is mediated by pyrazine, directly linking the two Ni ions. **b)** Lowest-energy levels of the molecular dimer as a function of the applied magnetic field B. The arrows indicate the two transitions detected by in-field INS. **c)** Measured INS spectrum (black points) and calculations (red line) for a collection of (Cr$_7$Ni)$_2$ crystals at T = 1.2 K and B = 2.5 T applied along the y-vertical axis, with an incident neutron wavelength λ = 7.5 Å and integrated over the full range of measured Q [4].

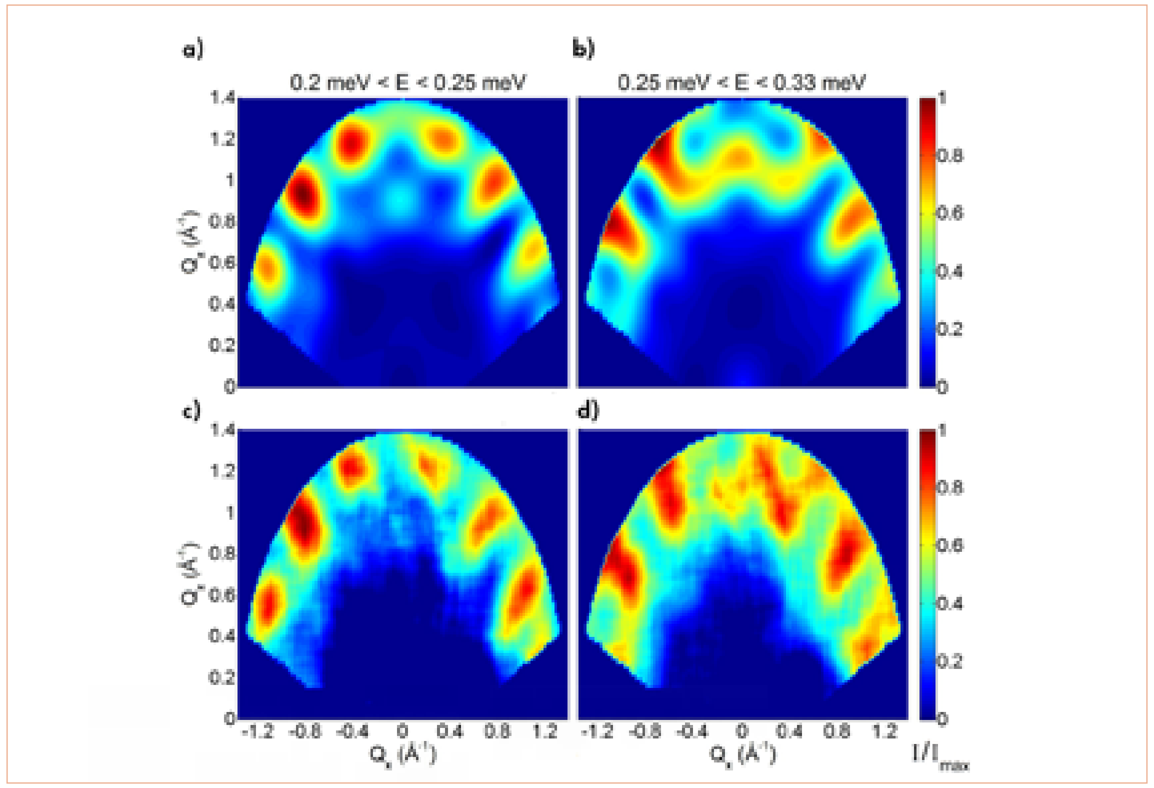

Figure 2

Constant-energy plots of the neutron scattering intensity [4]. **a**, **b)** The calculated dependency of the neutron scattering intensity of the two inelastic excitations on the two horizontal wave-vector components Q_x–Q_z, integrated over the full experimental Q_y. The cross-section has been integrated over energy ranges centred around the observed transition energies. **c**, **d)** The corresponding experimental measurements, carried out with a 7.5 Å incident neutron wavelength, a sample temperature of 1.2 K and a magnetic field B = 2.5 T. The colour bar depicts the transition intensity normalised for the maximum in each panel.

The dimer (**figure 1a**) consists of two Cr$_7$Ni antiferromagnetic rings. Strong exchange couplings between the eight spins within each ring lock them into a correlated S = 1/2 ground state, and a weaker antiferromagnetic inter-ring interaction leads to entanglement between the two molecular S = 1/2. The lowest-energy levels of the (Cr$_7$Ni)$_2$ dimer as a function of the applied magnetic field are presented in **figure 1b**. We performed our neutron scattering experiment on IN5 under an applied magnetic field, in order to place the system into a factorised ground state of the two rings (**figure 1b**). In this way, we are able to unambiguously attribute the observed dynamical inter-ring correlations to entanglement in the excited states. At 1.2 K and with an applied magnetic field of 2.5 T, we detected two inelastic peaks at 0.24 and 0.28 meV (**figure 1c**), corresponding to excitations from the factorised ground state towards two excited Bell states (red arrows in **figure 1b**). Exploiting the position-sensitive detectors of IN5, we also measured the four-dimensional scattering function S(**Q**,E), yielding direct information on the dynamical spin-spin correlation functions. If the excited state involved in the transition is entangled, the dynamical correlations are non-zero also for pairs of spins belonging to different rings. The spatial structure of these large-distance correlations produces short-Q modulations in S(**Q**,E), whose pattern is a 'portrayal' of the entanglement between the molecular qubits (see calculations in **figures 2a**, **b**). **Figures 2c**, **d** show the measured Q-dependence of the intensity of the two observed transitions, where short-Q modulations of the intensity are evident and clearly demonstrate the occurrence of entanglement.

We also developed a method to quantify entanglement, by extracting the concurrence of the two excited states from the data in **figure 2** [4]. Concurrence is one of the most commonly used measures of entanglement between a pair of qubits, ranging from 0 for factorised states to 1 for maximally entangled ones. The comparison between the data and our calculations clearly shows that concurrence is 1 for both excited states of the dimer, which are therefore maximally entangled states (for more details see [4]).

In conclusion, by using the (Cr$_7$Ni)$_2$ supramolecular dimer as a benchmark, we have shown that the richness of four-dimensional inelastic neutron scattering data enables us to portray entanglement in weakly-coupled molecular qubits and to quantify it. Our approach can also be applied to dimers of more complex molecular qubits, thus opening up remarkable perspectives in our understanding of entanglement in complex spin systems.

Polymer membranes for water desalination: neutron reflectivity elucidates links between nanostructure and performance

Reflectometer D17

AUTHORS
F. Foglia, A.G. Livingston, J.T. Cabral (Imperial College London, UK)
R. Barker (ILL)

ARTICLE FROM
Adv. Funct. Mater. (2017) – doi:10.1002/adfm.201701738

The scarcity of 'fresh' water, amounting to less than 1 % of the Earth's water, is one of the most pressing current societal challenges and is expected to increase in the foreseeable future in response to growing demand for human consumption, agriculture and industry. This challenge has ramifications that are far reaching, threatening nutrition and health but also geopolitical stability, and therefore constitutes an existential threat to future generations. Safe drinking water has a salinity level below approximately 150 ppm, while higher levels (1 000–3 000 ppm) are considered acceptable for irrigation. By contrast, brackish water has a level of salinity ranging between 3 000–10 000 ppm, whilst sea water is typically 30 000 ppm, depending on the source. Fresh water needs are increasingly being met by industrial membrane processes, including reverse osmosis (RO), over traditional thermal and vacuum distillation technologies. In recent years, however, RO has emerged as the leading membrane technology for new desalination plants for both brackish and sea water. Neutron reflectivity experiments have enabled us to correlate physical properties of membranes with their performance, in terms of salt rejection and permeability.

Significant challenges in RO membrane technology remain not only to reduce energy consumption during operation and achieve higher efficiency, but also to reduce performance losses during operation. In simple terms, the performance of a desalination membrane is measured by its *salt rejection*, the percentage of salt removed from the feedwater stream; and by its water *permeability*, the volume of water that passes through a membrane per unit time, unit area and unit pressure. Polymer scientists and membrane technologists seek to maximise both *selectivity* and *permeability*, and minimise loss of performance with time (ageing) and operational costs arising from the applied pressure (and temperature) to drive separation. Selectivity is generally inversely proportional to permeability, and despite considerable research in RO membrane structure and transport our fundamental understanding and thus ability to engineer high performance membranes remain limited and progress largely empirical.

RO membranes comprise a 'tight' separating polymeric layer, called the active layer, on a more 'open' support layer, often phase-inverted polysulfone, which is in turn mounted on a woven fabric backing, generally polyester, that imparts mechanical integrity. The top separating layer is usually synthesised by interfacial polymerisation (IP) at the organic/aqueous interface between an aromatic diamine (m-phenylenediamine, MPD) and trimesoyl chloride (TMC). IP is a polycondensation process between two multifunctional monomers dissolved in immiscible solvents, generally water and an organic phase, taking place at the interface between the two solvents. Formally, the organic-soluble component (acid chloride) is insoluble into the polymer, whereas the water-soluble component (diamine) diffuses through the film to react with the acid chloride at the film/organic phase interface, where the film grows. The resulting cross-linked polyamide (PA) film is extremely thin, approximately 10 nm, but is spontaneously crumpled and folded such that the overall membrane surface is rough and has a large surface area. This roughness has so far prevented the use of neutron (and X-ray) reflectivity approaches to resolve the membrane nanostructure at molecular resolution. Structural characterisation has instead relied on electron microscopy techniques that operate under vacuum (in the absence of water), as well as spectroscopic measurements and simulation.

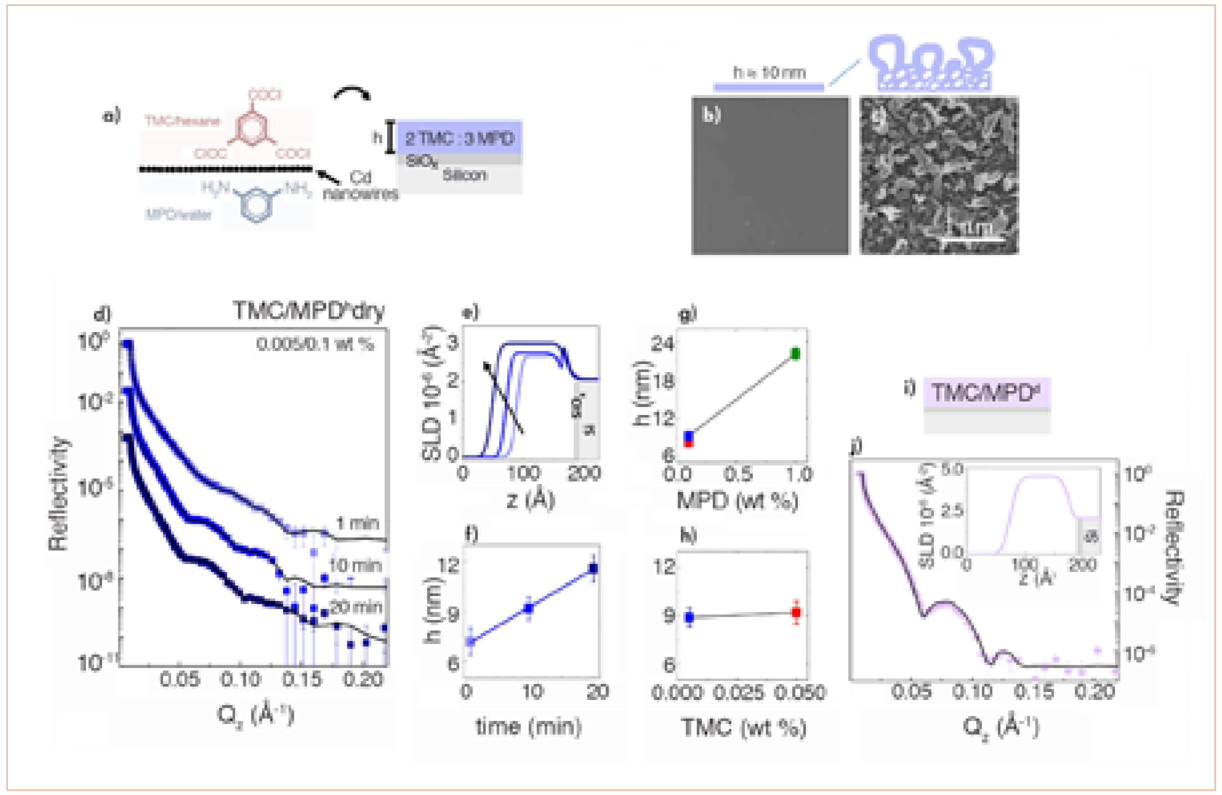

Figure 1

a) Schematic of the interfacial polymerisation (IP) reaction between TMC and MPD at the organic/water interface.
b) Scanning electron microscopy (SEM) image of smooth nanofilm from TMC/MPD with ~ 10 nm thickness.
c) SEM image of a representative crumpled nanofilm from TMC/MPD.
d) Neutron for dry TMC/MPD 0.005/0.1 wt % films obtained at reaction times 1, 10 and 20 min.
e) Corresponding SLD profile, where *z* is the distance normal to the film surface.
f) Film thickness *h* dependence on the reaction time.
g) Variation of *h* with MPD concentration after 10 min reaction time, with TMC 0.005 (blue, green) and 0.05 (red) wt %.
h) Variation of *h* with TMC concentration, with MPD 0.1 wt % (blue, red).
i–j) NR of a representative TMC/MPD^d membrane with 0.005/0.1 wt % and reaction time 1 min (corresponding to the first membrane in panel d), and the SLD profile, shown to be uniform across membrane thickness.

In this paper, we demonstrate the first neutron reflectivity study of polyamide RO membranes. By carefully tuning the reaction stoichiometry and time, planar PA membranes of a thickness of approximately 10 nm were successfully fabricated, exhibiting separation performances comparable with the crumpled counterparts extensively employed commercially. Moreover, we are able to controllably hydrate the membrane, and thus resolve its structure under *in operando* conditions.

Our neutron experiments are thus able to elucidate the nanoscale structure of single PA films, resolve the cross-sectional composition profile resulting from IP of TMC and MPD and the membrane response to water and, critically, correlate these physical properties with membrane performance. We find that PA film thickness increases linearly with reaction time, with a non-zero intercept interpreted as the onset of coherent film formation upon cluster aggregation. The cross-sectional profile is found to be uniform for the conditions investigated, which is a somewhat unexpected interfacial reaction, and water vapour hydration results in considerable swelling (up to 20 %). Importantly, film thickness appears to be predominantly set by MPD concentration, while TMC regulates water uptake and a favourable correlation between higher swelling and water uptake with permeance is found. Our data provide unique quantitative insight into the film nanostructure and performance, opening up pathways for the molecular engineering of polyamide membranes for desalination.

Gas confinement in compartmentalised coordination polymers for highly selective sorption

IN1-LAGRANGE and
time-of-flight spectrometer IN5

Metal-organic frameworks (MOFs) are hybrid, crystalline, porous materials composed of organic linkers and metallic nodes. Their exceptionally large porosity, flexible and dynamic networks and tuneable nature make them excellent candidates for multiple applications such as sorption and the storage of gases, catalysis, energy conversion and drug delivery [1]. In particular, MOFs with reduced pores have shown superior selectivity in gas separation, an improvement that is illustrated in this study using compartmentalised coordination polymers (CCPs). A combination of inelastic- and quasi-elastic neutron scattering, crystallographic and sorption studies, and magnetic measurements provides a complete understanding of the sorption process.

AUTHORS
M. Giménez-Marqués, **N. Calvo Galve**, **E. Coronado** and
G. Mínguez Espallargas (University of València, Spain)
M. Palomino, **S. Valencia**, **F. Rey**, **G. Sastre** and
J.L. Jordá (Polytechnic University of València, Spain)
I.J. Vitórica-Yrezábal (School of Chemistry, University of Manchester, UK)
M. Jiménez-Ruiz, **J.A. Rodríguez-Velamazán** and
M.A. González (ILL)

ARTICLE FROM
Chem. Sci. 8 (2017) 3109 – doi:10.1039/C6SC05122G

REFERENCES
[1] G. Maurin, C. Serre, A. Cooper and G. Férey, Chem. Soc. Rev. 46 (2017) 3104
[2] M. Giménez-Marqués, N. Calvo Galve, M. Palomino, S. Valencia, F. Rey, G. Sastre, I.J. Vitórica-Yrezábal, M. Jiménez-Ruiz, J.A. Rodríguez-Velamazán, M.A. González, J.L. Jordá, E. Coronado and G. Mínguez Espallargas, Chem. Sci. 8 (2017) 3109

One of the major challenges in our current society is climate change experienced through global warming as a result of human activity. In this scenario the efficient removal of greenhouse gases is required, and research has shown that this necessarily entails the capturing and further separation of those gases. Yet, the separation of gas mixtures with high selectivity is a challenging task that often requires an understanding of the specific interactions between the porous framework and the gases. In this context, MOFs with reduced pores have shown excellent separation performance with especially high selectivity.

For this purpose, herein [2] we propose the use of two isostructural, compartmentalised coordination polymers with confined cavities, CCP-1 and CCP-2, with general formula $[Fe(btzx)_3](X)_2$ (btzx = bistetrazole-*p*-xylene and X = ClO_4–, BF_4–), as shown in **figure 1a**.

These solids present ordered pockets (each with a volume of 132 Å³). Despite the lack of permanent channels, they can effectively trap a wide range of gas molecules in nanometer-sized internal cavities due to the flexible and dynamic nature of the framework, as shown in **figures 1b** and **1c**. More importantly, they are capable of capturing gas molecules from mixtures of gases in a highly selective manner, as unequivocally demonstrated by experimental breakthrough studies.

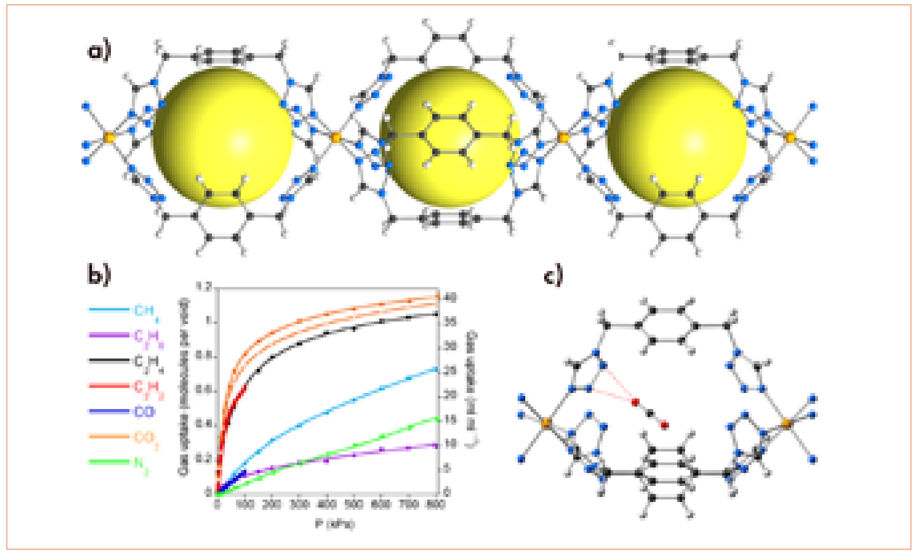

Figure 1
a) Partial crystal structure of the compartmentalised coordination polymers CCP-1 and CCP-2 emphasising the internal cavities (as yellow spheres).
b) Gas adsorption isotherms at 298 K.
c) Crystal structure of CCP-1/CCP-2 loaded with CO_2.

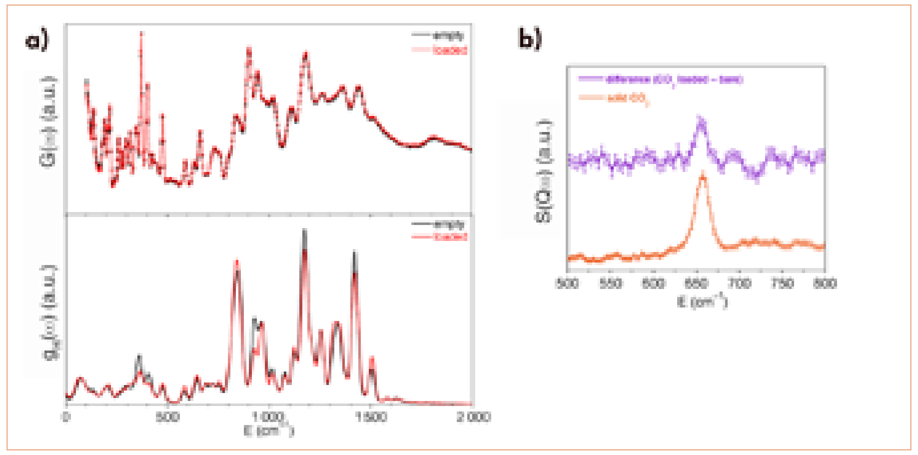

Figure 2
a) Comparison of the experimental INS spectra **(top)** and hydrogen partial density of states, $g_H(\upsilon)$, obtained from *ab initio* molecular dynamics simulations (AIMD) **(bottom)** for bare CCP-1 (black) and CCP-1 loaded with CO_2 (red).
b) Difference plot for experimental INS spectra CCP-1 loaded with CO_2 and bare CCP-1 (purple), and that of solid CO_2 (orange).

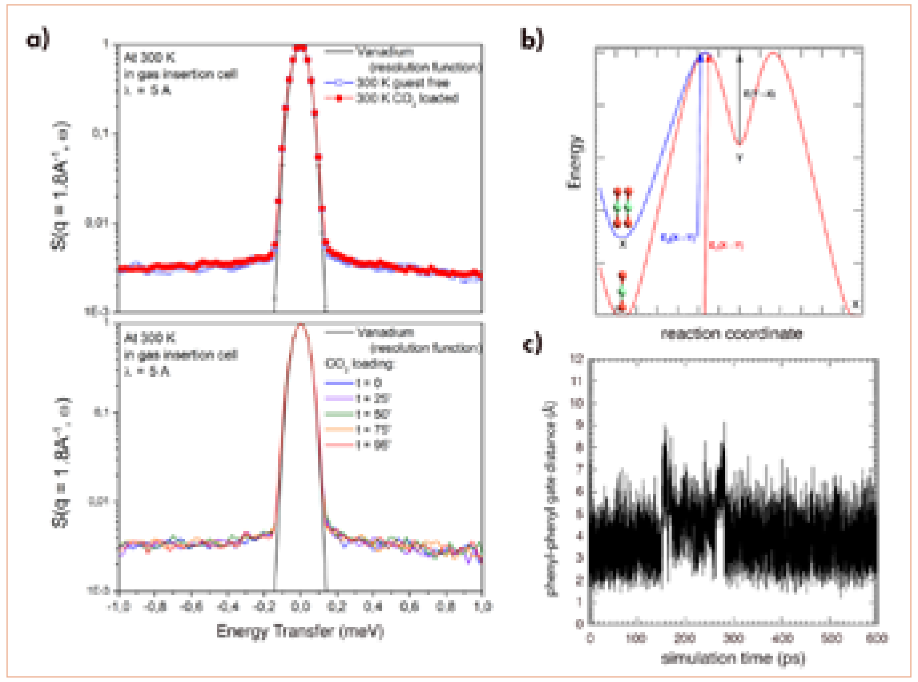

Figure 3
a) QENS spectra for bare and CO_2-loaded CCP-1 at 300 K **(top)** and *in situ* measurement during CO_2 loading **(bottom)**.
b) Energetic diffusion scheme.
c) Interphenyl distance showing the gate-opening mechanism in CCP-1 during the 600 ps molecular dynamics calculation where the intercavity transition of a CO_2 molecule can be observed.

Neutrons are an excellent tool for investigating the process of adsorption in these MOF materials. Inelastic neutron scattering (INS) and quasi-elastic neutron scattering (QENS), together with complementary molecular dynamics (MD) simulations (*ab initio* and classical), provided a sensitive means of determining the mechanism of entrance for CO_2 molecules into the framework and revealing the actual location and binding of the gas molecules in the cavities. The interaction between the adsorbed CO_2 molecules and the framework was studied by means of INS and *ab initio* MD simulations. Both results are in agreement and show minor changes in the peak intensities between the bare and loaded system, revealing a weak CO_2–framework interaction (**figure 2a**); more interestingly, the neutron vibrational spectrum of adsorbed CO_2 has been detected for the first time in a MOF material (**figure 2b**).

The gas diffusion mechanism was revealed through a combination of QENS and MD simulations (**figure 3**). QENS is highly sensitive to the movement of hydrogen atoms, and we used this technique to probe the dynamics of the framework upon CO_2 sorption. Thus, CO_2 diffusion into the internal cavities can be explained by a gate-opening mechanism of the phenyl rings, which affords a minor decrease in intensity in some Bragg peaks and no significant change in the QENS spectra after gas sorption (**figure 3a**). This minor change is probably due to the fast movement of the phenyl rings allowing the entrance of CO_2 molecules, with only some phenyl rings rotating at any specific moment and the vast majority remaining static as confirmed by MD simulations (**figure 3c**).

Finally, these pocket-like crystalline solids exhibit magnetic bi-stability, a spin-state switching that has been shown to be affected by the entrapment of different gases such as CO_2, CH_4, ethane or ethylene molecules. This intrinsic sensing behaviour has also served to elucidate the strength of the gas-framework interaction in these solids.

In summary, this multi-technique, detailed analysis has provided a clear assessment of the gas sorption process in these compartmentalised crystalline solids, which have been revealed to be excellent for selective sorption.

Making cars light and safe

Strain analyser for engineering applications SALSA

Materials are the basis of any technological product and determine its performance, lifetime and ecological impact to a large extent. Ductility, hardness, weight, formability and temperature-behaviour are parameters for selecting the optimum material for a specific application. Let us take the example of a car. The passenger cabin is reinforced using very hard and stiff material in order to protect its passengers. In contrast, the crumple zone is made of ductile steel in order to absorb and spread the energy of an impact by deformation and reduce the acceleration of the passengers.

Figure 1

Robotic spot welding in car manufacturing: thousands of spot welds are made when assembling the various steel parts of a car body. Image taken from http://weldingsource.org/new-study-finds-limits-spot-welding-boron-steel/

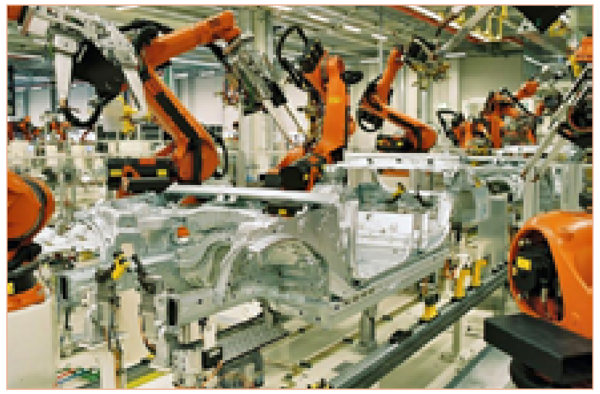

AUTHORS
N.D. Raath and **D. Hughes** (Warwick Materials group, Coventry, UK)
T. Pirling (ILL)

ARTICLE FROM
Metall. Mater. Trans. A 48A (2017)

REFERENCES

[1] A. Bardelcik, M.J. Worswick, S. Winkler and M.A. Wells, Int. J. Impact Eng. 50 (2012) 49
[2] D. Mohr and F. Ebnoether, Int. J. Solids Struct. 46 (2009) 3535
[3] M. Naderi, L. Durrenberger, A. Molinari and W. Bleck, J. Mater. Sci. Eng. A 478(1) (2007) 130
[4] H.S. Choi, G.H. Park, W.S. Lim and B.M. Kim, J. Mech. Sci. Technol. 25 (2011) 1543
[5] Y. Yu, C. Wang, S. Chen and Z. Lu, Adv. Mater. Res. 339 (2011) 375
[6] T. Lienert, T. Siewert, S. Babu and V. Acoff, *ASM Handbook Volume 6A Welding Fundamentals and Processes.* ASM International (2011) 488
[7] N.D. Raath *et al.*, Metall. Mater. Trans. A 48A (2017) 2900

Joining together all these different materials is no trivial task. Not only is not every material compatible with every joining method, but also the thermal impact involved changes the microstructure of the materials. As a result, the properties of the—initially so carefully tailored—materials change, making the joint the weakest part of the whole structure. Therefore, the optimisation of joining techniques and the characterisation of joints play an essential role in making mechanical structures functional and safe. This requires a combination of analysis tools. Neutron stress determination plays an important role here, since it is a non-destructive technique providing stress profiles from the bulk of the material to its surface.

Returning to car manufacturing, press-hardened boron steel is classed as an ultra-high-strength steel. It is used in the automotive industry in structural and anti-intrusion components such as B-pillars, bumper reinforcements, roofs and side rails [1–3]. The main attraction of using boron steel is the weight reduction achieved through gauge reduction, and the greater passenger safety it provides.

Figure 2

Experimental set-up for stress determination on SALSA. Two radial, focusing collimators provide the focused 0.6 mm-wide beam for the samples.

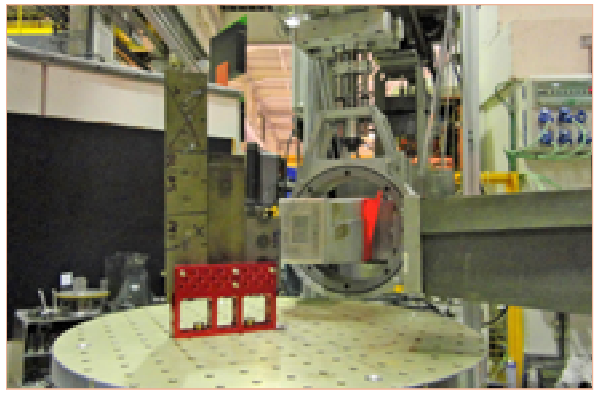

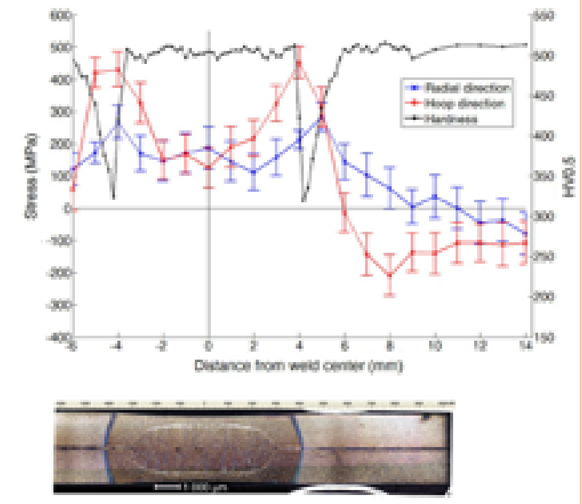

Figure 3

Comparison between hardness and residual stress. Tensile stresses that weaken the material correlate well with the hardness profile. The picture below shows the cross-section of the weld and the two metal sheets. Stresses and hardness have been determined in one of the sheets.

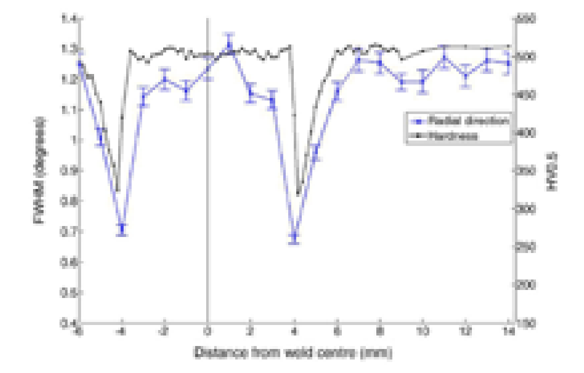

Figure 4

Hardness profile and width of diffraction peaks. The drop in peak width clearly indicates the presence of the softer, ferritic phase in the HAZ, which correlates with a drop in hardness.

Boron steel microstructure is chiefly composed of a very hard form of steel crystalline structure known as martensite. However, martensite easily decomposes to lower strength microstructures when the steel is exposed to beyond a certain temperature. This tempering effect becomes problematic when boron steel is welded.

A major joining method in the automotive industry is resistance spot welding, with several thousand welds being made on a single car. During resistance spot welding a high electric current is sent through the parts for a very short time. The metals melt instantaneously at the interface and cool down rapidly as a result of cooled welding grips and the surrounding base metal. A decreasing temperature gradient extends outwards from the weld centre (nugget), resulting in altered microstructures known as the heat-affected zone (HAZ). For boron steel welds in particular there is a steep gradient of material properties in the HAZ which, it has been established, is due to the tempering of martensite [4, 5]. This results in a soft area surrounded by a hard nugget and base material.

The difference in material properties between the HAZ and nugget/base material may enhance the stress concentration [6]. Therefore, it is crucial to characterise the gradients of material properties that occur through a spot weld. This has been done in a collaboration between the Warwick Manufacturing Group WMG of Warwick University and the SALSA team at the ILL [7].

Sheets of press-hardened boron steel and dual-phase steel were resistive spot-welded using standard industrial processes. The sheets were 1.5 mm thick and two different welds were compared.

A specific task of the project was to identify the correlation between hardness and residual stress. In order to access the weld nugget, samples had to be sliced for micro-hardness testing. Since cutting relaxes stresses, stress determination was performed beforehand. This is where our stress diffractometer SALSA comes into play: the neutron technique is non-destructive and provides maps of the full stress tensor with millimetre resolution. The 0.6 mm-wide beam on SALSA provides the required resolution for measurements in only 1.5 mm-thick steel sheets.

Figure 3 shows the stress profile of the boron steel sheet across the weld in comparison with the hardness profile. The photograph shows the weld region on the same scale. Stresses become tensile towards the nugget, with a maximum in the HAZ (4–5 mm from the weld centre), where the hardness shows a pronounced minimum. This can be explained by the fact that during tempering, martensite loses carbon, becomes less tetragonal and even reverts to a softer, ferritic phase. This is supported by the peak width evolution shown in **figure 4**. The width of diffraction peaks from the cubic ferritic phase is smaller than that of the different tetragonal martensitic phases. The coincidence with the hardness measurement is remarkable.

This study has demonstrated the need for alternative welding methods that can extend the lifetime of widely-used boron steel to its full potential. With several thousand welds being made on a single car, future work on non-destructive welding techniques and post-spot welding treatments will enable the boron steel components of cars to maintain their hardness and avoid residual stress. Importantly, this will ultimately provide top-tier passenger safety in stronger yet lighter vehicles.

Direct measurement of individual phonon lifetimes in the clathrate compound $Ba_{7.81}Ge_{40.67}Au_{5.33}$

Time-of-flight spectrometer IN5
Three-axis spectrometer IN22

The engineering of thermal conductivity in semiconducting materials is a central issue in the development of modern nano- and microtechnologies. Low thermal conductivity is important in materials used in technology products as it provides thermal insulation and thus the reduction of heat transfer, ensuring that products do not overheat. It is also important for thermoelectrics, as it drives its efficiency. This study provides a direct quantitative measurement of phonon lifetimes in a clathrate, providing a novel picture of thermal conductivity in complex materials.

Figure 1
Illustration of the atomic structure of the $Ba_{7.81}Ge_{40.67}Au_{5.33}$ clathrate.

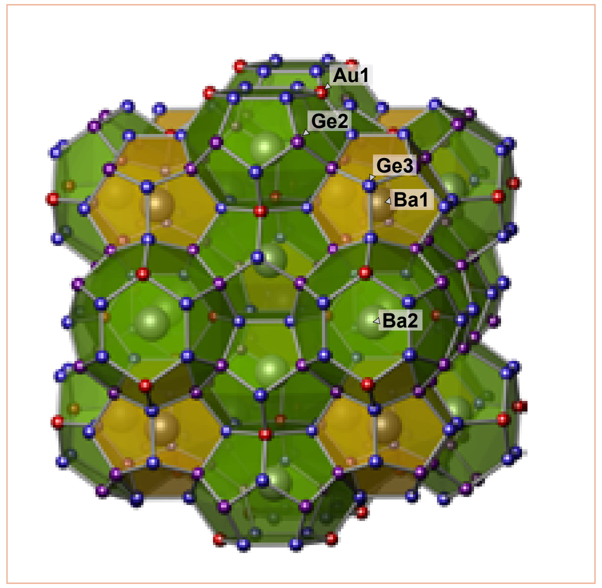

AUTHORS
M. de Boissieu (Université Grenoble Alpes, CNRS and INP Grenoble, France)
P.-F. Lory (ILL, Université Grenoble Alpes, CNRS and INP Grenoble, France)
S. Pailhès and **V.M. Giordano** (University of Lyon, France)
H. Euchner, **M. Ikeda**, **P. Tomeš** and **S. Paschen** (TU Vienna, Austria)
M. Baitinger and **Y. Grin** (Max Plank Insitute, Dresden, Germany)
M. Mihalkovič (Slovak Academy of Science, Bratislava, Slovakia)
C. Allio (Goethe University, Frankfurt, Germany)
M.R. Johnson, **H. Schober** and **J. Ollivier** (ILL)
Y. Sidis (LLB and CNRS, CEA, Gif-sur-Yvette, France)
F. Bourdarot and **L.P. Regnault** (Université Grenoble Alpes and CEA, INAC, Grenoble, France)

ARTICLE FROM
Nat. Commun. 8 (2017) – doi:10.1038/s41467-017-00584-7

REFERENCES
[1] H. Euchner, S. Pailhès, L.T.K Nguyen *et al.*, Phys. Rev. B 86 (2012) 224303
[2] S. Pailhès, H. Euchner, V.M. Giordano *et al.*, Phys. Rev. Lett. 113 (2014) 25506
[3] P.-F. Lory, S. Pailhès, V.M. Giordano *et al.*, Nat. Commun. 8 (2017) 491

Understanding how heat propagates in a material is a key issue in many different fields. For instance, with thermoelectric materials, which can transform heat into electricity, researchers try to reduce the thermal conductivity—a key parameter in the efficiency equation of these materials—as much as possible. However, an understanding of the detailed mechanism of heat propagation in structurally complex compounds is still lacking. The heat is carried out by quasi-particles named phonons that travel in the material at the speed of sound. While travelling in a material a phonon collides with defects or other phonons, as billiard balls would do, in turn reducing the thermal conductivity. The more collisions there are, the smaller the thermal conductivity. This is measured by the mean distance a phonon travels without collision (phonon mean free path) or by the mean time between two phonon collisions (phonon lifetime—the phonon mean free path is the product of the phonon lifetime by phonon velocity).

A multi-partner study within the European C-MAC network has experimentally measured at the ILL, for the first time, the phonon lifetime of a thermoelectric material clathrate renowned for its very low, 'glass-like', thermal conductivity. This material is a periodic packing of cages constructed with Ge and Au atoms enclosing heavy Ba atoms, as illustrated in **figure 1**. For a long time it was believed that the glass-like thermal conductivity of clathrates resulted from 'phonon glass' behaviour, with very short mean free paths of the order of interatomic distances (*i.e.* 0.3-0.5 nm).

As has been shown in previous experiments on clathrates [1, 2], an overview of the dispersion measured on three-axis instruments at the LLB and on the time-of-flight spectrometer IN5 at the ILL demonstrates that the acoustic phonons that are effective in carrying heat are in fact confined to a very limited wave vector and energy range, typically of between 0 to 6 meV as shown in **figure 2**.

Measuring long lifetime with triple-axis instruments is challenging because of the phonon energy resolution that can be achieved. Using a high resolution set-up and detailed comparison with a Ge reference sample already gives a very long, measured phonon mean free path. However, a more conclusive experimental input is achieved using the neutron spin-echo resonance (NRSE) techniques installed on the ILL's IN22 three-axis spectrometer. Thanks to the extremely high quality of the single grain sample used, with an overall mosaic spread equal to 0.01 °, a phonon mean free path larger by one order of magnitude can be measured.

Our results were very surprising: a phonon mean free path ranging from tens to hundreds of nm, much larger than that expected in the 'phonon glass' scenario [3]. In particular, even close to the Brillouin zone boundary, phonon mean free paths were of the order 15 nm, *i.e* 10 unit cells. This is shown in **figure 3**, where the phonon lifetime is illustrated by the decay of the wave representing the phonon frequency.

Such a result can in fact be reconciled with a simple theory of heat propagation, once the number of acoustic phonons carrying heat is properly taken into account.

These new experimental results challenge current phonon lifetime simulations and will serve as a reference for any future proposed model.

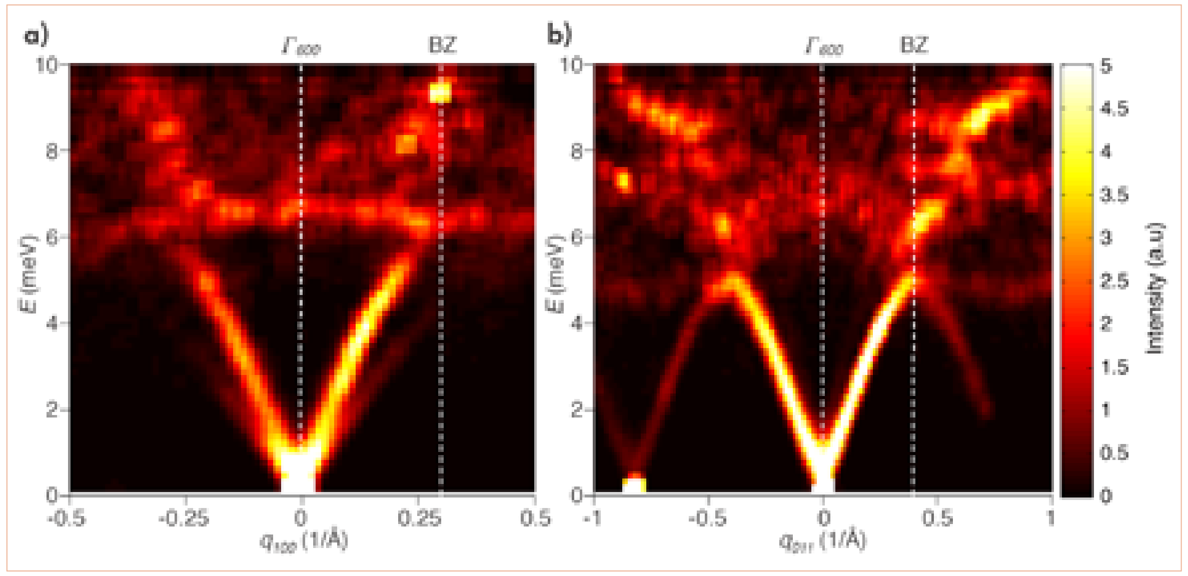

Figure 2
Two-dimensional inelastic neutron scattering intensity distribution as measured on the neutron time-of-flight spectrometer IN5 at room temperature around the strong zone centre Γ_{600} ($Q = 3.6$ Å^{-1}).
a) Longitudinal acoustic (LA) phonons measured along the [100] direction. Well-defined propagating excitations are only observed for LA modes with an energy lower than 6 meV.
b) Transverse acoustic (TA) phonons propagating along [011] and polarised along [100]. Well-defined propagating excitations are only observed for TA modes with an energy lower than 5 meV.

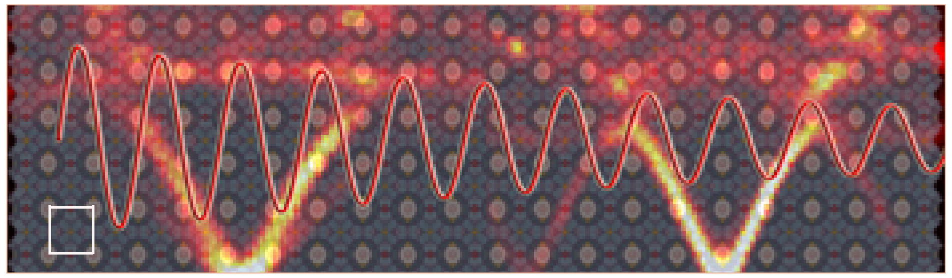

Figure 3
The background illustrates the periodic structure of the clathrate, with a unit cell (shown as a white square in on the left with a parameter 1 nm). The Ba atoms in red are enclosed in the cages. The coloured curved is the inelastic neutron scattering as measured on the neutron time-of-flight spectrometer IN5 at room temperature around the strong zone centre Γ_{600} ($Q = 3.6$ Å^{-1}). The decaying sinusoidal curve illustrates the phonon propagation and its time decay (or lifetime) for a phonon wavelength equal to 2 nm.

What is the actual local crystalline structure of uranium dioxide? A new perspective for the most used nuclear fuel

Disordered materials diffractometer D4

Up until now, uranium dioxide (UO_2), the most used nuclear fuel, was said to have an Fm-3m crystalline structure and its properties were modelled under this assumption. Recent X-ray diffraction results [1] have questioned this assumption by finding evidence of shorter than expected U-O bonds. We investigated the atomic structure of UO_2 using neutron diffraction to shed light on this apparent contradiction, since neutrons are more sensitive than X-rays to O atoms.

AUTHORS

L. Desgranges, **Y. Ma** and **Ph. Garcia** (CEA, DEN, DEC Saint-Paullèz-Durance, France)
G. Baldinozzi and **D. Siméone** (SPMS, LRC Carmen, CNRS Centrale Supélec and CEA, DEN, DMN Gif-sur-Yvette, France)
H.E. Fischer (ILL)

ARTICLE FROM

Inorg. Chem. (2017) – doi:10.1021/acs.inorgchem.6b02111

REFERENCES

[1] B. Skinner *et al.*, Science 346 (2014) 984
[2] L. Desgranges, Y. Ma, Ph. Garcia *et al.*, Inorg. Chem. 56 (2017) 321
[3] P. Ruello *et al.*, J. Phys. Chem. Solids 66 (2005) 823

The neutron diffraction experiment was performed using the D4 neutron diffractometer on a UO_2 sample having the form of two sintered pellets (8.3 mm in diameter and 14 mm in height), from 300 K to 1 273 K. We first analysed the diffraction pattern using the Rietveld-refinement software JANA, by putting uranium and oxygen atoms in their regular positions in the Fm-3m space group but giving them anharmonic thermal motion. Thermal motion parameters describe how, on average, an atom moves away from its central equilibrium position. While the uranium atoms in UO_2 have an isotropic thermal motion distribution, Rietveld refinement showed that the oxygen atoms move preferentially along four different directions that correspond to the four equivalent [1 1 1] vectors in the Fm-3m crystalline structure.

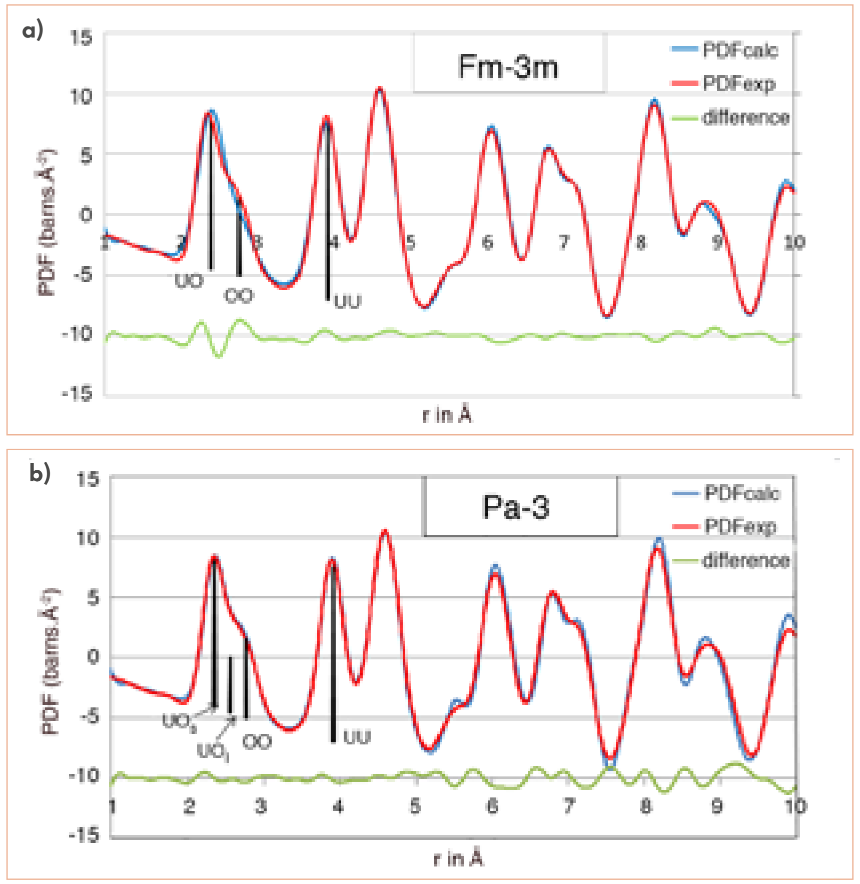

Figure 1

Experimental PDF(r) at 1 273 K (red) compared with fitted PDF(r) (blue) using Fm-3m space group **(a)** and Pa-3 space group **(b)**. The difference between fitted and observed curves is represented as the green curve, and the first three distances, UO (UO_s and UO_l corresponding to short and long UO distance in Pa-3), OO and UU are indicated by black sticks.

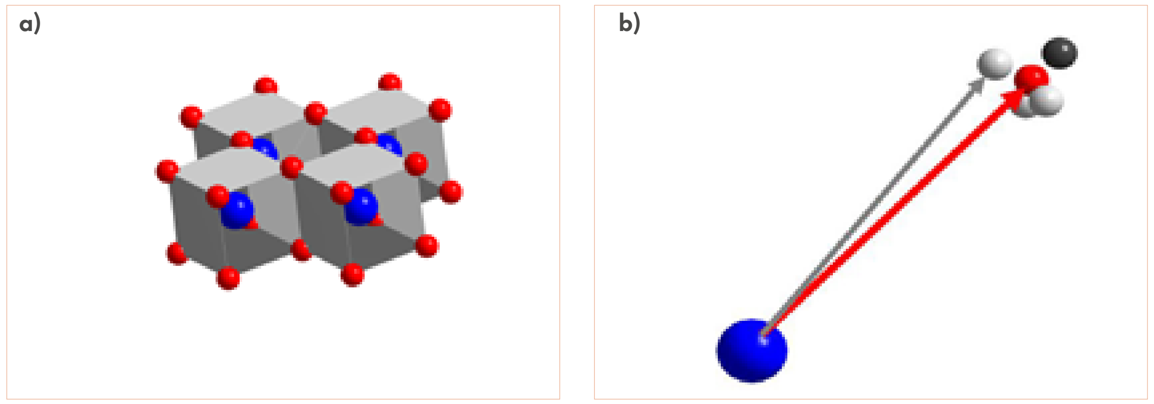

Figure 2

a) Crystal structure of UO_2 in Fm-3m space group.
b) Oxygen position as a function of the structural model: oxygen atom at its regular position in Fm-3m space group (red); oxygen atom in Pa-3 having short UO distance (grey); oxygen atom in Pa-3 having long UO distance (black). Averaging black and grey atoms leads to the regular Fm-3m configuration.

However, since Rietveld refinement analyses only the elastic part of Bragg peak intensities, disregarding diffuse scattering, it represents the crystal structure of the sample as averaged over time and also over all the unit cells in the sample. It is therefore possible that different oxygen atoms in UO_2 have different equilibrium positions in different unit cells, but when averaged over all the sample's unit cells it looks like a single position but with a particular shape of thermal motion as described above. In order to clarify this, we turned to PDF-analysis, a technique that makes use of all the scattered intensity, including the diffuse scattering that results from local variations in atomic structure, *i.e.* from local structural disorder [2].

The pair-distribution function PDF(r) is obtained by Fourier transform of the diffraction pattern after correction for experimental factors, and represents an ensemble-average of quasi-instantaneous local structures in the sample in the form of a real-space function whose amplitude is proportional to the probability of finding an atom at a distance r from an average atom at the origin.

Our UO_2 sample's PDF(r) was fitted with the Fm-3m space group at 1 273 K. The fit converged quite well for $r > 6$ Å but was not able to fit the first two peaks corresponding to UO and OO distances properly (**figure 1a**). The measured UO distance was indeed a bit shorter than that in the Fm-3m structure, which is consistent with [1]. In order to determine the nature of the local disorder, the same PDF(r) at 1 273 K was fitted with the Pa-3 space group. Pa-3 symmetry can be obtained from Fm-3m symmetry by moving the oxygen atoms out of their regular positions along (1 1 1) directions, generating a distorted oxygen cube with two longer distances and six shorter distances, as shown in **figure 2**. The Pa-3 symmetry was chosen firstly because this oxygen displacement is consistent with the direction of apparent oxygen thermal motion resulting from Rietveld refinement, and secondly by comparison with other metal dioxides (SnO_2, GeO_2, SiO_2) that adopt Pa-3 or Fm-3m crystalline structures depending on pressure. The Pa-3 fit to the PDF(r) was very good for short-range order ($r < 6$ Å) but poor for longer range order (**figure 1b**). Therefore the UO_2 crystalline structure can be interpreted as domains of Pa-3 local symmetry but with different orientations that spatially average over longer distances to the Fm-3m symmetry observed by Rietveld refinement. These domains could be either static or dynamic (*i.e.* changing or moving with time); this could not be identified by the PDF(r) representing an ensemble-average of quasi-instantaneous 'snapshots' of local structures across the sample.

Our neutron diffraction data have shown convincingly that UO_2 has Fm-3m symmetry only when averaged over long distances, having Pa-3 symmetry at short range. Although unexpected, this finding is consistent with some properties already observed in UO_2. In particular, the specific heat of UO_2 shows an unexpected increase, starting from around 1 000 K and ending up at nearly twice the value expected from the Dulong–Petit Law [3]. This very unusual behaviour has been fitted empirically but is still misunderstood. The existence of disorder induced by Pa-3 domains could increase the entropy of UO_2 and thus be the reason for the increased specific heat.

More work is needed to understand what causes the local Pa-3 order, whether it is static or dynamic, and especially, what is the nature of the interface between different Pa-3 domains. This new description of uranium dioxide at high temperature, in terms of Pa-3 domains, could provide new leads for improving the understanding of high temperature UO_2 behaviour.

Investigation of the relationship between the structure and electrical conductivity of the novel oxide ionic conductor $Ba_3MoNbO_{8.5}$

High-resolution two-axis diffractometer D2B

In a fuel cell the reaction between hydrogen and oxygen produces water and electricity and provides a clean and more efficient alternative to fossil fuels. An important ambition is to lower the running temperature of solid oxide fuel cells (SOFCs) to temperatures above 650 °C, as this will reduce costs, increase reliability and lifetime, and make the wide range of SOFC applications more economical [1]. We have recently identified a novel hexagonal perovskite derivative oxide ion conductor, $Ba_3MoNbO_{8.5}$ [2], which exhibits significant oxide ion conductivity comparable with other prominent oxide ion conductors at 600 °C.

AUTHORS

S. Fop, **E.J. Wildman**, **J.M.S. Skakle** and **A.C. McLaughlin**
(University of Aberdeen, UK)
J.T.S. Irvine and **P.A. Connor** (University of St Andrews, UK)
C. Ritter (ILL)

ARTICLE FROM

Chem. Mater. 29 (2017) – doi:10.1021/acs.chemmater.7b01298

REFERENCES

[1] E.D. Wachsman and K.T. Lee, Science 334 (2011) 935
[2] S. Fop, J.M.S. Skakle, A.C. McLaughlin, P. Connor, J.T S Irvine and E J. Wildman, J. Am. Chem. Soc. 138 (2016) 16764
[3] S. Fop, E.J. Wildman, J.T.S. Irvine, P.A. Connor, J.M.S. Skakle, C. Ritter and A.C. McLaughlin, Chem. Mater. 29 (2017) 4146

$Ba_3MoNbO_{8.5}$ crystallises in a crystal structure that is a hybrid of the 9R hexagonal perovskite and palmierite structures (**figure 1**). This is a novel and so far unique crystal structure. Units of $(Mo/Nb)O_4$ and $(Mo/Nb)O_6$ coexist within the structure, forming a disordered arrangement of Mo/Nb tetrahedra and octahedra. $Ba_3MoNbO_{8.5}$ is an oxide ion conductor with negligible electronic conductivity in air/O_2. A small amount of electronic conduction is observed in air/5 % H_2 in Ar. $Ba_3MoNbO_{8.5}$ is the first hexagonal perovskite to display such promising oxide ion transport at low temperature with a bulk conductivity of 2.2 x 10^{-3} S cm^{-1} at 600 °C [2].

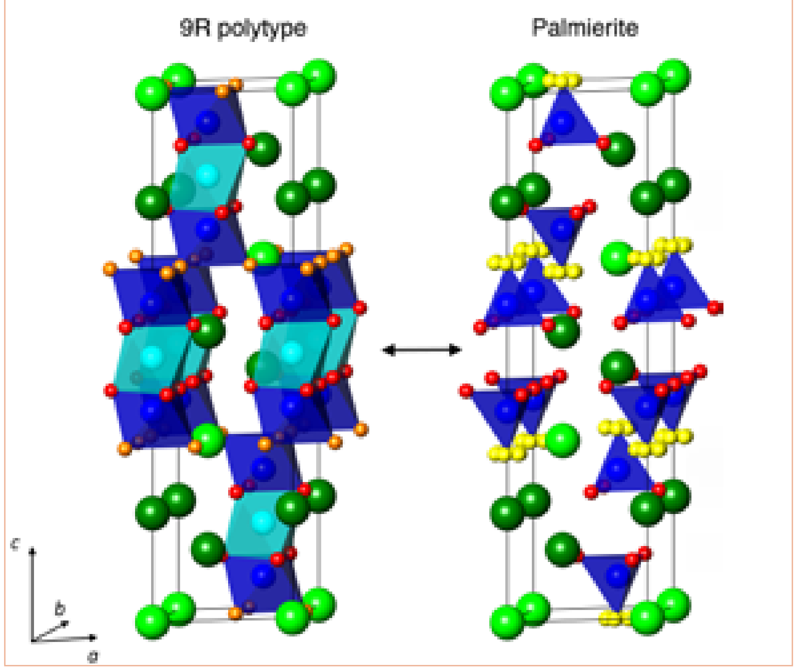

Figure 1

Crystal structure of $Ba_3MoNbO_{8.5}$. The hybrid structural model formed by the superimposition of the 9R-polytype and the palmierite sub-units representing the average structure of the system. Colours indicate: light green Ba(1), dark green Ba(2), blue M(1), cyan M(2), red O(1), orange O(2) and yellow O(3).

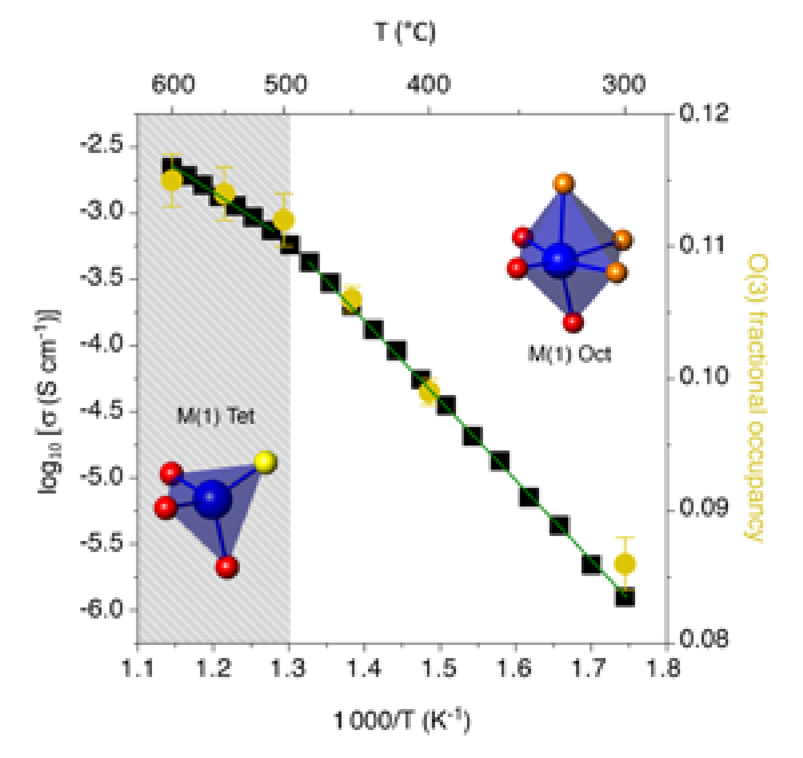

Figure 2

A comparison of the thermal variation of the fractional occupancy of O(3) and the Arrhenius plot of the bulk conductivity of $Ba_3MoNbO_{8.5}$.

In order to determine whether there is a relationship between the electrical properties and crystal structure, we performed a variable temperature, powder neutron diffraction study of $Ba_3MoNbO_{8.5}$ on the high-resolution D2B diffractometer between 25 °C and 600 °C. The powder neutron diffraction data confirm that $Ba_3MoNbO_{8.5}$ is phase-pure and crystallises in the hybrid 9R/palmierite structure (space group *R*-3*m* H, **figure 1**) at all temperatures. The temperature dependency of the *a* and *c* cell parameters exhibits non-monotonic behaviour with a clear change in slope observed above 300 °C [3], suggesting a possible structural modification. Large changes to the Mo/Nb and oxygen site occupancies are observed above 300 °C. Above this temperature a sudden increase in the M(1) (Wykoff site 6*c*) fractional occupancy, with a concomitant decrease in the M(2) fractional occupancy, is apparent. The same behaviour is observed for the O(2) and O(3) (Wykoff site 3*b*) fractional occupancies, which respectively decrease and increase above 300 °C. Above 500 °C there is little further variation in the fractional occupancies of M(1), M(2), O(2) and O(3). An overall oxygen stoichiometry of 8.5 was obtained at all temperatures. Ba(1), Ba(2) and O(1) form the rigid part of the $Ba_3MoNbO_{8.5}$ structure, while M(1), M(2), O(2) and O(3) are responsible for the variable tetrahedral/octahedral coordination. Therefore, changes in the occupancies of the latter atoms indicate that the structure is able to adjust the ratio of tetrahedra to octahedra and, consequently, the oxygen/vacancy distributions as the temperature increases. The results demonstrate that the number of $(Mo/Nb)O_4$ tetrahedra increases upon heating above 300 °C.

Figure 2 shows the temperature variation of the fractional occupancy of O(3) (situated at the apex of the tetrahedra (**figure 1**)), and the Arrhenius plot of the bulk conductivity of $Ba_3MoNbO_{8.5}$. There is a clear correlation between the number of tetrahedra within the crystal lattice and the electrical properties at temperatures between 300 °C and 600 °C. The results clearly demonstrate that the magnitude of ionic conductivity observed in $Ba_3MoNbO_{8.5}$ is strongly related to the number of $(Mo/Nb)O_4$ tetrahedra within the average crystal structure. Increasing the number of $(Mo/Nb)O_4$ tetrahedra most likely offers more low-energy transition paths for transport of the O^{2-} ions, further enhancing the conductivity.

In summary, this variable temperature neutron diffraction study demonstrates an unusual structural rearrangement in $Ba_3MoNbO_{8.5}$ above 300 °C so that the ratio of tetrahedra to octahedra increases and, consequently, the oxygen/vacancy distribution changes as the temperature increases. We propose that the conductivity is enhanced by the increase in the proportion of MO_4 tetrahedra between 300 °C and 600 °C, and that substitution of Nb^{5+} with an aliovalent cation with preferential tetrahedral co-ordination may be a way to further optimise conductivity at low temperature in $Ba_3MoNbO_{8.5}$.

CHEMISTRY AND CRYSTALLOGRAPHY

$Mg_xMn_{2-x}B_2O_5$ pyroborates (2/3 ≤ x ≤ 4/3): high-capacity and high-rate cathodes for Li-ion batteries

High-resolution two-axis diffractometer D2B

The inherent stability and high operating voltage of polyanion materials makes them attractive candidates for positive electrodes in Li-ion batteries. However, low capacities and poor ionic conductivity reduce their potential applications. In this work we demonstrate that following electrochemical demagnesiation, magnesium manganese pyroborates can act as high-capacity, high-rate cathodes in Li-ion batteries. In $MgMnB_2O_5$ we demonstrate complete removal of Mg^{2+} and the subsequent reversible intercalation of 1.5 Li^+ ions per formula unit.

AUTHORS

H.F.J. Glass, **Z. Liu**, **P.M. Bayley**, **C.P. Grey** and **S.E. Dutton** (University of Cambridge, UK)
E. Suard (ILL)
S.-H. Bo (Stony Brook University and Lawrence Berkeley National Laboratory, US)
P.G. Khalifah (Stony Brook University and Brookhaven National Laboratory, US)

ARTICLE FROM

Chem. Mater. 29 (2017) – doi:10.1021/acs.chemmater.7b00177

ACKNOWLEDGEMENTS

This work was supported by the EPSRC Cambridge NanoDTC, EP/G037221/1, and the Winton Programme for the Physics of Sustainability.

Pyroborates, $M_2B_2O_5$, are a class of borate polyanion containing divalent ions. The structure of pyroborates (**figure 1**) is highly versatile, with a wide range of divalent ions found to occupy the two *M* sites. The low mass and reduced oxygen content of the pyroborate means that a change in the polyanion unit, from borate BO_3^{3-} to pyroborate, does not result in a significant drop in theoretical capacity as is found for the heavier pyrophosphate, $P_2O_7^{2-}$, unit. Prior work on $Mg_xFe_{2-x}B_2O_5$ proposed the presence of mobile magnesium ions, but these have not been studied in Li-ion batteries. We studied the magnesium manganese solid solution $Mg_xMn_{2-x}B_2O_5$ (where x = 2/3, 1 or 4/3), exploring both the removal of Mg-ions and the subsequent Li-ion intercalation in a Li-ion battery.

Figure 1
a) Polyhedral model of $M_2B_2O_5$; in the case of $Mg_xMn_{2-x}B_2O_5$ the Mg and Mn ions are disordered over the two *M* sites.
b) Cycling of $MgMnB_2O_5$ at C/25: initial charge (Mg removal), red line; subsequent cycling *vs* Li for ten cycles, grey lines; and cycling *vs* Li after 100 cycles, black line.

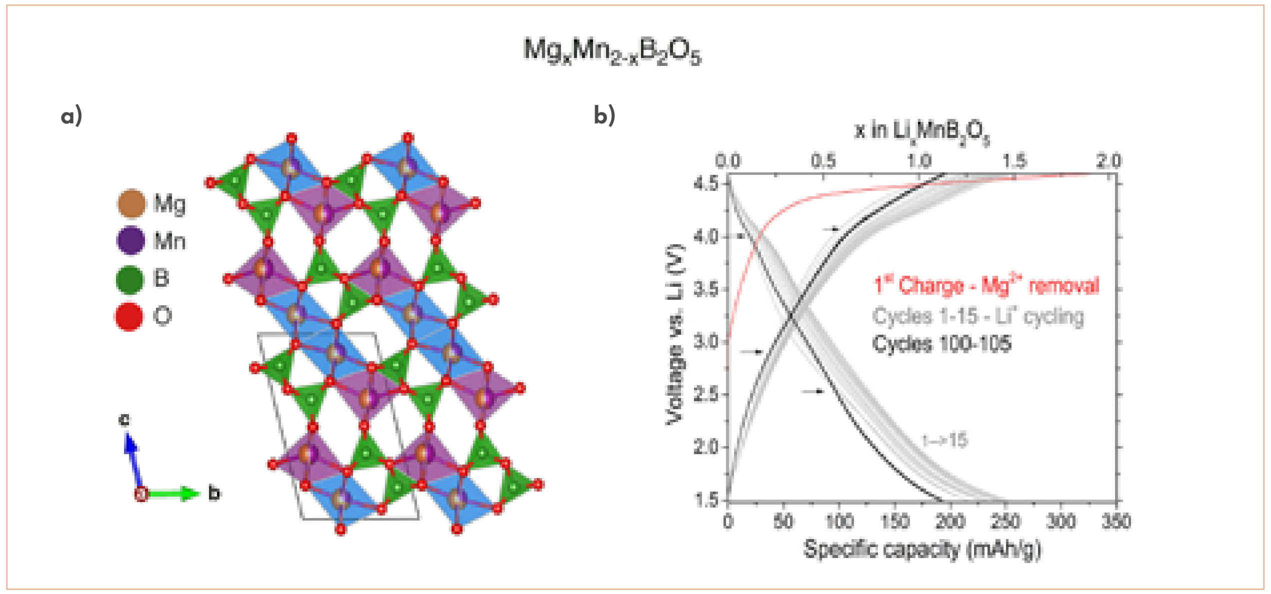

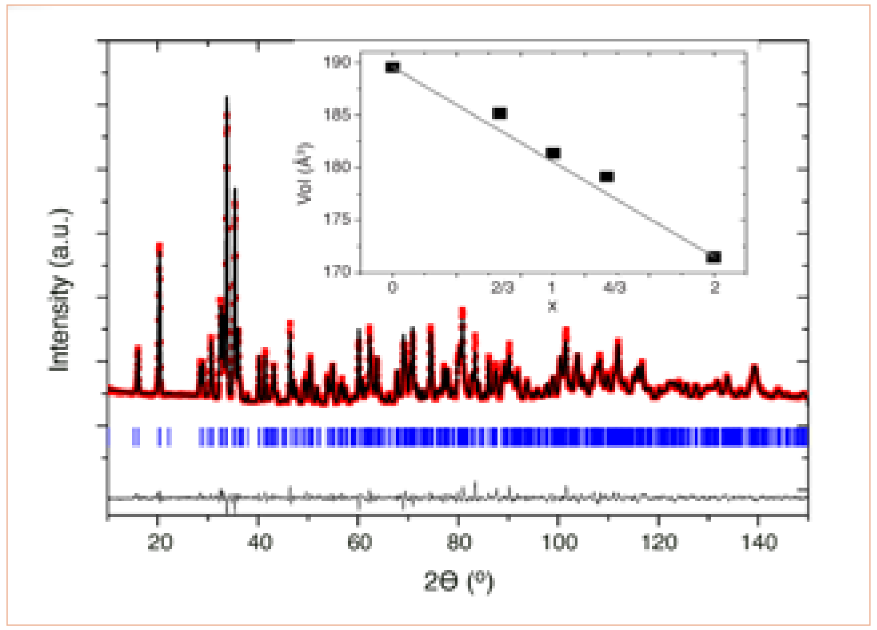

Figure 2

Neutron diffraction pattern (red dots) and fit (black line) of $Mg_{4/3}Mn_{2/3}B_2O_5$. Allowed Bragg reflections are shown as blue tick marks. **Inset)** The change in cell volume in $Mg_xMn_{2-x}B_2O_5$ as a function of x, as determined from neutron and X-ray powder diffraction.

We used neutron diffraction on the high-resolution powder diffractometer D2B to study changes in the structure of the $Mg_xMn_{2-x}B_2O_5$ solid solution (**figure 2**). We found that the Mn and Mg are disordered over the two metal sites, with some preference for Mn to occupy the larger, more distorted, site. The refined volumes shown in the inset of **figure 1** vary according to Vegard's law, with higher Mn content increasing the unit cell volume.

Despite the disorder in the occupation of the Mg and Mn sites in $MgMnB_2O_5$, we found that it is possible to remove all the Mg (**figure 1b**). The presence of labile Mg^{2+} differs from other Mg-containing cathodes, where Mg^{2+} doped on transition metal sites is assumed to be electrochemically inactive. Further cycling *vs* lithium results in reversible intercalation of ~ 1.5 Li^+ ions (250 mA h g^{-1}). We studied the changes on cycling through *ex situ* ^7Li NMR, magnetometry and neutron diffraction measurements. Our results show that the pyroborate structure is retained, even when 50 % of the divalent ions are removed from the structure. Furthermore, whilst there is a large change in volume following removal of Mg^{2+} (4.2 %), subsequent Li^+ insertion results in an expansion of just 1 %; an unusually small volume change given the relatively high capacity.

We found that all members of the $Mg_xMn_{2-x}B_2O_5$ solid solution were electrochemically active. In the case of Mg-rich $Mg_{4/3}Mn_{2/3}B_2O_5$ we were able to remove ~ 0.5 Mg^{2+} ions and subsequently reversibly intercalate ~ 1 Li^+ ion, whereas in the case of Mg-poor $Mg_{2/3}Mn_{4/3}B_2O_5$ we observed significantly lower reversible capacity. We interpret this as being the result of poor ionic and/or electrical conductivity, possibly due to excess manganese blocking pathways for the diffusion of Li/Mg.

This study shows that the pyroborates are a promising family of materials for high-capacity, high-rate, Li-ion cathodes. The lightweight borate framework leads to significantly higher gravimetric capacities than those observed for the pyrophosphate polyanions. The use of polyanion structures where Li^+ can replace labile Mg^{2+} without disrupting crystal structure opens up a new avenue for novel Li-ion cathode material with high-energy densities. Facile Mg^{2+} removal in $Mg_xMn_{x-1}B_2O_5$ means that these materials may also be of interest for Mg-ion battery systems.

Addressed realisation of multi-cation complex arrangements in metal-organic frameworks

Powder diffractometer DIB

Combining different metals provides new or enhanced physical properties that cannot be achieved with just one metal. The difficulty of obtaining multi-metal materials with desired properties is mainly twofold: on the one hand are the complexities associated with incorporating more than one element into the atomic arrangement of the material, and on the other, is controlling the location where the second metal element is incorporated into the other. Metal-organic frameworks (MOF) are crystalline materials formed by metal clusters coordinated with organic linkers. We have developed a strategy to synthesise a platform of MOF that allows the incorporation of more than one metal into the structure, where the arrangement of elements in the crystalline structure is controlled at various length scales [1].

AUTHORS
C. Castillo-Blas, **E. Gutiérrez-Puebla**, **F. Gándara** and **Á. Monge** (CSIC, Madrid, Spain)
V.A. de la Peña-O´Shea (IMDEA Energy Institute, Spain)
J. Romero de Paz and **R. Sáez Puche** (Universidad Complutense de Madrid, Spain)
I. Puente Orench (CSIC, Madrid, Spain and ILL)

ARTICLE FROM
Sci. Adv. (2017) – doi:10.1126/sciadv.1700773

REFERENCES
[1] C. Castillo-Blas *et al.*, Sci. Adv. 3 (2017) 1
[2] H.C. Zeng, Curr. Nanosci. 3 (2007) 177

Incorporation of more than one metal into an MOF structure is possible in those in which the formation of the crystalline structure is kinetically governed, such as in the case of ZnPh-1, formed with 4,4'-(hexafluoroisopropylidene)*bis*(benzoic acid) (H_2hfipbb) as the organic linker. It crystallises in the hexagonal P6$_4$22 space group (a = 21.22(1) Å, c = 7.710(5) Å), where Zn atoms are arranged in a helical rod-shaped structure, tetrahedrally coordinated. By maintaining the metal to linker molar ratio constant at 1.65 it has been possible to incorporate a second cation, such as Co, Mn or Ca, into the structure. The term 'molar code' indicates the molar relation between metal elements (*e.g.* Zn:Co 1:2).

The combination of single crystal X-ray diffraction together with high-resolution and high-intensity neutron diffraction techniques is of utmost relevance in the crystallographic characterisation of these compounds. At room temperature Zn:Co, up to molar ratio 1:2, is isostructural to the original ZnPh-1 with the crystallographic metal position occupied by both Zn and Co tetrahedrally coordinated. The crystals are found to be hollow (**figure 1**) and the amount of Co, moreover, is larger in the external areas of the crystals, which is consistent with the hollow morphology found [2]. Thus, the core of the crystal is composed of Zn atoms and the shell formed by Zn and Co atoms all tetrahedrally coordinated.

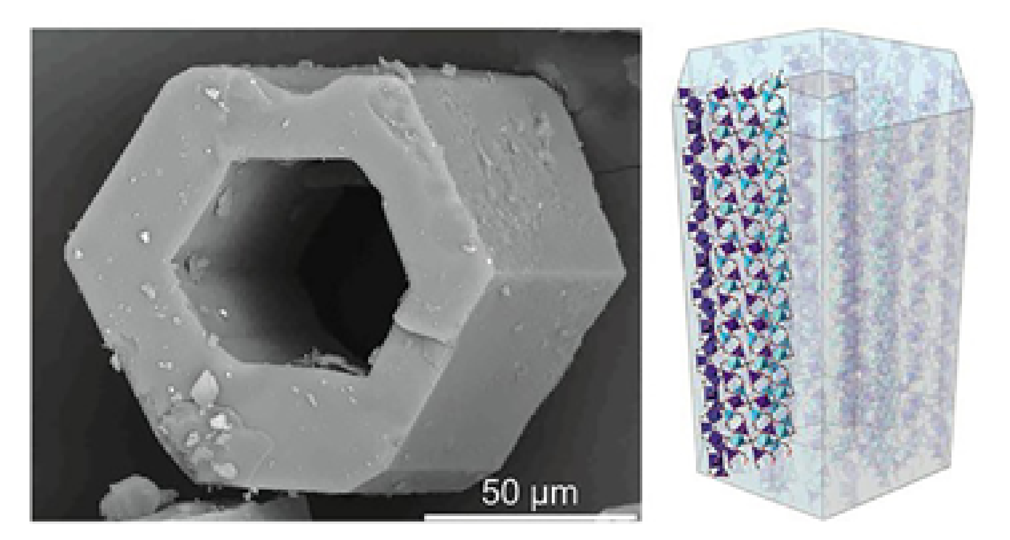

Figure 1
SEM image of Zn:Co 1:2 and the mesoscopic arrangement of the metal clusters.

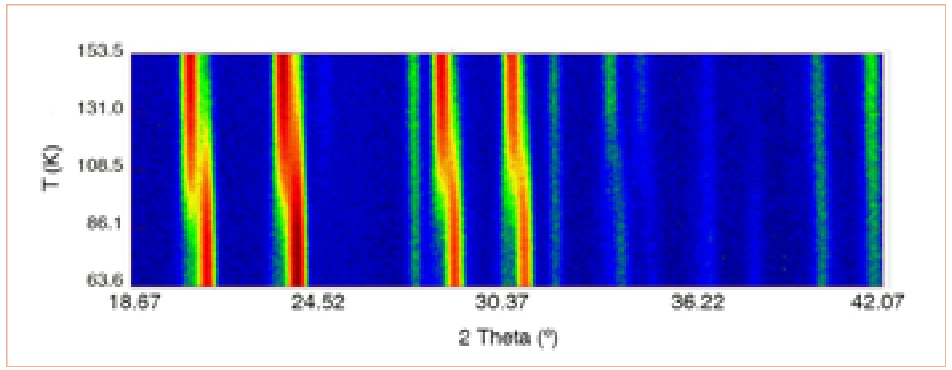

Figure 2
Neutron diffraction pattern of Zn:Co 1:2 as a function of temperature, measured on the CRG powder diffractometer D1B.

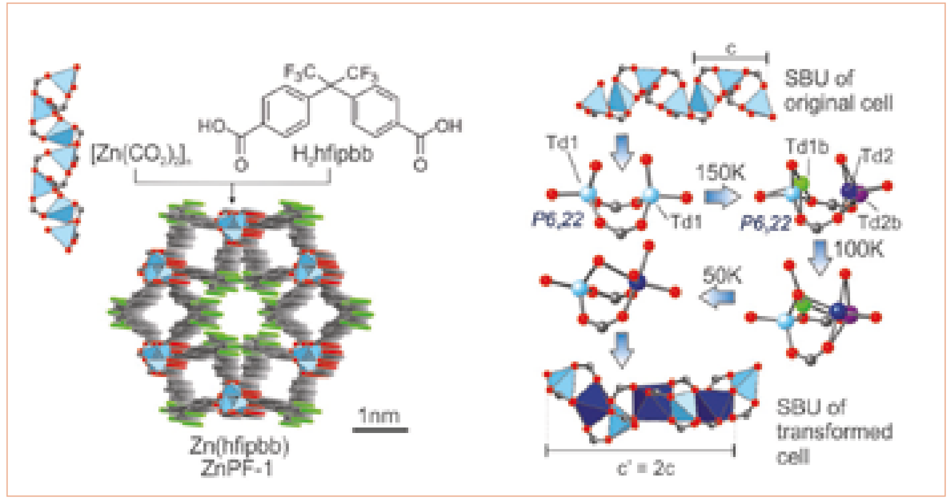

Figure 3
Transformation from two independent tetrahedral sites of group P6$_4$22 to an alternating tetrahedral-octahedral one of group P6$_5$22 where the c parameter is doubled.

The coordination environment of Co changes, however, at low temperatures. The unit cell has a doubled c parameter and the space group that describes the low temperature crystalline structure is P6$_5$22. **Figure 2** illustrates the thermodiffraction data from D1B where the phase transformation is observed. It is worth mentioning that there is a region of temperatures in which both crystalline structures coexist. The lattice constant change is caused by the splitting of the metal site, which is now formed by tetrahedral and octahedral sites. **Figure 3** summarises the transformation from two independent metal tetrahedral sites at temperatures above 150 K to a tetrahedral and octahedral coordination environment.

In conclusion, at room temperature both atoms are in a tetrahedral coordination environment while at low temperatures only Co atoms become octahedral, resulting in the c parameter change. Increasing the molar ratio of Co in the structure has a direct impact on the presence of the crystalline phases. Zn:Co 1:10 exhibits both phases at room temperature, indicating that the presence of cobalt in the structure has a stabilising effect on the octahedral site. This MOF has three domains, in which Zn and Co have a different coordination environment: a small core with only Zn atoms tetrahedral coordinated; a shell of Zn and Co in tetrahedral coordination at room temperature; while at low temperature Co is octahedrally coordinated and an outer shell forms only with Co atoms in alternating tetrahedral and octahedral coordination environments.

Therefore, it is possible to obtain metal clusters with more than one metal with variable coordination environments while maintaining the overall morphology. This method opens up alternatives for the preparation of new materials with specific applications.

London Dispersion enforces the shortest C–H•••H–C contact recorded to date

Single-crystal diffractometer D19

London Dispersion (LD)—the main attractive interaction of the van der Waals forces—arises from pairwise correlated electron movement between atoms [1]. For a long time LD was considered largely negligible, but it grows rapidly with increasing size of the molecular system. Recent investigations provide ample evidence of the decisive influence of LD in multiple scientific fields [2]. Dimeric all-*meta tert*-butyl triphenylmethane 1_2 hereby embodies a milestone as the LD interactions overcome the immense Pauli repulsion of the *tert*-butyl groups, resulting in the shortest known C–H···H–C contact [3].

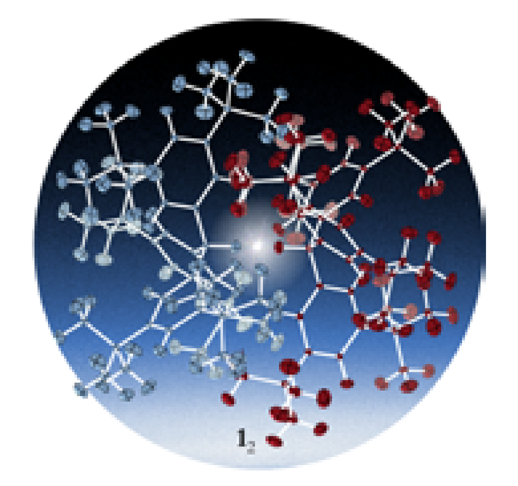

AUTHORS

S. Rösel and **P.R. Schreiner** (Justus-Liebig University, Giessen, Germany)
E. Mossou (ILL and Keele University, UK)
L. Cañadillas-Delgado (ILL and Centro Universitario de la Defensa de Zaragoza, Spain)

ARTICLE FROM

J. Am. Chem. Soc. 139 (2017) – doi:10.1021/jacs.7b01879

REFERENCES

[1] F. London, Trans. Faraday Soc. 33 (1937) 8
[2] J.P. Wagner and P.R. Schreiner, Angew. Chem. Int. Ed. 54 (2015) 12274
[3] S. Rösel, H. Quanz, C. Logemann, J. Becker, E. Mossou, L. Cañadillas-Delgado, E. Caldeweyher, S. Grimme and P.R. Schreiner, J. Am. Chem. Soc. 139 (2017) 7428
[4] S. Grimme, J. Antony, S. Ehrlich and H. Krieg, J. Chem. Phys. 132 (2010) 154104
[5] B. Kahr, D.v. Engen and K. Mislow, J. Am. Chem. Soc. 108 (1986) 8305
[6] S. Grimme, R. Huenerbein and S. Ehrlich, Chem. Phys. Chem. 12 (2011) 1258
[7] O. Ermer, S.A. Mason, F.A.L. Anet and S.S. Miura, J. Am. Chem. Soc. 107 (1985) 2330

The design of molecular systems and the prediction of their properties depend on a full understanding of chemical interactions that are often dissected with the help of computational methods. The lack of inclusion of LD in commonplace density functional theory (DFT) methods has led to the realisation that LD is critical to describing structures and reactivities fully. *A posteriori* LD corrections such as Grimme's D3 term allow dispersion to be switched on and off, thereby providing fundamental insights [4]. Such LD corrections require molecular model systems with accurately defined properties, as provided by the hexaphenylethane scaffold. While parent hexaphenylethane has not yet been observed, due to steric repulsion of the phenyl rings, the introduction of bulky *tert*-butyl groups in all *meta*-positions leads to an isolable compound with a very long central bond of R_{C-C} = 1.67 Å {R_{C-C} (common): 1.54 Å} [5]. We have shown that the *tert*-butyl groups stabilise the molecule, not kinetically by steric shielding but thermodynamically by strong attractive LD forces between the *tert*-butyl moieties. Such groups are now termed dispersion energy donors (DED) [6]. In our previous computational studies we found that large, symmetric and rigid alkyl moieties like *tert*-butyl and 1-adamantyl are excellent DEDs. Upon extension of the DED concept to the all-*meta tert*-butyl triphenylmethane dimer 1_2, formally the hydrogenation product of all-*meta tert*-butyl hexaphenylethane, we were able to prepare a unique dispersion dimer displaying the shortest C–H···H–C contact known (**figure 1**).

Figure 1

The ND structure of dimeric all-*meta tert*-butyl triphenylmethane 1_2. The monomers are indicated in blue or red for better visibility. The very short central H···H contact appears in the middle. Ellipsoids are drawn at 50 % probability.

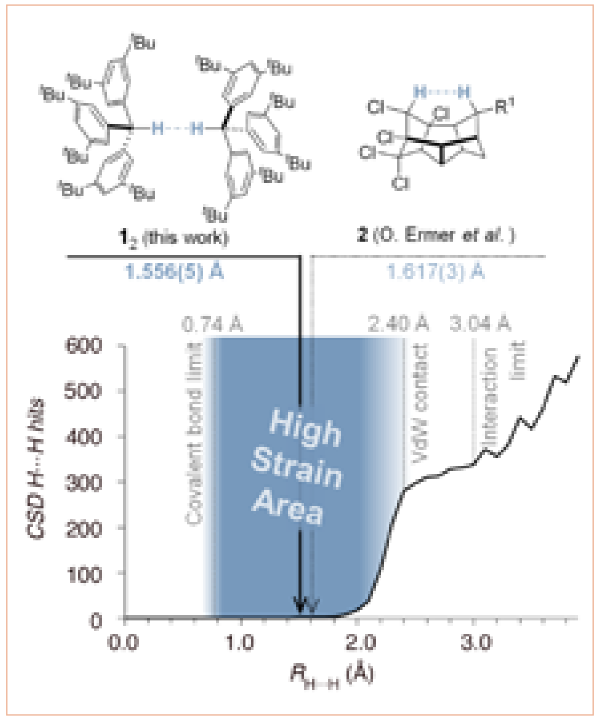

Figure 2

Top) Structures of dimeric all-*meta tert*-butyl triphenylmethane 1_2 **(left)** with its short H···H contact and former record-holder 'half-cage' 2 **(right)** R^1: OBn.
Bottom) Hits for H···H contacts determined by ND in the Cambridge Crystal Structure Database (V5.38 + two updates) rise quickly, starting from distances around the sum of the van der Waals (vdW) radii of hydrogen. The repulsive region below $R_{H...H} < 1.9$ Å contains only seven non-bonded H···H contacts in six molecules, revealing the difficulties of preparing structures with such short contacts.

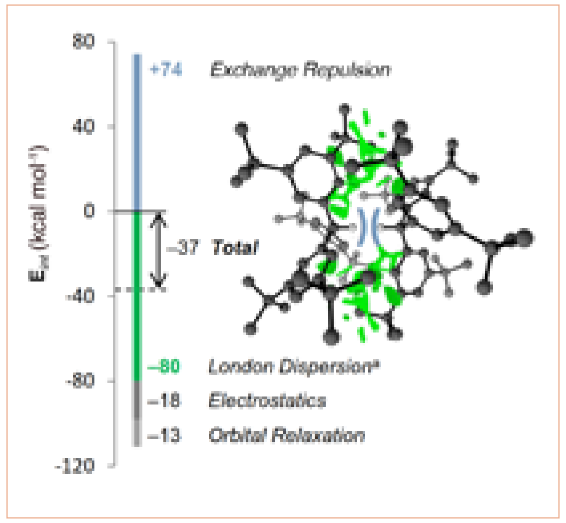

Figure 3

The energy decomposition analysis (EDA) of 1_2 at the B3LYP-D3^{ATM}(BJ)/def2-TZVPP level of theory shows the high repulsion within the dimer (blue) that is outbalanced by LD interactions between the monomers (green). ^{a} This EDA scheme obtains the LD interaction from the (partly DFT method-inherent) electron correlation (–28 kcal mol^{-1}) and additionally the D3^{ATM}(BJ) correction (–52 kcal mol^{-1}), accounting for the insufficient correlation treatment in DFT.

To date, most very short H···H contacts have been obtained intramolecularly. The former record-holder is the bowl-shaped, 'half-cage' pentacyclododecane **2** with an H···H distance of 1.617(3) Å, determined by neutron diffraction (ND) at 113 K (**figure 2**) [7]. This contact is 27 % closer than expected from the sum of the van der Waals radii and is therefore highly repulsive. The energy needed to overcome the repulsion results in severe deformations of the molecular structure.

All-*meta tert*-butyl triphenylmethane crystallises in the $P2_13$ space group (R = 0.03) as a dispersion-bound dimer. The short C–H···H–C contact is *intermolecular* and both parts of the head-to-head arrangement are contained in the asymmetric unit. Neutron data collected on the ILL single-crystal diffractometer D19 at 20 K revealed that this H···H contact is as short as 1.566(5) Å. Unlike in previous molecules containing short, transannular H···H contacts, **1** does not seem to suffer from severe geometric distortions: the bond angles around the central bond of 1_2 and the corresponding C–H bonds length are ordinary.

A computational analysis (HSE-3c/CRYSTAL14) of the periodic crystal structure was performed to rationalise this surprisingly short contact. The computed periodic structure is in good agreement with the ND structure [V(exp.) = 7833.1(4) $Å^3$; V(comp.) = 7676.9 $Å^3$] and it reproduces the H···H distance within the error bar. Comparison with the gas phase dimer reveals a minor crystal packing effect. The energy decomposition analysis (B3LYP-D3^{ATM}(BJ)/def2-TZVPP) shows a large Pauli repulsion of +74 kcal mol^{-1}, which is mainly outbalanced by –80 kcal mol^{-1} of LD (**figure 3**). The large contribution of the *tert*-butyl groups as DEDs becomes evident when all-*meta tert*-butyl substituted 1_2 is compared with the unsubstituted parent triphenylmethane dimer: 77 % of the LD is lost and the head-to-head arrangement becomes thermodynamically unfavourable. Hence, LD can become *the* decisive quantity determining hitherto unrealised chemical structures. This demonstrates the applicability of the DED concept and the notion of LD as an integral part of molecular design.

Fast diffusion of methane at the interface of clathrate structures I and II

Time-of-flight spectrometer IN6

Methane clathrate hydrates are inclusion compounds in which methane molecules are caged in open crystalline frameworks of water molecules. Using quasi-elastic neutron scattering measurements we observed a remarkably fast diffusion of methane at the interface of the two most common clathrate hydrate structures, sI and sII, whose coexistence was promoted by applying high pressure. This result could considerably improve our understanding of non-equilibrium phenomena in methane hydrates, such as clathrate formation and gas exchange, and indicate new routes for exploiting these materials as energy resources.

AUTHORS

U. Ranieri (EPSL, ICMP, Lausanne, Switzerland and ILL)
M.M. Koza (ILL)
W.F. Kuhs and **A. Falenty** (University of Göttingen, Germany)
S. Klotz (CNRS UMR 7590, Université Pierre et Marie Curie, Paris, France)
P. Gillet (EPSL, ICMP, Lausanne, Switzerland)
L.E. Bove (CNRS-UMR7590, Université Pierre et Marie Curie, Paris France and EPSL, EPFL, Lausanne, Switzerland)

ARTICLE FROM

Nat. Commun. (2017) – doi:10.1038/s41467-017-01167-2

REFERENCES

[1] L.E. Bove, S. Klotz, Th. Strässle, M. Koza, J. Teixeira and A.M. Saitta, Phys. Rev. Lett. 111 (2013) 185901
[2] U. Ranieri, M.M. Koza, W.F. Kuhs, S. Klotz, A. Falenty, P. Gillet and L.E. Bove, Nat. Commun. 8 (2017) 1076
[3] R.E. Lechner, Solid State Ion. 77 (1995) 280
[4] K.R. Harris and N.J. Trappeniers, Physica A 104 (1980) 262
[5] P.S. Van der Gulik, R. Mostert and H.R. Van den Berg, Physica A 151 (1988) 153

Methane clathrate hydrates are ice-like solids in which methane molecules are enclosed inside polyhedral cages formed by hydrogen-bonded water molecules. They form naturally in large quantities within marine sediments and within and below continental permafrost, and have therefore attracted considerable attention in the last decade for their potential as powerful geo-organic fuel resources. Exchanging the guests in existing methane hydrate deposits with CO_2 has recently been indicated as a promising two-in-one approach to energy recovery and concomitant carbon dioxide mitigation.

Assessing the technological viability of such energy applications and then implementing them requires a complete understanding of the non-equilibrium phenomena involving methane clathrate hydrates—something that has still not been achieved. For example, very little is known about the microscopic diffusion of methane during conversion between different clathrate structures, although methane diffusion certainly plays a paramount role in that process. The transport properties of methane clathrate hydrates under high pressure are also important in planetary science, as clathrate hydrate layers are believed to exist at pressure in the interiors of large icy bodies in the universe.

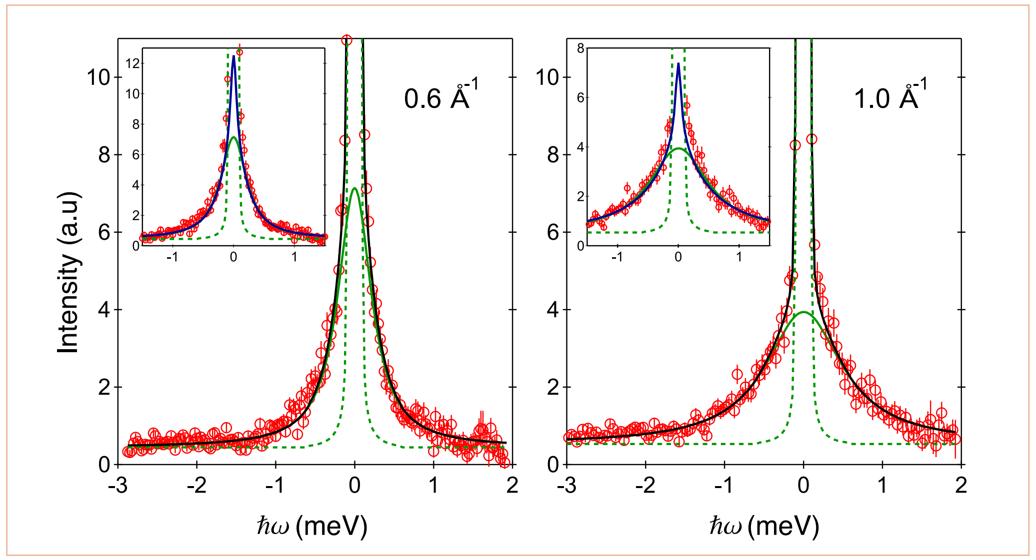

Figure 1

Examples of measured QENS spectra at 0.8 GPa, 282 K and two momentum transfer values. Experimental data (empty circles) are compared with their best fits (black lines) within the 3D diffusion model. Quasi-elastic Lorentzian (solid green lines) and elastic (dashed green lines) components are also shown. **(Insets)** The Lorentzian fits are compared with the fits obtained within the 2D diffusion model (blue lines).

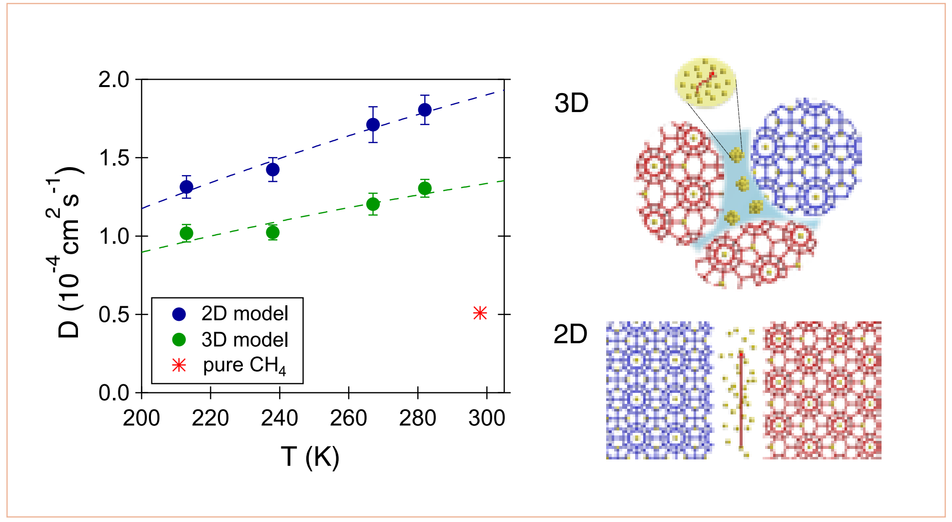

Figure 2

Left) Temperature dependence of the translational diffusion coefficient D at 0.8 GPa, as obtained in the 3D and 2D diffusion models. Arrhenius fits of D are shown as dashed lines. The estimated value for D in pure methane from the literature [4, 5] is also reported. **Right)** Schematic views of the 3D and 2D diffusion processes are presented.

For clathrate hydrates of methane, structure I is the thermodynamically preferred phase, while structure II is a metastable form that is kinetically favoured and transiently detected in the initial stages of the hydrate formation process. Remarkably, structure II can persistently coexist with structure I in methane clathrate hydrate under high pressure. We therefore took advantage of the novel possibility of performing quasi-elastic neutron scattering measurements under pressures of the order of gigapascals [1], and directly measured the diffusion of methane molecules at the interface of clathrate structures I and II as a function of temperature between 212 and 282 K at 0.8 GPa [2]. The starting structure I clathrate was constituted by a frame-deuterated (CH_4-D_2O) sample containing approximately one methane molecule for every six water molecules.

Experiments were performed on the time-of-flight spectrometer IN6 using a Paris-Edinburgh press. Analysis of the QENS spectra revealed a fast, extra-cage translational diffusion on the picosecond time scale, involving a sizeable fraction (approximately one third) of the methane molecules in the sample. The existence of such a high fraction of fast-diffusing methane molecules strongly suggests that an appreciable fraction of water molecules is in a disordered state during structural coexistence. Such disordered regions would form at the front line of the transformation between clathrate structures I and II, and their sizes would be below the typical size of the crystallites of a few micrometres.

The quasi-elastic signal was fitted assuming a three-dimensional (3D) diffusion process at the grain boundaries, *i.e.* using a simple Lorentzian function (see typical QENS spectra in **figure 1**), and a planar (2D) diffusion model, *i.e.* using the complex formula reported in reference [3] (see insets in **figure 1** for examples of fits and reference [2] for details). The second model corresponds to the scenario in which the grain boundary network or the intercalated disordered regions between crystals of structure I and structure II are thin compared with the typical length scale probed by the instrument (that is, 1-10 Å) so that the methane molecules essentially diffuse bi-dimensionally. The fits obtained within the two models are actually indistinguishable outside the instrumental resolution-dominated region close to $\omega = 0$ (**figure 1**), and therefore it is not possible to unequivocally establish whether bulk or planar diffusion is taking place.

In both cases, the obtained translational diffusion coefficients D turn out to be of the order of 10^{-4} cm^2 s^{-1}—*i.e.* seven to eight orders of magnitude higher than those reported in the literature for cage-to-cage hopping of methane through clathrate structure I at low pressure, up to one order of magnitude higher than that of a supersaturated water-methane solution at low pressure and a factor of two to three times higher than that expected for pure bulk supercritical methane at the same pressure and comparable temperature (**figure 2**). The remarkable enhancement of the methane diffusion observed can be ascribed either to fast diffusion within methane nanobubbles forming at structure I–structure II grain boundaries, or, alternatively, to a hyper-diffusion phenomenon associated with a peculiar layered structure of the interface [2]. Further investigation will be needed to distinguish between these two scenarios.

The hydrogen-bond collective dynamics in liquid methanol

Brillouin spectrometer BRISP

Despite thorough scrutiny, the microscopic behaviour of hydrogen-bond (HB) systems still presents many mysterious aspects. Their elucidation could clarify both why this elusive interaction is key to biological functioning and the origin of unusual properties of aqueous solutions and alcohols, undoubtedly the classes of liquids most directly affecting life and daily human activity and development.

AUTHORS

S. Bellissima (CNR-IFAC, Sesto Fiorentino, Italy)
S. De Panfilis (IIT, Centre for Life Nanoscience, Roma, Italy)
U. Bafile (CNR-IFAC, Sesto Fiorentino, Italy.
A. Cunsolo (BNL, National Synchrotron Light Source II, Upton, NY, US)
M.A. González (ILL)
E. Guarini (Physics and Astronomy Department, University of Firenze, Italy)
F. Formisano (CNR-IOM, Grenoble, France)

ARTICLE FROM

Sci. Rep. 6 (2016) – doi:10.1038/srep39533

REFERENCES

[1] M. Sampoli *et al.*, Phys. Rev. Lett. 79 (1997) 1678
[2] E. Pontecorvo *et al.*, Phys. Rev. E 71 (2005) 011501
[3] G. Garberoglio *et al.*, J. Chem Phys. 117 (2002) 3278

The two most studied members of these two families—water and methanol—share many features, their relevant difference consisting in the replacement of a proton by a methyl group that bestows on alcohols their amphiphilic character and different solvent properties. Therefore, a sensible question to ask is whether methanol shares with water the anomalous dynamic behaviour of collective molecular excitations (CME), namely a remarkably fast high-frequency wave propagation and its unusual coupling with transverse molecular movements [1, 2].

Comparing the phenomenology of CMEs in water and methanol is of prominent scientific interest, not so much for the analogies between them as for their main structural difference: unlike methanol, water has an HB network with a tetrahedral symmetry, which has indeed often been identified as responsible for the above-mentioned anomalies.

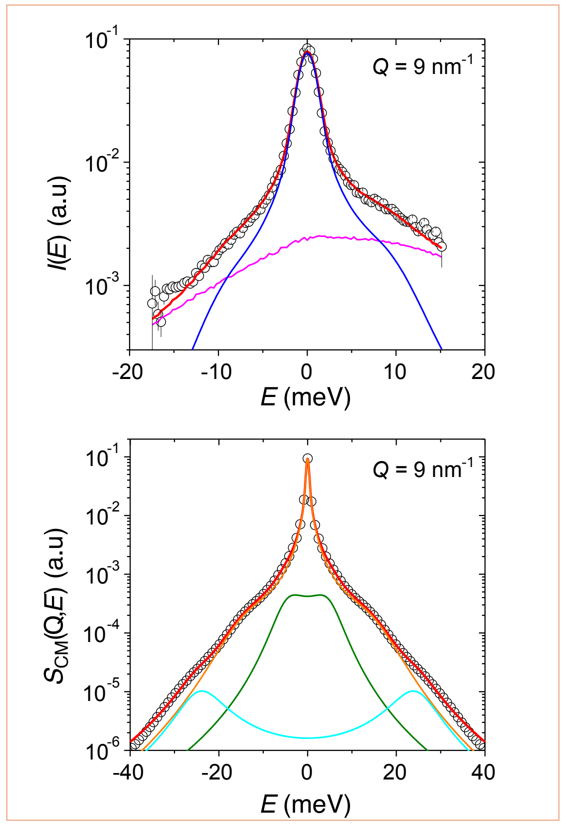

Figure 1

Upper panel) Fit of neutron Brillouin data obtained for liquid deuterated methanol at 298 K. The total fit (red line) is a linear combination of simulation (blue line) and multiple scattering (magenta line) data.

Lower panel) Fit of MD results to the theoretical model for liquid deuterated methanol at 298 K. The total fit (red line) is the sum of a viscoelastic (orange line) and two damped harmonic oscillators' (green and cyan lines) line shapes.

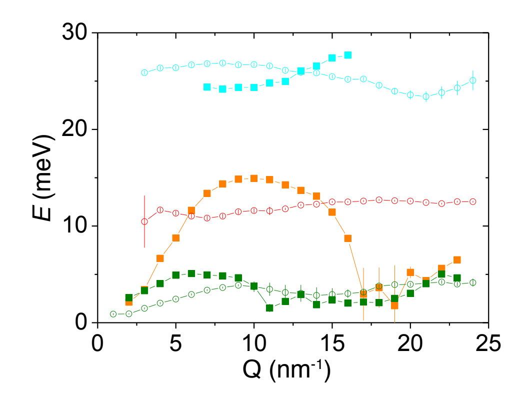

Figure 2

Energies of longitudinal and transverse modes for liquid methanol at 298 K. The energies obtained by modelling the $S_{CM}(Q,\omega)$ are indicated by squared symbols and colours as in **figure 1**. The energies obtained from the analysis of current spectra are indicated by open circles.

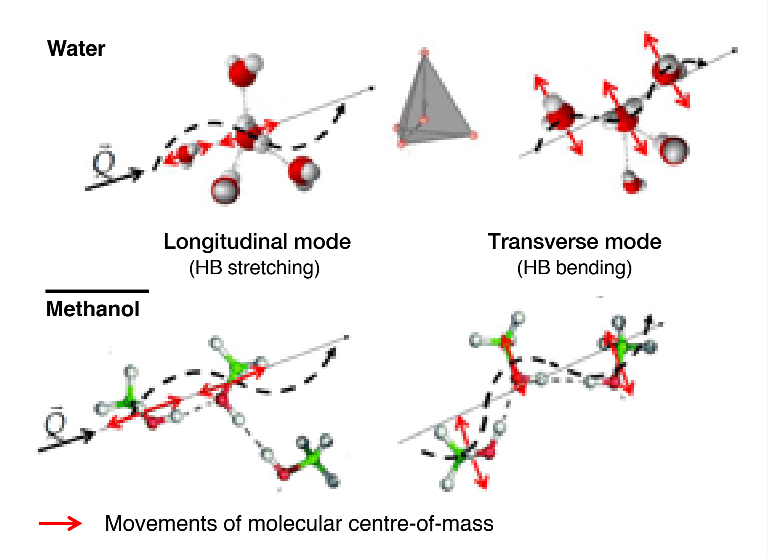

Figure 3

Sketch of longitudinal and transverse modes contributing to the THz spectrum of liquid water and methanol.

A direct characterisation of CMEs in a liquid can be gained using scattering methods, through the measurement of the dynamic structure factor $S(Q,\omega)$, which depends uniquely on the momentum and energy exchanged between the target sample and the beam of probe particles (neutrons, for instance)—$\hbar Q$ and $\hbar\omega$ respectively—with $\hbar$ being the reduced Planck constant. Most importantly, $S(Q,\omega)$ can be independently determined by molecular dynamics (MD) computer simulations, whose synergic employment in experiments is essential. Indeed, on the one hand experiments represent the ideal benchmark for interaction models employed in MD routines; on the other, MD methods can cover much broader dynamic windows and probe properties not accessible experimentally.

On the experimental side, the neutron BRIllouin SPectrometer, BRISP, at the ILL, is an ideal tool for pursuing the above research programme, as it can access the Q and ω regions in which CMEs dominate the $S(Q,\omega)$ of liquid methanol at T = 298 K. The line shape measured by this instrument on the methanol sample is presented in the upper panel of **figure 1** for one example Q value.

An ideal complement of $S(Q,\omega)$ measurements is provided by computations of $S_{CM}(Q,\omega)$, the centre-of-mass dynamic structure factor, which is not accessible experimentally and is closely connected to statistical correlations between molecular centres of mass movements. This spectral function is in principle strongly affected by interactions involving distinct molecules such as HBs. The $S_{CM}(Q,\omega)$ profile of methanol computed at one example Q value is presented in the lower panel of **figure 1**.

Overall, both measured and computed spectra in **figure 1** reveal the presence of CMEs through side shoulders in the line shapes, whose presence is emphasised by comparison with best fitting models of the total spectral shape and the individual CME contributions. The $S(Q,\omega)$ so obtained mostly describes a so-called 'longitudinal' dynamics because the system is probed along directions parallel to $\mathbf{Q}$. We have therefore computed the current spectra which is a quantity allowing us also to characterise the dynamics transverse to $\mathbf{Q}$. In this way, we obtain a set of data describing both longitudinal and transverse modes, reported as a function of Q in **figure 2**. These data clearly indicate that some modes have frequencies linearly vanishing in the $Q = 0$ limit, thus revealing their acoustic nature, *i.e.* their ability to propagate over macroscopic times and distances, with a travelling speed given by the slope of the curve. Conversely, other modes instead exhibit a non-propagating, rather localised, nature, as suggested by the vanishing 'group velocity', *i.e.* the essentially flat Q dependence of their frequencies. The similarity between the longitudinal and transverse flat modes calls for global reconsideration of the popular attribution of this coupling to the tetrahedral character of the HB network. A schematic representation of both modes in water and methanol is shown in **figure 3**.

This complex phenomenology closely resembles that previously observed in other HB systems [3], which suggests some universality in the high-frequency collective dynamics of HB network liquids.

One-dimensional phase diagram for simple glass formers

Time-of-flight spectrometers IN5 and IN6
Backscattering spectrometer IN16B

For simple van der Waals glass formers, we show that the dynamics over 14 orders of magnitude in time scale can be expressed as a function of a single parameter, reducing the usual temperature–pressure phase diagram into one of just one dimension in accordance with isomorph theory. For the investigated simple van der Waals systems, this is found to be true even when the vibrational and fast relaxational dynamic contributions on a picosecond time scale are completely separated from the alpha relaxation at the glass transition, which is on a time scale of seconds. The scaling to one control parameter also works for the alpha relaxation dynamics in a studied hydrogen-bonding system on a large range of time scales, but in this case it breaks down close to the glass transition.

AUTHORS

H.W. Hansen, **A. Sanz** and, **K. Niss** (Roskilde University, Denmark)
K. Adrjanowicz (University of Silesia, Katowice, Poland)
B. Frick (ILL)

ARTICLE FROM

Nat. Commun. (accepted) – arXiv:1709.08953

REFERENCES

[1] M.D. Ediger and P. Harrowell, J. Chem. Phys. 137 (2012) 080901
[2] J.C. Dyre, J. Phys. Chem. B 118 (2014) 10007
[3] H.W. Hansen, A. Sanz, K. Adrjanowicz, B. Frick and K. Niss, accepted in Nat. Commun. (2017) arXiv:1709.08953
[4] A. Sanz, H.W. Hansen, B. Jakobsen, I.H. Pedersen, S. Capaccioli, K. Adrjanowicz, M. Paluch, J. Gonthier, B. Frick, E. Lelièvre-Berna, J. Peters and K. Niss, arXiv:1709.09859.
[5] H.W. Hansen, PhD thesis (2018), Roskilde University, IMFUFA teskst 507, ISSN: 0106-6242
[6] H.W. Hansen, B. Frick, T. Hecksher, J.C. Dyre and K. Niss, Phys. Rev. B 95 (2017) 104202

The ability to form a glass is a universal property of materials. When a liquid is supercooled below its melting point, avoiding crystallisation, the molecules will stay disordered as in the liquid but movement will eventually be so slow that the material is considered a solid. The glass transition is defined as occurring when the structural alpha relaxation reaches $\tau_\alpha \approx 100$ s. Molecular movement can be slowed down by cooling as well as by compression. The nature of the glass transition remains a puzzling phenomenon, and a complete understanding must include temperature as well as pressure dependencies of the dynamics [1].

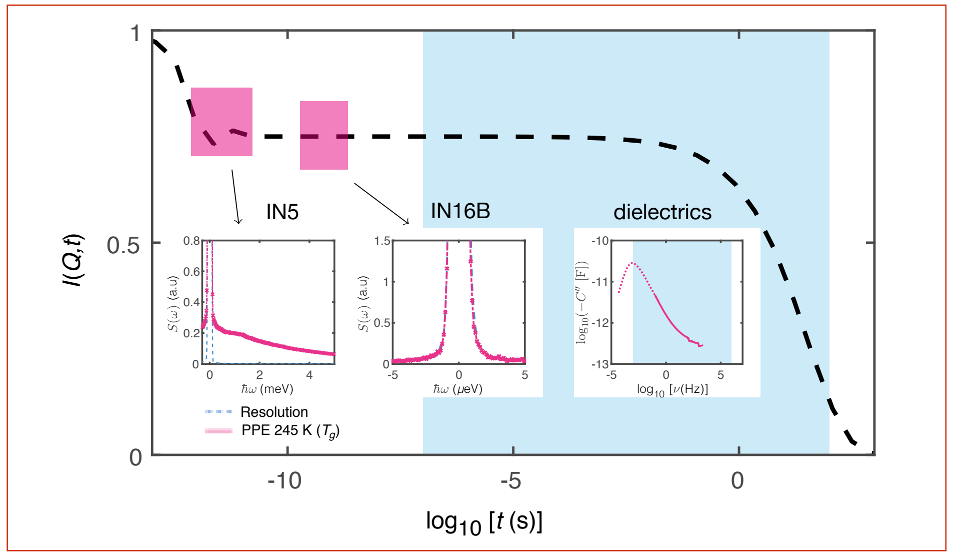

Figure 1

Illustration of an incoherent intermediate scattering function, I(Q, t), at the glass transition. One observes a complete separation of time scales: vibrations and fast relaxation at short times and the alpha relaxation at long times. A combination of TOF (ps), BS (ns) and dielectrics (μs to 10^2 s) spans a large dynamic range.

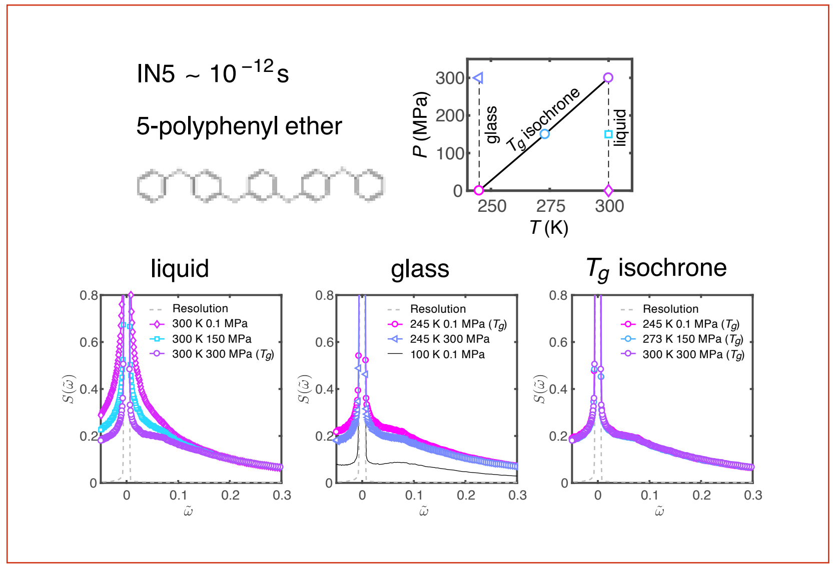

Figure 2

IN5 spectra of a simple glass former (PPE) shown as a function of energy transfer on reduced energy unit scale in accordance with isomorph theory, $\tilde{\omega} = \omega\rho^{-1/3}T^{-1/2}$. All spectra are shown summed over Q. The state points of the two isotherms and the T_g isochrone (τ_α = 100 s) are shown in the (T,P) phase diagram.

Isomorph theory proposes the existence of isomorphs, which are curves in the phase diagram along which dynamics and structure are invariant on all time scales after appropriate scaling. The idea is that two state points are isomorphic if their potential energy landscapes are the same after scaling, *i.e.* one landscape can be mapped onto the other [2]. Experimentally, we can identify potential isomorphs by isochrones, which are lines in the temperature–pressure phase diagram of constant alpha relaxation time, *e.g.* the glass transition line (**figure 2**). The alpha relaxation time is one parameter that should be constant along an isomorph. If isomorphs exist, dynamics on all time scales should then be invariant along isochrones. Isomorph theory is an approximate theory and therefore only expected to work for simple systems.

We measured three different systems using a high-pressure cell for performing simultaneous dielectric and neutron spectroscopy [3]. This newly developed cell was a collaboration between ILL services (SANE and SCI) and Roskilde University and has been used with time-of-flight (TOF) on IN5 and IN6, and backscattering (BS) on IN16B, accessing a large range of time scales [4]. Two of the systems were van der Waals liquids without secondary relaxations, *i.e.* systems we consider to be simple. The third system was a hydrogen-bonding system with more complex dynamics, *e.g.* a methyl-group rotation visible in BS and an excess wing in the dielectrics. With the dielectrics covering time scales from 10^{-6} to 10^{2} s, using IN16B which covers nanosecond dynamics and IN5 covering picosecond dynamics we were able to explore the temperature and pressure dependence of the dynamics on a large range of time scales.

We found the alpha relaxation dynamics measured with TOF and BS, *i.e.* pico- and nanosecond dynamics, respectively, to scale for all three systems along isochrones determined from dielectrics when the alpha relaxation time was faster than milliseconds [5]. As the temperature is lowered (or pressure increased) approaching the glass transition, the alpha relaxation dynamics separates from fast relaxations and vibrations on picosecond time scales. This final state is illustrated in **figure 1**, while there is no relaxational signal within the instrumental resolution of IN16B, *i.e.* at nanosecond time scales. In the TOF window of IN5, *i.e.* at picosecond time scales, we observe dynamic contributions from vibrations and fast relaxations.

In **figure 2** we show picosecond dynamics from IN5 for 5-polyphenyl ether (PPE), a simple van der Waals liquid [6]. While the picosecond dynamics is observed to change along the two isotherms in the glass and in the liquid, we observe that it is invariant along the glass transition isochrone found from the dielectrics. This non-trivial collapse of the picosecond dynamics at the glass transition, where the dynamics is completely separated from the alpha relaxation, was shown for two simple van der Waals systems, while it was shown not to hold for the more complex hydrogen-bonding system.

For the simple van der Waals systems, the collapse of the picosecond dynamics along the glass transition implies that dynamics on all time scales can be expressed as a function of just one parameter instead of the usual two (T,P), and this is interpreted as a genuine signature of real simple glass formers having isomorphs. The implication of this finding is that if a universal theory of the glass transition exists, it must be in agreement with the one-dimensional phase diagram of isomorph theory.

Coexistence of spherical and deformed structures in the ^{96}Y nucleus: the onset of a quantum shape-phase transition in the A = 100 mass region

Polarised cold-neutron beam facility PF1B

Nowadays, sophisticated nuclear models can predict the very different observed structures of nuclei, astrophysical observations and fission mechanisms. Key observables to validate such models are, in turn, provided by technologically challenging experiments. In our recent publication [1] based on the EXILL campaign at PF1B, the energy level scheme of ^{96}Y (a nucleus with $N = 57$ neutrons, lying in the proximity of the r-process nucleosynthesis path) was significantly extended following neutron-induced fission of ^{235}U and ^{241}Pu targets. The coexistence of spherical and deformed shapes was observed, indicating that deformed structures are already apparent three neutrons away from the $N = 60$ isotone chain where the quantum shape-phase transition from spherical to deformed occurs.

AUTHORS

Ł.W. Iskra and **B. Fornal** (Institute of Nuclear Physics PAN, Krakow, Poland)
S. Leoni (University of Milan and INFN, Italy)
U. Köster (ILL)

ARTICLE FROM

Europhys. Lett. 117 (2017) 12001

REFERENCES

[1] R.F. Casten, Prog. Part. Nuc. Phys. 62 (2009) 183
[2] T. Togashi *et al.*, Phys. Rev. Lett. 117 (2016) 172502
[3] Ł.W. Iskra *et al.*, Europhys. Lett. 117 (2017) 12001
[4] W. Urban *et al.*, Phys. Rev. C 96 (2017) 044333
[5] J.K. Hwang *et al.*, Phys. Rev. C 58 (1998) 3252
[6] N. Shimizu *et al.*, Prog. Theor. Exp. Phys. (2012) 01A205
[7] Tokyo K supercomputing system: http://www.aics.riken.jp/en/
[8] E.M. Burbidge *et al.*, Rev. Mod. Phys. 29 (1957) 547

The shape of a particular nucleus results from the interplay between the collective (macroscopic) and single (microscopic) particle nature of such a complex many-body quantum system, and therefore strongly depends on both the atomic number Z and the neutron number N. Neutron-rich nuclei around $Z = 40$ and $N = 60$ provide one of the best territories for exploring this duality. Indeed, the sudden onset of deformation observed for neutron-rich nuclei with $Z = 37–40$, near $N = 60$, is considered the most dramatic shape change in the nuclear chart, with typical characteristics of quantum-phase transition phenomena [1, 2]. This abrupt shape change can be interpreted in terms of the interchange between coexisting spherical and deformed configurations: while in isotopes with $N < 60$ the former are energetically favoured, for $N \geq 60$ the situation is inverted with the deformed structure becoming the lowest in energy. The question that arises is whether deformed structures appear in close proximity to $N = 60$ (*i.e.* in ^{95}Rb, ^{96}Sr, ^{98}Y, $^{98\text{-}99}$Zr, with $N = 58$ and 59, deformed rotational bands built on excited isomeric states exist) or whether they also reside in lighter isotopes.

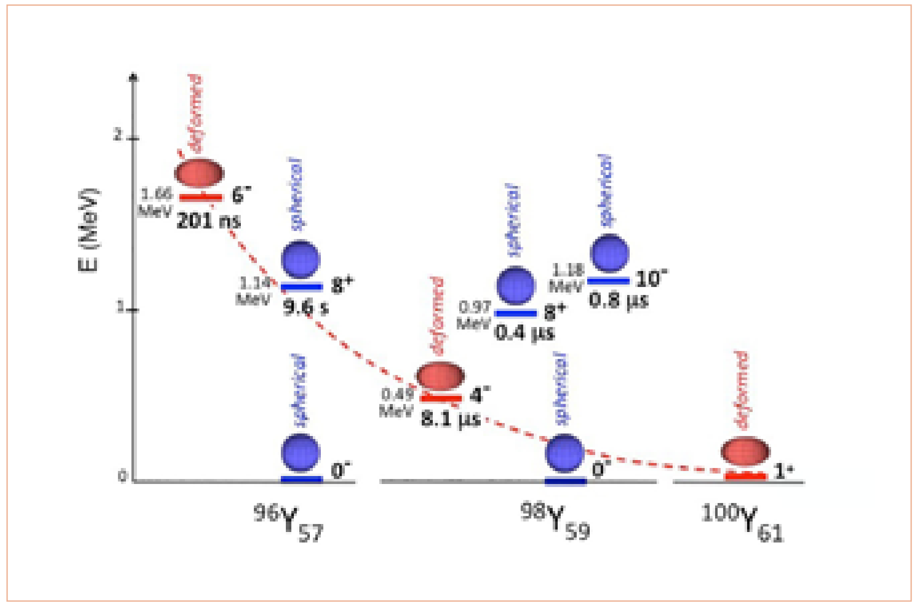

Figure 1

Evolution of the deformed structures across the Y ($Z = 39$) isotopic chain [3,4,5].

To shed light on this issue we have studied in detail the structure of the $N = 57$ yttrium isotope, *i.e.* ^{96}Y [3], which prior to our work was very poorly understood. The nucleus of interest was produced by cold-neutron-induced fission of ^{235}U and ^{241}Pu targets at the PF1B facility. An extensive spectroscopic investigation was possible by employing a highly efficient HPGe array (consisting of up to 49 Ge crystals) installed at the ILL, during the EXILL experimental campaign. The level scheme of ^{96}Y was significantly extended on the basis of the gamma-coincidence spectroscopy technique. A new 201(30)-ns isomeric state at 1 655 keV excitation energy was also discovered and the structure feeding this isomer identified: it resembles the beginning of a rotational band, analogous to the 4^- isomeric state in the ^{98}Y isotope. The results point to the existence of deformed structures already apparent at $N = 57$ which, with increasing number of neutrons, gradually decrease in energy to become dominant at $N \geq 60$ (**figure 1**).

The observed structure evolution can be used to validate sophisticated nuclear structure models such as, for example, large shell-model calculations based on ingenious computational schemes [6] and very powerful computing systems (with a million parallel processors, *e.g.* the Tokyo K supercomputing system [7]), which can predict the properties of nuclei lying on the r-process nucleosynthesis path [8]. This has significant implications for computing the abundance of elements heavier than Fe in the universe, which so far remain largely uncertain.

NUCLEAR AND PARTICLE PHYSICS

Direct tomographic quantum state reconstruction in neutron interferometry

Neutron interferometer S18

Quantum state tomography is one of the major resources in quantum information science, quantum communications and computing. However, quantum state tomography requires a lot of data post-processing. Consequently, an alternative, more direct, tomographical method was implemented in 2011 [1] using minimally disturbing measurements—so called weak measurements [2]. Recently, theorists have predicted better performance by utilising weak values obtained not *via* weak measurements but *via* conventional strong ones [3]. Using a silicon perfect-crystal interferometer we clearly demonstrate that strong interactions outperform weak ones for tomographic accuracy [4].

AUTHORS
T. Denkmayr, **H. Geppert**, **Y. Hasegawa** and **S. Sponar** (Atominstitut, TU Wien, Austria)
H. Lemmel (ILL and Atominstitut, TU Wien, Austria)

ARTICLE FROM
Phys. Rev. Lett. 118 (2017) – doi:10.1103/PhysRevLett.118.010402

REFERENCES
[1] J.S. Lundeen, B. Sutherland, A. Patel, C. Stewart and C. Bamber, Nature (London) 474 (2011) 188
[2] Y. Aharonov, D.Z. Albert and L. Vaidman, Phys. Rev. Lett. 60 (1988) 1351
[3] G. Vallone and D. Dequal, Phys. Rev. Lett. 116 (2016) 040502
[4] T. Denkmayr, H. Geppert, H. Lemmel, M. Waegell, J. Dressel, Y. Hasegawa and S. Sponar, Phys. Rev. Lett. 118 (2017) 010402

Consider a two-level quantum system or **qubit**, *e.g.* a spin state, which is the fundamental building block of quantum computing. The qubit is characterised not only by the populations of its two eigenstates but also by the relative phase between them. The standard method of determining the complete state is called **quantum state tomography**. Repeated measurements project the state in different directions in phase space, then finally the original state can be reconstructed. Nevertheless, this requires a lot of computational post-processing of the measured data in order to infer the initial quantum state.

In 2011 a novel, more direct, tomographical method was implemented that makes it possible to determine the quantum state without the need for post-processing [1]. However, that novel method has a major drawback—namely, that minimally disturbing measurements, referred to as weak measurements, are involved. The basic principle of **weak measurements**, a procedure introduced by Yakir Aharonov in 1988, is to keep the back-action of the measurement on the system small [2]. The price for this is that one can gain only very little information about the observed system for a single measurement. Thus the measurement has to be repeated multiple times, which is the main disadvantage of this procedure.

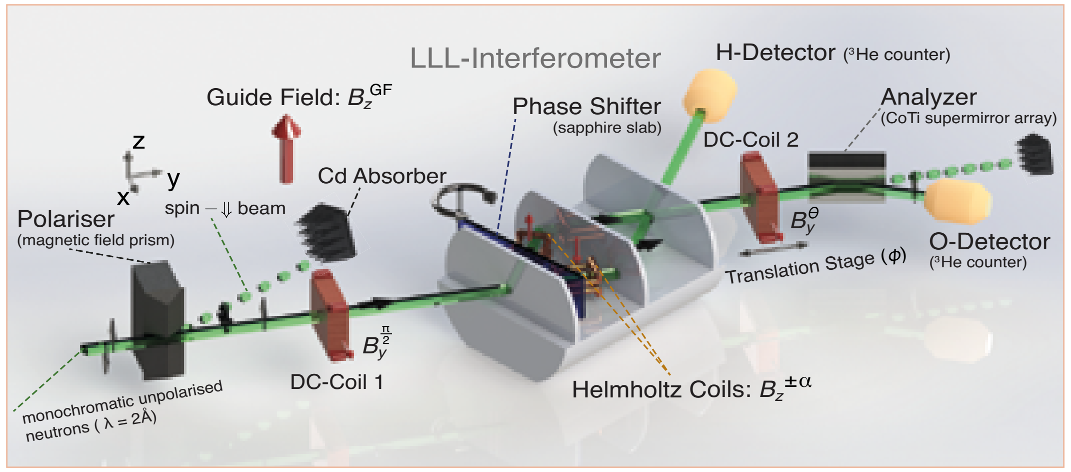

Figure 1
Schematic illustration of the experimental set-up for the neutron path system's quantum state characterisation *via* direct—or more precisely, strong—measurements. At the centre, the triple Laue perfect-silicon neutron interferometer surrounded by numerous neutron optical components.

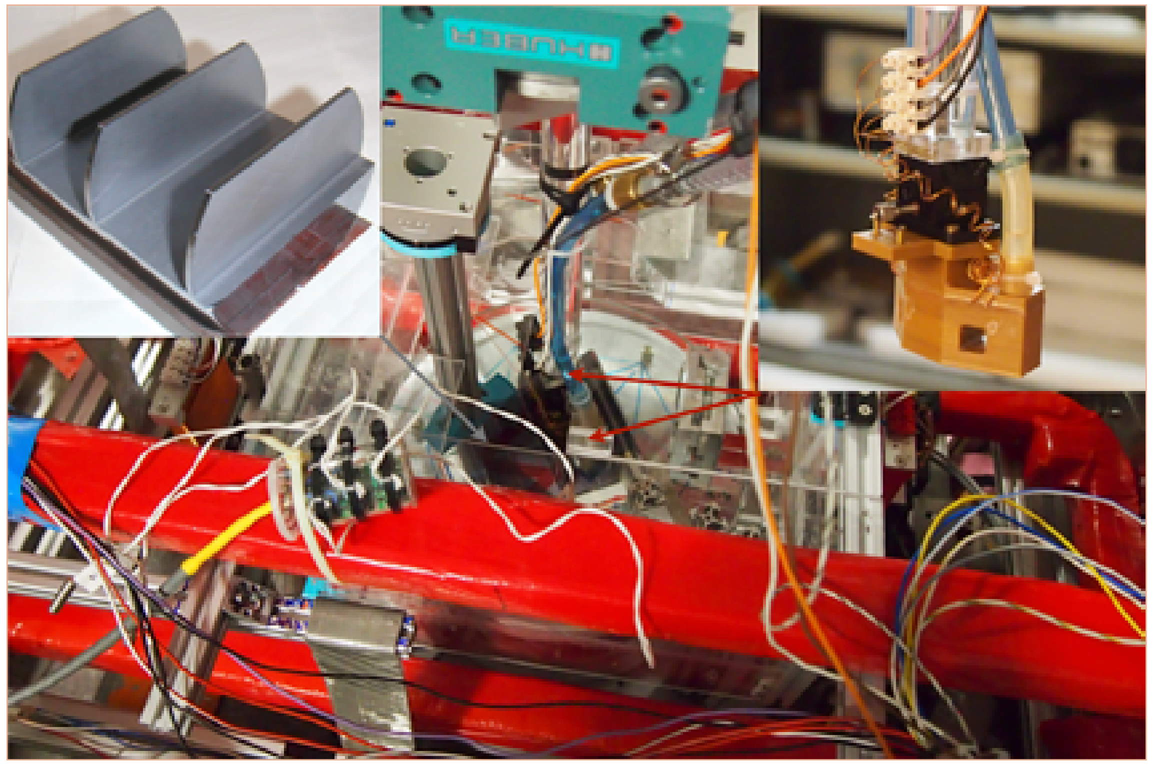

Figure 2
Photograph of the experimental set-up at S18, with the neutron interferometer on a fully vibration-damped platform and covered by a magnetic guide field (red) as well as magnetic and thermal sensors: **(upper left corner)** a zoomed-in picture of the triple Laue interferometer; **(upper right corner)** a cropped version of the water-cooled Helmholtz coils, constructed using a state-of-the-art 3D-printer.

We have now managed to integrate conventional, so-called **strong measurements**, in the tomographic procedure, thereby improving performance. As a result, it is possible to determine the quantum state with higher precision (measure of fluctuation) and accuracy (deviation from the theoretical prediction), all in a much shorter time compared with the approach using weak measurements.

Our neutron interferometric experiment, which is schematically illustrated in **figure 1**, was the first realisation of this procedure which works in the following way: at the first plate of the neutron interferometer, an incident neutron beam is split into two separate beams that travel along different regions in space. The two sub-beams are recombined at the last plate of the interferometer, giving rise to interference. The state of the neutron inside the interferometer is described as a **coherent superposition** state of the two **path eigenstates** associated with the two beam paths. The purpose of the small Helmholtz coils inside the interferometer is to couple the neutron's spin to the path by tuneable spinor rotations. The angle of rotation accounts for the measurement strength of the tomographic procedure, aiming to determine the neutron's path state. **Figure 2** shows a photograph of the actual neutron interferometric set-up. The two paths of the interferometer form, similar to the spin, a two-level system or qubit.

Two-level systems, albeit the simplest quantum systems, are of considerable interest because they are the fundamental building block of any quantum information process.

Our experiment confirms the advanced character of modern techniques applied in quantum physics: it should be noted here that neutron interferometric methods are well suited to this kind of high-tech research. The validity of our results is not limited to the quantum system formed by single neutrons, but can in fact be generalised to other systems. Neutron interferometric investigation may have a major impact on how quantum state estimation will be performed in the future in the rapidly evolving field of quantum information science.

Anomalous diffusion of water in membranes for fuel cells

Performance optimisation of fuel cells implies a complete understanding of the correlation between the structure of the membrane where proton transport takes place and the dynamics of the absorbed water molecules. Neutron scattering is the inevitable tool for revealing the details of this complex multiscale dynamics. By jointly analysing quasi-elastic neutron scattering (QENS) and molecular dynamics (MD) simulation data for a range of materials, we demonstrate that the sub-diffusion of water molecules is the crucial mechanism underlying experimental observations.

AUTHORS

Q. Berrod (LLB, CEA, CNRS, Université Paris-Saclay, France and Lawrence Berkeley National Laboratory, US)
S. Hanot (ILL and Pasteur Institute, Paris, France)
A. Guillermo, **S. Mossa** and **S. Lyonnard** (Université Grenoble Alpes, CEA, CNRS, INAC, SYMMES, Grenoble, France)

ARTICLE FROM

Sci. Rep (2017) – doi:10.1038/s41598-017-08746-9

REFERENCES

[1] K.-D. Kreuer *et al.*, Chem. Rev. 104 (2004) 4637
[2] K.A. Mauritz and R.B. Moore, Chem. Rev. 104 (2004) 4535
[3] J.-C. Perrin *et al.*, J. Phys. Chem. C 111 (2007) 3393
[4] F. Volino *et al.*, J. Phys. Chem. B 110 (2006) 11217

The dynamics of absorbed water determines proton transport in membranes employed in polymer electrolyte membrane fuel cells [1]. Among these soft charged materials, perfluoro-sulfonic acid compounds like Nafion [2] and Aquivion (differentiated by the length of their grafted side chains, shorter in the latter) play a crucial role in technology. However, due to their complexity they still constitute an extreme challenge. Simpler systems, like the perfluorooctanesulfonic acid ionic surfactant with a structure very similar to that of the Nafion side chain, also show similar properties.

Where do the challenges come from? In the presence of water, all these materials phase-separate, assuming intricate, multiscale, hydration-dependent morphologies where mechanical strength is provided by a hydrophobic host matrix and proton transport takes place in randomly distributed, irregular ionic nanodomains. Conductivity in these structures therefore depends on both the macroscopic total amount of water absorbed in the network of interconnected channels and the microscopic structure of the fluid molecules, making comprehension of this interplay very difficult to achieve.

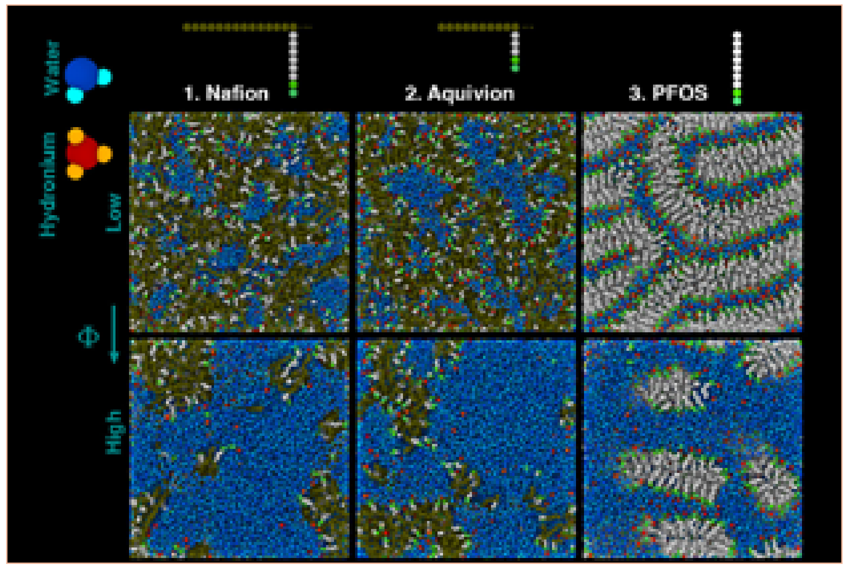

Figure 1
Sketches of the molecular models used in the MD simulations, together with typical snapshots of the considered systems at different water volume fractions, **Φ**. We represent in brown the polymer backbones, in white the side chains. Green beads schematise the SO_3^- groups, water is in blue and the protonated complexes (hydronium) in red (figure taken from doi:10.1038/s41598-017-08746-9).

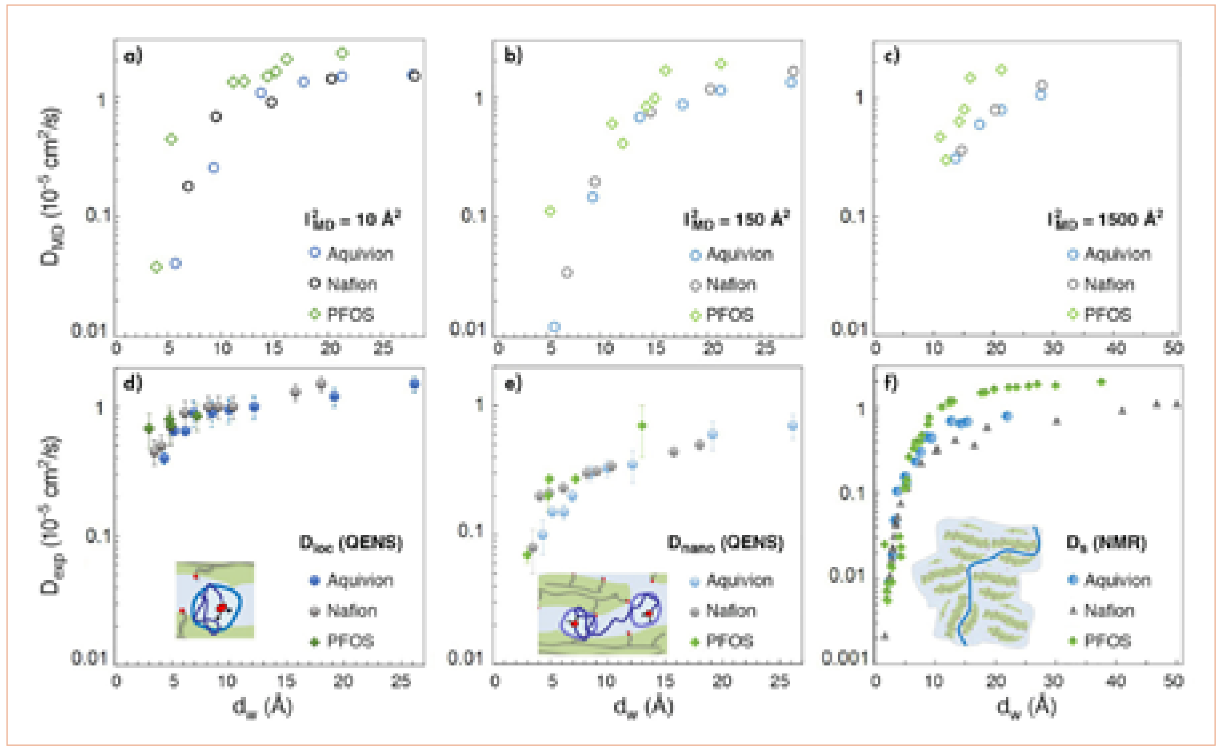

Figure 2
a), **b)**, **c)** MD diffusion coefficients of the water molecules, at the indicated length scales and hydrations for all materials, versus the size of ionic domains, d_w. Local **(d)** and nano-scale **(e)** diffusion coefficients determined by QENS using the generalised Gaussian model for localised translational motions [4]. **f)** Water self-diffusion coefficient measured by PFG-NMR. The data are plotted as a function of d_w to highlight the complex interplay between the structure of the confining environment and the dynamics of the absorbed fluid (figure taken from doi:10.1038/s41598-017-08746-9).

When complex dynamics at the nano-scale are involved, QENS experiments are inevitable [3]. In our work, we have complemented such experiments using small-angle X-ray scattering (SAXS) to gather specific information about the main features of the confining matrix, such as the typical size of the ionic domains, d_w and PGF-NMR measurements, which allow perfect control of the long-time self-dynamics limit. MD simulation supplies further help by providing, for instance, synthetic three-dimensional system templates that are useful for mere visual inspection or information of a kind that cannot be extracted from experiments. Such possibilities often enable additional arguments to be put forward in order to better justify or extend the interpretation of experimental results. Typical MD snapshots of the investigated materials, as well as sketches of the coarse-grained numerical models used in our simulations, are shown in **figure 1**.

By jointly analysing experimental and simulation data we have been able to distil two important main messages. First, by following the water molecules' trajectories generated by MD we have made an observation that would have been impossible under experimental conditions: the squared distance covered by the confined molecule over a certain interval of time is not linear in the latter, as it is in the case of in bulk. In contrast, it varies as a power law, with an exponent less than one and decreasing as hydration decreases. This is the hallmark of sub-diffusion and implies that water diffusion coefficients measured on different time (length) scales will be different, in contrast with Fick's law. The second conclusion originates from the data shown in **figure 2**: the diffusion coefficients that we 'read' in MD at well-chosen length scales in different hydration conditions reproduce analogous values extracted from experiments *via* extremely complex fitting procedures. These assume different dynamical mechanisms active at increasingly large length scales (cartoons in **figure 2**). In fact, at a few points the experiments probe the underlying anomalous dynamics of confined water which is tracked continuously by MD simulation.

Our work has a potential impact in all contexts where water confined at nanometric scales controls important phenomena, from biology to materials science.

(This is part of the ILL thesis work of Samuel Hanot)

What can we learn from magnetic oscillations in cuprate superconductors: planar coupling or fine details of Fermi surface reconstruction?

Thirty years after the discovery of high-temperature cuprate superconductors, while we have amassed a wealth of experimental information using many techniques it is sobering to admit that we still lack a convincing understanding of why they are special and how to calculate their superconducting temperature. A more profound examination using techniques pushed to new limits may not immediately solve the mystery, but may nevertheless stimulate the development of new methods that are applicable throughout condensed matter physics and may lead to the discovery of more fascinating new materials. One contribution of theory can be to help to put together pieces of the puzzle coming from different measurements. Important new data for the cuprates concerning the occurrence of charge density waves are now emerging, based on neutrons and X-rays and including those generated in free electron lasers combined with extreme conditions such as the simultaneous application of pulsed high magnetic fields [1]. We need to understand their significance: are they just interesting phenomena that are competing with the superconductivity, or do they provide vital clues as to the root causes? Is all the physics in the electronics of copper oxide planes or should we focus on interactions in the third dimension?

AUTHORS

P.D. Grigoriev (Landau Institute for Theoretical Physics, Moscow, Russia)
T. Ziman (ILL)

ARTICLE FROM

Phys. Rev. B 96, 165110 (2017);
https://doi.org/10.1103/PhysRevB.96.165110

REFERENCES

[1] S. Sebastien and C. Proust, Annual Rev. Cond. Mat. Phys. 6 (2015) 411
[2] H. Jang *et al.*, PNAS 113, 14645 (2016)
[3] P.D. Grigoriev and T. Ziman, JETP Lett. 106, 349 (2017); Phys. Rev. B 96 (2017)165110

Renewed interest in density waves in fact began with a rather surprising discovery made a decade ago using magnetotransport [2], when the transport coefficients in strong magnetic fields of under-doped cuprate superconductors were shown to display oscillations as a function of an inverse applied magnetic field. This is just like a weakly correlated metal with a regular Fermi surface, where the frequencies are the extremal values of cuts in the surface by planes perpendicular to the direction of the applied magnetic field. The dominant oscillations, expressed as a fraction of the first Brillouin zone (about 2 %), are, however, tiny compared with those expected for the doped bilayer compound YBa$_2$Cu$_3$O$_{6+\delta}$, and show a pattern of three slightly split frequencies with the central frequency greater than that of its two neighbouring shoulders. From angularly resolved photoemission spectroscopy (ARPES) experiments, features have emerged that indicate the appearance of Fermi surfaces, but they are peculiar in that they seem to be at most Fermi 'arcs'—one side only of complete closed pockets—but the areas, if closed off, are still much larger than the magnetic oscillations would indicate. In the experimental literature, it has generally been assumed that spin or charge density waves reconstruct the Fermi surface and give the low frequencies seen. In fact, there has since appeared more and more direct evidence of charge density order from both neutron and X-ray diffraction [1], and actually in the high magnetic fields needed to measure magnetic oscillations this order is of longer range than that in low fields. There have been several attempts to understand the observed oscillations in terms of a very fine-grained reconstruction of the Fermi surface *via* charge density waves compatible with diffraction studies. The significance of the charge density order is thus a new element under hot debate.

Figure 1

a) The crystal structure of YBa$_2$Cu$_3$O$_{6+\delta}$ showing the double layers of CuO$_2$ separated by chain layers. This gives rise to a band structure that can be understood as that of weakly coupled bilayers. Just as an electron propagating in a single layer with weak transverse coupling would have a Fermi surface corresponding to a corrugated cylinder, the bilayer structure with stronger intra-bilayer coupling than the three-dimensional dispersion gives rise to two concentric corrugated cylinders, as shown in **c)**. In ARPES there appear to be only 'Fermi Arcs', *i.e.* only one half of the expected cut of the cylinders, as shown in **b)**. In our theory the strongest frequency corresponds to the difference in areas F$_\alpha$ shaded in **b)**.

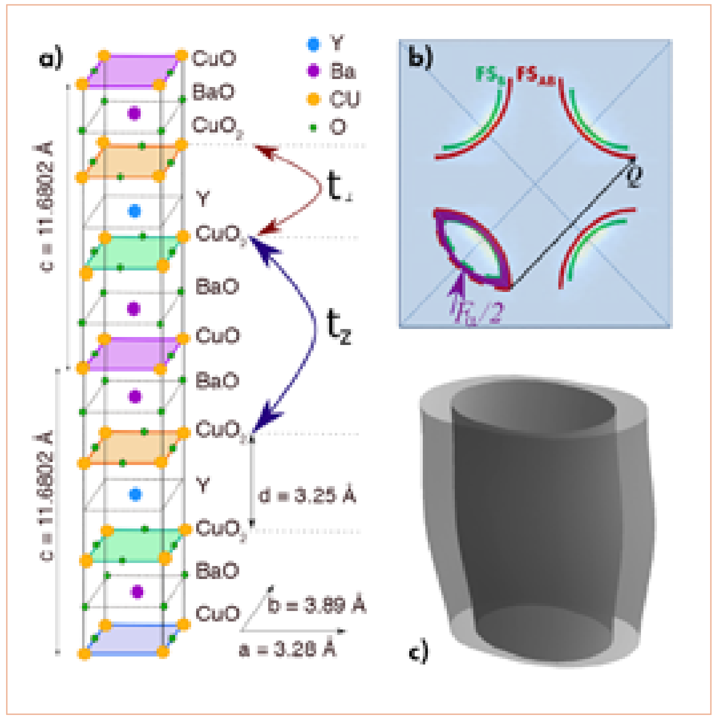

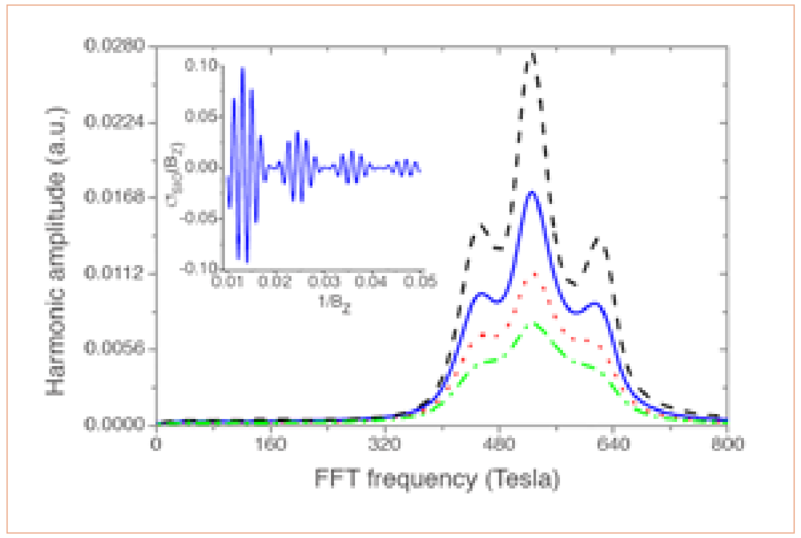

Figure 2

Magnetic oscillation amplitudes as a function of frequencies as calculated for different Dingle temperatures, as shown by the solid and dotted lines [3]. **Inset)** the calculated conductivity as a function of inverse field.

We have come up with a new interpretation [3] which we feel explains the experimental results and resolves certain puzzles much better, in particular: why, for a whole range of doping, do we see just three frequencies more or less independent of doping, with a stronger central peak flanked by two weaker shoulders? Why do the two shoulders vary with the angle of the field orientation with respect to the copper oxide planes? We propose that the three frequencies in fact correspond not to cross-sectional areas of the Fermi surface but rather to 'beats': differences of higher frequencies coming from the dependence of the conductivity on the products of oscillatory factors of density of states and diffusivity. The numerical values of the central peak F$_\alpha$ = 550 Tesla determines the intra-planar coupling, and the splitting 90 Tesla, the inter-planar dispersion. Of course, it is natural to ask why such non-linear terms may have amplitudes larger than the primary terms: the answer lies in the dependence on temperature and inhomogeneity, as our calculations indicate. Our theory very naturally reproduces the doping-independent pattern of a central frequency flanked by two weaker peaks, and in addition the angular dependence of the observed peak can be used to predict a primary, truly cross-sectional, Fermi surface area at 1 650 T, which may have been seen but whose existence is contested.

In conclusion, we have constructed a new theory for magnetic oscillations in the cuprates that successfully explains features of the experimental data and allows one to extract important parameters for the three-dimensionality of the electrons. Whether the theory is complete, and why the observed charge order does *not* lead to extra reconstruction, should lead to future exciting theory and experiments. Whether the issues of three-dimensionality and charge densities are interesting but peripheral details or are central to our future understanding of the ever enigmatic high-temperature superconductors is, of course, an open question.

MODERNISATION PROGRAMMES AND TECHNICAL DEVELOPMENTS

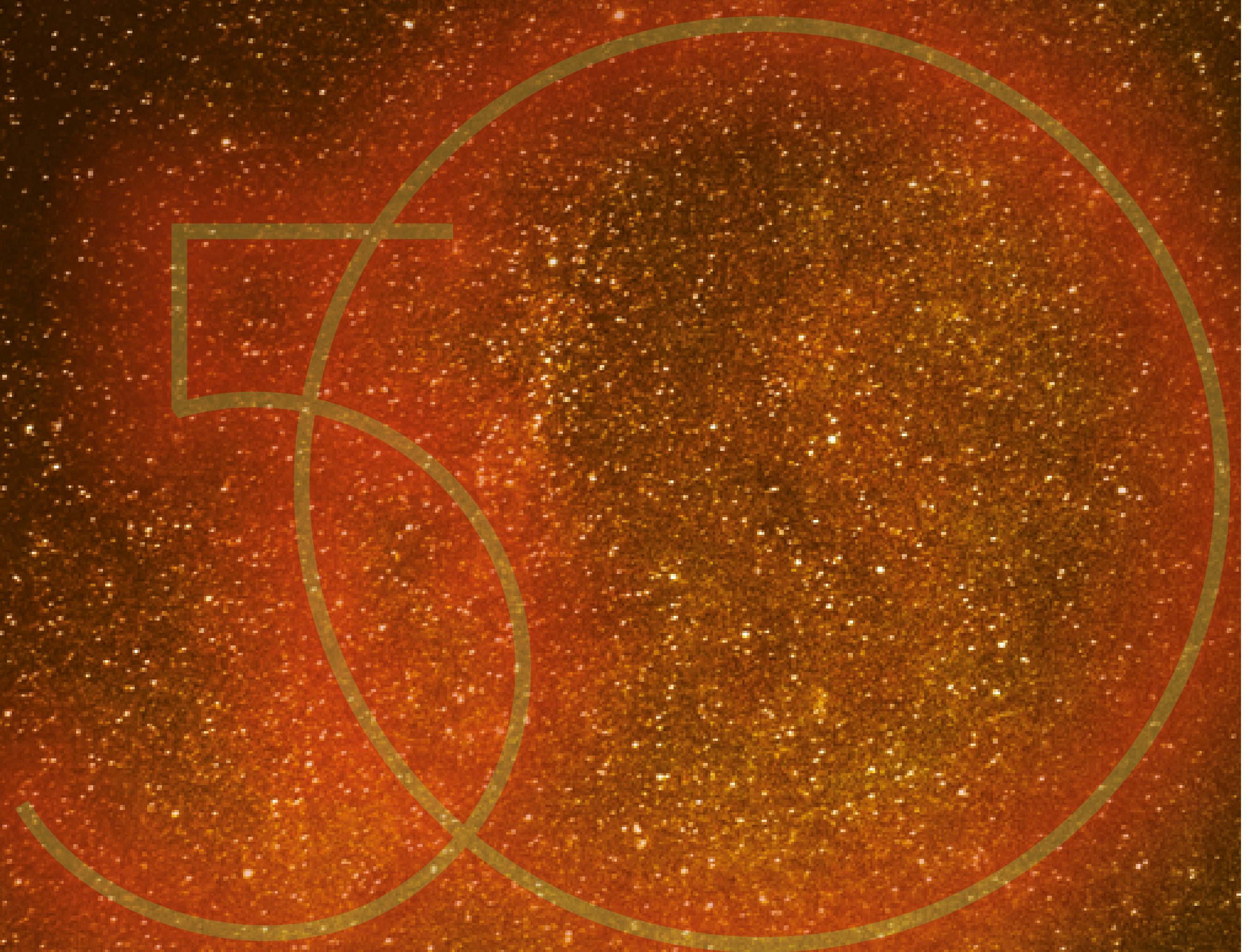

The ILL has maintained its international leadership by constant attention to its capacity for innovative engineering and the construction of ever more powerful instrumentation. The Millennium Programme is a fine example of this; it is now ending with the commissioning of WASP, which will receive its first neutrons in 2018. Millennium has been succeeded by Endurance, whose first phase started in 2016.

The call for proposals for Endurance phase 2 was very successful. The selection process carried out by the ILL and its partners has resulted in a plan for Endurance 2 contained in four different packages to be deployed between 2018 and 2023. Depending on the funding made available, this new programme will ensure even better performance from the instruments, enhancing the quality of research our users can produce with our neutrons.

The Projects and Techniques Division is at the centre of all this activity. Its operations are project-oriented and conducted in close liaison with the Science Division, which is principally responsible for determining the scientific framework and the level of performance to be achieved.

The performance gains expected from the new instruments will also call for research and innovation in other technical fields, including simulation techniques such as calculations and virtualisation, to improve the design of the instruments and their environment. These additional projects—new detectors and guides to be built as well as innovative data acquisition and storage techniques—will ensure that the instruments set new standards in their fields.

The level of experience acquired by the Projects and Techniques Division has naturally led to its participation in a number of European projects and conferences with a view to both sharing and developing its capacity, whether with regard to the development of new instruments (detectors, guides, instrumentation, electronics, and so on), data-sharing systems or a new reactor fuel design. All this, from the perspective of continuously renewing our capacity for collaboration.

The Division also has its part to play of course, on a daily basis, in the routine running of a research facility, such as the maintenance and renewal of the ILL's software applications or the renovation and improvement of its buildings and infrastructure.

The continuous improvement of the ILL's instrumentation is the force at the heart of the Division's activities.

Jérôme Estrade
Associate Director
Head of the Projects and Techniques Division

MODERNISATION PROGRAMME

Endurance: the ILL instrument upgrade programme

AUTHORS
C. Dewhurst and J. Estrade (ILL)

Over the last decades, neutron scattering in Europe has seen a big step forward both in capacity and capability. New sources aside, progress has been primarily fuelled by technological improvements in neutron delivery and neutron detection combined with computer-aided instrument optimisation. At the ILL this process has led to a series of ambitious upgrades managed under the Millennium and Endurance Programmes. The Millennium M-0 phase saw 14 projects completed by 2009, while the M-1 phase is entering its final stage with the commissioning of WASP in 2018. In total, the Millennium Programme has seen 26 new or upgraded instruments with a financial volume (exclusive of in-house staff costs) of ~ 80 M€ over a period of 15 years. The return on this investment, which is small on the scale of the operational budget, is nevertheless impressive, and as a result the ILL can offer its users state-of-the-art experimental facilities. The constant high demand for beamtime and concomitant high-quality publication output demonstrates the attractiveness of the services provided. Modernisation of the ILL instrument suite and support infrastructure continues under the Endurance Programme.

The first phase, Endurance1, running from 2016 to 2018, is well underway having benefited from an additional contribution from the ILL's Associates of 4.5 M€/year. The new fission fragment spectrometer, **FIPPS**, was the first instrument to begin commissioning and delivering new science at the end of 2016. The new thermal time-of-flight (TOF) spectrometer, **PANTHER**, is anticipated to begin commissioning in 2019, along with the new source of ultra-cold neutrons (UCN), **SuperSUN**. The backbone of Endurance1 is the 'Chartreuse' project, involving the renewal of the **H24** thermal neutron guide and the upgrade of the **D10$^+$** single crystal diffractometer, the **IN13$^+$** (CRG) backscattering spectrometer and a new extreme conditions powder and single crystal diffractometer, **XtremeD** (CRG). Each instrument will benefit from a dedicated end-of-guide position allowing for optimised beam-shaping and monochromator optics. Importantly, the new H24 guide will also leave potential for further high-performance instrumentation. Due to constraints on the functioning of the ILL reactor during 2017 the 'Chartreuse' projects, H24, D10$^+$, IN13$^+$ and XtremeD, will now be delivered upon completion of the H1-H2 in-pile guide renewal at the end of 2020. A rollout of data treatment work packages as part of the **BASTILLE** project sees the ILL join the multi-facility Mantid project, while the **NESSE** project is already delivering new and upgraded sample environment capabilities and support infrastructure.

The year 2017 saw the scope and strategy of a second phase, Endurance2, begin to take shape. In December 2016 the ILL invited expressions of interest and proposals for flagship instruments to exploit the full scientific potential of the ILL's high-flux reactor and to help define a coherent scientific strategy and capabilities within the landscape of existing and emerging neutron sources. Following an unprecedented response from the community, a dedicated Instrument Subcommittee of neutron instrumentation experts reviewed proposals for new and upgraded instruments in order to advise the Scientific Council as to the priorities and strategy for Endurance2. During 2018 the final scope and strategy of Endurance2 will be presented to the ILL Steering Committee with the aim of securing additional funding and getting the go-ahead, thus allowing the ILL to continue instrument and infrastructure modernisation and secure its leading role in neutron sciences well into the 2020s. Briefly, projects within the scope of Endurance2 are as follows:

Endurance
Setting the pace

Large-Scale Structures: Detector upgrades providing greater area to the SANS instruments **D11** and **D22** and the cold diffractometer **D16**. An upgrade of the collimation section of D11 is also proposed. A second **LADI-B** protein crystallography station is envisaged, doubling capacity and improving instrument resolution. In order to fully exploit the **Rainbows** option on **D17** and **Figaro**, the purchase of a high spatial resolution, high-count-rate and large-area detector is envisaged when the technology being developed at the ESS becomes available. It is also anticipated that the ILL will engage in new activities centred around neutron imaging with the provision of a public neutron imaging instrument, **IM2020**.

Diffraction: The powder and single crystal diffractometers **D20** and **D19**, respectively, are to expect a replacement of their ageing detectors. An upgrade to the primary spectrometer of the **D7$^+$** diffuse scattering instrument promises gains of more than x10 in intensity. An upgrade to the polarised hot-neutron diffractometer, **D3**, with a position-sensitive detector and upgraded polarisation components will allow for efficient measurement of hydrogen-containing liquid samples.

Spectroscopy: The world-leading **IN5$^+$** spectrometer will be upgraded with a new high-performance, elliptically focusing guide, while the full scope of the new **PANTHER** thermal TOF spectrometer and the new spin-echo spectrometer **WASP** is expected to be achieved. The **SHARP** (CRG) TOF spectrometer (formerly IN6) will be upgraded by the CRG team with a new large-area position-sensitive detector, while the primary spectrometer will be renewed along the lines of the **RAMSES** concept when relocated onto a newly rebuilt **H15** guide. Upgraded Silicon-311 analyser options for **IN16B** are also being considered, while the thermal TAS instrument **IN20** should benefit from upgraded monochromators, polarisation equipment and higher-order wavelength filtering using a velocity selector. The **MARMOT** upgrade will add a multiplexed analysis option to the cold TAS spectrometer **THALES**.

Nuclear & Particle Physics: The new fission-fragment spectrometer, FIPPS, begun under Endurance1, should see additional performance under the FIPPS2 project in terms of gamma-ray discrimination with the addition of anti-Compton discrimination detectors and an additional gas-filled-magnet mass spectrometer to directly measure the mass of fission fragments.

Infrastructure: Two cold neutron guides, **H15** and **H16** are expected to be renewed under Endurance2, providing intense cold neutron beams to the instruments **IN5$^+$**, **SHARP**, **D7$^+$** and **D11** as well as providing beam positions for potential further instrumentation. A renovation of the thermal **H23** guide may also allow for further thermal instrumentation on either H23 or H24. Thus, Endurance2 also includes scope for infrastructure requirements for future instrumentation. The sample environment project **NESSE** and data treatment and analysis project **BASTILLE**, begun under Endurance1, are expected to continue through Endurance2.

Once the programme is established, funding will be sought from the ILL's Associates as well as through other channels. Ideally Endurance2 should be approved by the Steering Committee by Autumn 2018 at the latest in order to begin promptly in 2019, commensurate with the termination of Endurance1. The expected funding of Endurance2 should be of a level similar to that of Endurance1, with a dedicated contribution from the Associates and the ILL's own budget over the five-year period 2019–2023. French national funds and Grenoble regional funds, the so-called CPER grant, are providing additional monies on top of those requested from Associates. The CPER funds are allowing us to inject additional resources and provide a smooth interface between the first and second phase of the Endurance Programme. On the recommendation of the Instrument Subcommittee and Scientific Council, the CPER funds have been allocated to permit full specification of Endurance1 projects such as **PANTHER**, advance some Endurance2 projects such as **IN5$^+$**, **FIPPS2**, **IN20** and **LADI-B** and allow for early planning and design studies for infrastructure such as **H15** in advance of the official start of Endurance2.

FIPPS – the ILL's new nuclear physics instrument

What is the origin of heavy elements? What is the force keeping nucleons together in the atomic nuclei? To answer questions like this we need nuclear physics observables. The combination of an intense pencil-like neutron beam and a high-sensitivity nuclear spectrometer can reveal the properties of nuclei in many different regions of the nuclear chart. This is the principle underlying FIPPS, the ILL's new nuclear physics instrument.

AUTHOR

C. Michelagnoli (ILL) on behalf of the FIPPS team

REFERENCES

[1] M. Jentschel *et al.*, JINST. 12 (2017) 11003
[2] G. Bocchi *et al.*, Phys. Lett. B 760 (2016) 273
[3] N. Cieplicka *et al.*, Phys. Rev. C 93 (2016) 054302

There has been a host of international collaborations, using many different techniques, focusing on atomic nuclei. The search for answers to fundamental questions in nuclear theory and nuclear astrophysics has also led to practical applications in the fields of nuclear waste and nuclear medicine. At the ILL the nuclear physics instruments Lohengrin and GAMS have been providing a wealth of nuclear information for several decades, thanks to the extraordinary resolutions available and the use of in-pile targets. The recent EXILL campaign [1] demonstrated the unique advantages provided by an efficient spectrometer on a neutron beam.

FIPPS is a FIssion Product Prompt-gamma-ray spectrometer arising from this experience. It consists (in its first phase, operational since December 2016) of a pencil-like thermal neutron beam and an array of HPGe clover detectors mounted symmetrically around the target position (**figure 1**). The detectors detect the γ-rays emitted by excited nuclei produced by neutron-induced reactions with 2 keV energy resolution at 1.3 MeV. The 'add-back' of Compton scattered γ-rays in the different germanium crystals of the same clover produces additional efficiency (compared with traditional coaxial germanium detectors). We thus achieve gains of up to 55(6) % of statistics at 6.8 MeV (from γ-rays measured for the ^{49}Ti nucleus). The signals are processed with digital electronics (CAEN V1724 cards, 100 MHz) and the energy information is extracted by applying a trapezoidal filter (moving window deconvolution) to the digital waveforms. This provides for high count rates (~ 10 kHz per crystal) without any loss in detection.

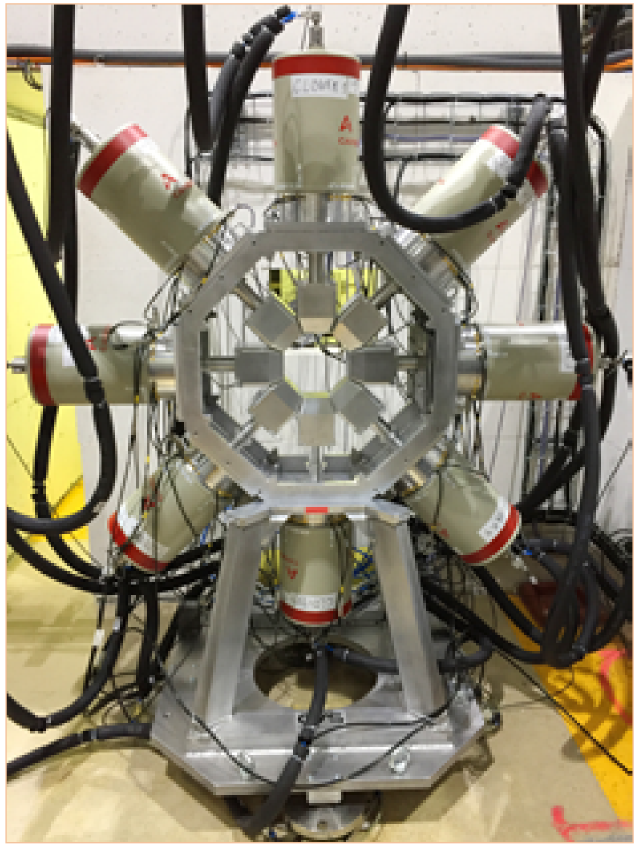

Figure 1

The FIPPS phase I spectrometer.

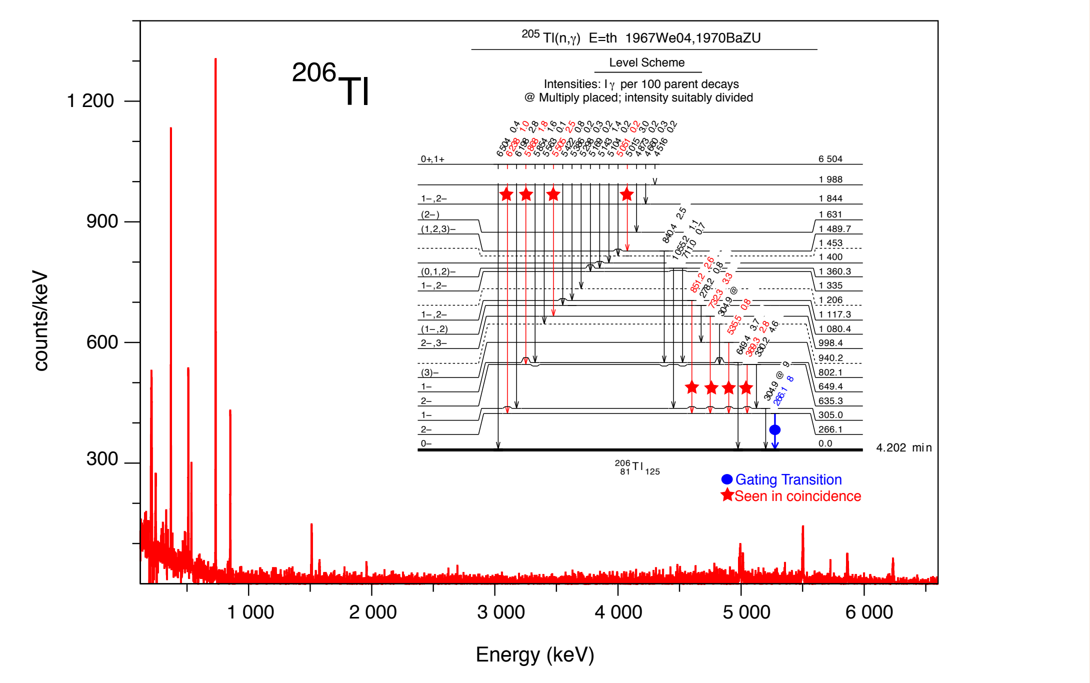

Figure 2

Coincidence γ-ray spectrum of the ^{206}Tl nucleus, obtained at FIPPS after ~ 40 minutes of beam on target.

The instrument is located on the H22 thermal neutron guide. The beam from the guide (7 x 10^8 ncm^{-2}s^{-1}, diameter of about 2 cm) is collimated up to the target position. The 2.20 m collimation system consists of a series of apertures in natural boron carbide. There are thick (5 cm) lead absorbers at the exit of each aperture to reduce the neutron-induced gamma background. The collimation system is installed in a round vacuum tube, coated with 1 cm of borated plastics. The thermal neutron flux at the target position has been measured at 10^8 ncm^{-2}s^{-1}, 1 cm diameter.

The set-up was commissioned in December 2016 and six different experiments took place during the first experimental campaign, from December 2016 to January–March 2017. Over 30 users from 11 universities and laboratories were involved. Fifteen different targets were used to study the structure of nuclei produced in neutron-capture reactions. The research focused on different nuclear phenomena, and on the study of the interplay between collective and single-particle structures in nuclei in particular.

The first experiment examined the structure of the ^{206}Tl nucleus after neutron-capture reactions, using a ^{205}Tl target. This nucleus consists of 81 protons and 125 neutrons, one neutron and one proton outside the doubly magic shell closure corresponding to the ^{208}Pb nucleus. This is an ideal test for nuclear models using ^{208}Pb as a core and the remaining valence particles determining the observed structure as a consequence of the occupation of the single particle orbitals outside the doubly-magic core. As recent publications from the EXILL campaign at the ILL have highlighted [2, 3], we can expect to discover more complex structures arising when collective states couple onto single particle ones.

Figure 2 shows the first coincidence spectrum for ^{206}Tl obtained at FIPPS, with the corresponding transitions highlighted.

The next experimental campaigns will see new methods being used (fast scintillators, for example). A casemate has already been installed for dynamic confinement of the atmosphere in the experimental zone for radioactive and fissile targets. We are planning experiments with ^{233,235}U fissile targets for 2018, including the testing and use of fission event tags.

In a second phase of the project (planned to be operational in four years) the γ-ray detection system will be coupled to a fission fragment separator based on gas-filled technology. This will significantly increase the sensitivity of the spectrometer for fission studies, making new investigations into the fission phenomenon and the structure of neutron-rich nuclei on the r-process nucleosynthesis path possible.

Search for sterile neutrinos: the STEREO experiment

STEREO searches for oscillations of reactor antineutrinos at very short baseline from the ILL reactor core. A first phase of data-taking (November 2016 to March 2017) has been successfully completed, with results expected in 2018. STEREO has been reinstalled after being withdrawn for reactor maintenance and resumed data-taking in October 2017.

AUTHORS
S. Fuard and T. Soldner (ILL)

REFERENCES
[1] C. Patriganani *et al.*, (Particle Data Group), Chin. Phys. C 40, 100001 (2016) Chapter 14
[2] T.A. Mueller *et al.*, Phys. Rev. C 83 (2011) 054615
[3] G. Mention *et al.*, Phys. Rev. D 83 (2011) 073006

Oscillations between the three neutrino flavours, electron-neutrino, muon-neutrino and tau-neutrino, of the standard model of particle physics have been observed by many experiments. They can be explained by the mixing of three neutrino mass eigenstates. One consequence is the disappearance of about 10 % of the electron-antineutrinos produced by beta decay of the fission products in a nuclear reactor at about 1 km from the reactor core. This has been measured with high precision by the experiments Daya Bay (China), Double Chooz (France) and RENO (South Korea) [1]. At distances below 100 m from reactors the disappearance is negligible. However, a re-evaluation of predicted spectra of reactor-antineutrinos [2] and subsequent analysis of experiments at such short baselines [3] have revealed a deficit of about 6 % of detected antineutrinos compared with what was predicted. This unexpected deficit cannot be described by the standard three-neutrino mixing, and is called 'Reactor Antineutrino Anomaly' [3]. It might be explained by an oscillation to a new neutrino species, called 'sterile neutrinos', since they do not participate in weak interactions.

The use of STEREO was proposed to confirm or refute the sterile neutrino hypothesis. It requires searching for neutrino oscillations at very short baseline. The ILL reactor provides optimum conditions for this research. The core is very compact (it should be small compared with the expected oscillation length) but provides sufficient power for the experiment. The highly-enriched fuel allows for direct comparison with the antineutrino spectrum predicted for ^{235}U, whereas contributions from several fissile isotopes superpose in power reactors. Finally, the location chosen for STEREO, about 10 m from the reactor core, is protected from cosmic background radiation by the transfer channel, a large volume of water just above it.

Conversely, the extraction of neutron beams into the reactor hall for scattering instruments creates challenging background conditions for neutrino experiments, namely a high flux of fast and thermal neutrons and capture gammas. The STEREO collaborators have quantified the background through a series of measurements and have designed the shielding accordingly: the walls of neighbour instruments and casemates were reinforced by 50 tonnes of lead and three tonnes of borated polyethylene. The STEREO detector itself (**figure 1**) is shielded by another 60 tonnes of lead and six tonnes of borated polyethylene. A two-layer shielding of soft iron and mu-metal suppresses magnetic fields from neighbour experiments and prevents a deterioration in STEREO energy measurement.

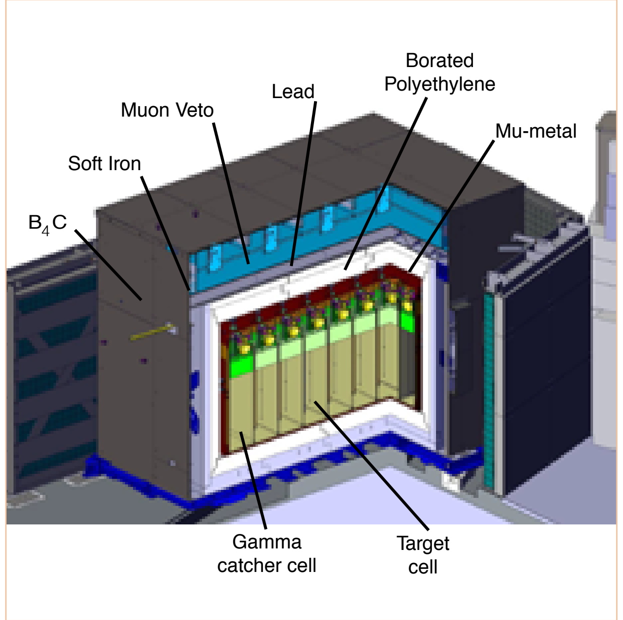

Figure 1

Cut through of the STEREO detector. The target is split into six cells along the propagation direction of the antineutrinos and surrounded by four gamma catcher cells.

Figure 2

Preparation for the last metres of STEREO's journey to its measuring position. The assembled detector and shielding structure, in total about 90 tonnes, were transported by air cushions.

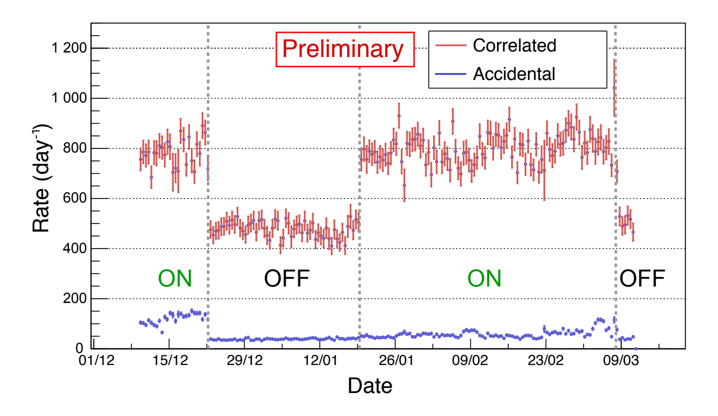

Figure 3

Rate of correlated and accidental coincidences of a positron candidate and a neutron candidate by date. The correlated background (measured with reactor-OFF) is caused by cosmic radiation and has been corrected for atmospheric pressure variations. The rate increase for reactor-ON is due to reactor antineutrinos. The signal-to-background ratio being close to 1, STEREO needs to measure roughly equal periods of reactor-OFF and reactor-ON.

STEREO detects electron-antineutrinos by inverse beta decay in a Gd-loaded liquid scintillator: the antineutrino and a proton from the hydrogen-rich scintillator convert into a positron and a neutron. The positron carries almost all the antineutrino's energy and is used for spectral measurement. The neutron of a few keV kinetic energy is moderated before its detection *via* capture, dominantly on Gd. This delayed coincidence of neutron and positron signal provides a specific signature used to suppress background from uncorrelated events. The STEREO target consists of two tonnes of Gd-loaded scintillator separated into six cells along the propagation direction of the antineutrinos. Comparing the spectra measured in the different cells as a function of the distance to the reactor core reduces sensitivity to the predicted antineutrino spectrum. The target is surrounded by two tonnes of Gd-free scintillator, the gamma-catcher, which detects gammas escaping from the target and thus improves energy reconstruction. Atmospheric muons can create high-energy neutrons by spallation in heavy materials and are therefore a source of coincident background that needs to be subtracted by measurements with the reactor off. A water Cherenkov detector installed on top serves as a muon veto, improving the signal-to-background ratio.

STEREO was designed and built by a collaboration between CEA-IRFU Saclay, LAPP Annecy, LPSC Grenoble, MPIK Heidelberg and the ILL. The STEREO structure, detector and shielding were assembled in an area with crane access and moved by air cushions to the measuring position below the transfer channel (**figure 2**). STEREO is designed to resist earthquakes, is protected against fire and has been reviewed by the French authority for nuclear safety, ASN. With the strong support of several ILL teams STEREO became operational in November 2016. STEREO took data continuously until March 2017 over 1.5 reactor cycles and including reactor shutdowns, which were essential to subtract the coincident background. Overall, detector performance and background levels fulfilled the requirements. Data analysis is ongoing (**figure 3**) and we expect complete results for this first data set in spring 2018.

In March 2017 STEREO had to be retracted temporarily for reactor works. This time was used to repair some faulty components in the detector. Since October 2017 STEREO has been taking data again, with improved performance. We are planning to collect statistics for at least six reactor cycles and shutdowns, which should allow us to confirm or refute the sterile neutrino hypothesis.

INSTRUMENT UPGRADES

GAMS6 – the world's highest resolution gamma-ray spectrometer

AUTHOR
M. Jentschel (ILL)

The new double-crystal spectrometer GAMS6 was commissioned in 2017. It offers world-leading energy-resolution power at E/ΔE = 10^6, outstanding drift stability of about 10 nrad / day and absolute energy measurement capabilities with 10 meV accuracy. Its first users performed experiments in 2017 on photon matter interaction, nuclear structure physics and metrology.

Figure 1

The interior of the GAMS6 vacuum chamber, showing the optical angle interferometers and the goniometer axes.

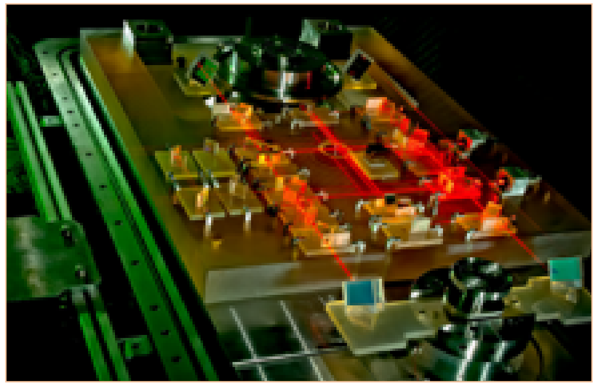

Gamma-ray spectroscopy scientists use detectors that absorb radiation and convert the energy released *via* internal quantum effects (band gap, optical transition) into a discrete number of events (conduction electrons, optical photons). The conversion into a finite number of quantum events induces statistical uncertainty, resulting in an intrinsic limitation of energy resolution and dynamic range. An alternative approach to gamma-ray spectroscopy relies on the diffraction of gamma rays at perfect crystals. Knowing the crystals' lattice spacing and diffraction angle, we can obtain the gamma rays' wavelength and therefore their energy. Dynamical diffraction theory predicts the theoretical resolution of such crystal spectrometers as being up to three orders of magnitude superior to that of absorption spectrometers. There are other advantages: a superior dynamic range (up to two orders of magnitude) and the possibility of self-calibration. However, crystal spectrometers require an extremely well-collimated beam that reduces the solid angle and needs to be compensated for by substantial source activities. Crystal spectrometers are therefore difficult to use in combination with other detector systems. Both types of spectrometer are used at the ILL: conventional absorption detectors grouped into two arrays around a neutron or particle beams (PN1, FIPPS) and ultra-high resolution crystal spectrometers pointing to a target inside the ILL reactor.

The ILL has a long history of operating crystal spectrometers. It started in the '70s with GAMS1-3, bent-crystal spectrometers, which were later replaced by the double-flat crystal spectrometers GAMS4-5. These instruments were installed at the two exits of the H6/H7 tangential beam tube, taking advantage of the extraordinary neutron flux of 5 x 10^{14} n s^{-1} cm^{-2} at the in-pile target position. GAMS4 made it possible, for the first time, to achieve resolution power close to the theoretical prediction. This triggered the development of new experimental techniques. Due to the ultra-high resolution, it was possible to deduce nuclear state lifetimes and study atomic motion by measuring Doppler-broadened gamma profiles. It also became possible to measure absolute gamma-ray energies with 0.1 ppm accuracy. This enabled the neutron mass to be determined to ten-figure accuracy and Einstein's mass/energy equivalence principle to be tested directly with unprecedented accuracy.

Crystal spectrometers face the particular challenge of measuring the diffraction angle. Sub-nanoradian angular resolution is required over a range of 30 degrees. This is achieved using dedicated optical angle interferometers. Over the ten years of operation on GAMS4 and GAMS5, the spectrometers' main limitations were the time drifts of these optical interferometers, obliging users to perform fast scans or accept certain systematic errors. The drifts were essentially due to the spectrometer being operated under (albeit well-controlled) atmospheric conditions. As it was not possible to convert the old spectrometers to operate under vacuum conditions, it was decided to develop a completely new instrument. The aim was to measure gamma-ray energies with 10 ppb accuracy and gain an order of magnitude in stability.

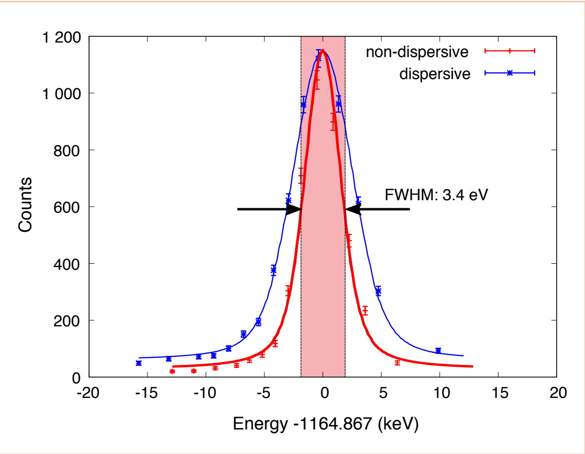

Figure 2

Measured resolution of GAMS6 at 1.1 MeV (non-dispersive blue curve). The red curve shows the instrument operating in energy dispersive mode and measuring Doppler-broadening due to thermal motion of the emitting atoms.

GAMS6 now boasts many technological improvements.

The first step was to develop and test a new interferometer layout. GAMS4-5 operated with two independent interferometers for each crystal, thus generating individual drifts for each axis. By working under vacuum conditions we were able to develop a common interferometer layout using the same optical components to measure the angle of both axes. This compensated for any drift in the optical components and allowed us to monitor the vibrations and stability of the interferometer itself. We reduced long-term drift by replacing the chemical epoxy bonding by a silica bonding technique, with all the optical components linked to a block of ultra-low expansion ceramics. New electronics developed in-house recover the interferometer signals and provide feedback control for positioning.

The next challenge was to protect the interferometer and the goniometer axes in the vacuum chamber from vibration (from the vacuum pumps and other sources of vibration in the reactor). For stable operations the spectrometer requires temperature variations of less than 10 mK/day; this implies the elimination of all heat sources from the vacuum chamber (motors, light sources, detectors, etc). We therefore designed a vacuum chamber with the main interferometer table mechanically decoupled from the vacuum chamber walls. The vacuum chamber is positioned on a 2 m^2-wide air pad over a polished granite block; the spectrometer can thus be manoeuvred according to the diffraction angles. The entire system weighs almost three tonnes and is suspended on air cushions. Pressure in the cushions is actively controlled to maintain the orientation of the granite block independent of the vacuum chamber position within 10 microradian with respect to the H6/H7 beam axis. The development, mounting and commissioning period took over ten years and was carried out in close collaboration with a number of other institutions, including Italy's and Germany's national metrology institutes INRIM and PTB.

GAMS6 was commissioned in late 2016 and received its first users in March. The first experiments performed aimed to measure the refractive index of materials at gamma-ray energies; these were followed by a first ever campaign to study mixed symmetry in the octupole deformations and double octupole phonon excitations of 144Nd. More recently, measurements have been performed to improve the current value of the neutron mass. The results are particularly sensitive to systematic error and remain statistically limited, but the data are currently being evaluated and publications being prepared.

GAMS6 is now shut down for the exchange of the H6/H7 tangential beam tube, anticipated for 2019-20. This gives us time to make further improvements, including work to reduce the impact of mechanical vibration on the measurement process.

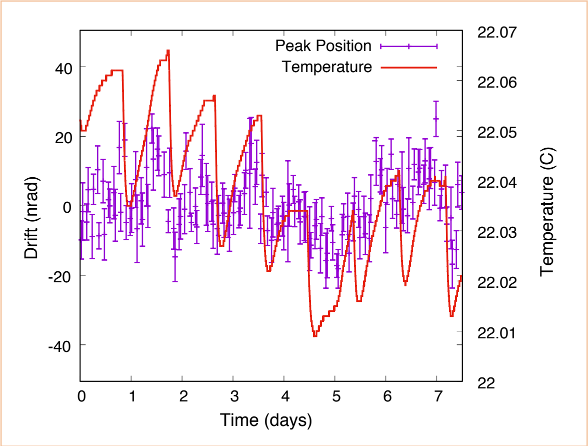

Figure 3

Measured drift of the instrument (error bars). These data result from an experiment to measure the neutron mass by periodically scanning the deuterium gamma-ray transition. No substantial drift can be detected within the statistical uncertainty. A slight correlation with residual temperature variation requires further investigation. The red line shows the temperature drift of the instrument. The main temperature modulation results from periodic filling of GAMS's Ge-detector.

TECHNICAL AND COMPUTING DEVELOPMENTS

A record in backscattering energy resolution — first tests on IN16B with the GaAs prototype

Since late 2013 we have been developing a prototype neutron backscattering spectrometer using the GaAs 200 reflection to achieve a significant increase in energy resolution. We report here on the first test measurements conducted on IN16B, which have yielded an unprecedented resolution of (76.5 ± 3.3) neV FWHM, an order of magnitude narrower than the current standard.

Figure 1

GaAs prototype.
Top left: Monochromator, mounted on goniometers, with water cooling circuit and power supply. **Bottom left:** Side view of an analyser segment, with alignment mechanics and temperature control. **Right:** Analyser mounted inside the spectrometer. (Photos: Markus Appel, Bernhard Frick)

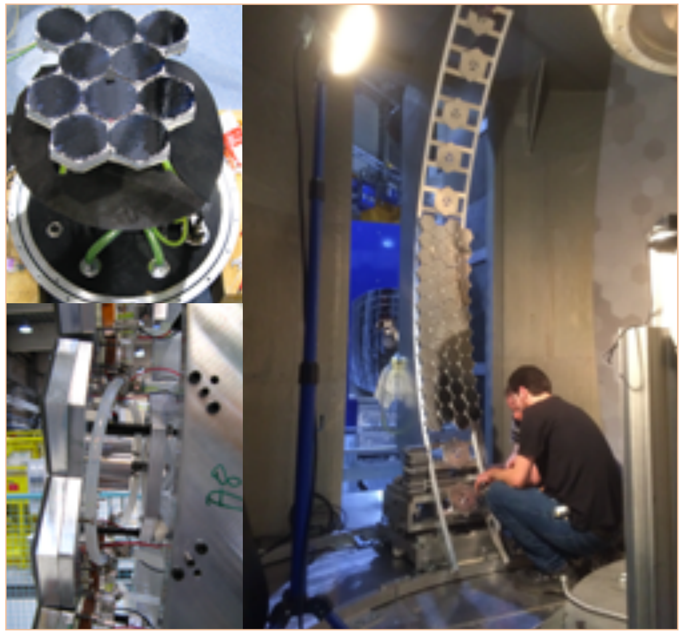

AUTHORS
K. Kuhlmann and **M. Appel** (ILL and Friedrich-Alexander University Erlangen-Nürnberg, Germany)
B. Frick (ILL)
A. Magerl (Friedrich-Alexander University Erlangen-Nürnberg, Germany)

REFERENCES
[1] K. Kuhlmann, M. Appel, B. Frick and A. Magerl (in preparation)
[2] https://www.ill.eu/instruments-support/instruments-groups/instruments/in16b

A backscattering spectrometer uses Bragg reflections of single crystals to determine the energy of the neutrons before and after scattering from the sample. Since the crystals are mounted at a Bragg angle of 90° ('backscattering'), the energy resolution is in first order independent of the beam divergence and—aside from the technical limitations discussed below—limited by the Darwin width $(\Delta\boldsymbol{\tau}/\boldsymbol{\tau}) = (16\pi N_c\, F_{\boldsymbol{\tau}})/\boldsymbol{\tau}^2$ of a Bragg reflection with a reciprocal lattice vector $\boldsymbol{\tau}$. The Darwin width is a material property and depends on the structure factor $F_{\boldsymbol{\tau}}$ of a Bragg reflection. We used the GaAs 200 reflection for the prototype, with $(\Delta\boldsymbol{\tau}/\boldsymbol{\tau}) = 1.55 \times 10^{-6}$, an order of magnitude narrower than the current standard (Si 111), where $(\Delta\boldsymbol{\tau}/\boldsymbol{\tau})_{\mathrm{Si\ 111}} = 18.6 \times 10^{-6}$. This makes it possible to gain a factor of ten in energy resolution.

To achieve this, several constraints need to be mediated. For instance, in order to avoid deformation of the crystals inducing strain, the monochromator and analyser were constructed using 4 x 4 mm^2 crystals; these need to be installed with a misalignment of less than 0.1°. In addition, since thermal expansion changes the lattice parameter and thus the reflected wavelength, the variation in temperatures across the crystal area (10 m^2 for a fully equipped spectrometer) has to be stabilised homogeneously to less than 0.3 K. Moreover, since neutrons undergo an energy change of 103 neV/m against the Earth's gravity, the energy acceptance of the crystals needs to be adapted using a temperature gradient of 3.3 K/m along the 3 m-high analyser. We therefore devised a technique for manufacturing the crystal components, a support with alignment mechanics and a temperature control system fulfilling these requirements (**figure 1**).

Since the crystals are the centrepiece of the instrument, an extensive study of the structural quality of commercially available GaAs wafers was required. Over the last three years we have investigated some 50 GaAs wafers with different specifications using a two-crystal backscattering test set-up specifically built for this purpose on IN10. The average two-crystal convolved FWHM within this sample system was found to be 19.5 neV, only 50 % higher than the ideal crystal limit of 13.2 neV. We also measured variations of the lattice parameter caused by the incorporation of dopant atoms (boron and silicon) into the crystal structure during the growth process. These amounted to up to 10^{-5} in relative lattice parameter variation—much larger than the Darwin width—but we found that this effect can be tolerated if the concentrations of both B and Si are limited to less than 10^{18} cm^{-3}. In the prototype, any residual variations of the lattice parameter are mediated by adapting the temperature of the crystals.

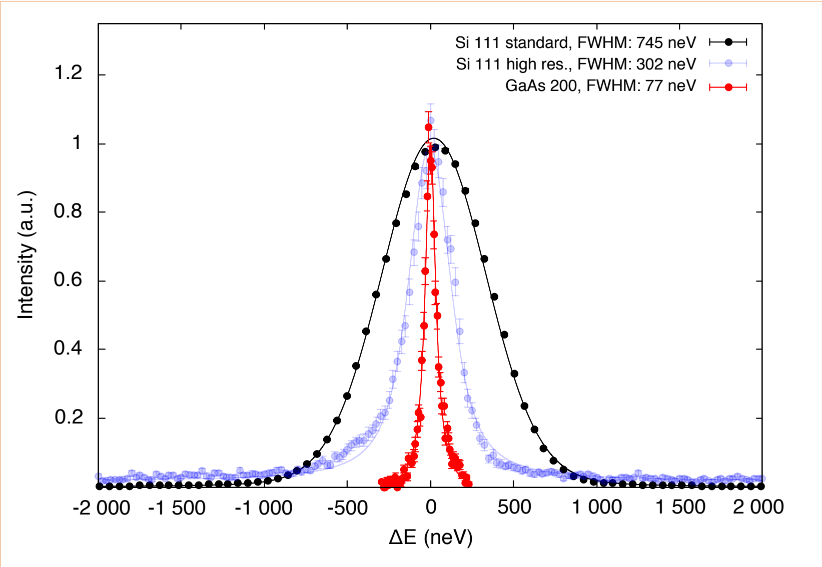

Figure 2

Resolution function of the GaAs prototype obtained using a Ø8 mm wooden ball as strong elastic scatterer, compared with the resolutions of two available Si 111 configurations of IN16B.

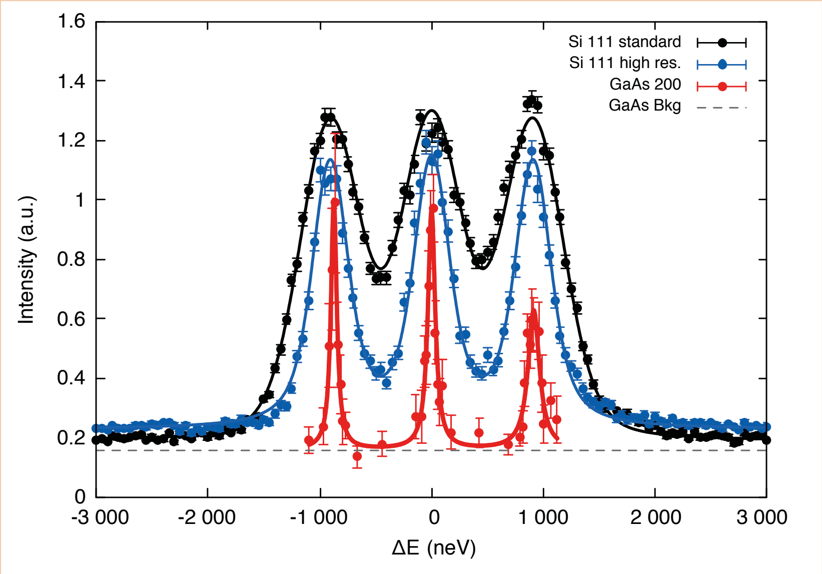

Figure 3

Hyperfine splitting in cobalt, compared with measurements in two Si 111 configurations of IN16B.

To illustrate the potential of a GaAs-based spectrometer we installed a monochromator and an analyser in the geometry of a user instrument, covering approximately 3 % of IN16B's crystal surface. The resolution line width of (76.5 ± 3.3) neV FWHM (**figure 2**), measured under usual instrument operating conditions, is a world record for neutron backscattering [1], a factor of ten narrower than the standard IN16B resolution of 750 neV FWHM and a factor of four narrower than the highest currently available resolution of 300 neV FWHM [2].

To demonstrate the feasibility of inelastic neutron scattering experiments, we measured the hyperfine splitting in cobalt as a benchmark (**figure 3**). Compared with previous measurements on IN16B in two Si 111 configurations, we obtained a largely improved resolution but also recognised a deterioration of the line width and height of one of the inelastic peaks. We explain this by temperature inhomogeneities caused by the mechanical support of the monochromator.

During these first tests, temperature scans of the monochromator were used to perform energy scans. The accuracy of the measured energy transfer is limited by the precision to which the temperature dependence of the thermal expansion coefficient of GaAs is known. This could explain the discrepancy in the position of the inelastic peak at negative energy transfer of 30 neV between the GaAs measurements and data taken with IN16B's Doppler drive in both Si 111 set-ups. In the next stage of development, a monochromator using the Doppler drive will be built, which should do away with this issue.

These first results provide proof of concept for the construction of a full-scale user instrument using GaAs 200. We also see potential for further improving the manufacturing technique to enhance the energy resolution, and we will continue development along these lines.

This work was supported by the German Federal Ministry of Education and Research through grants 05K13WE1 and 05K16WEA.

Dynamics in pressure-temperature space by coupling dielectric and neutron spectroscopy: a new experimental tool

Time-of-flight and backscattering spectrometers

Temperature and density play a crucial role in controlling the molecular motions of liquids [1]. When supercooled liquids approach the glass transition on cooling, on the one hand density increases, resulting in a more tightly packed structure; on the other, thermal energy decreases, trapping the molecules in the wells of the potential energy landscape. With the general aim of fostering knowledge about the dynamics of liquids and glasses, we have designed and developed a novel experimental set-up to perform dielectric and neutron spectroscopy simultaneously, varying pressure and temperature. This novel set-up is a unique tool for studying dynamics on different timescales, from kilo- to picoseconds, covering universal dynamic features such as relaxation and fast vibrations at the same time.

AUTHORS

A. Sanz, **H.W. Hansen**, **B. Jakobsen**, **I.H. Pedersen** and **K. Niss** (Department of Science and Environment, Roskilde University, Denmark)
S. Capaccioli (Department of Physics, University of Pisa, Italy)
K. Adrjanowicz and **M. Paluch** (Institute of Physics, University of Silesia, Katowice, Poland)
J. Gonthier, **B. Frick**, **J. Peters** and **E. Lelièvre-Berna** (ILL)

ARTICLE FROM

arXiv:1709.09859 [physics.ins-det]

REFERENCES

[1] C. Alba-Simionesco, A. Cailliaux, A. Alegria and G. Tarjus, EPL. 68 (2004) 58.
[2] A. Sanz, H.W. Hansen, B. Jakobsen, I.H. Pedersen, S. Capaccioli, K. Adrjanowicz, M. Paluch, J. Gonthier, B. Frick, E. Lelièvre-Berna, J. Peters and K. Niss, accepted in Rev. Sci. Instrum. (2018) arXiv:1709.09859
[3] E. Lelièvre-Berna, B. Demé, J. Gonthier, J.-P. Gonzales, J. Maurice, Y. Memphis, C. Payrea, P. Oger, J. Peters and S. Vial. JNR. 19 (2017) 77
[4] H.W. Hansen, A. Sanz, K. Adrjanowicz, B. Frick and K. Niss, Nat. Commun. 9 (2018) 518

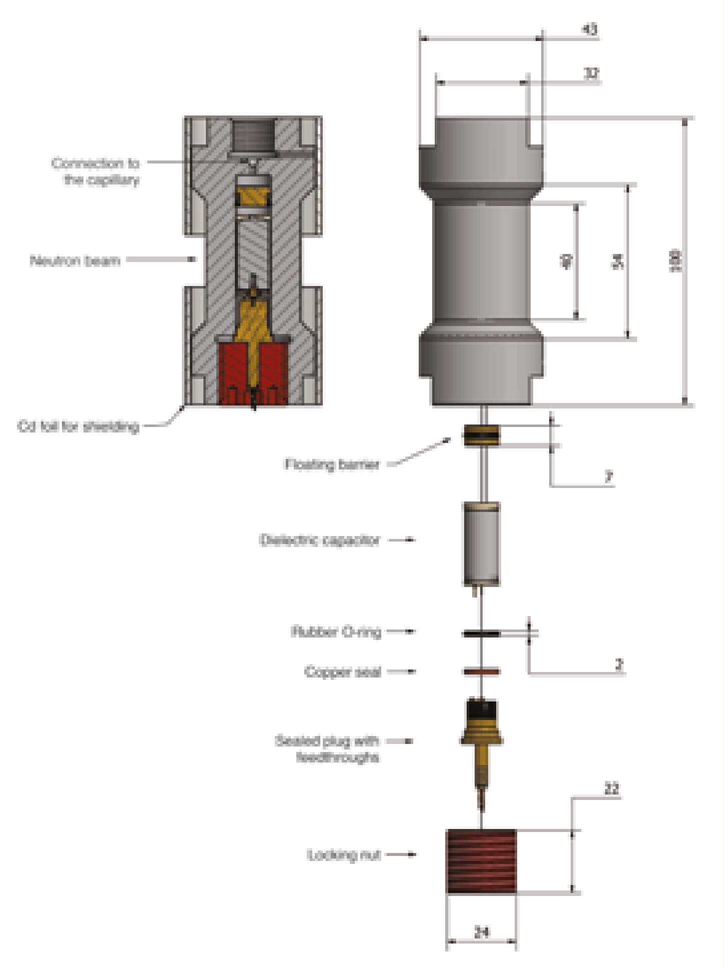

Figure 1
Exploded-view technical drawing of the high-pressure cell for simultaneous dielectric and neutron spectroscopy measurements (dimensions in mm).
Top left: Cross-sectional view of the assembled cell.

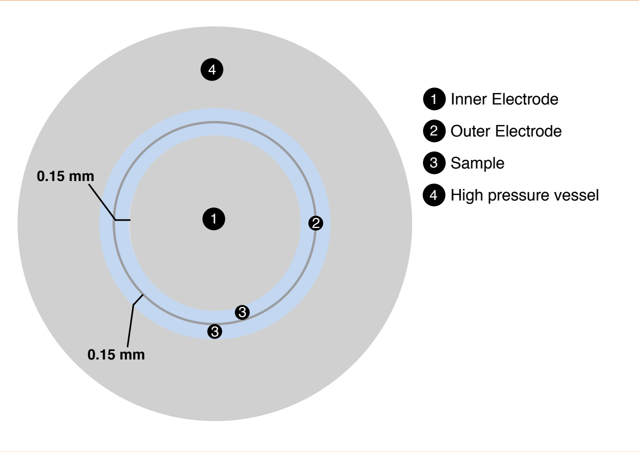

Figure 2
Schematic cross-sectional top view (orthogonal to the plane of the incident neutron wave) of the sample geometry for the high-pressure dielectrics-neutron cell. Dimensions are not to scale for the sake of clarity.

Figure 3
Picture of the assembled cell seen from the bottom. It shows the cadmium shielding and the connection point where coaxial cables plug the electronics into the dielectric capacitor.

We have developed a high-pressure cell for a temperature range of approximately 2–320 K and a maximum pressure of 500 MPa, which is 5 000 times atmospheric pressure. By performing simultaneous dielectric and neutron spectroscopy measurements, we are able to monitor slow and fast dynamics under exactly the same conditions, precluding potential unwanted external effects associated with different environments. Simultaneous measurements are especially important when a sample is not stable due, for instance, to physical or chemical processes. This set-up can be used on different neutron spectrometers in order to explore different energy transfers and energy resolutions, thus accessing a wide spectrum of time scales across a broad range of temperatures and pressures. We demonstrated the successful performance of the cell by simultaneously collecting dielectric and neutron data on the spectrometers IN5, IN6 and IN16B. Energy resolution on IN5 and IN6 corresponds to ~ 10 picoseconds, while on IN16B it corresponds to ~ 1 nanosecond. The dielectric set-up covers dynamics from kilo- to microseconds.

One advantage of coupling dielectric spectroscopy and incoherent neutron scattering is that the optimal cell geometry is identical for both methods. The area should be as large as possible and the thickness of the sample should be small. For a capacitor, the dielectric signal scales with the height of the capacitor and is inversely proportional to the distance between the electrodes. For incoherent quasi-elastic neutron scattering, the sample thickness must remain small in order to minimise multiple scattering effects, while a large sample area enhances the signal. This high-pressure dielectric-neutron cell is presented in the exploded-view drawing in **figure 1** [2]. We used the aluminium alloy EN AW-7049A-T6 for constructing both the high-pressure container and the electrodes of the capacitor, after the performance of detailed stress calculations by the Service for Advanced Neutron Environment (SANE) at the ILL and material tests on IN6, IN13 and IN16B.

Figure 2 shows a schematic representation of the sample geometry illustrating the location of electrode-electrode and cell-electrode sample volumes. To perform the experiments, we connected the cell to a neutron sample stick specially optimised for these high pressure and dielectric measurements. The stick was designed and developed by SANE [3]. The sample stick drives a pressure-transmitting liquid from the compressor to the sample through a heated capillary, avoiding freezing of the pressure-liquid at the cold point of the cryostat, and brings two coaxial cables that are connected through the plug to the capacitor. We integrated our Matlab-based dielectric software into the NOMAD instrument control software in order to synchronise the processes of neutron and dielectric data collection as well as temperature and pressure control.

The relaxation probed with dielectric spectroscopy is extremely sensitive to pressure and/or temperature changes and a dielectric spectrum can be acquired in a minute. It acts like an internal probe to define the thermodynamic state of the system precisely. This new experimental set-up can provide information on, for example, whether the sample is in thermal equilibrium or if pressure is transmitted properly to the sample, which is particularly important when the liquid approaches the glassy state either by cooling or compression. This aspect is critical for viscous liquids, in which the characteristic time of relaxation often changes with an order of magnitude in response to small changes in temperature and/or pressure. In the search for new physics, we have successfully employed this set-up to explore the phase diagram of simple van de Waals liquids in an unprecedented range of timescales. Our results agree with the predictions of isomorph theory, and allowed the phase diagram to be reduced to a single variable in which fast and slow relaxations are controlled by a single thermodynamic parameter [4].

This project was made possible under the ILL Long-Term Proposal LTP-6-7. For future collaborations or for more information on the availability of the set-up, please contact Henriette Wase Hansen (hansenhw@ill.fr), currently a postdoctoral researcher at the ILL, or Kristine Niss (kniss@ruc.dk).

Low gas pressure operation to improve Multi-Grid detectors

The neutron detector service (SDN, ILL)

Multi-Grid detectors have shown great potential to replace Helium-3-based detectors [1, 2]. However, a limitation of this technique, particularly for time-of-flight instruments, comes from the mechanical constraint on the detector vessel in a vacuum environment. Filling the detector at low pressure, typically 50 mbar, drastically reduces this constraint; it also helps to improve detector performance by increasing the counting rate capability and reducing the gamma sensitivity. Future instruments will derive considerable benefit from this new operating mode, as well as from the large grid currently in development under the BrightnESS project.

AUTHORS

J.C. Buffet, **V. Buridon**, **J.F. Clergeau**, **S. Cuccaro**, **B. Guerard**, **F. Lafont**, **J. Marchal**, **J. Pentenero** and **D. Roulier**

REFERENCES

[1] J. Correa, '$^{10}B_4C$ Multi-Grid as an alternative to ^{3}He for large area neutron detectors', PhD thesis, ILL and Zaragoza University (2012)

[2] A. Khaplanov *et al.*, JINST 12 (2017) P04030

[3] A. Khaplanov *et al.*, J. Phys. Conf. Ser. (2014) 528 012040

Multi-Grid detectors are made up of one or several columns of grids mounted in a gas vessel; each grid is composed of thin aluminium blades coated on both sides with a ^{10}B-isotope-enriched B_4C thin film to convert neutrons into ionising particles. The standard grid used in several of our prototypes contains 60 cells of 2 cm x 2 cm x 1 cm (**figure 1**), hence one column of n grids is equivalent to 60 proportional counter tubes segmented in n independent voxels. Anode wires are mounted in the middle of these tubes. Cathode grids and anode wires are connected to the front-end electronics *via* high-voltage decoupling capacitors; the analogue signals are processed to determine the voxel of interaction. Three grids are fired on average for each event, hence, the following algorithm can be used to optimise the position measurement along the wires: the first active channel corresponding to grid N is virtually divided into two equal parts—the bottom half-grid N- and the top half-grid N+—then the pulse heights from the two neighbouring grids (N-1) and (N+1) are compared. The neutron is localised in N- if the pulse height on grid (N-1) is larger than on grid (N+1), or in N+ in the opposite case. This algorithm is relatively simple to implement in ILL standard data acquisition systems.

One of the prototypes, called MG12, contains a unique column of 12 standard grids mounted in a vacuum-tight vessel. This detector was filled with different values of gas pressure $Ar\text{-}CO_2$ (90:10), from 50 mbar to 1 bar, and the 'Counting versus Anode Voltage' curve measured in each case. The resulting curves were constant between 50 and 200 mbar, indicating that the detector is insensitive to slight changes in pressure when operated in this pressure regime. The MG12 detector, filled with 50 mbar of gas, was also exposed to a neutron beam of 50 KHz/cm^2 for 15 hours, and showed less than 0.15 % variation in the counting rate.

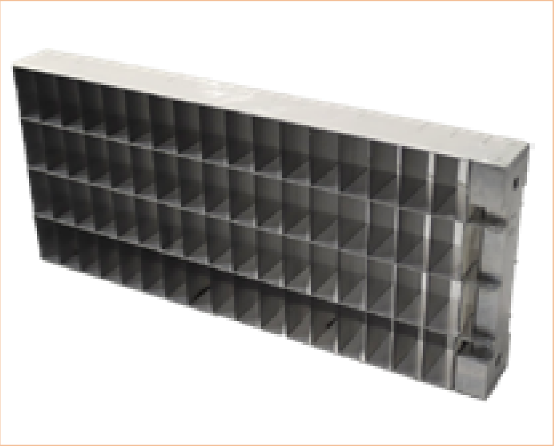

Figure 1

Picture of a standard grid with 4*17 rows of cells; the grid described in this paper has 4*15 rows.

Figure 2

Inside view of the MG_IN6 prototype. Standard grids are on the left, new grids on the right.

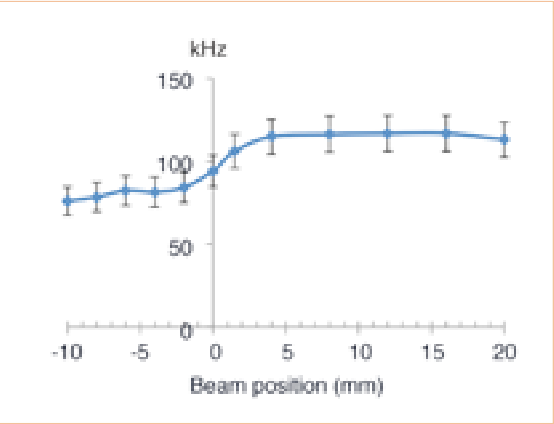

Figure 3

Detector counting rate measured during irradiation of standard grids (beam position < 0 mm) and new grids (> = 0 mm) while scanning the detector with a beam of 100 mm x 100 mm in the direction perpendicular to the anodes.

Another prototype, called MG_IN6 [3], is separated into two sectors mounted side by side, each of them occupying the same sensitive volume. One sector is made up of three columns of 16 standard grids, the other, one single column of 16 large grids (**figure 2**). These large grids contain 384 detection cells. A significant gain in detection efficiency is expected from this new grid: first, there is no dead space in the whole sector; second, the reduced dimension of the cell allows an increase in the number of convertor layers in the depth direction (48 instead of 30); and finally, the radial blades that are not B_4C-coated in the standard design, are now coated. Another advantage of the new grid comes from its cylindrical geometry, which provides better response uniformity.

Since the MG_IN6 detector cannot stand more than 50 mbar of pressure difference between the inside and outside of its vessel, the detection gas must be at 1 bar when used in an atmospheric environment. This was the case for the test at the LLB on the G4.3 instrument equipped with a graphite monochromator. The intrinsic detection efficiency was measured for a monochromatic narrow (3 mm x 3 mm) beam centred in the middle of the cells. Detection efficiency at 2.8 Å is 56 % + -3 % for the standard grid, and 66 % + -3 % for the new one. Experimental data have been corrected to take the λ/2 and λ/3 harmonics into account. This gain with the new grids comes only from the higher number of convertor layers. A further gain in detection efficiency is provided by the radial blades and the absence of dead zones. This is shown by comparing the counting rate measured in the two sectors with a large beam of 100 mm x 100 mm: at 2.8 Å the sector with the new grids counts 45 % more than the sector with the standard grids (**figure 3**).

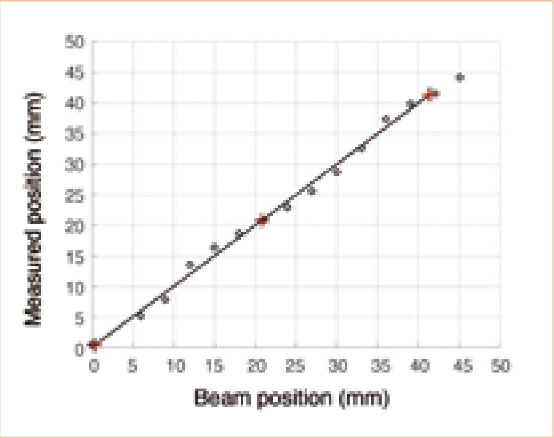

Figure 4

Position measurement along the wires while scanning the detector with a beam of 3 mm x 3 mm in the direction parallel to the anodes. The middle of the grids are represented by red crosses. The dark line represents the ideal response of the detector.

The MG_IN6 was then moved in the direction parallel to the wires in front of the narrow beam of 3 mm x 3 mm; **figure 4** shows the average value of the measured position as a function of the real position, showing a maximum deviation from the real position of only 1 mm.

In conclusion, the implementation of large grids in a reasonably light-pressure vessel filled at low gas pressure is optimal for operating the detector in a vacuum environment. The next step is to equip the MG_IN6 prototype with large grids only, and to test it with 50 mbar of detection gas in a vacuum environment using a gas flow monitoring system.

This work has been financed by the EU BrightnESS project, an H2020 grant agreement 676548. We would like to thank the people at the LLB for their support in the test of the MG_IN6 prototype.

NOMAD 3D – seeing through walls

The progress being made in 3D graphics and the soaring levels of computational power on even small portable devices have generated great possibilities in the field of instrument control. The superposition of data or synthesised imagery on real-world modelling has been providing benefits in fields as diverse as video gaming, medical applications and military technology. We will show in the following how virtualisation and augmented reality have been applied to scientific instrument control at the ILL in Grenoble.

Figure 1

Screenshot of the Editor. The front wall is selected and appears transparent.

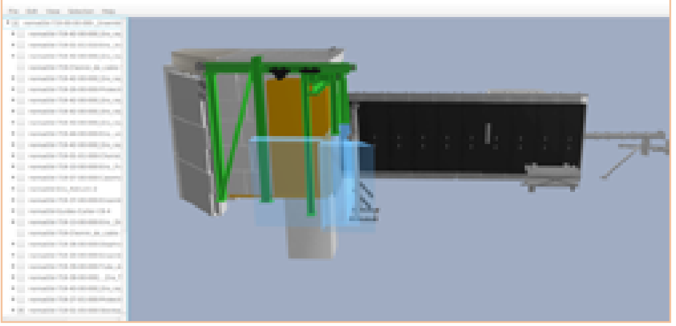

AUTHORS

P. Mutti, F. Cecillon, C. Cocho-Martinez, A. Elaazzouzi, Y. Legoc, J. Locatelli and H. Ortiz (ILL)

REFERENCES

[1] SolidWorks: http://www.solidworks.com/
[2] Nomad: P. Mutti *et al.*, Proc. ICALEPCS (2011), Grenoble, France.
[3] .stl files: https://all3dp.com/what-is-.stl-file-format-extension-3d-printing/
[4] Blender: https://www.blender.org/
[5] LOD: https://www.computer-graphics.se/TSBK07-files/pdf/PDF09/10%20LOD.pdf/
[6] WebGL: https://www.khronos.org/webgl/

From SolidWorks to Nomad 3D

Most of the ILL's recent instruments were designed using SolidWorks [1]. The design plans are extremely detailed, including every component of the instrument down to the smallest screw. Therefore the associated files can be extremely large. The model produced presents a scaled view of the different instruments, as the real parts are to be built from it. Nomad [2] is the software used to control the instruments. It moves the motors at the user's request and monitors the position of the axes by reading the associated encoder.

The goal of our project is to transform the SolidWorks model into an animated 3D one loaded onto a dedicated viewer application. No major assumptions have been made as regards the client-computer specifications; the viewer application will therefore have to be scalable and capable of displaying different degrees of detail. The Instrument Control Service has developed a set of applications to achieve this.

The first application is a SolidWorks plugin, which converts the geometric parts into a set of triangles. The Converter plugin is written in C#; it preserves the SolidWorks hierarchy and geometries and loads information from the constraints and configurations. The API provides full access to the model data and offers a native function to convert the geometries into .stl files [3] containing a set of triangles. At this point a first step is taken to simplify the model's geometries with an Exporter plugin. This configures the export with a threshold to eliminate minor parts, such as screws, which we do not need in our final visualisation.

The second step in the conversion uses a Blender script [4] to transform the .stl files and clean up the geometries (poor triangle orientation, double vertices, etc.). The Blender script can also generate different levels of detail [5] for the geometries. In addition to the cleaned-up *exported* geometries, we also generate *decimated* geometries with different levels of detail. This is useful for the scalability of the viewer application as the number of triangles is reduced accordingly.

Whilst the Exporter and Converter applications reduce and reorganise the SolidWorks model data, the Editor application adds information that cannot be obtained automatically. It is principally used to define the axes and their type (*e.g.* rotation, translation), and to set the walls around the instrument for collision detection. The Editor is written in JavaFX [6]; it provides a 3D view of the model and a tree view of the hierarchy of components. **Figure 1** shows the Editor screen with an overall view of the FIGARO reflectometer. We decided to use a 3D engine based on WebGL [6] for the viewer application; this offers the best compromise currently available between performance and portability for different platforms. **Figure 2** shows a virtual view of FIGARO with all the surrounding structures rendered transparent. The viewer application asks Nomad for the positions of the axes at each frame, thus enabling real-time animation of the model.

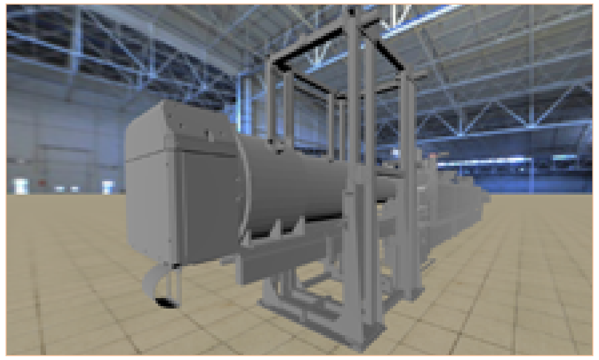

Figure 2

Virtual view of the Figaro reflectometer. The walls and other unnecessary structures have been rendered transparent.

Figure 3

Screenshot of the vExp application prototype. It provides a 3D view of virtual space.

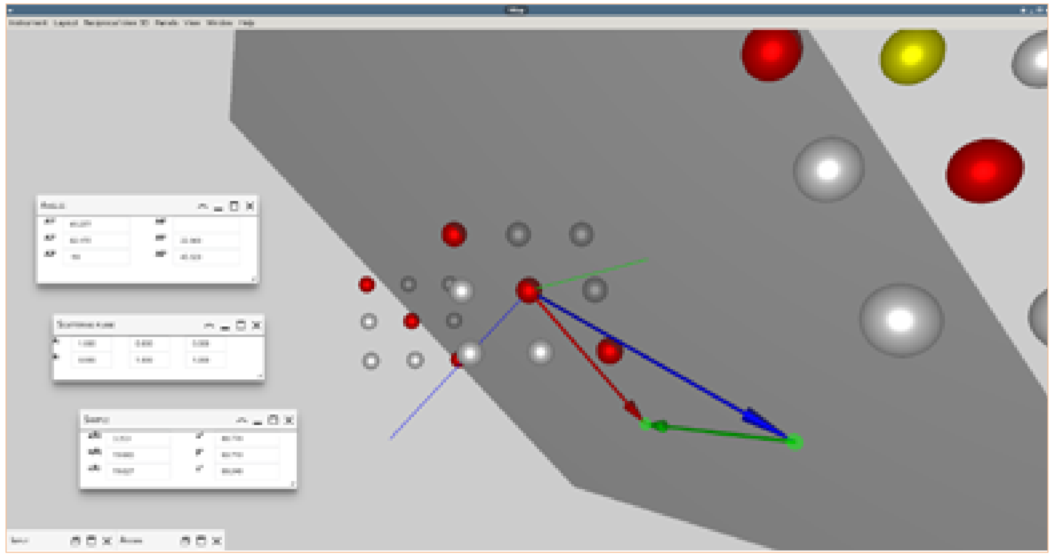

Augmented reality in instrument control

By providing users with virtual access to instruments and the environments in which the instruments operate, the ILL offers users the possibility of simulating entire experiments. Users can now verify, before their arrival at the Institute, the feasibility of their experimental programmes. By performing the experiment virtually they can detect, for example, any possible collisions with walls or surrounding materials. By changing the physical parameters of an instrument or its environment in virtual space they can visualise the consequences in real space. The possibility of incorporating real data in simulations will help users determine the measurement strategy.

Figure 3 shows the vExp prototype, an application developed in collaboration with the ILL's Spectroscopy group, for exploring virtual space without losing sight of the real one. We have also developed an augmented-reality Android application for mobile devices such as tablets; this is designed essentially for instrument maintenance. The application identifies and displays all the available parameters of the electronics boards and can help configure the instrument. The software recognises where the user is located by reading the information stored on dedicated near-field communication tags. A recognition algorithm uses the image taken with the tablet's on-board camera to extract relevant information from the electronic crates and displays important settings and configuration parameters. In the near future we will be able to add invisible elements such as the neutron beam to the real view, making rough pre-alignments of the sample possible.

The development work performed over the last year has shown that the next generation of instrument control software, with user experience at its heart, is on the point of arrival. Nomad 3D is a powerful mix of mechanics, computer-assisted design and 3D graphics, proving that the future of instrument control will depend on cross-disciplinary innovation. Advanced instrument simulation techniques and real-time collision detection will help both the ILL and its users to fine-tune measurement strategies and optimise space use. And, last but not least, we can now anticipate the integration of virtual reality devices such as Oculus Rift for a complete immersion experience.

INDUSTRIAL ACTIVITIES

The ILL provides industrial users with access to state-of-the-art neutron instrumentation and the expertise of its scientific and technical staff.

Contact: industry@ill.fr
http://www.ill.eu/neutrons-for-society/industry-and-business/

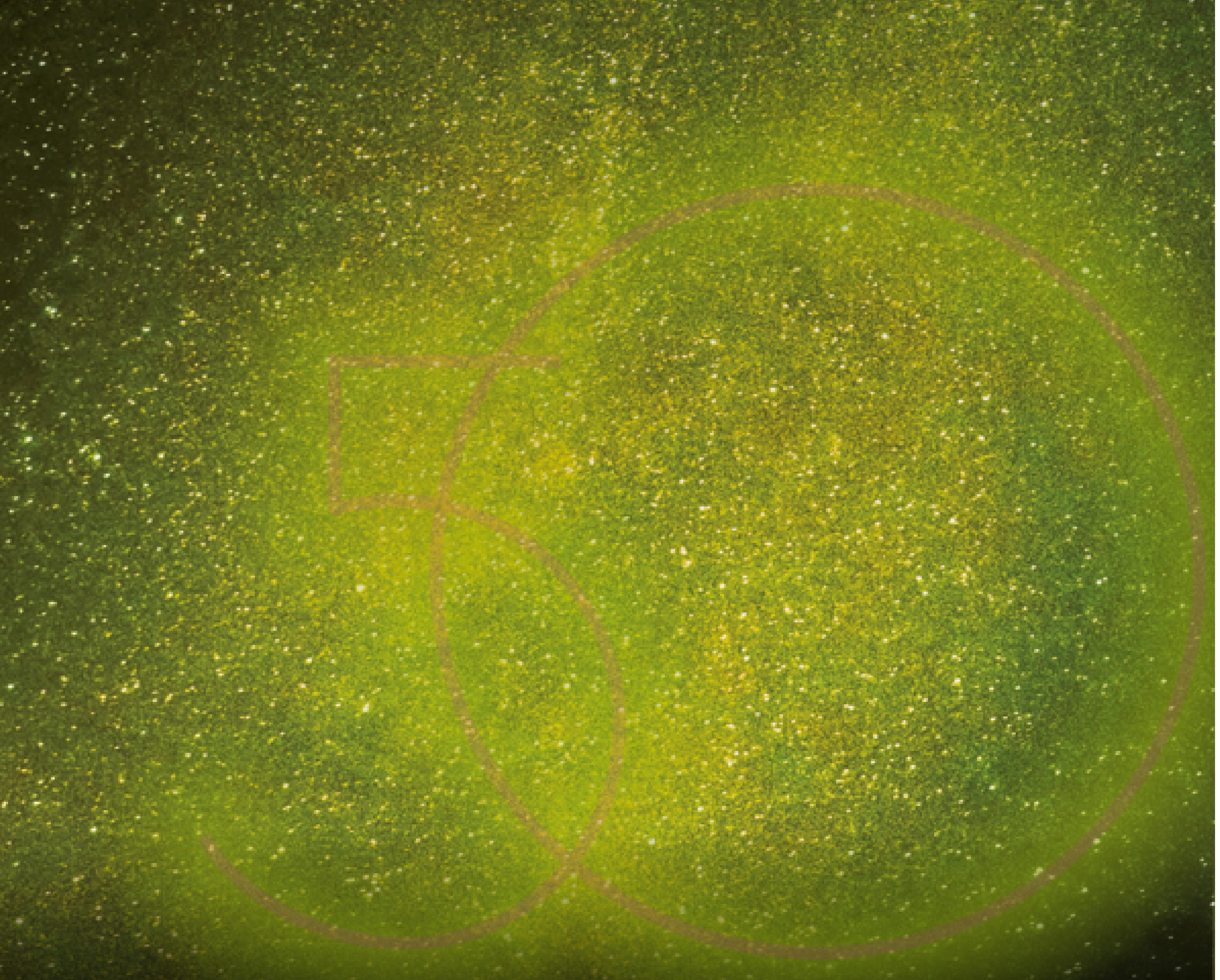

Industrial activities at the ILL

The year 2017 saw the consolidation of several key projects involving the Industrial Liaison Unit (ILU). These included IRT Nanoelec and SINE2020 Industry Consultancy, the first industrial and academic imaging experiments on the D50 tomograph extension in collaboration with Université Grenoble Alpes and the redefinition of the ILL's stress-scanning instrument SALSA for wider industrial use. At the same time, strong proprietary beamtime sales and the inclusion of industrial implications in proposals for experiments underline the ILL's relevance to applied research and development in numerous domains, such as health science, renewable energies and advanced materials.

The second phase of the IRT Nanoelec (2015–2017) project came to fruition in 2017 following final technical fine-tunings to D50's reflectometry/irradiation set-up, thus paving the way for full operation of the ILL's industrial instrument. Companies such as Airbus, SdH, SwissNeutronics and Irotech have already been involved in successful proof-of-concept tests on D50.

A major achievement obtained within IRT Nanoelec was the operational launch of the Platform for Advanced Characterisation – GRENOBLE (PAC-G), a joint venture between the ILL, ESRF, CEA and CNRS/LPSC to provide innovative characterisation services to industry. A business developer has been recruited to the ILU on a 24-month contract, with the task of bridging the gap between IRT PAC-G and the nano- and micro-electronics industry and consolidating a competitive and relevant service offer.

Also, as far as D50 is concerned, the NeXT (Neutron and X-ray Tomography) collaboration with Université Grenoble Alpes (UGA) (**https://next-grenoble.fr/**) reached its first milestone with academic and industrial use of its newly operational medium-resolution neutron imaging station. Financed by the UGA with industrial backing from Total and EDF, this instrument, implanted in the bespoke extension to the D50 casemate, is currently undergoing technical upgrades to achieve the final goal of high resolution bi-modal neutron and x-ray tomography capable of simultaneous and rapid x and n imaging.

The ILL's management took the decision to devote 50 % beamtime of the stress-scanning instrument SALSA directly to industrial-related activities. In order to develop this new orientation (including the definition of a business strategy blueprint for the next 3–5 years) and fully operate the instrument, a second beamline scientist was appointed in April 2017. Following this, an intense period of outreach activity has resulted in the activation of more than 20 company links with the objective of establishing medium- and long-term industrial collaborations as well as direct proprietary access, and the organisation of the workshop 'Challenges in additive manufacturing industrial qualification: key solutions at large scale infrastructures' in Grenoble on 9–10 April 2018.

The ILL plays a key role in the Industry Consultancy work package (WP4) of the European Union's Horizon SINE2020 programme, aimed at strengthening cooperation between European Industry and neutron research facilities through a campaign of networking and communication. In practice, more than 20 outreach events have been organised/attended, culminating in a major industry event planned for 2018 **www.synergi2018.eu**. A growing repository of industrial case studies can be consulted on its website, **www.sine2020.eu/industry/case-studies.html**, and so far, four free industrial feasibility tests have been carried out at the ILL.

Towards the end of 2017, the ILL, CEA and ESRF co-organised a local workshop on modern Li-ion battery developments with the objective of creating a forum for dialogue between battery researchers and instrument scientists. More than 100, mainly locally-based scientists attended and follow-up activities such as laboratory visits, newsletters and a series of seminars are planned to promote this promising collaboration.

With regard to beamtime sales, revenue from this and other ILU activities during the last cycle in 2016 and the first cycle in 2017 amounted to 96 908 €, thus continuing the upward trend in sales since 2014.

Recent studies by the ILU have revealed the true extent of industrial involvement in ILL academic experiments. A systematic analysis of proposals from 2012 to 2014 showed that 25 % had either direct or indirect industrial/commercial applications; it has been estimated that this figure is around at least 15 % for 2016 and the first cycle in 2017. New directives to users requiring complementary information on industrial applications on their proposal forms have been put into place, in order to obtain a more accurate and 'real time' overview of this important indicator.

Lastly, a strategic decision was taken by the ILL management to integrate the ILU into the Science Division. This reflects the close working relationship between the ILU and scientists at the ILL, and will give further impetus to this vital synergy.

EXPERIMENTAL AND USER PROGRAMME

Neutron beams and instrument facilities are free of charge for proposers of accepted experiments. Scientists affiliated to the Institute's member countries will also, in general, be assisted with necessary travel and daily subsistence for a limited period. The User Support team makes all arrangements for accommodation and will process claims for expenses after users have completed their experiments.

The ILL **User Office** is dedicated to helping all visiting researchers to make the most of its facilities. If you are coming to the ILL to carry out experiments, the User Office will give you the organisational and administrative support you need to successfully perform your experiments.

All administrative tools and information for our scientific visitors are grouped together and directly accessible on the web, courtesy of our user-friendly, online **User Club**. Club members can log on using their own personal identification to gain direct access to all the information they need. Users with particular responsibilities have privileged access to other tools, according to their role. **http://www.ill.eu/users/user-club/**

The opportunities we offer to our users extend beyond the privilege of access to the world's leading suite of neutron instruments. The ILL—in collaboration with the European Synchrotron Radiation Facility (ESRF) and other institutes—is actively responding to the needs of scientists unfamiliar with neutron techniques and in need of training and support facilities. New support facilities have been already set up on the ILL site. For more information see p.106.

Our users can now electronically flip through our **User Handbook** (containing practical information on their stay) at **http://www.ill.eu/users/user-guide/**.

For further information about the Institute's facilities, applications for beamtime, user support and the experimental programme, please visit our website at **http://www.ill.eu/users/**.

User programme

PROPOSAL SUBMISSION

There are different ways of submitting a proposal to the ILL:

- Standard submission—twice a year—*via* the User Club
- Long-Term Proposals (LTPs)—once a year, autumn round—*via* the User Club
- Easy access system (EASY)—throughout the year—*via* the User Club
- Test time (TEST)—throughout the year—*via* the instrument responsible
- Director's Discretionary Time (DDT)—throughout the year—*via* the Head of Science Division
- Special access for proprietary research and industrial users

All types of access (except DDT) are reserved for users from ILL member countries or for collaboration between non-member and member teams.

Detailed information can be found at **http://www.ill.eu/users/applying-for-beamtime/**.

Submission of a standard research proposal

Proposals can be submitted to the ILL twice a year, usually in February and September, *via* the User Club. Submitted proposals are divided amongst the different colleges (**see box below**) according to their main subject area.

THE ILL SCIENTIFIC LIFE IS ORGANISED INTO 10 COLLEGES:

College 1	Applied Metallurgy, Instrumentation and Techniques
College 2	Theory
College 3	Nuclear and Particle Physics
College 4	Magnetic Excitations
College 5A	Crystallography
College 5B	Magnetic Structures
College 6	Structure and Dynamics of Liquids and Glasses
College 7	Spectroscopy in Solid-state Physics and Chemistry
College 8	Structure and Dynamics of Biological Systems
College 9	Structure and Dynamics of Soft Condensed Matter

Proposals are judged by peer review panels, one for each college, which usually meet eight weeks after the deadline and evaluate the proposals purely on scientific excellence.

Easy access system – EASY

The EASY route has been used to grant limited beamtime on the diffractometer D2B to scientists from ILL member countries for short measurements at room temperature. In 2018, EASY access will be extended to all instruments, except those in the NPP group, with an increased range of sample environments. Access is open all year round. Users are not invited to the ILL but send their samples to us.

Long-term proposals

The purpose of a Long-Term Proposal is to facilitate the development of instrumentation, techniques or software—that could be beneficial to the ILL community as a whole—through the award of beamtime over several cycles (typically three years). Projects are monitored through compulsory annual reports. A final report is also required at the end of each project.

Submission of a proposal to the Director's Discretionary Time

Five per cent of ILL beamtime is reserved for proposals outside the twice-yearly proposal rounds. Primarily these concern urgent experiments. Proposals can be submitted at any time, and will be reviewed by the panel concerned and the ILL Science Director. If successful, beamtime will be awarded quickly. DDT may also be used to award beamtime to excellent proposals from non-member countries. These proposals must go through the usual proposal rounds so that the level of excellence can be compared against that of other proposals.

Experimental reports

Users must complete an experimental report on the outcome of their experiments. Failure to do so may lead to the rejection of any subsequent continuation proposals.

USER PROGRAMME, USER AND BEAMTIME STATISTICS

INDUSTRY-SPONSORED ACADEMIC RESEARCH AND INDUSTRIAL USERS

Neutrons have significant, specific applications for industry. Beamtime can be sold directly for proprietary research, in which case the experimental data are not made publicly available. The Industry Liaison Unit (ILU) is the single point of contact for industry looking to use the ILL's facilities (see p. 91).

However, industry use of the ILL often takes place *via* academia, at a level between 10 and 25 % depending on how this is evaluated. The data from these experiments are publicly available and the results should be published. The ILL now measures the number and nature of industry-*via*-academia experiments more precisely, with a view to promoting and potentially enhancing this use of neutrons in the future.

COLLABORATIVE RESEARCH GROUP INSTRUMENTS

The ILL provides a framework in which Collaborative Research Groups (CRGs) can build and manage instruments at the ILL to carry out their own research programmes. These groups enjoy exclusive access to the instrument for at least half of the beamtime available. They provide their own scientific and technical support, and cover the general operating costs of the instruments. The beamtime reserved for the ILL is made accessible to users *via* the standard proposal rounds.

There are currently three different categories of CRG instruments:

- **CRG-A**: external groups lease an instrument owned by the ILL, having 50 % of the beamtime at their disposal.
- **CRG-B**: groups own their instrument and retain 70 % of the available beamtime.
- **CRG-C**: instruments are used full time for specific research programmes by the external group, which has exclusive use of the beam.

User and beamtime statistics

THE ILL USER COMMUNITY

The ILL welcomed 721 users in 2017, including 207 from France, 123 from Germany and 101 from the UK (**figure 1**). Many of our visitors were received more than once (making a total of 942 user visits).

We value feedback from our users as an indicator of how well our facility is fulfilling their needs and to initiate action when this is not the case (**figure 2**). Users who have just finished an experiment are asked to complete a User Satisfaction Form. User feedback is made available to managers for action when appropriate.

Figure 1: National affiliation of ILL users in 2017.

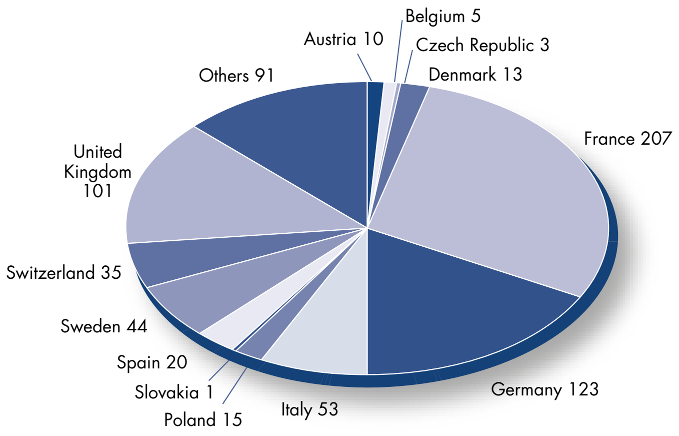

Figure 2: User satisfaction survey results for 2017 compared with those obtained in previous years. User feedback rate was around 65 % in 2017.

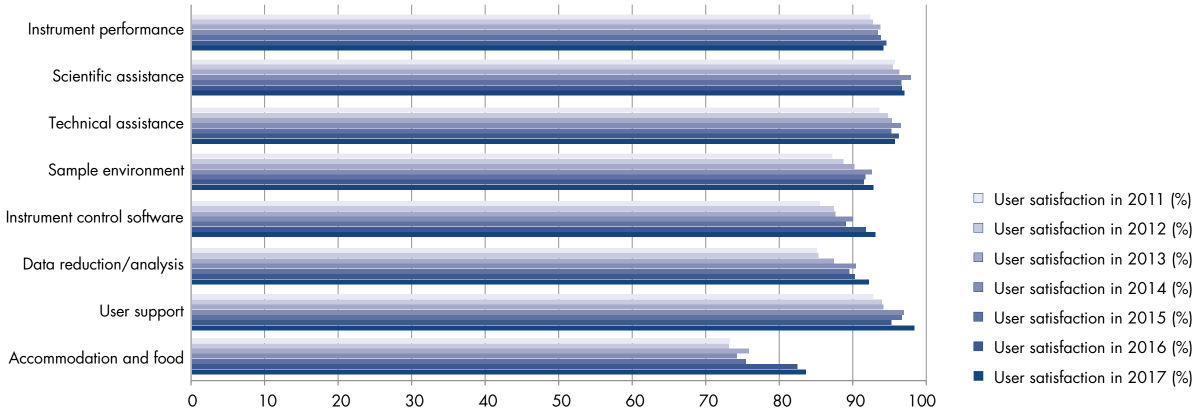

INSTRUMENTS

The instrument facilities at the ILL are shown in the plan on p. 99. Besides the 27 ILL instruments there are 10 Collaborative Research Group (CRG) instruments.

All current CRGs are A- or B-type, the only exception being GRANIT which as a CRG-C instrument is not available as a 'user' instrument. IN15 has special status since it is a joint venture between the ILL and FZ Jülich. The instrument STEREO is jointly funded by the ILL and CEA Saclay, LAPP Annecy, LPSC Grenoble and MPIK Heidelberg.

BEAMTIME ALLOCATION AND UTILISATION FOR 2017

During 2017 the reactor was anticipated to operate for 3 cycles, representing 158 days of neutrons. The allocation of beamtime during November 2016 and April 2017 was made on the basis described in **table 2** (see p. 97, first three columns).

Overall, the panel meetings examined 1 017 proposals requesting 7 010 days in 2017. Of these, 609 proposals received beamtime requiring the allocation of 3 199 days of beamtime on the different instruments. Since some proposals are for more than one experiment, a total of 656 experiments were approved for scheduling in 2017. The distribution of accepted proposals amongst the different research areas and colleges is given in **figure 3**.

However, the ILL was not able to run two of the originally planned three cycles (see § Reactor Operation, p.102). This meant that only 48 days were actually available on most instruments (**table 2**). Consequently, all of them accumulated a backlog, to be cleared by the allocation of additional time scheduled during the first two cycles of 2018.

Please note that access to PN3 was not offered *via* the subcommittees; because a considerable backlog had taken up most of the available beamtime on this instrument, the remaining time was used internally (before the instrument's three-year shutdown).

In 2017, the member countries of the ILL were as follows: France, Germany, UK, Austria, Belgium, the Czech Republic, Denmark, Italy, Poland, Slovakia, Spain, Sweden and Switzerland.

Table 1 (see p. 96) gives the beamtime distribution amongst the different member countries (for beamtime scheduled in 2017). In calculating the statistics of beamtime per country, the attribution is based on the location of the laboratory of the proposers, not their individual nationality. For a proposal involving laboratories from more than one member country, the total number of days is divided amongst the collaborating countries and weighted by the number of people from each. Local contacts are not counted as proposers, except when they are members of the research team. The beamtime requested by and allocated to scientists from the ILL, ESRF or EMBL is allocated to the member countries according to a weighting system based on the fractional membership of the country of the institute concerned. When a proposal involves collaboration with a non-member country, the allocated time is attributed entirely to the collaborating member country (or countries). Proposals in which all proposers are from non-member countries therefore do not appear in this table. This explains why the total number of allocated days can differ from that in **table 2**.

A more complete view of beamtime use is given in **table 2**. Requests for and allocation of beamtime, as well as the number of originally planned experiments, refer to standard submissions to the subcommittee meetings. The effective number of days given to our users also takes into account Director's Discretion Time and CRG time for CRG instruments.

Figure 3: Beamtime allocation in 2017: distribution amongst the different research areas (**a**) and colleges (**b**).

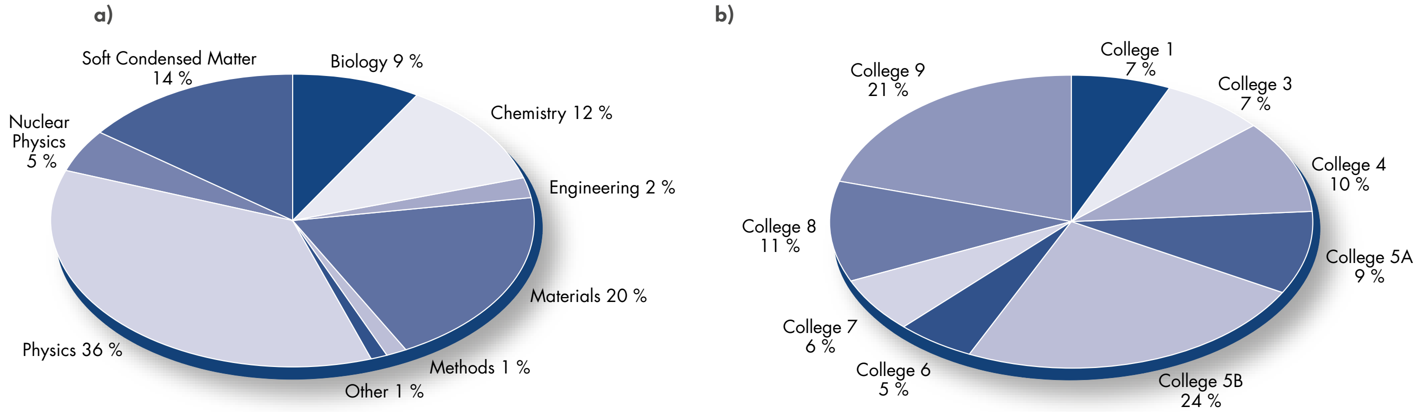

USER AND BEAMTIME STATISTICS

Table 1: Distribution amongst the Associate and Scientific Member countries of beamtime requested and allocated in 2017 during the subcommittees of the Scientific Council. *Proposals from purely non-member countries and purely ESRF proposals do not appear in this table, and therefore the total request and allocation is different in table 2.*

	Request days	Request %	Allocation days	Allocation %	Allocation days	Allocation %
Member countries only			Before national balance		After national balance	
AT	127.43	1.82	100.88	3.11	100.99	3.16
BE	27.02	0.39	19.17	0.59	19.22	0.60
CH	441.30	6.30	209.14	6.45	132.44	4.14
CZ	61.07	0.87	43.82	1.35	43.87	1.37
DE	1 764.03	25.17	737.94	22.76	740.95	23.16
DK	82.51	1.18	40.26	1.24	40.33	1.26
ES	308.18	4.40	127.19	3.92	127.40	3.98
FR	1 830.16	26.12	828.54	25.55	842.83	26.35
GB	1 452.99	20.74	678.10	20.91	697.94	21.82
IT	400.86	5.72	205.84	6.35	192.96	6.03
PL	145.71	2.08	104.34	3.22	104.39	3.26
SE	352.94	5.04	140.51	4.33	148.39	4.64
SK	13.10	0.19	7.21	0.22	7.23	0.23
Total	**7 007.30**	**100.00**	**3 242.94**	**100.00**	**3 198.94**	**100.00**

INSTRUMENT PERFORMANCE

Table 2 also gives a summary of instrument performance for 2017. For each cycle a record is kept of the use of the total available beamtime for all the instruments. The table gives a global summary for the year.

Overall 1 295 days were made available to our users in 2017 on ILL and CRG instruments, which represents about 72 % of the total days of operation. A total of 153 days was used by ILL scientists to carry out their own scientific research. About 12 % of the total beamtime available on the ILL instruments was allowed for tests, calibrations, scheduling flexibility, recuperation from minor breakdowns and student training. A significant fraction of this time and the 8.5 % internal research is used for collaboration with users. In 2017, 136 out of 1 792 days were lost as a result of various malfunctions, which represents about 7 % of the total available beamtime. This higher than usual value was due to major problems on two instruments (explained below).

Beam days given to science in 2017 amounted to 1 448 (used for users and internal research), which is the correct figure for a single cycle.

The majority of instruments lost only a few days, for various reasons.

IN20 lost about 40 days because of broken sensors and mechanics that drive the monochromator shielding. The repair necessitated a complete dismantling of the monochromator drum. The instrument was back in operation at the end of the cycle.

PN1 lost an entire cycle because the main vacuum valve could not be opened. Making the repair, which required beam-tube venting, was only possible during the subsequent shutdown.

Please note that access to PN3 was not offered *via* the subcommittee, as a considerable backlog took up most of the available beamtime on the instrument. The remaining beamtime was used internally.

Figure 4: Use of ILL beamtime

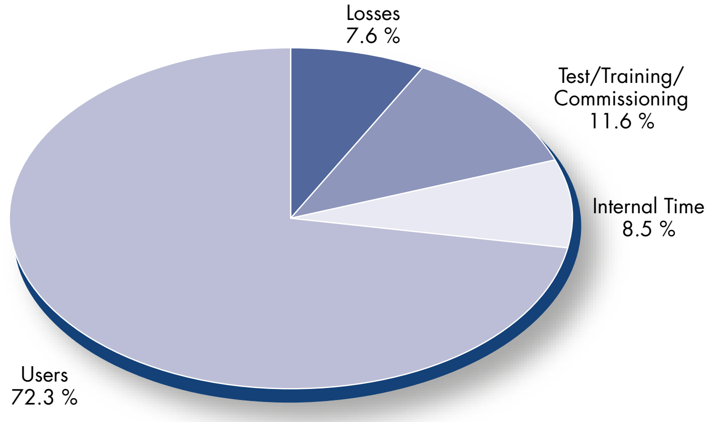

Table 2: Beamtime request/allocation (*via* standard subcommittees and Director Discretion Time – DDT combined) by instrument and instrument performance.
CRG instruments are in blue.
* 'days allocated' refers only to those days reviewed by the subcommittees (*i.e.* excluding CRG days and DDT)
**'days used' refers to the total number of days given to users (*i.e.* including CRG days for CRGs and DDT)
PF2 consists of different set-ups where several experiments are running simultaneously. The values given are averages for these positions.
D4 and IN1 share the same beam port and cannot be run simultaneously.

Instrument	Outcome of the panel meetings, originally planned use in 2017			Effective use in 2017				
	Days requested	Days allocated*	Number of accepted experiments	Available days	Days used for users**	Days lost	Days for test/ commissioning /training	Days for internal research
BRISP	44	36	3	48	18	6	12	12
D1B	68	63	24	48	44	1	2	1
D10	240	113	19	48	43	0	5	0
D11	215	90	45	48	36	1	10	1
D16	192	106	20	48	36	0	4	8
D17	225	95	32	48	30	2	7	9
D19	210	111	13	48	40	1	7	0
D2B	210	109	50	48	41	0	1	6
D20	246	105	39	48	34	5	6	3
D22	237	76	33	48	37	0	9	2
D23	68	39	6	48	47	0	1	0
D3	140	116	14	48	43	1	4	0
D33	238	75	27	48	39	1	6	3
D4	113	46	11	14	11	0	1	2
D7	241	109	20	48	42	0	6	0
D9	137	94	12	40	34	5	1	0
FIGARO	182	98	32	48	41	3	5	0
FIPPS	401	327	18	48	48	0	0	0
IN1-LAGRANGE	99	25	9	11	6	0	1	4
IN11	254	91	12	48	45	1	2	1
IN12	136	26	5	48	41	0	7	0
IN13	154	56	5	48	38	0	5	5
IN15	237	51	9	48	32	1	11	4
IN16B	200	84	30	48	20	5	23	0
IN20	192	51	8	48	0	45	0	3
IN22	128	33	5	48	41	2	5	0
IN4	166	96	26	48	43	0	2	3
IN5	334	97	28	48	38	0	10	0
IN6	196	67	18	48	45	1	0	2
IN8	158	41	7	48	24	3	10	11
LADI	419	112	15	48	38	0	7	3
PF1B	212	134	8	48	34	1	7	6
PF2 normalised	97	84	2	48	33	0	15	0
PN1	111	78	8	48	0	48	0	0
PN3-GAMS				48	0	0	0	48
SALSA	158	60	15	48	31	3	5	9
SUPERADAM	129	45	8	48	34	1	7	6
S18	62	62	3	48	48	0	0	0
THALES	161	98	17	48	41	0	5	3
Total	**7 010**	**3 199**	**656**	**1 793**	**1 295**	**136**	**208**	**153**
Percentage of the total beamtime					72.3 %	7.6 %	11.6 %	8.5 %

INSTRUMENT LIST

Instrument list – January 2018

ILL INSTRUMENTS		
D2B	powder diffractometer	operational
D3	single crystal diffractometer	operational
D4 (50 % with IN1-LAGRANGE)	liquids diffractometer	operational
D7	diffuse-scattering spectrometer	operational
D9	single crystal diffractometer	operational
D10	single crystal diffractometer	operational
D11	small-angle scattering diffractometer	operational
D16	small momentum-transfer diffractometer	operational
D17	reflectometer	operational
D19	single crystal diffractometer	operational
D20	powder diffractometer	operational
D22	small-angle scattering diffractometer	operational
D33	small-angle scattering diffractometer	operational
FIGARO	horizontal reflectometer	operational
FIPPS	fission project prompt x-ray spectrometer	operational
IN1-LAGRANGE (50 % with D4)	three-axis spectrometer	operational
IN4	time-of-flight spectrometer	operational
IN5	time-of-flight spectrometer	operational
IN8	three-axis spectrometer	operational
IN11	spin-echo spectrometer	operational
IN16B	backscattering spectrometer	operational
IN20	three-axis spectrometer	operational
PF1	neutron beam for fundamental physics	operational
PF2	ultra-cold neutron source for fundamental physics	operational
PN1	fission product mass-spectrometer	operational
PN3 – GAMS	gamma-ray spectrometer	operational
SALSA	strain analyser for engineering application	operational
ThALES	three-axis spectrometer	operational
WASP	wide-angle spin-echo spectrometer	commissioning

CRG INSTRUMENTS		
BRISP	Brillouin spectrometer	CRG-B operational
D1B	powder diffractometer	CRG-A operational
D23	single crystal diffractometer	CRG-B operational
GRANIT	gravitation state measurement	CRG operational
IN6-SHARP	time-of-flight spectrometer	CRG-A operational
IN12	three-axis spectrometer	CRG-B operational
IN13	backscattering spectrometer	CRG-A operational
IN22	three-axis spectrometer	CRG-B operational
SuperADAM	reflectometer	CRG-B operational
S18	interferometer	CRG-B operational

JOINTLY FUNDED INSTRUMENTS		
LADI (50 %)	Laue diffractometer	operated with EMBL
IN15	spin-echo spectrometer	operated with FZ Jülich
GRANIT	gravitation state measurement	operated with LPSC (UJF, CNRS)
STEREO	search for sterile neutrino	operated with CEA Saclay, LAPP Annecy, LPSC Grenoble, MPIK Heidelberg

TEST AND CHARACTERISATION BEAMS	
CT1, CT2	detector test facilities
CYCLOPS	Laue diffractometer
TOMOGRAPHY	neutrography
OrientExpress	Laue diffractometer
T3	neutron optics test facility
T13A, C	monochromator test facility
T17	cold neutron test facility

Details of the instruments can be found at **http://www.ill.eu/users/instruments/**.

Instrument layout – January 2018

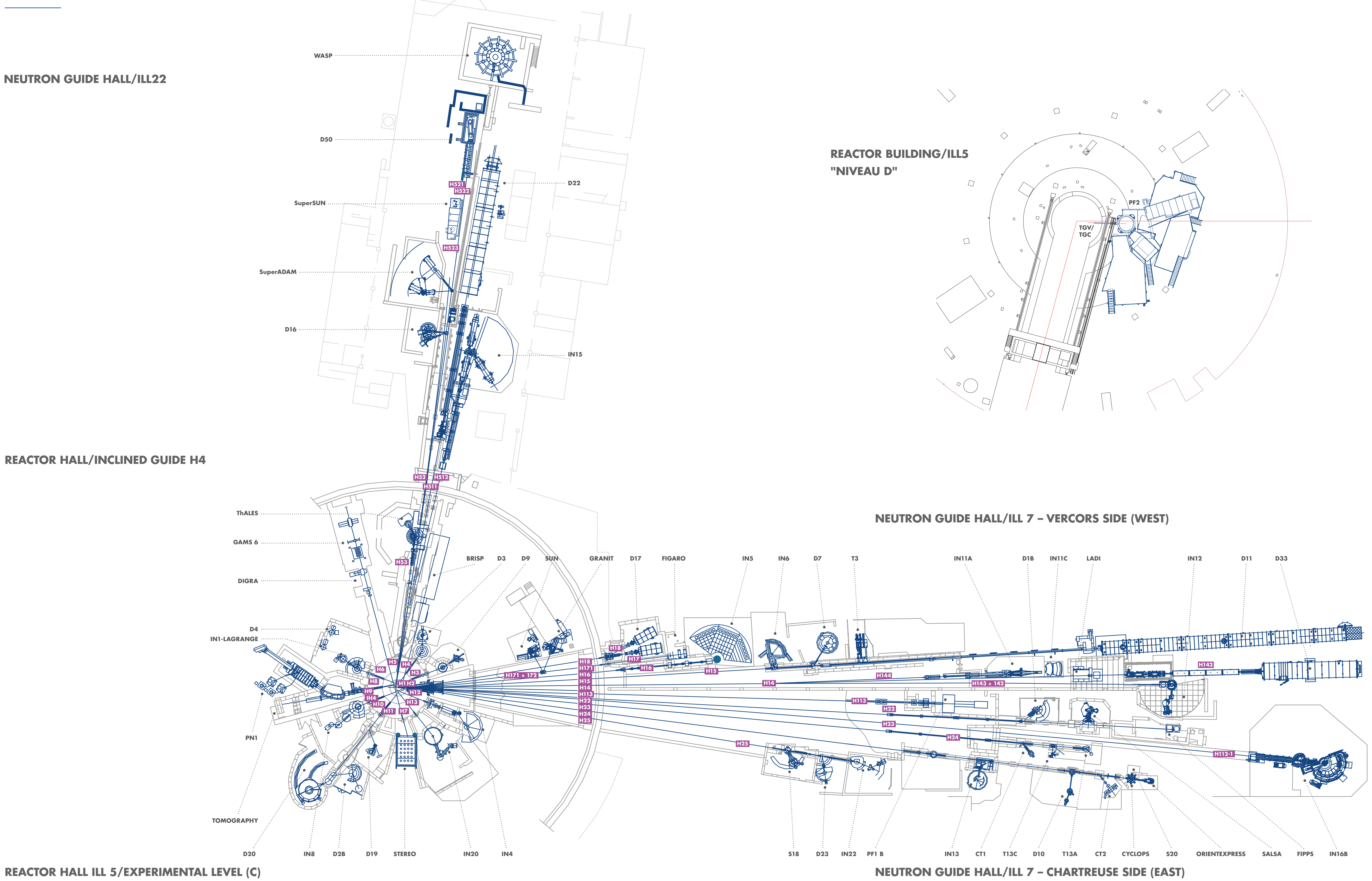

INSTRUMENT LAYOUT

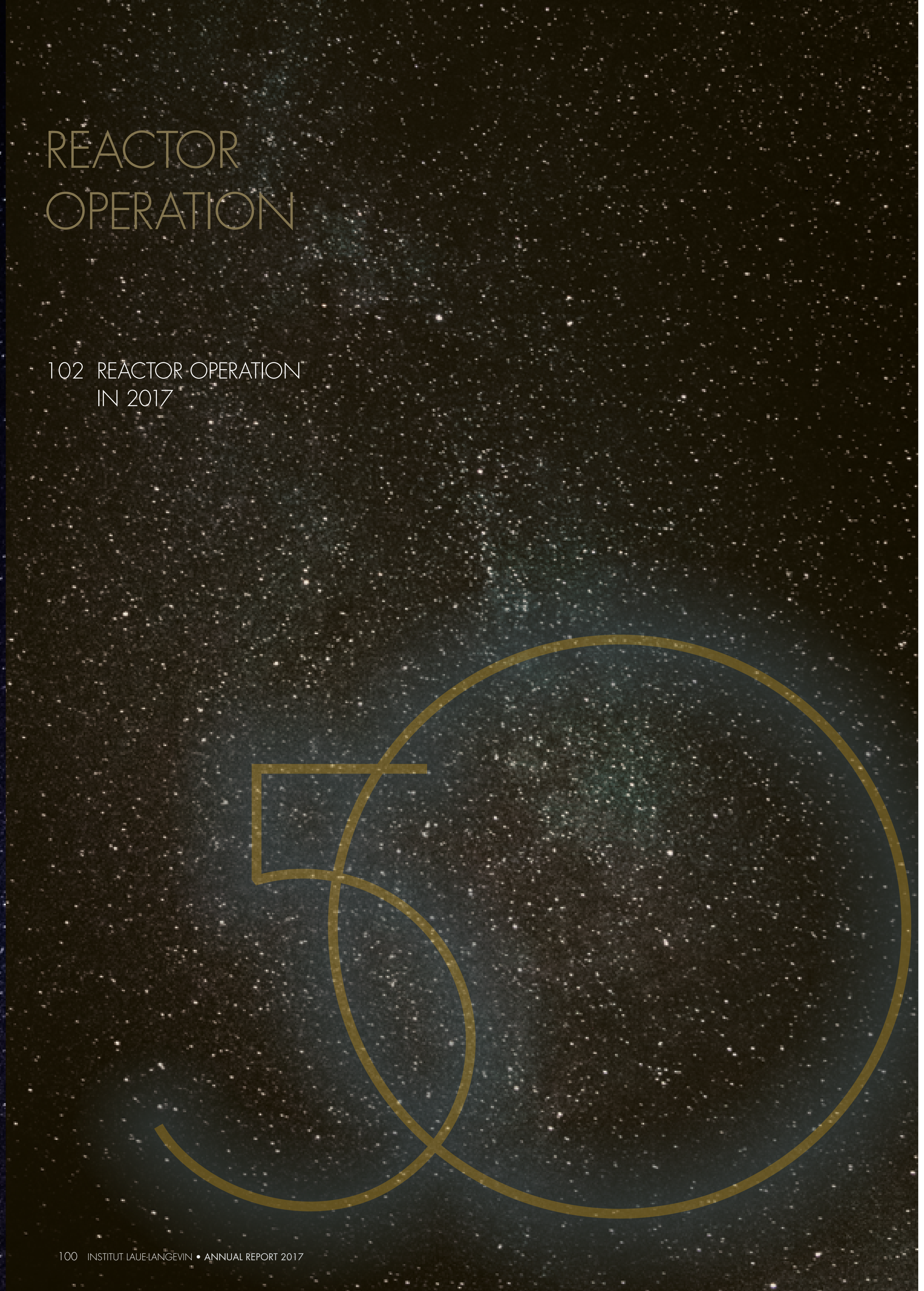

REACTOR OPERATION

The ILL's High-Flux Reactor (HFR) produces the most intense neutron flux in the world: 1.5×10^{15} neutrons per second per cm^2, with a thermal power of 58.3 MW. The reactor normally operates 4 reactor cycles per year. At the end of each cycle there is a shutdown period during which the fuel element is changed and a number of checks are carried out. Occasionally longer shutdowns are scheduled to allow for equipment maintenance.

At maximum power, the reactor's fuel element can provide 46 days of operation per cycle. For almost the last ten years, our 'contract' with our scientific users has been to provide 200 days of operation per year (excluding maintenance and upgrade work). At nominal power this allows for 4.5 cycles per year. For obvious practical reasons, this number of annual cycles is not ideal for the Reactor Division because it involves the same amount of work as having 5 operating cycles: the tests and fuel loading operations to be carried out are the same before every start-up, irrespective of the length of the cycle. As the performance of the instruments has generally been increased by a factor of 20, thanks to the Millennium Programme, we have recently decided to provide the 200 days of operation over four 50-day cycles at slightly lower power.

Following the nuclear disaster at Fukushima in 2011, the French nuclear safety authority (ASN) ordered additional safety assessments to be carried out on all French basic nuclear installations (INBs), including the ILL. This has had a major impact on the ILL and its budget over the past few years. Studies were performed by the Reactor Division teams to analyse the behaviour of the ILL reactor under extreme conditions, in particular an earthquake scenario involving major damage to Grenoble and the failure of all the dams on the river Drac—a scenario that would leave the city centre under 10 m of water.

The post-Fukushima programme has now ended, and the safety of the reactor is guaranteed even in the event of an extreme earthquake-and-flood combination involving the rupture of the dams upstream, well beyond previous dimensioning standards.

The ILL's High-Flux reactor (HFR) produces the most intense neutron flux in the world.

REACTOR OPERATION

Reactor operation 2017

A total of 48 days of scientific activity was provided in 2017, although only one reactor cycle could be delivered, using 1 fuel element.

Cycle n°	Start of cycle	End of cycle	Number of days of operation	Number of days scheduled	Power in MW	Number of unscheduled shutdowns
181	19.01.17	08.03.17	48	48	55.8	0
Total			**48**	**48**	**55.8**	**0**

The reactor cycle was completed without incident.

The winter shutdown was used for various important maintenance and other operations:

- emptying and cleaning of the pump basin
- installation of a protective barrier for the 45-metre high reactor exhaust stack
- preventive replacement of the batteries on the backup safety circuits
- maintenance of the natural convection flow valves (CN1/CN2/CN3/CN4) and siphon-breaker (two-yearly maintenance)
- maintenance of the NS network's uninterruptible power supply
- qualification of the new pumps on the shutdown cooling system with their new bearings.

Later in 2017 we were informed that the nuclear safety authorities were extending the period required to examine our request to bring our new emergency circuits into operation. We took advantage of the longer-than-expected reactor shutdown period to carry out a number of challenging technical operations:

- decommissioning of Emergency control room 2 (PCS2), following the transfer of operations to PCS3
- commissioning of the emergency groundwater circuit and its connection with the emergency core reflood system
- commissioning of the complementary seismic reactor shutdown circuit
- commissioning of the automatic power supply cut-off in case of earthquake
- commissioning of the automatic valve on the secondary circuit to guarantee the integrity of the containment
- commissioning of the seismic annular space pressurisation system
- commissioning of the emergency radiological monitoring laboratory
- construction of an airlock system for the reactor truck entrance
- reinforcement of the fuel-handling column and maintenance stand to resist extreme earthquake conditions
- replacement of three beam tubes and extraction of a fourth
- heavy maintenance on one of the principal diesel generators.

The post-Fukushima programme has now ended, and the safety of the reactor is guaranteed even in the event of an extreme earthquake-and-flood combination involving the rupture of the dams upstream, well beyond previous dimensioning standards.

In 2017 we also prepared and submitted all the reports required for our ten-yearly safety review. On 2 November 2017 the safety authorities were sent the following documentation:

- safety review report
- statutory conformity report
- mechanical conformity report for Safety-critical Items (EIS)
- conformity report for critical instrumentation and controls
- decommissioning report
- updated safety report
- updated operation rules
- updated emergency plan
- numerous studies in support of the reports
- numerous on-site controls and documentation reviews as part of the demonstration of conformity.

The safety review will determine whether any further work is required to ensure that the ILL reactor installations comply with the latest safety standards. This is likely to be limited given the extent of the reinforcement already carried out under the Reactor Refit programme (2002 to 2007) and post-Fukushima programme (2012 to 2017).

THE KEY REACTOR COMPONENTS (KRC) PROGRAMME

The aim of the KRC programme is to ensure the upgrade and maintenance of the reactor's most important components, thus guaranteeing the reliability of reactor operations for the future. The programme was launched in 2005 and is run as a continuous process.

OPERATIONS PLANNED FOR 2018

Maintenance operations:

- Major maintenance on the second principal diesel generator.

Work on the Key Reactor Components programme:

- Replacement of a safety rod
- Replacement of beam tubes H4 and H10.

RADIOACTIVE WASTE AND EFFLUENTS

The ILL's activities in 2017 generated waste and effluents respecting the regulatory limits applicable to our installation, as follows:

Evacuation of radioactive waste	Quantity
Decay bin (60 L)*	4
5 m³ pre-concreted crate (low and intermediate level waste)	0
5 m³ crate (low and intermediate level waste)	0
HDPE 200 L drums of 'incinerable' waste	74
HDPE 120 L drums of 'incinerable' waste	3
HDPE 120 L drums (laboratory waste)	6
30 L cylinders (liquid)	3

** The decay bins contain very active waste. They will be transferred to ANDRA's new storage centre CIGEO as soon as it becomes available, after an interim period in special storage.*

Gaseous effluents	Released in 2017 (TBq)
Tritium	13.0
Rare gas	0.42
Carbon-14	0.046
Iodine	0.00000055
Aerosols	0.00000015

Liquid effluents	Released in 2017 (TBq)
Tritium	0.19
Carbon-14	0.00029
Iodine	0.00000087
Other activation products	0.00014

Left to right:

Rosaline: The Rosaline container used in December 2017 to transfer highly active waste to its storage site.

Passerelle: The metal walkway ensuring the movement of personnel even in the event of extreme flooding following a breach of the dams on the river Drac.

Well: The lining for one of the wells to be used for the emergency groundwater supply.

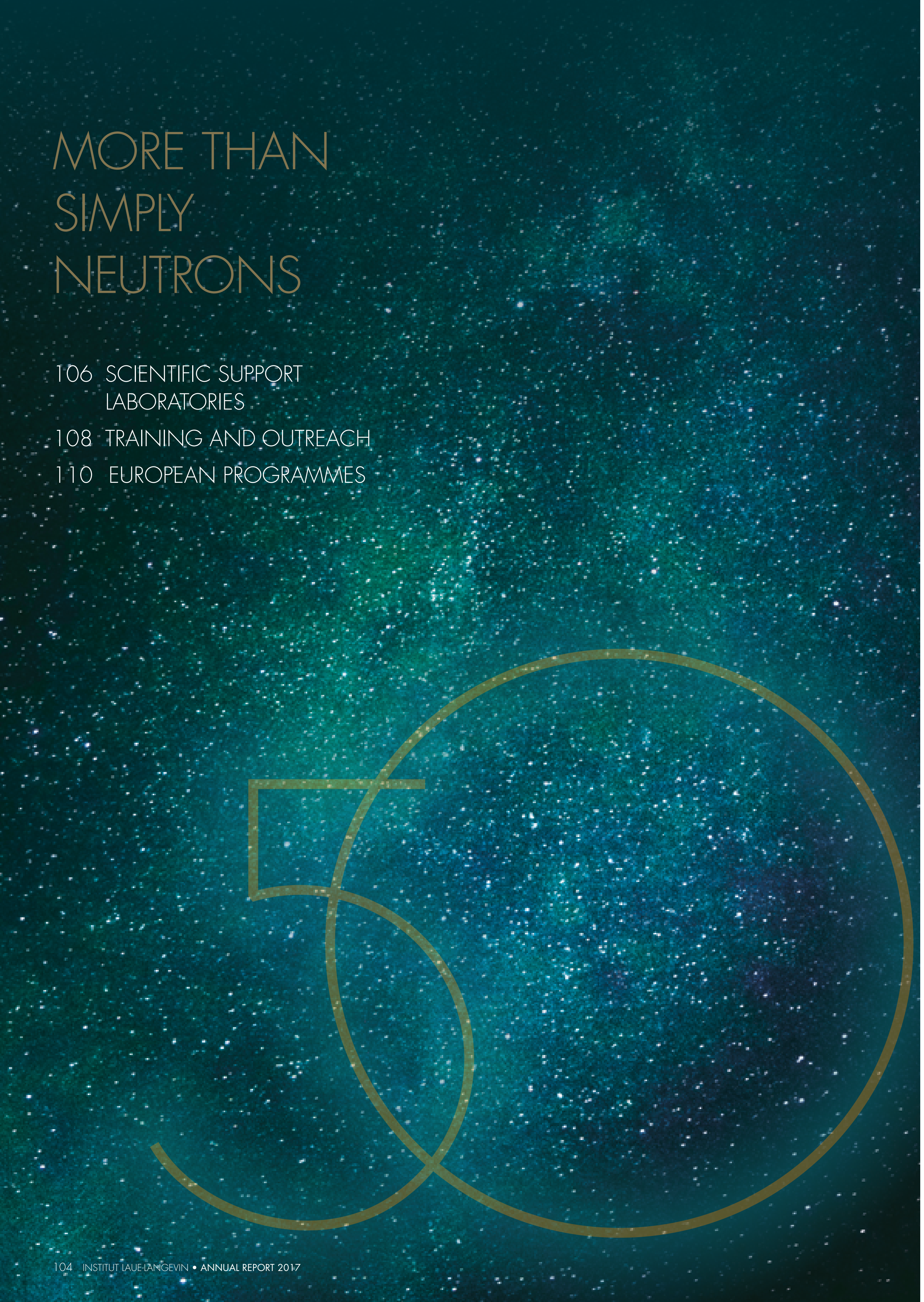

MORE THAN SIMPLY NEUTRONS

In order to maintain their ranking on the international scene, European research institutes must optimise their resources and develop synergies at every level.

The ILL is firmly committed not only to building high-performance instruments but also to offering the best scientific environment to the user community. We have established successful collaborations with neighbouring institutes over the years and launched many successful scientific and support partnerships.

The history of the ILL is that of European collaboration, and the Institute is today involved in no fewer than eight different projects funded by the European Commission. The benefits are not merely financial—the ILL also benefits from the networks and resources, which improve its integration with other facilities and the user community. This article focuses in particular on the activities being developed by the SINE2020 and FILL2030 projects—both coordinated by the ILL.

In addition, the ILL and the ESRF have transformed our joint site into a research campus—the European Photon and Neutron science campus, or EPN-campus for short—with a truly international reputation. The EPN science campus is a unique international science hub in Grenoble, hosting three major European institutes—the European Molecular Biology Laboratory (EMBL), the European Synchrotron Radiation Facility (ESRF) and the ILL—along with the Institut de Biologie Structurale (IBS) (**http://www.epn-campus.eu/**).

Last but not least, training and outreach forms a major part of the ILL programme and takes a wide variety of forms.

The ILL Graduate School and PhD programme are intended to train the next generations of neutron users. In parallel, schools, training sessions and local initiatives for Masters and PhD students are organised throughout the year.

In addition, through regular open days on the EPN-campus and yearly participation in the local science festival we hope to inspire new vocations in science disciplines, or at least to broaden the general public's awareness of science.

SCIENTIFIC SUPPORT LABORATORIES

PARTNERSHIP FOR SOFT CONDENSED MATTER

The Partnership for Soft Condensed Matter (PSCM) is a joint initiative established by the ILL and the European Synchrotron Radiation Facility (ESRF) here in Grenoble. The main PSCM mission is to provide enhanced support services to ILL and ESRF users addressing contemporary challenges in soft matter research, including nanomaterials, environmental and energy sciences, biotechnology and related fields. Currently the PSCM offers access to 13 laboratories hosting 25 major pieces of equipment as well as sample preparation facilities. Recently the PSCM instrument suite was expanded by the incorporation of the ESRF-AFM platform and the acquisition of both a gas chromatography set-up and zeta-sizer apparatus.

In addition to normal user operations, the PSCM is continually searching for new collaborative partners in order to strengthen the soft matter research community through the establishment of long-term collaborations devoted to the joint development of specialised sample environments and instruments.

In 2017, the PSCM was subjected to its first five-year review, which was conducted by a panel of four experts from France, the UK, Sweden and Italy. As a result, the PSCM agreement was renewed for the next five years.

The PSCM is located on the 2nd floor of the Science Building, along with the Soft Matter Science and Support group. Users wishing to use the PSCM laboratories and equipment in conjunction with neutron measurements should indicate this when submitting their request for beamtime. Further details can be found at **http://www.epn-campus.eu/pscm/**.

PARTNERSHIP FOR STRUCTURAL BIOLOGY

The Partnership for Structural Biology (PSB) contains a powerful set of technology platforms, contributed and operated by the various partner institutes (ILL, ESRF, EMBL, IBS). These platforms include advanced capabilities that strongly complement the neutron-scattering facilities available to ILL users: synchrotron X-rays, electron microscopy, high-field nuclear magnetic resonance (NMR), high-throughput methods (*e.g.* soluble expression and crystallisation) and a range of biophysical techniques such as isothermal calorimetry (ITC) and surface plasmon resonance (SPR). The PSB includes the Deuteration Laboratory (see below), operated as a user platform within the ILL's Life Sciences Group. It also includes the joint SANS/SAXS platform. In addition, there is strong connectivity and collaboration between the ILL and ESRF life sciences/structural biology and industry groups. The aim of the PSB is to enhance the interdisciplinary capabilities of each of the facilities co-located on the site and to widen the scientific scope of external user communities.

The Carl-Ivar Brändén building (CIBB) is the principal site for the PSB and its partner organisations. Check the website for more information: **http://www.psb-grenoble.eu/**.

DEUTERATION LABORATORY

The Deuteration Laboratory (D-Lab) is located and operated within the ILL's Life Sciences Group. Its user programme uses *in vivo* recombinant expression approaches to provide deuterated analogues of proteins, nucleic acids and lipids for the study of structure (crystallography, SANS, fibre diffraction, reflection) and dynamics (EINS) using neutron scattering. The platform is therefore of central importance to the activities of biological work relating to all the ILL instrument groups. The Group is involved in a wide variety of externally funded programmes that exploit the capabilities of the PSB as well as promoting interdisciplinary structural biology. It also interacts strongly with industry. Each year it takes on a small number of undergraduate students who are trained in many of these techniques and who contribute to method development activity. It is also engaged in the operation and exploitation of the cryo-EM capabilities being set up with the installation of the Titan Krios at the ESRF, in partnership with ESRF, IBS and EMBL.

Access to the D-Lab platform is through a rapid peer-review proposal system and is available to all ILL member state countries regardless of where the neutron scattering study will be carried out. The facility may also be made available to users from non-member state countries, but it is expected that the costs of the work involved will be covered by the user. Users can apply to use the D-Lab at **http://www.ill.eu/users/support-labs-infrastructure/deuteration-laboratory/**.

CHEMISTRY LABORATORIES

The Chemistry Laboratories are managed by the Soft Matter Science and Support Group (SMSS). The main purpose of the laboratories is to allow ILL users to prepare samples for their neutron experiments on site. Support for in-house research conducted by instrument scientists and PhD students is also provided.

The main facilities include an advanced sample preparation lab, a bio-preparation lab, a laboratory for handling corrosive substances, an oven room and a cold room, and are located on the first floor of the Science Building. Three sample preparation laboratories can be found in the guide halls ILL7 and ILL22. The labs provide users with basic lab equipment, glassware, consumables and chemicals necessary to prepare samples for a variety of different neutron experiments. A glovebox to handle air-sensitive compounds and an enclosure to work with nano-powders are also available. Different equipment for sample characterisation can be accessed *via* the PSCM laboratories. Further information on the Chemistry Laboratories can be found at **https://www.ill.eu/users/support-labs-infrastructure/chemistry-laboratories/**.

MATERIALS SCIENCE SUPPORT LABORATORY

The Materials Science Support Laboratory (MSSL) provides a range of support to our users, from advice with experiment proposals through sample preparation to the running of the experiment. We provide equipment for tensile testing, hardness testing and microscopy as well as 3D-scanning of samples. In particular, the Laboratory works with users to optimise their experimental methodology before the start of an experiment. This takes the form of standardised specimen mounting, digitisation of samples and the definition of measurement macros. It is recommended that users contact us well in advance and arrive at the ILL a day or two prior to the start of an experiment to enable these off-line preparations to be performed.

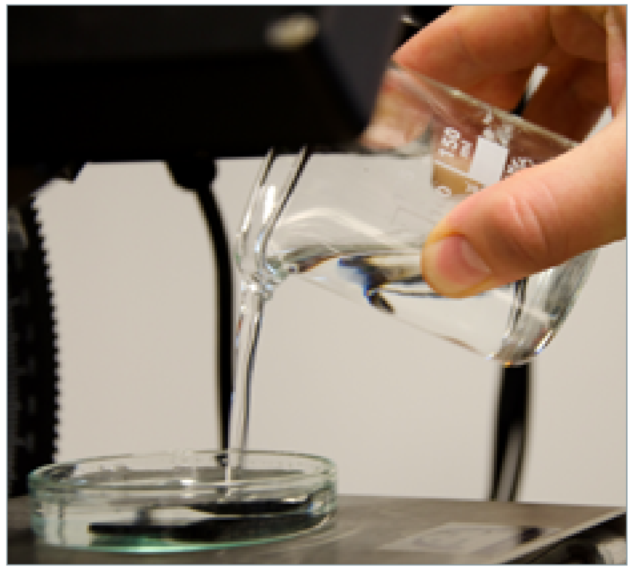

TRAINING AND OUTREACH

STUDENT TRAINING

Through the **ILL PhD programme**, the **ILL Graduate School** has grown in strength over recent years and now involves approximately 50 students of many different nationalities. Most are wholly or partially supported by the ILL, while a few are also financed by other sources. In the recent 2017 call for proposals for PhD projects 41 applications were submitted, from which 8 full-time-equivalent projects will be selected in spring 2018 and the students subsequently recruited.

Since the students work in different disciplines, their annual **clip session** gives them the opportunity to exchange ideas and get to know one another better. This is also an occasion for the ILL staff at large to meet the students and learn about their projects. The 2017 clip session on 24 May once again challenged the students to present their work in five minutes, and the event was as entertaining as ever.

Running throughout the year, a set of seminars (titled '**All you need is neutrons**' in 2016–2017) is held on a weekly basis. The speakers are the PhD students themselves and the topics range over all aspects of neutron science and current PhD projects.

In 2017, the ILL again offered Masters and PhD students from the local university 'Université Grenoble Alpes' (UGA) the opportunity to take part in real neutron scattering experiments, under the framework of the so-called **TP CESIRE**. Coordinated by Paul Steffens, and with thanks to the various ILL scientists interested in this project, experiments with appropriate topics and experimental set-ups are constantly selected for this purpose. This year, 15 UJF (Université Joseph Fourier) Masters students participated in some of the TP CESIRE experiments performed on both ILL and CRG instruments.

For the fourth time the ILL organised its undergraduate summer programme, in collaboration with the ESRF, for students from all universities in its member countries. The invited students spent a month on a scientific project and attended a series of seminars given by the Institute's scientists.

TRAINEES

In 2017 the ILL welcomed a total of 72 trainees (including 8 from the ILL–ESRF summer school and 2 from the STFC) of 24 different nationalities (including 8 German, 30 French, 11 English and 14 from other ILL member countries).

The ILL's PhD students during their clip session on 24 May.

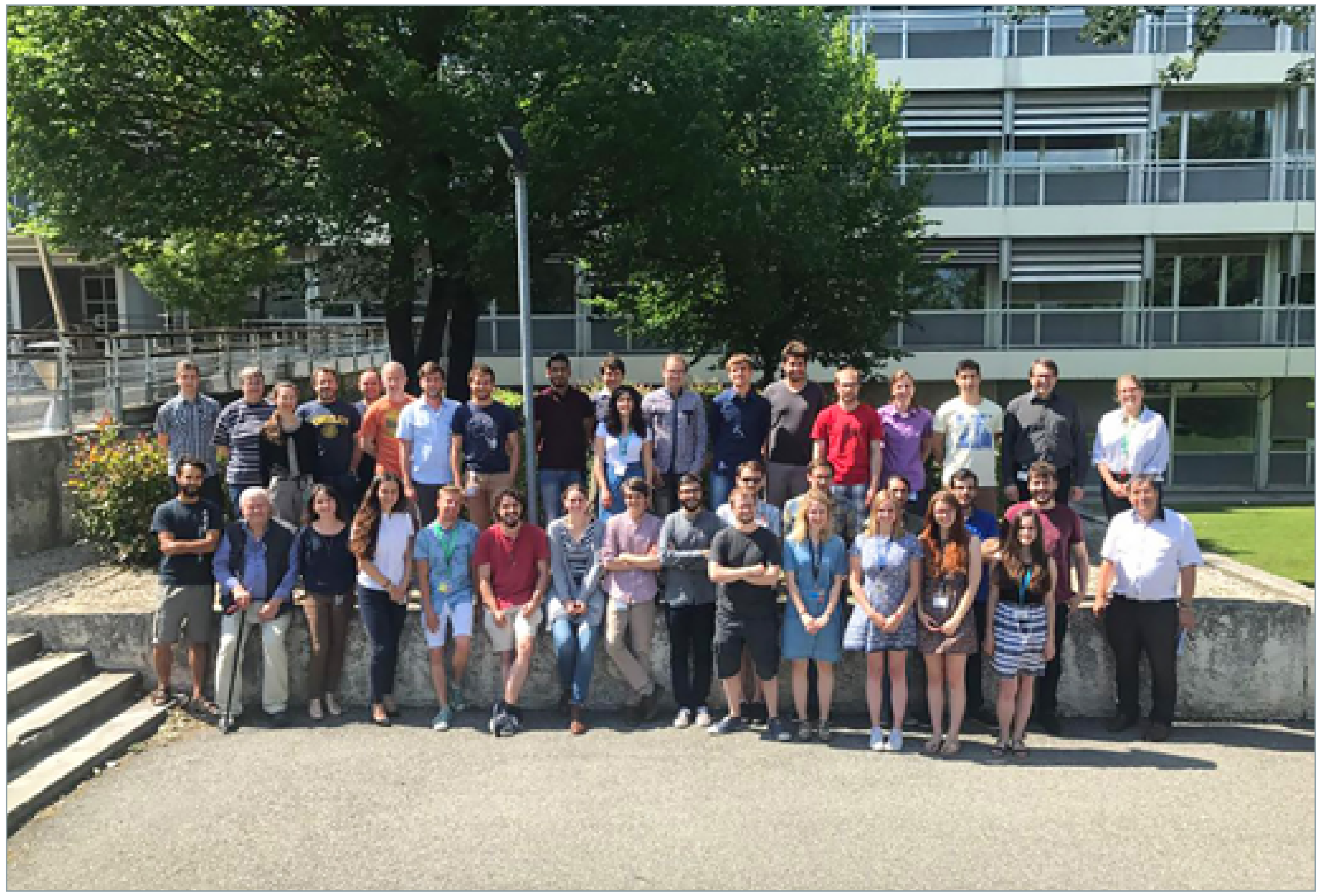

Participants of the HERCULES 2017 school.

HERCULES SCHOOL

This one-month course, coordinated by the Université Grenoble Alpes, is designed to provide training for students as well as postdoctoral and senior scientists in the field of neutron and synchrotron radiation for condensed matter studies (biology, chemistry, physics, materials science, geosciences, industrial applications), from European and non-European universities and laboratories.

The course includes lectures, practicals and tutorials, visits to large facilities and a poster session (each participant puts up a poster about her/his thesis or research topic for a day). A special 'Practicals and Tutorials' programme is included, hosted in a partner institution (including one full day at the ILL).

The 2017 HERCULES took place from 27 February to 30 March 2017. It welcomed 77 participants (including 5 part-time), of 20 different nationalities working in 19 different countries (including France 18, Germany 14, Denmark 10, Italy 5, Russia 5, UK 5, Sweden 4, Czech Republic 3, Taiwan 3, Spain 2, Hungary 2), and coming from as far as India (1). The students were selected from more than 160 applicants.

More information is available at **http://hercules-school.eu/**.

SCIENCE FESTIVAL

On Saturday 20 October, the four EPN-campus institutes fielded a stand at the French Science Festival 'Fête de la Science'. We welcomed many of the 2 800 curious and enthusiastic visitors who came to the Grenoble 'Parvis des Sciences' that day. The public learnt about the different activities and research carried out on the EPN science campus guided by more than 30 passionate volunteers from the four institutes, demonstrating once more their complementarity and the importance of geographical proximity.

Half of the stand highlighted the large-scale facilities (ILL/ESRF) and their wide range of scientific activities. The other half was dedicated to structural biology, with many hands-on activities from EMBL Heidelberg. Without doubt, a great success.

Science festival – Explaining the "magic" of diffraction.

EUROPEAN PROGRAMMES

SINE2020—SCIENCE AND INNOVATION WITH NEUTRONS IN EUROPE IN 2020

SINE2020 (**http://sine2020.eu**) was initiated in October 2015. It is a four-year 12 M€ infrastructure development project under the Horizon2020 Framework Programme federating 18 facilities and academic partners. The main objective of the project is twofold: to prepare the European community for the first neutrons at the ESS (European Spallation Source) in 2020, and to explore the innovation potential of neutron facilities and their scientific partners.

SINE2020 is largely user-oriented. Its so-called 'Joint Research Activities' (JRAs) focus accordingly on key techniques for present and future neutron experiments. These activities cover issues of sample preparation, such as novel techniques in deuteration and macromolecular crystallogenesis, sophisticated equipment for sample environment and software development. For example, the project is actively involved in the Mantid project for data reduction (**http://www.mantidproject.org**), a framework for high-performance computing and the visualisation of materials science data across specialised European facilities. SINE2020 promotes a collective approach to the processing of data generated by a wide range of techniques (SANS, reflectometry, imaging, INS, QENS and atomistic simulations).

A promising, though still under-explored, area is that of research collaborations with industry. SINE2020 is committed to strengthening direct links with industrial users, by demonstrating the potential of neutron techniques and the value of access to the network's facilities. Thanks to SINE2020 industrial users can now easily perform feasibility studies in eight different European neutron centres, in areas such as failure analysis or materials and component development. The March 2016 invitation generated 27 applications—half of which came from the engineering and metallurgy sector—which almost tripled the combined annual industrial demand of the centres involved. The campaign effectively highlights the need of industrial partners for strain scanning, imaging and SANS.

A special focus of SINE2020 is the education of future neutron generations. To this end the virtual e-learning platform has been further developed, with SINE2020 supporting introductory and specialised neutron schools all over Europe. The opportunities now cover a wider range of audiences, applications and levels of learning, with demand already expanding the scope of training available.

SINE2020 illustrates the ever-growing commitment of the neutron community in Europe to demonstrate the potential of neutron science. Its collaborators have expanded the capacity of the community to provide tailor-made solutions capable of boosting innovation and addressing the challenges facing our society.

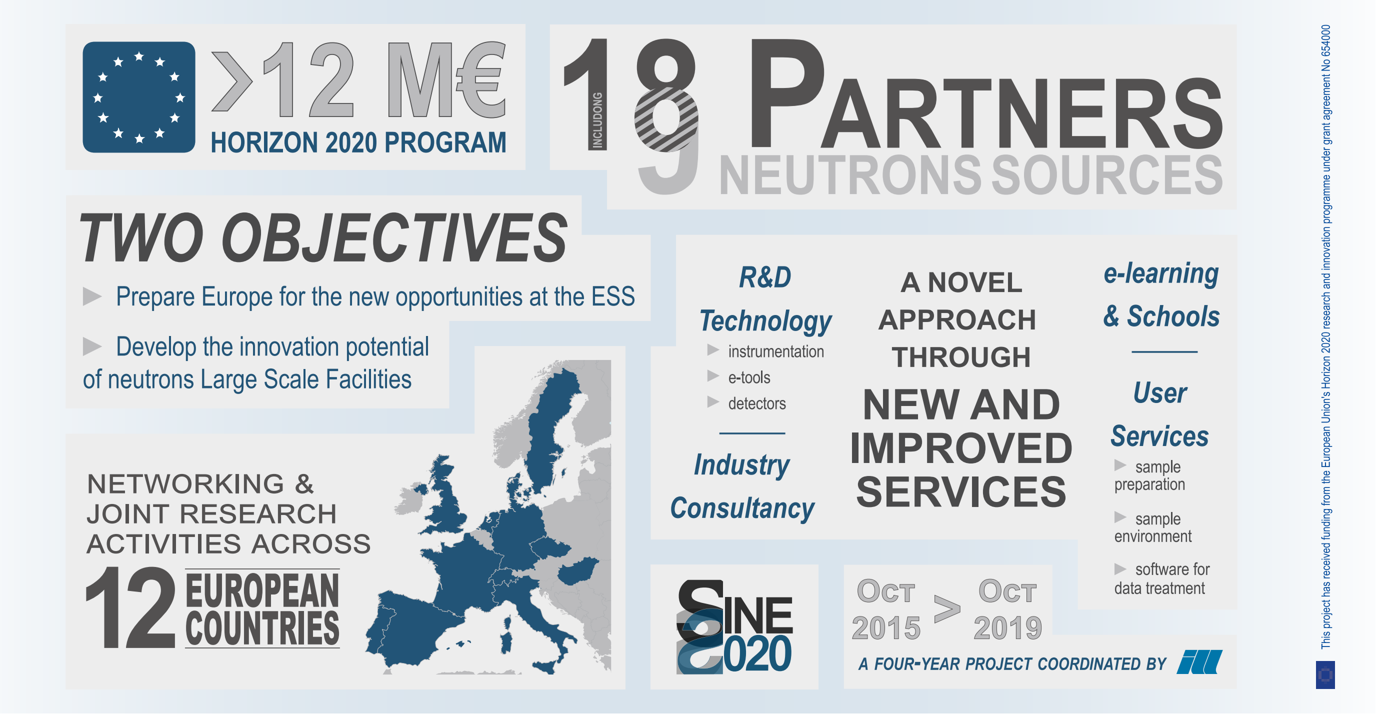

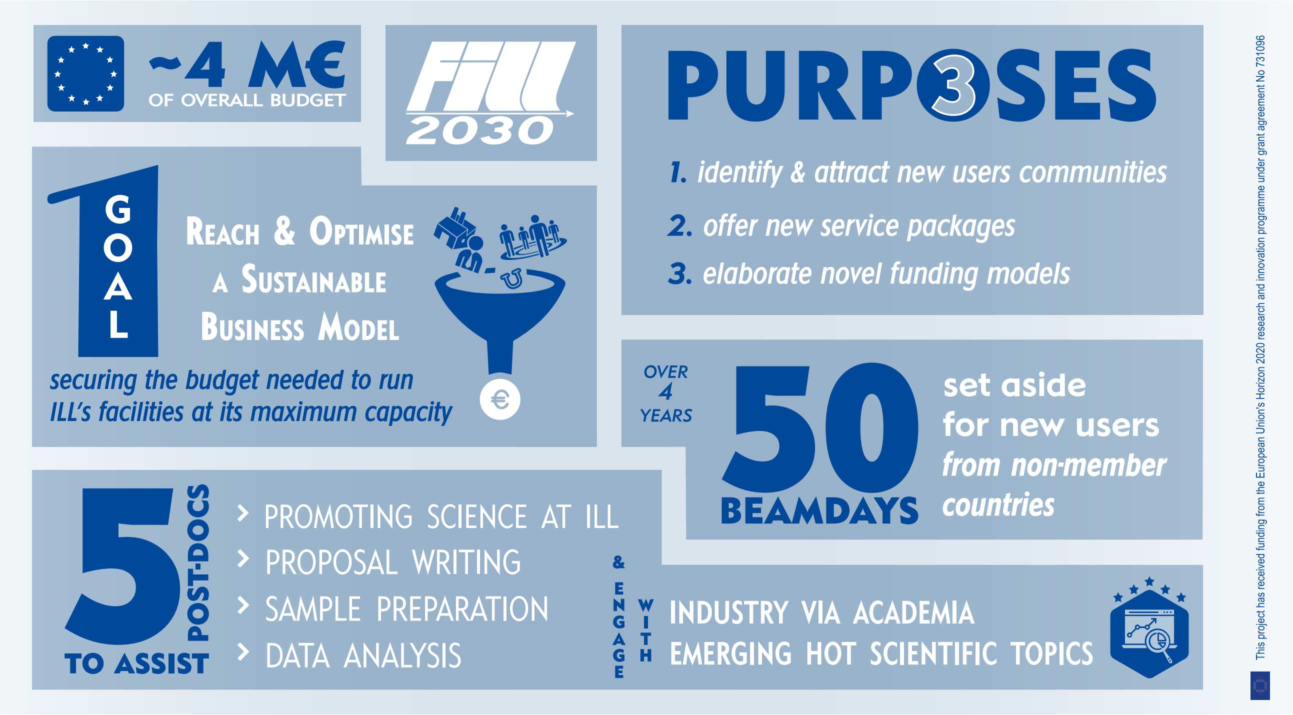

FILL2030—THE FUTURE OF ILL, UNTIL AT LEAST 2030

Unlike most of the other projects funded by the European Commission, FILL2030 is a mono-beneficiary project, entirely dedicated to ensuring the long-term sustainability of the ILL business model.

Part of the EU's Horizon 2020 research and innovation programme, FILL2030 has been granted 3.98 M€ to achieve its mission. This budget will finance the development of the following:

- new service packages for academia and industry
- innovation of the ILL's funding model
- tools to identify emerging user groups
- demonstrations of the socio-economic impact of ILL research.

FILL2030's overall objective is to achieve an increase of 5 M€ in the ILL's annual budget (~ 5 % of its current budget), equivalent to the cost of one extra fuel cycle. Its initial efforts will concentrate on securing continuous income from the existing Associate and Scientific Member countries. Relations are being strengthened in this respect, focusing on the needs and expectations of each partner country. The ILL is now actively promoting, country by country, the impact of the neutrons it produces and the return on investment its funders receive.

Simultaneously, FILL2030's outreach activities (including tours of installations, roadshows, workshops and media communications) will extend the pool of potential new partners, in Europe and beyond. The ILL's online activity is also being renewed, starting with a new design for the ILL website which will now also present an attractive showcase of the Institute's many achievements.

The ILL's strategy to engage with new users and attract sources of additional funding will be based on a much clearer picture of the European neutron scattering landscape. The aim is to identify new international partners, attract new scientific communities and ensure that current users are exploiting to the full the potential Europe can offer.

FILL2030 will therefore develop a set of bibliometric tools capable of analysing the activity of European and other neutron scattering communities. This will help both to unravel existing complex, trans-national networks of collaboration and identify potential areas of growth. The new tools will also allow for regular monitoring of the changes underway in neutron science. Most crucially they will help to measure societal impact—a major factor in the endeavour to win over potential new funders. The same is true of course for our existing supporters, who must justify their on-going investment in the ILL.

By establishing relationships with new member states, FILL2030 will almost certainly be changing the framework conditions. Existing paradigms will be adapted and extended, with the introduction of new mechanisms for access and funding corresponding more closely to the new community's needs.

WORKSHOPS AND EVENTS

ILL Chronicle 2017

19 JANUARY
Celebration of the ILL's 50th anniversary (World Trade Centre, Grenoble)

23 JANUARY
Visit by the head of Italy's CNR, Corrado Spinella

4–7 APRIL
Meetings of the ILL's Scientific Council and its Subcommittees

18–19 MAY
Meeting of the Subcommittee on Administrative Questions (SAQ)

20 JUNE
Signing of a Memorandum of Understanding between the ESS and the ILL on neutron research and technology

20–21 JUNE
Meeting of the Steering Committee

12 SEPTEMBER
Visit by Don Pablo Benavides Orgaz, the new Consul General of Spain in Lyon

18 SEPTEMBER
Signing of a Master Collaboration Agreement between the international company Procter & Gamble (P&G), the ESRF and the ILL

12–13 OCTOBER
Instrument Subcommittee meeting: ILL Modernisation Programme Endurance II

17–18 OCTOBER
Meeting of the Subcommittee on Administrative Questions (SAQ)

10 NOVEMBER
Inauguration of the Cryo-EM platform (EPN Campus)

16–17 NOVEMBER
Meetings of the ILL Scientific Council

29–30 NOVEMBER
Meeting of the Steering Committee

4 DECEMBER
Visit by Mr Jérôme Gercet, Headmaster of Grenoble International School

The ILL Instrument Subcommittee met on 12–13 October to discuss the Modernisation Programme Endurance II.

EVENTS 2017

Scientific events

In 2017, the ILL organised (or co-organised) 21 scientific events (workshops, conferences and schools).

13 JANUARY
Discussion Group for macromolecular crystallogenesis

20–24 MARCH
6th Workshop on Nuclear Fission and Spectroscopy of Neutron-Rich Nuclei

23–24 MARCH
ChEMWood: Chemical Engineering and Mechanics in Wood: X-ray and neutron scattering, microscopy and modelling

3 APRIL
PSB student day

9–11 MAY
Advances in neutron scattering for soft matter and biology

24 MAY
PhD students' clip session

24–26 MAY
International Workshop on Particle Physics at Neutron Sources

7–9 JUNE
Neutrons in Structural Biology

19–20 JUNE
Optics and neutrons experimental approaches to THz spectroscopy—SON2017

28–30 JUNE
Stereo collaboration meeting

6–7 JULY
NDMeso2017 Neutron Diffraction and the Mesoscale

6–7 JULY
Neutron Diffraction and the Nanoscale 2017 (NanoDif 2017) satellite meeting

7–14 AUGUST
International Conference of Physics Students

3–30 SEPTEMBER
X-Ray and Neutron Science, international student summer programme at ILL/ESRF

11–15 SEPTEMBER
EMBO SAXS/SANS course

16–25 SEPTEMBER
Giornati Didattiche

28–29 SEPTEMBER
Students' workshop

9 OCTOBER
3ème journée thématique du GDR, Bio-inginérie des interfaces

10–13 OCTOBER
40th anniversary of Neutron Spin Echo

16–20 OCTOBER
Annual School on Neutron Diffraction Data Treatment using the FullProf Suite

23 NOVEMBER
CARAC

1


2
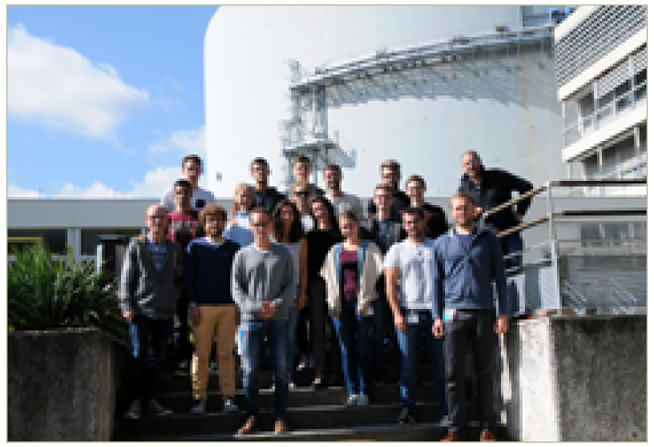

3


1. Participants of the Neutrons in Structural Biology workshop.
2. Group photo during the undergraduate summer school co-organised by the ILL and the ESRF.
3. Attendees at the 'Chemical Engineering and Mechanics in Wood' workshop.

ILL seminars organised in 2017

A total of 58 general seminars were organised at the ILL in 2017, in addition to 12 colloquia. The list of colloquia can be found at **http://www.ill.eu/news-press-events/events-calendar/**.

23 January W. Press
Is rotational tunnelling still alive? Questions concerning solid methane

26 January P. Regan
Characterising & standardising 'interesting' radioisotopes at the UK National Physical Laboratory

26 January R. Bilewicz
Lipidic cubic-phase carriers of anticancer drugs: drug release profiles and interactions with phospholipid membranes

26 January G. Burca
'IMAT—the new neutron imaging and diffraction beamline at ISIS'

31 January A. Popov
Basic properties of radiation defects in halides, oxides and perovskites

7 February T. Reimann
Vortex matter beyond SANS

10 February D. Price
The influence of water on the structure and relaxation of a prototype ionic liquid

13 February T. Weber
The triple-axis resolution software 'Takin'

13 February M. Stachura
When NMR spectroscopy is not enough: applications of ß-radiation-detected NMR in chemistry and biochemistry

16 February A. Sundaresan
Magneto(di)electric effect in spinel oxides

22 February N. Kardjilov
Neutron imaging in materials research

23 February J. Jäckel
WISPy dark matter

8 March C. Michelagnoli
FIPPS— The new Fission Product Prompt X-ray spectometer

10 March C. Garvey
Molecular insights into small molecule anhydro- and cryo-protectants

4 April A. Serebrov
Measurements of neutron lifetime with Big Gravitational Trap

25 April M. Doser
Experiments on antimatter at CERN

9 May S. Perkins
Atomistic modelling of scattering data in the Collaborative Computational Project for Small-Angle Scattering (CCP-SAS): new insights into antibody conformations

15 May C. Vendrely
Amyloids in extracellular matrices

18 May G. Jackeli
Spin-orbital frustration in Mott insulators

23 May F. Cantargi
LAHN: The Argentinian Neutron Beams Laboratory Project

30 May M. Berritta
Theory of laser-induced magnetism from first principles

6 June F. Ferdeghini
Ionic liquids under nanometric unidimensional confinement: a route to a better electrolyte?

6 June N. Martinez
Nanoscale water dynamics *in operando* fuel cells

6 June J-P. Melchior
A multiscale study of proton dynamics and ionic transport in phosphoric acid: the substance with the highest intrinsic proton conductivity

6 June J. Peet
Investigation of oxide ion conduction *via* neutron scattering techniques and *ab initio* molecular dynamics

6 June A. Perrichon
Ionic diffusion mechanisms investigated through lattice and vibrational dynamics: the cases of the oxide-ion conductor Nd_2NiO_{4+d}, and Ba_ZrO_3-based proton conductors

7 June C. Bidinosti
NMR phase encoding using twisted B1 fields

16 June Z. Fakhraai
Long-range correlated dynamics in organic glasses

16 June J. Dawidowski
Multiple scattering corrections: possible applications for SANS techniques

19 June X. Ledoux
A new neutron facility at SPIRAL-2

19 June C. Breton
Glycosyltransferases: the enzymes that build complex sugars

20 June T. Roger
The new generation active target ACTAR TPC

26 June S. Chernyshev
Quantum order-by-disorder and excitations in kagome-lattice magnets

27 June N. Ashby
Relativistic theory of a falling cube gravimeter

28 June C. Wiebe
Confinement of magnetic monopole quasiparticles in a quantum spin ice

30 June E. Farhi
Automated lattice dynamics with iFit, using ASE, PhonoPy, VASP and more…

3 July C. Weinheimer
The quest for the neutrino mass

6 July I. Zaliznyak
Polarised neutron scattering on HYSPEC (the Hybrid SPECtrometer at SNS): temperature evolution of dynamical magnetism in $FeTe_{(1-x)}Se_{(x)}$

18 July N. Manohar
Solvent-driven infiltration of polymer (SIP) into nanoparticle packings

25 July B. Aoun
Fullrmc, stochastic fitting to reverse engineering atomic and molecular systems enabled with Machine Learning

15 September D. Svergun
State-of-the-art of SAS data analysis

18 September A. Tremsin
MCP neutron detector imaging—towards the um resolution for *e.g.* SANS and diffraction

25 September V. Lauter
Magnetism reflectometer: grazing incidence polarised neutron scattering at SNS

26 September G. Balik
Vibration analysis and control for scientific experiment

4 October J. Wilson
Spectroscopic studies of the ^{238}U(n,f) and ^{232}Th(n,f) fission reactions with fast neutrons at LICORNE/nu-ball

11 October G. Lane
Creation and survival of ^{180}Ta in stellar environments plus a brief overview of nuclear research at the ANU

23 October L. Udby
E-neutrons for everyone

13 November N. Zaccai
Oil and water don't mix but have to: insights into cell membrane biogenesis from neutron scattering

15 November C. Masquelier
Crystal chemistry of positive electrode materials for Li- and Na-ion batteries probed at large-scale facilities

17 November T. Chupp
The new muon g-2 experiment at Fermilab

22 November A. Franck
Neutron waves in an accelerating matter

29 November J. Ljungvall
Picosecond lifetime measurements using Recoil Distance Doppler Shift method (an opportunity at FIPPS?)

30 November S. Ulvenlund
How neutrons help us design the green surfactant technology of tomorrow

4 December K. Bodek
Search for BSM physics at TeV scale by exploring the transverse polarisation of electrons emitted in neutron decay—the BRAND project

6 December F. Müller
Innovation in the chemical industry

7 December A. Senyshyn
Neutron scattering studies on Li-ion batteries

11 December V. Monti
Intense thermal neutron fields from a medical-type LINAC: the e_LIBANS project

12 December L. Oberauer
Neutrino astrophysics at low energies—status and prospects

FACTS AND FIGURES

STAFF ON 31/12/2017

501.5 people, including 73 experimentalists in the scientific sector and 37 thesis students.

347 French; 45.5 German; 38.5 British; 45 scientific participating countries and 25.5 others.

Nationality		**%**
French	343.5	69.2 %
German	45.3	9.1 %
British	38.4	7.7 %
Member countries	44.0	8.9 %
Others	25.2	5.1 %
Total	**496.4**	**100 %**

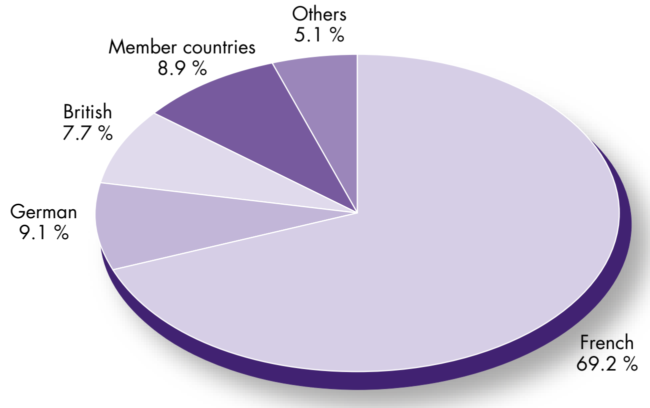

REVISED BUDGET 2017: 100.694 M€ (excluding taxes)

Income	**M€**	**%**
Income from Associates (incl.Endurance Progamme, Nucl. insurance & add. nuclear tax)	65.068	64.62 %
Income from Scientific Members	20.118	19.98 %
Own income	2.940	2.92 %
Carry forward from 2016	1.645	1.63 %
Movement from reserves	9.873	9.81 %
Contribution from national/regional/ local authorities	1.050	1.04 %
Total	**100.694**	**100.00 %**

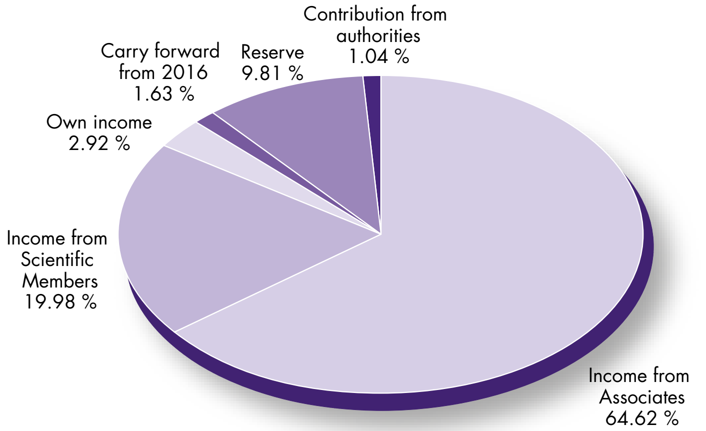

Expenditure	**M€**	**%**
Staff costs	46.260	45.94 %
Operating costs	19.363	19.23 %
Investment costs	20.486	20.34 %
Fuel cycle	14.585	14.48 %
Total	**100.694**	**100.00 %**

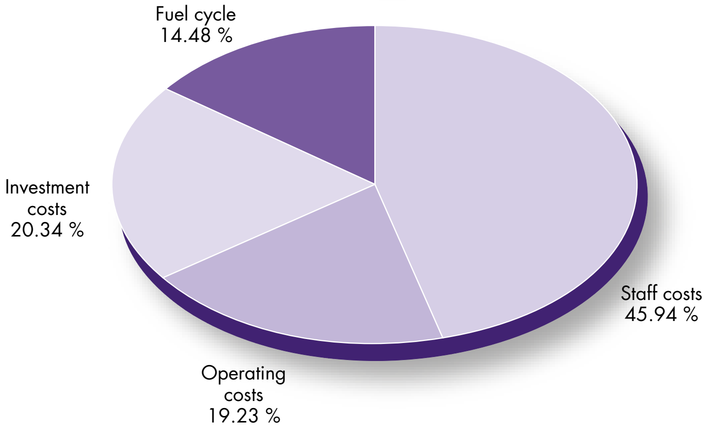

PURCHASING STATISTICS (Figures 2017 to December 2017)

	M€	**%**
France	18.05	51.58 %
Germany	4.39	12.55 %
United Kingdom	2.16	6.17 %
Scientific Members	4.61	13.17 %
Others	5.78	16.53 %
Total	**34.988**	**100.00 %**

France captif market	6.28	15.22 %
Total captif/non captif	**41.270**	**0**

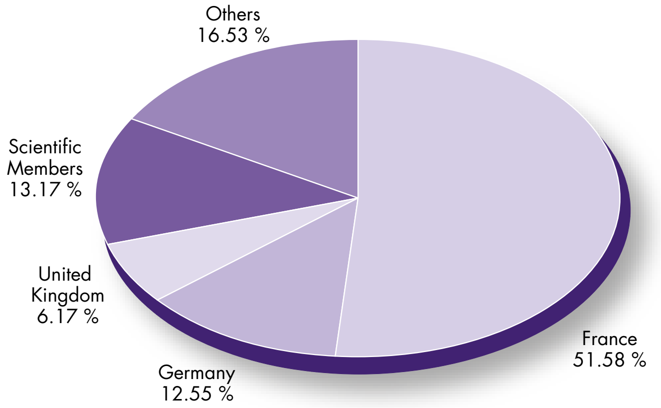

FACTS AND FIGURES

NAME
Institut Max von Laue-Paul Langevin (ILL)

FOUNDED
19 January 1967

Intergovernmental Convention between France, Germany and United Kingdom (19/07/1974)

ASSOCIATES
France

Commissariat à l'Energie Atomique et aux Energies Alternatives (CEA)

Centre National de la Recherche Scientifique (CNRS)

Germany

Forschungszentrum Jülich (FZJ)

United Kingdom

Science & Technology Facilities Council (STFC)

COUNTRIES WITH SCIENTIFIC MEMBERSHIP
Spain

MINECO Ministerio de Economia y Competitividad

Switzerland

Staatssekretariat für Bildung, Forschung und Innovation (SBFI)

Italy

Consiglio Nazionale delle Ricerche (CNR)

CENI (Central European Neutron Initiative)
Consortium composed of:

Austria: Österreichische Akademie der Wissenschaften

Czech Republic: Charles University of Prague

Slovakia: Comenius University, Bratislava

TRANSNI
(Belgian-Danish-Swedish Transnational Neutron Initiative Consortium)

Belgium: Belgian Federal Science Policy Office (BELSPOL)

Sweden: Swedish Research Council (VR)

Denmark: Danish Agency for Science, Technology and Innovation (DASTI)

Poland: ILLPL Consortium of Polish Scientific and Research Institutions

SUPERVISORY AND ADVISORY BODIES
Steering Committee, which meets twice a year

Subcommittee on Administrative Questions, which meets twice a year

Audit Commission, which meets once a year, and statutory auditor

Scientific Council with 9 Subcommittees, which meets twice a year

REACTOR
Operating 1 cycle in 2017
48 days in total, average power 55.8 MW (p.102)

EXPERIMENTAL PROGRAMME
268 experiments out of the 656 allocated by Subcommittees on 28 ILL-funded and 9 CRG instruments

721 visitors from 33 countries

Publications in 2017

In 2017, the ILL received notice of 572 publications by ILL staff and users.

They are listed on the ILL website:
https://www.ill.eu/about-ill/documentation/scientific-publications/scientific-publication-list/.

THE DISTRIBUTION BY SUBJECT IS AS FOLLOWS

Applied Physics, Instrumentation and Techniques	36
Biology	57
Crystallography and Chemistry	64
Liquids and Glasses	19
Magnetic Excitations	50
Magnetic Structures	97
Materials Science and Engineering	46
Medicine	4
Nuclear and Particle Physics	64
Soft Matter	82
Spectroscopy in Solid State Physics and Chemistry	40
Theory	12
Other	1

ILL PHD STUDENTSHIPS

PhD students at the ILL in 2017*	44
PhD theses completed in 2017*	6
PhD theses completed in 2017**	4

* *Receiving a grant from the ILL.*
** *Receiving an external grant.*

ORGANISATION CHART IN DECEMBER 2017

Review panels

Key
Chair/focus group Chair
ILL college secretary/focus group secretary
ILL specialist

REVIEW PANELS

APPLIED METALLURGY, INSTRUMENTATION AND TECHNIQUES
G. Bruno (BAM, Berlin, Germany)
E. Farhi
T. Pirling/A. Wildes

NUCLEAR AND PARTICLE PHYSICS
M. Van der Grinten (STFC, UK)
T. Jenke
P. Geltenbort

MAGNETIC EXCITATIONS
A. Boothroyd (Oxford University, UK)
J. Ollivier
B. Fåk

CRYSTALLOGRAPHY
C. Masquelier (CNRS Amiens, France)
E. Mossou
C. Ritter

MAGNETIC STRUCTURES
F. Damay (LLB Saclay, France)/**M. Laver** (Birmingham University, UK)
N. Qureshi/T. Saerbeck
J. Rodriguez Carvajal

STRUCTURE AND DYNAMICS OF LIQUIDS AND GLASSES
L. Bove (Pierre and Marie Curie University, Paris, France)
G. Cuello
T. Seydel

SPECTROSCOPY IN SOLID STATE PHYSICS AND CHEMISTRY
M. de Boissieu (Simap, Grenoble, France)
A. Piovano
M. Zbiri

STRUCTURE AND DYNAMICS OF BIOLOGICAL SYSTEMS
R. Biehl (JCNS and ICS-1 Jülich, Germany)
A. Martel
M. Blakeley/J. Peters

STRUCTURE AND DYNAMICS OF SOFT CONDENSED MATTER
R. Jacobs (Oxford University, UK)/**A. Zarbakhsh** (University of London, UK))
I. Hoffman/P. Gutfreund
O. Czakkel/I. Grillo

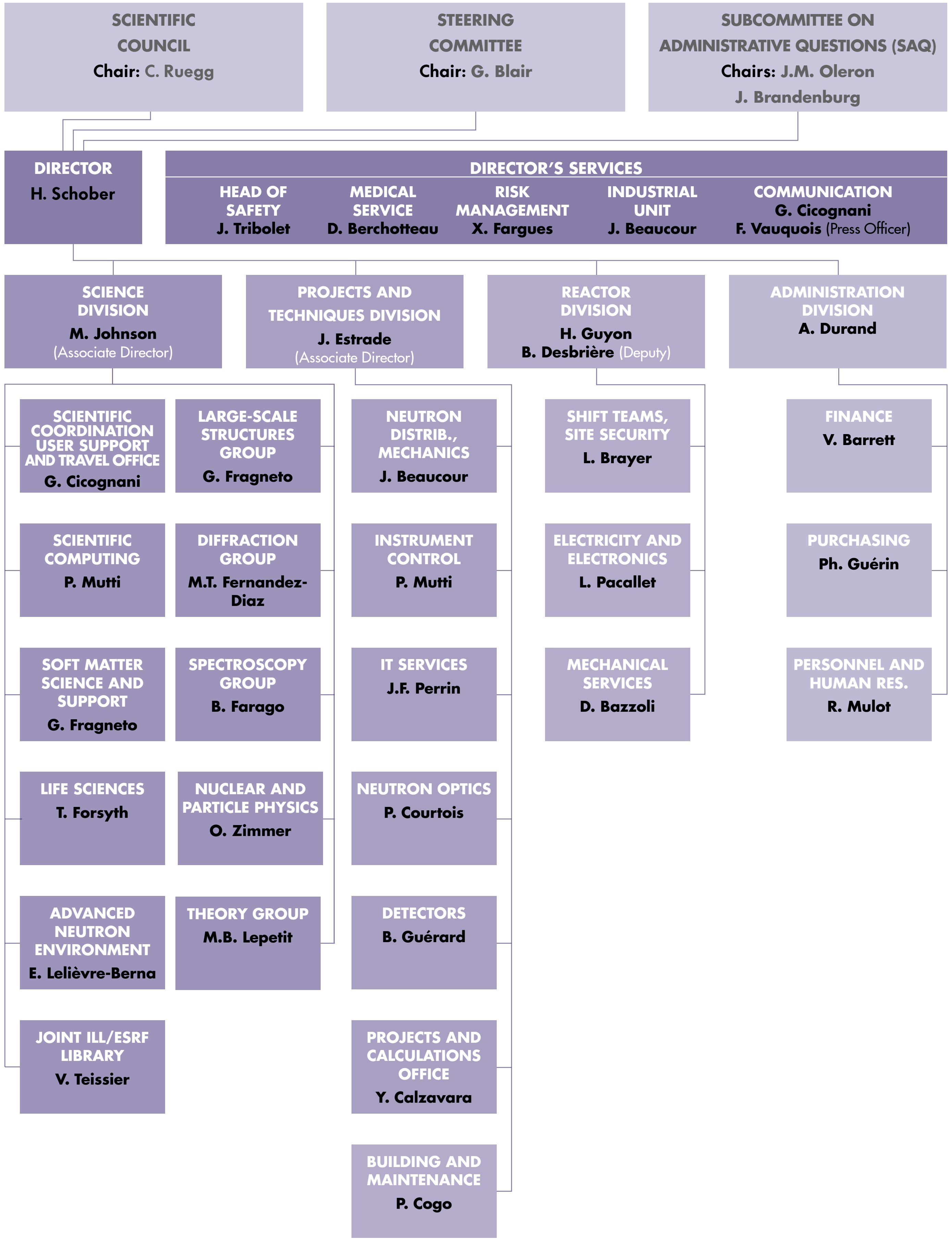

SCIENTIFIC COUNCIL
Chair: C. Ruegg

STEERING COMMITTEE
Chair: G. Blair

SUBCOMMITTEE ON ADMINISTRATIVE QUESTIONS (SAQ)
Chairs: J.M. Oleron
J. Brandenburg

DIRECTOR
H. Schober

DIRECTOR'S SERVICES
- **HEAD OF SAFETY** J. Tribolet
- **MEDICAL SERVICE** D. Berchotteau
- **RISK MANAGEMENT** X. Fargues
- **INDUSTRIAL UNIT** J. Beaucour
- **COMMUNICATION** G. Cicognani; F. Vauquois (Press Officer)

SCIENCE DIVISION
M. Johnson
(Associate Director)
- **SCIENTIFIC COORDINATION USER SUPPORT AND TRAVEL OFFICE** G. Cicognani
- **LARGE-SCALE STRUCTURES GROUP** G. Fragneto
- **SCIENTIFIC COMPUTING** P. Mutti
- **DIFFRACTION GROUP** M.T. Fernandez-Diaz
- **SOFT MATTER SCIENCE AND SUPPORT** G. Fragneto
- **SPECTROSCOPY GROUP** B. Farago
- **LIFE SCIENCES** T. Forsyth
- **NUCLEAR AND PARTICLE PHYSICS** O. Zimmer
- **ADVANCED NEUTRON ENVIRONMENT** E. Lelièvre-Berna
- **THEORY GROUP** M.B. Lepetit
- **JOINT ILL/ESRF LIBRARY** V. Teissier

PROJECTS AND TECHNIQUES DIVISION
J. Estrade
(Associate Director)
- **NEUTRON DISTRIB., MECHANICS** J. Beaucour
- **INSTRUMENT CONTROL** P. Mutti
- **IT SERVICES** J.F. Perrin
- **NEUTRON OPTICS** P. Courtois
- **DETECTORS** B. Guérard
- **PROJECTS AND CALCULATIONS OFFICE** Y. Calzavara
- **BUILDING AND MAINTENANCE** P. Cogo

REACTOR DIVISION
H. Guyon
B. Desbrière (Deputy)
- **SHIFT TEAMS, SITE SECURITY** L. Brayer
- **ELECTRICITY AND ELECTRONICS** L. Pacallet
- **MECHANICAL SERVICES** D. Bazzoli

ADMINISTRATION DIVISION
A. Durand
- **FINANCE** V. Barrett
- **PURCHASING** Ph. Guérin
- **PERSONNEL AND HUMAN RES.** R. Mulot

THE ILL IN THE PRESS

1. Published in *Research Match* on 19 January 2017
2. Published in *Phys.org* on 3 February 2017
3. Published in *Pan European Networks* in April 2017
4. Published in *Phys.org* on 7 July 2017
5. Published in *The Manufacturer* on 18 July 2017

1.

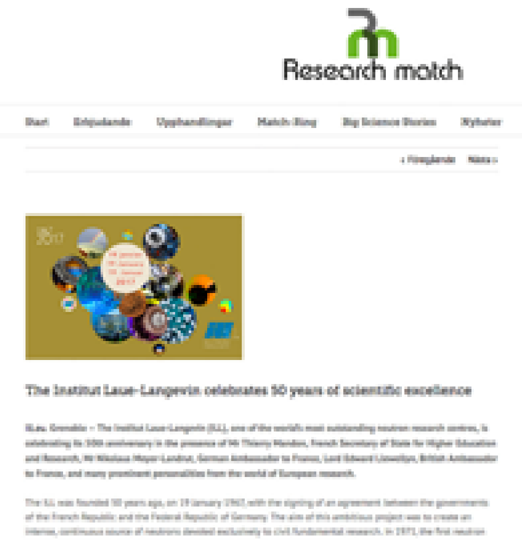

Research match

The Institut Laue-Langevin celebrates 50 years of scientific excellence

2.

Neutrons reveal 'quantum tunnelling' on graphene stars

3.

CHEMISTRY & PHYSICS

PROFESSOR HELMUT SCHOBER, DIRECTOR OF THE INSTITUT LAUE-LANGEVIN, SPOKE TO PEN ABOUT THE EVOLUTION OF THE SCIENCE THAT TAKES PLACE AT THE INSTITUTE

More than simply neutrons

4.

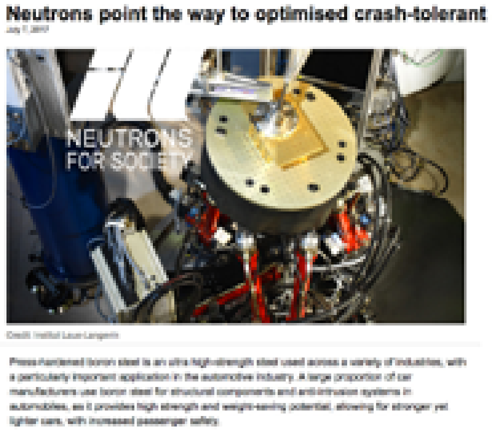

Neutrons point the way to optimised crash-tolerant

Credit: Institut Laue-Langevin

Press-hardened boron steel is an ultra high-strength steel used across a variety of industries, with a particularly important application in the automotive industry. A large proportion of car manufacturers use boron steel for structural components and anti-intrusion systems in automobiles, as it provides high strength and weight-saving potential, allowing for stronger yet lighter cars, with increased passenger safety.

5.

The Manufacturer

Nuclear technology to help manufacture safer cars

Warwick Manufacturing Group (WMG) at the University of Warwick has announced it is using a stream of neutrons from the Institut Laue-Langevin's nuclear reactor in France to examine the safety critical welds in cars made with boron steel.

The WMG research team formed a partnership between the Institut Laue-Langevin's (ILL), Tata Steel, and the UK's EPSRC, which has now begun to use neutrons generated from ILL's nuclear reactor in its SALSA (Strain Analyser for Large Scale Applications) beamline to examine the welds in boron steel.

The collaboration is reportedly already getting useful data thanks to the neutron beam's ability to penetrate heavy materials and the fine resolution it provides.

Press-hardened boron steel is an ultra-high strength steel used across a variety of industries, with a particularly important application in the automotive industry. A

6.

Pan European Networks

A spotlight on spot welding

7.

e-EPS

Facts and info from the European Physical Society

Italy and the ILL: two decades of successful collaboration in neutron science

8.

A stronger interface

Jaime Segura-Ruiz, **Frank Fournel** and **Gregory Imbert** explain how advanced neutron characterization techniques can aid R&D within the microelectronics industry

Grenoble is sometimes regarded as France's version of Silicon Valley. Several important microelectronics firms, including ST Microelectronics, Soitec,

9.

news wise

DOE SCIENCE NEWS SOURCE

The DOE Science News Source is a Newswise initiative to promote research news public and news media.

Neutrons Observe Vitamin B6-Dependent Enzyme Activity Useful for Drug Development

Credit: Genevieve Martin/Oak Ridge National Laboratory, U.S. Dept. of Energy

ORNL's Steven Dajnowicz (left) and Andrey Kovalevsky prepared a sample to begin neutron structural analysis of a vitamin B6-dependent protein using the IMAGINE beamline at ORNL's High

6. Published in *Pan European Networks* on 21 August 2017
7. Published in *EPS* on 26 September 2017
8. Published in *Physics World* in October 2017
9. Published in *News Wise* on 16 October 2017

More articles at
http://www.ill.eu/en/news-press-events/press-corner/ill-in-the-media/

50 YEARS OF THE ILL – SOME LANDMARKS

With over 50 years of achievements, the ILL has firmly established itself as a pioneer in neutron science. The ILL 50th anniversary (celebrated on 19 January 2017) was more than an occasion to look back at a successful past: it should also be seen as a major milestone on the road to an equally bright future.

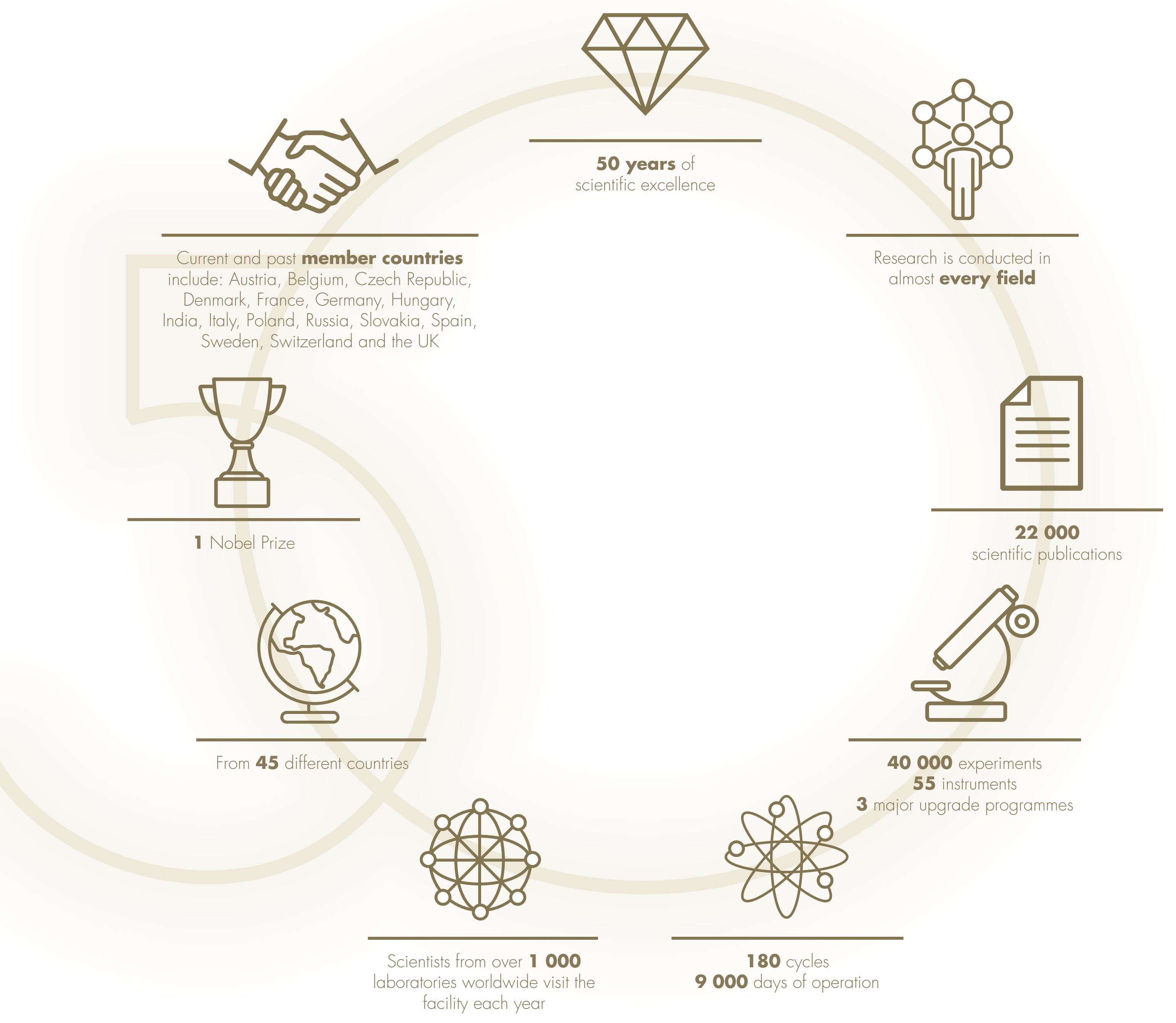

50 years of scientific excellence

Research is conducted in almost **every field**

22 000 scientific publications

40 000 experiments
55 instruments
3 major upgrade programmes

180 cycles
9 000 days of operation

Scientists from over **1 000** laboratories worldwide visit the facility each year

From **45** different countries

1 Nobel Prize

Current and past **member countries** include: Austria, Belgium, Czech Republic, Denmark, France, Germany, Hungary, India, Italy, Poland, Russia, Slovakia, Spain, Sweden, Switzerland and the UK

1961-1970

	1961	1962	1963	1964	1965	1966	1967	1968	1969	1970
THE ILL STORY	J. Horowitz to R. Dautray: *'Draw me a reactor'*	First plans for a heavy water reactor		The Geneva conference: J. Horowitz suggests a Franco-German initiative H. Maier-Leibnitz puts the ILL on the map (at Grenoble!)			19 January: signing of the Inter-governmental Convention		Work starts on the reactor	
WORLD HISTORY	12 April, Y. Gagarin: the first man in space		Paris, 22 January: the signing of the Franco-German Elysée Treaty						Neil Armstrong walks on the moon	
WORLD SCIENCE		Nobel Prize for the work by F. Crick, J. Watson and M. Wilkins on DNA	USA: the world's first human heart transplant				Tectonic plate theory	Description of the molecular structure of insulin		Néel wins Nobel Prize for discoveries in magnetism
ILL SCIENCE										
ILL & NEUTRON TECHNOLOGY						H. Maier-Leibnitz and B. Alefeld invent neutron backscattering A. Heidemann brings it back to the ILL with IN10 (commissioned in 1974)				

1971-1980

	1971	1972	1973	1974	1975	1976	1977	1978	1979	1980
THE ILL STORY	31 August: Reactor goes critical	The founders confirm a user service philosophy for the ILL	UK joins the ILL						The 'deuxième souffle'	
WORLD HISTORY		First Earth Summit (Stockholm)	UK joins the EEC							
WORLD SCIENCE	G. de Gennes' reptation theory		Gavaler discovers Nb_3Ge, a superconductor at 22 K				The first complete genome sequence		First 'World climate conference', Geneva	The world awakes to AIDS
ILL SCIENCE	Neutron bottles for ultracold neutron storage (F.L. Shapiro *et al.*)	First experiment on ILL's IN2 (B. Dorner & M. Steiner)		First neutron scattering experiment on (normal) liquid ^3He (Cowley, Scherm & Stirling) Stuhrmann develops the mathematical formula for the contrast variation method	Key experiments on IN10 and D1A: tunnelling motions of CD_4 and CD_3 groups and Rietveld refinement First QNS experiment in a polymer (Higgins, IN10)			Experimental evidence for dynamic scaling predictions in polymer solutions (F. Mezei, D. Richter *et al.*)	Structural characterisation of a natural biological membrane (J. Zaccai) Spin-wave observations in the actinide α–uranium compounds (J.C. Marmeggi) Discovery of the dynamic nature of spin glass transitions by NSE polarisation analysis (F. Mezei & A. Murani)	Incommensurate phase of biphenyl (C. Zeyen *et al.*)
ILL & NEUTRON TECHNOLOGY		D2, D4, IN1, IN2 First tanzbonden instruments at the ILL (IN2, IN3, ..) Neutron spin-echo invented and tested by F. Mezei	D1A, D1B, D5, D8, IN3, IN4, IN5,IN7, IN10, PN1 PN2-BILL, PN3, 4-GAMS Ibel and Roth build SANS D11 and D17 on cold source guide		D3, D17 Orange cryostat built at the ILL (D. Brochier & S. Pujol) J. Paureau (CNRS) and C. Vettier develop the first high pressure cells (5–6 kbar) and first Al_2O_3 clamps (20–30 mbar)	D18, IN8 F. Mezei invents supermirrors	IN11 PN5/SN5 (FUTURE PF2) PN7 (FUTURE PF1)	P. Aldebert's neutron furnace for solid samples reaches 2 400°C	IN12 PN8	D5

1981-1990

	1981	1982	1983	1984	1985	1986	1987	1988	1989	1990
THE ILL STORY				Green light for the ESRF		Horizontal cold source & second guide hall built	Spain joins the ILL	Switzerland joins the ILL Construction of the ESRF starts		Austria joins the ILL
WORLD HISTORY						26 April: the Chernobyl disaster			Fall of the Berlin wall	
WORLD SCIENCE				Quasi-crystals discovered		Bednorz & Muller: a high-temperature oxide superconductor	First Alzheimer drug trials	NASA's Hansen warns USA of 'global warming'	First human gene transfer experiment	
ILL SCIENCE	New model for molecular dynamics (J. Dianoux & F. Volino)					Determination of the structure of an organic conductor in the superconducting phase (A. Schultz & A.Filhol) Time-resolved neutron powder diffraction on D1B opens up a large research field (J. Pannetier)	Testing the mode coupling theory using spin-echo and backscattering (B. Frick & B. Farago) Fruitful period for the structure and dynamics of quasi-crystals at the ILL (C. Janot & M. de Boissieu)	A. Hewat *et al.* publish the major work on a high-temperature copper oxide superconductor	Unprecedented precision on the neutron lifetime with stored ultracold neutrons (W. Mampe & P. Ageron)	
ILL & NEUTRON TECHNOLOGY	D3, D4, IN1, IN6, IN5, IN8, IN10, IN13		D2 → D2B		D8 → D19 D18 → S18 IN2 → IN20	DB21, D23, IN11	D20 D5	Microstrip gas chamber invented at the ILL (A. Oed)	IN14 Cryopad, a zero-field spherical neutron polarimeter, built at the ILL (F. Tasset)	EVA, LADI

🟦 Instrument start 🟨 First upgrade 🟥 Second upgrade ⬛ Instrument closure

50 YEARS OF THE ILL – SOME LANDMARKS

1991-2000

	1991	1992	1993	1994	1995	1996	1997	1998	1999	2000
THE ILL STORY				First CRGs at the ILL	Reactor restarts with new reactor vessel	Russia joins the ILL	Italy joins the ILL		Czech Republic joins the ILL	The Millennium Programme is launched
WORLD HISTORY	Dissolution of the Soviet Union	Signing of the Maastricht Treaty								
WORLD SCIENCE	Carbon nanotube discovered		Andrew Wiles proves Fermat's Last Theorem							
ILL SCIENCE			Advances in the magnetic structure determination with neutron powder diffraction (J. Rodriguez-Carvajal, most cited ILL paper)		Explanation of why alkaline batteries cannot be recharged – Real-time powder neutron diffraction on D1B (J. Pannetier)				Discovery of ICE XII in two different regions of water's phase diagram (W. Kuhs & M. Koza)	
ILL & NEUTRON TECHNOLOGY	PN2-BILL, PN8		Three-directional neutron polarisation analysis (O. Shärpf)			D23	IN16, ADAM	S18 IN22 LADI	D17, IN15 The Xenocs spin-off (optics for industry and research – P. Høghøj)	IN8

2001-2010

	2001	2002	2003	2004	2005	2006	2007	2008	2009	2010
THE ILL STORY					Sweden joins the ILL	Belgium, Poland and Hungary join the ILL The PSB and D-Lab move into the Carl-Ivar Brändén building			Denmark and Slovakia join the ILL	
WORLD HISTORY	9/11 attacks in New York									
WORLD SCIENCE			First details of cosmic microwave background	Experimental evidence for the solid Bose-Einstein condensate effect	World Year of Physics, honouring the 100th anniversary of Einstein's papers	Neanderthal nuclear DNA sequenced			Water ice discovered on the moon	
ILL SCIENCE	Previously 'impossible' experiments on D20 due to the new microstrip detector (P. Convert & T. Hansen)	Quantum states of neutrons in the Earth's gravitational field (V. Nisvizhevsky *et al.*)			Einstein's $E = mc^2$ confirmed to very high accuracy – GAMS (M. Jentschel *et al.*)				Spin ices reveal magnetic monopole behaviour (T. Fennel *et al.* D7)	
ILL & NEUTRON TECHNOLOGY	FLATCONE: A TAS option combining a set of analysers and detectors in a very compact design (J. Kulda)	D19	IN20 ADAM → SuperADAM VIVALDI	EVA	SALSA IN16	IN3, LADI	IN4, D2B	BRISP	D1A IN5 FIGARO WASP (under construction)	D17 DB21 GRANIT

2011-2017

	2011	2012	2013	2014	2015	2016	2017
THE ILL STORY	India joins the ILL	Post-Fukushima reinforcement work starts	The Inter-governmental Convention is extended to 2023			The Endurance Programme is launched	50th anniversary of the ILL 20th anniversary of Italy's membership Memorandum of understanding between ILL and ESS
WORLD HISTORY	The Fukushima nuclear accident				Major terrorist attacks in Paris	The Brexit vote	
WORLD SCIENCE		Higgs boson discovered at CERN	Creation of human embryonic stem cells by cloning			Gravitational waves detected	Google's AlphaGo defeats Chinese Go Master in Win for A.I.
ILL SCIENCE	Radioisotope production for cancer treatment (U. Koester *et al.*)		Experimental observation of a 'quantum Cheshire cat' (H. Lemmel *et al.*, S18)		Protein water mobility studies (Härtlein & Weik, IN16) improve detection of Alzheimer's disease	Observation of proton transfer by neutron crystallography: key to future HIV drugs (M. Kowalevski & M. Blakeley. LADI) The 2016 Nobel Prize for Physics awarded to Duncan Haldane – previous post-doctoral researcher in the ILL's Theory group	Neutrons reveal that 'quantum tunnelling' on graphene enables the birth of stars (S. Rols *et al.*, IN4) Investigation into the entanglement between molecular qubits brings molecular magnets closer to application in quantum computing (H. Mutka & J. Ollivier, IN5)
ILL & NEUTRON TECHNOLOGY	VIVALDI	IN12 IN16 → IN16B	IN1 → LAGRANGE	IN14 → ThALES IN10		FIPPS	

🟦 Instrument start 🟨 First upgrade 🟥 Second upgrade ⬛ Instrument closure

INSTITUT LAUE-LANGEVIN
71, avenue des Martyrs
38000 Grenoble
France

www.ill.eu